This electronic thesis or dissertation has been downloaded from Explore Bristol Research, http://research-information.bristol.ac.uk

Author:
Almuqrin, Abdulaziz M

Title:
Molecular biology of the human coronaviruses, MERS-CoV and SARS-CoV

Molecular Biology of the human coronaviruses, MERS-CoV and SARS-CoV-2

Abdulaziz Almuqrin

A thesis submitted to the University of Bristol in accordance with the requirements for the award of the degree of Doctor of Philosophy in the School of Cellular and Molecular Medicine

Abstract

MERS-CoV and SARS-CoV-2 cause respiratory illnesses that may lead to severe respiratory diseases in humans. To help answer the question of why some coronaviruses are lethal to humans but not to their animal hosts, I used high-throughput quantitative proteomics to analyze the expression of proteins involved in the innate immune system response in bat, camel, and human cells. Bioinformatic analysis showed a difference in the expression levels of proteins involved in the innate immune response between the three species, especially the pro-inflammatory cytokines associated with viral diseases' severity and mortality.

Due to the limited information regarding the role of MERS-CoV accessory proteins ORF4A and ORF4B in virus replication, our lab investigated MERS-CoV ORF4A and MERS-CoV-ORF4B host protein-protein interactions using high-throughput quantitative proteomics in HEK293 cells. Based on the generated data, I selected six proteins (NDH II, NF45, HNRNPAB, HNRNPC, KPNA4, and HNRNPA2B1) to validate their interactions with the MERS-CoV ORF4A or MERS-CoV ORF4B in human cells. The interactions of MERS-CoV ORF4A & ORF4B proteins with bat and camel equivalent proteins were also examined to investigate whether they interact with these viral proteins with higher or lower affinity than their human counterparts or whether these interactions are species-specific. This analysis could help understand the potential roles of MERS-CoV ORF4A & ORFB proteins in virus replication and why MERS-CoV infection is lethal for humans but not for its animal hosts.

Open reading frame 10 (ORF10) is one of the unique features of the SARS-CoV-2 genome, and its potential function remains controversial. One aim of this work is to shed light on the possible role of ORF10 in SARS-CoV-2 infection. In this study, I used immunoprecipitation of FLAG-tagged ORF10 proteins to identify its cellular-interacting partners. In addition, reverse genetics techniques were used to rescue the SARS-CoV-2 virus with either the ORF10 protein knocked out or replaced with fluorescent markers. The cellular proteome of SARS-CoV-2 ORF10 mutant infected cells was investigated using high-throughput proteomics analysis to uncover more information on how ORF10 protein may be modulating the host's innate immune proteins or other aspects. Finally, the replicative fitness of the SARS-CoV-2 ORF10 mutant was characterized in different cell lines.

ACKNOWLEDGMENTS

In the name of Allah, the infinitely Compassionate and Merciful

AUTHOR'S DECLARATION

I declare that the work in this dissertation was carried out in accordance with the requirements of the University's Regulations and Code of Practice for Research Degree Programmes and that it has not been submitted for any other academic award. Except where indicated by specific reference in the text, the work is the candidate's own work. Work done in collaboration with, or with the assistance of, others, is indicated as such. Any views expressed in the dissertation are those of the author.

SIGNED: .... DATE:........................

Table of Contents

List of Tables

Abbreviations

- 3CLpro   3C-like protease
- A2RE   A2 response element
- ACE-2   Angiotensin-converting enzyme 2
- BAC   Bacterial Artificial Chromosome
- C8B   Complement component C8 beta chain
- CARD   Caspase activation and recruitment domains
- CCL2   C–C motif chemokine ligand 2
- CCL5   C-C Motif Chemokine Ligand 5
- CHIKV   Chikungunya Virus
- COVID-19   Coronavirus 2019
- CTLs   Cytotoxic T lymphocytes
- CXCL10   C–X–C motif chemokine 10
- DDX58   Antiviral innate immune response receptor RIG-I
- DENV   Dengue virus
- DPP4   Dipeptidyl peptidase 4
- E   Envelope
- EMCV   Encephalomyocarditis virus
- ER   Endoplasmic reticulum
- GRD   Arginine/glycine-rich domain
- GRP78   Membrane-associated 78 kDa glucose-regulated protein
- HAdV-2   Human adenovirus-2
- HAdV-5   Human adenovirus-5
- HAstV1   Classic Human Astrovirus 1
- HBV   Hepatitis B virus
- HCC   Hepatocellular Carcinoma
- HCV   Hepatitis C virus
- HEV   Hepatitis E Virus
- HNRNPA2B1   Heterogeneous nuclear ribonucleoproteins A2/B1
- HNRNPAB   Heterogeneous nuclear ribonucleoprotein A/B
- HNRNPC   Heterogeneous nuclear ribonucleoproteins C1/C2
- hnRNPs   Heterogeneous nuclear ribonucleoproteins
- HVR   Hyper-variable region
- IBDV   Infectious Bursal Disease Virus ()
- IFI16   Interferon Gamma Inducible Protein 16
- IFI44   Interferon Induced Protein 44
- IFI44L   Interferon Induced Protein 44 Like
- IFIGBP   Interferon-induced guanylate-binding protein 1
- IFIT1   IFN-induced protein with tetratricopeptide repeats 1
- IFIT2   IFN-induced protein with tetratricopeptide repeats 2
- IFIT3   IFN-induced protein with tetratricopeptide repeats 3
- IFN   Interferons
- Importin subunit alpha 3   KPNA4
- IP-Western   Western Blot Analysis of Immunoprecipitation
- TMT/MS-MS   Tandem mass spectrometry
- IRF3   Interferon Regulatory Factor 3

- IRF7   Interferon Regulatory Factor 7
- ISG15   Ubiquitin-like protein ISG15
- ISG20   Interferon-stimulated gene 20 kDa
- ISGs   Interferon-stimulated genes
- JAK1   Janus kinase 1
- JEV   Japanese encephalitis virus
- M   Membrane protein
- MAVS   Mitochondrial antiviral-signaling protein
- MAVS   Adaptor protein mitochondrial antiviral signaling
- MBP   Myelin basic protein
- MDA5   Melanoma differentiation-associated protein 5
- MDA5   Melanoma differentiation-associated protein 5
- MERS-CoV   Middle East respiratory syndrome coronavirus
- Mpro   Chymotrypsin-like or main protease
- MX1   Interferon-induced GTP-binding protein Mx1
- N   Nucleocapsid
- NDH II   Nuclear DNA helicase II or ATP-dependent RNA helicase A
- NF45   Nuclear factor 45 or Interleukin enhancer-binding factor 2
- NF-κB   Nuclear factor kappa-light-chain-enhancer of activated B cells
- NIX   Nip3-like protein X
- NLRP3   NOD-, LRR- and pyrin domain-containing protein 3
- NRGN   Neurogranin
- Nsp1   Non-structural protein 1
- OAS2   2'-5'-oligoadenylate synthase 2
- OASL   2'-5'-oligoadenylate synthase-like protein
- ORF10   Open reading frame 10
- PAMPs   Pathogen-associated molecular patterns
- PARP14   Poly (ADP-Ribose) Polymerase Family Member 14
- PDAC   Pancreatic ductal adenocarcinoma
- PHB1 and PHB2   prohibitin 1 and prohibitin 2
- PIT   Proteomics Informed by Transcriptomics
- PLpro   papain-like protease
- PolyI: C   Polyinosinic:polycytidylic acid
- PRRs   Pattern recognition receptors
- RBD   Receptor binding domain
- RH   Relative humidity
- RIG-I   Retinoic acid-inducible gene I
- RIG-I   Retinoic acid-inducible gene I
- RBPs   RNA-binding proteins
- RNP   Ribonucleocapsid
- RRM   RNA recognition motif
- RTC   RNA replication- transcription complex
- S   Spike protein
- S2M   Stem-loop II-like motif
- SARS   Severe acute respiratory syndrome
- SARS-CoV-2   Severe acute respiratory syndrome coronavirus 2
- STAT1   Signal transducer and activator of transcription 1
- STAT2   Signal transducer and activator of transcription 2

- TAR Transformation-associated recombination
- TBK1 TANK Binding Kinase 1
- TLRs Toll-like receptors
- TMPRSS2 Transmembrane serine protease 2
- TMT/MS-MS Tandem Mass Tag spectrometry
- TNFSF10 Tumor necrosis factor ligand superfamily member 10
- TNFSF18 TNF Superfamily Member 18
- TNF-α Tumor necrosis factor α
- TRAF3 TNF Receptor Associated Factor 3
- TRAF3 TNF Receptor Associated Factor 3
- TRAF6 TNF receptor-associated factors 6
- TRIF TIR-domain-containing adapter-inducing interferon-β
- TRS Transcription-regulating sequence
- TYK2 Tyrosine kinase 2
- VA1 Astrovirus VA1
- VOC Variants of concern
- VSV Vesicular Stomatitis Virus
- WHO World Health Organization
- YAC Yeast Artificial Chromosome
- ZC3H12A Zinc finger CCCH-type containing 12A
- ZC3H12A Zinc finger CCCH-type containing 12A

Chapter 1. General introduction

1.1 Coronaviruses classification

Coronaviruses are the largest known RNA viruses, with genomic sizes ranging from 25.5 - 32 kb and a crown-like appearance under the electron microscope. This unique appearance is due to the spike glycoprotein on the surface of the virus envelope (1).

They are part of the Coronaviridae family, which is classified under the Nidovirale order. Based on sequence comparisons of the whole viral genome, coronaviruses are categorized into four genera, Alphacoronaviruses, Betacoronaviruses, Deltacoronaviruses, and Gammacoronaviruses (1) (2).

Human coronaviruses are all members of the Alphacoronaviruses or Betacoronaviruses genera. HCoV-229E and HCoV-NL63 belong to the Alphacoronavirus family and only cause mild disease in the upper respiratory tract (3). HCoV-OC43, HCoV-HKU1, Severe acute respiratory syndrome (SARS), Middle East respiratory syndrome coronavirus (MERS-CoV), and severe acute respiratory syndrome coronavirus 2 (SARS-CoV-2) belong to the Betacoronaviruses (Figure1) (2) (4).

Betacoronaviruses are divided into four lineages (A, B, C, and D). SARS-CoV and SARS-CoV-2 are grouped in lineage B, while MERS-CoV is classified in lineage C. SARS-CoV, MERS-CoV, and SARS-CoV-2 cause life-threatening diseases (3–5) (4).
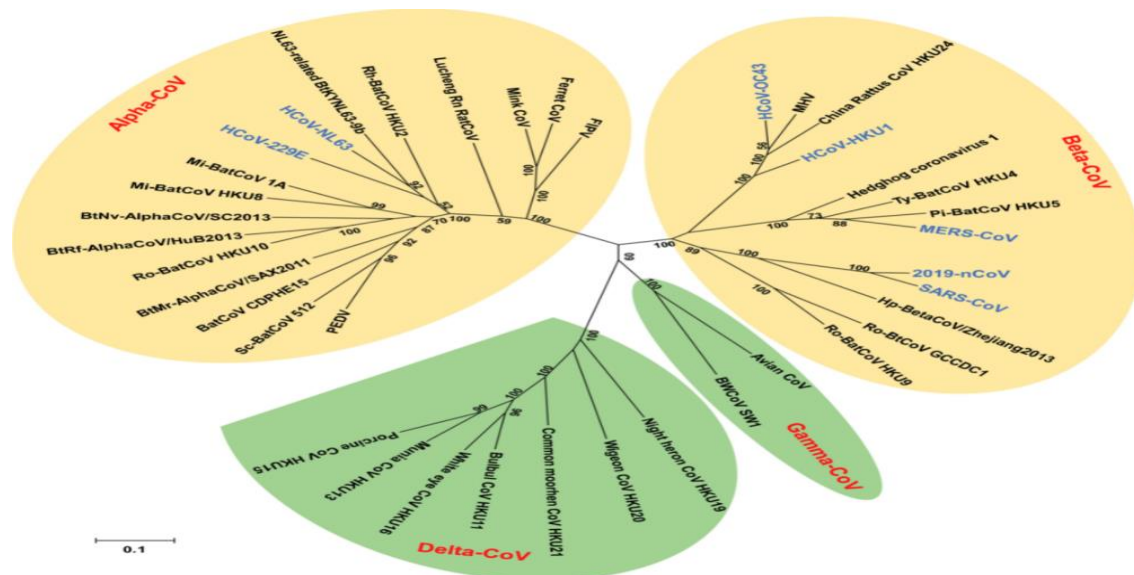
Figure 1. **Phylogenetic tree of Human and animal coronaviruses based on RNA-dependent RNA polymerase nucleotide sequences**. The four major phylogenetic clusters are Alphacoronaviruses, Betacoronaviruses, Deltacoronaviruses, and Gammacoronaviruses. SARS, MERS-CoV, and SARS-CoV-2 belong to the Betacoronaviruses. The figure adapted from "Subunit Vaccines Against Emerging Pathogenic Human Coronaviruses", Wang N, Front. Microbiol. 2020 (7).

1.2. Coronaviruses as a global public health challenge

Until 2002, only a few coronaviruses were known to be circulating in humans, causing asymptomatic or mild diseases. These diseases were mainly caused by four human coronaviruses, including HCoV-NL63, HCoV-229E, HCoV-OC43, and HCoV-HKU1 (1). However, SARS-CoV emerged in 2003 in Guangdong Province, China, causing a life-threatening form of pneumonia and respiratory failure. The virus spread to more than 27 countries infecting around 9000 people with a mortality rate of 10% (8). The SARS-CoV pandemic was an obvious sign that more coronaviruses could cross the species barrier and cause severe illness in humans.

1.3. MERS-CoV: History and Epidemiology

In 2012, MERS-CoV was isolated for the first time from a 60 year old patient who died from acute pneumonia and renal failure in Jeddah, Saudi Arabia (KSA). The isolated virus was the second highly pathogenic human coronavirus after the SARS-CoV in 2003 (9). Within the same year, hundreds of cases were confirmed in KSA, and currently, MERS-CoV is considered endemic. A WHO report showed that 2578 cases had been confirmed in KSA, including 810 related deaths with a case-fatality rate of around 38% until August 2021 (10). MERS infections have also been reported in different Middle Eastern countries, e.g., Egypt, Qatar, Iran, Kuwait, and UAE. In 2015, the largest outbreak of MERS outside Middle Eastern countries occurred in South Korea, with around 200 confirmed infections, including 39 related deaths (11). In addition, travel-associated cases have also been reported in Turkey, the United Kingdom, Italy, the United States, France, China, and Germany (11).

1.3.1 MERS-CoV: Host reservoirs and transmission

Phylogenetic and sequencing data analysis of the MERS- CoV genome suggests that bats are the main natural reservoir of the virus and dromedary camels are the intermediary host before dissemination to humans (Figure 2) (13) (14). A range of evidence supports this suggestion. For example, it was found that MERS-CoV antibodies were prevalent among dromedary camels across the Arabian Peninsula. Stored serum samples of camels dating back to the 1980s in the Middle East and North Africa were positive for MERS-CoV antibodies indicating that the virus had been circulating in dromedary camels for some time before it disseminated into humans (14). Several reports indicate that MERS-CoV RNA has

been isolated from milk of infected dromedary camels in KSA (15) . Moreover, a phylogenetic study of 182 full-genomes or genome fragments from viruses isolated from human and dromedary camels showed that MERS-CoV genomes share more than 99% sequence identity (14)(16).

Solid line, documented direction of MERS-CoV transmission
Dashed line, hypothetical direction of MERS-CoV transmission
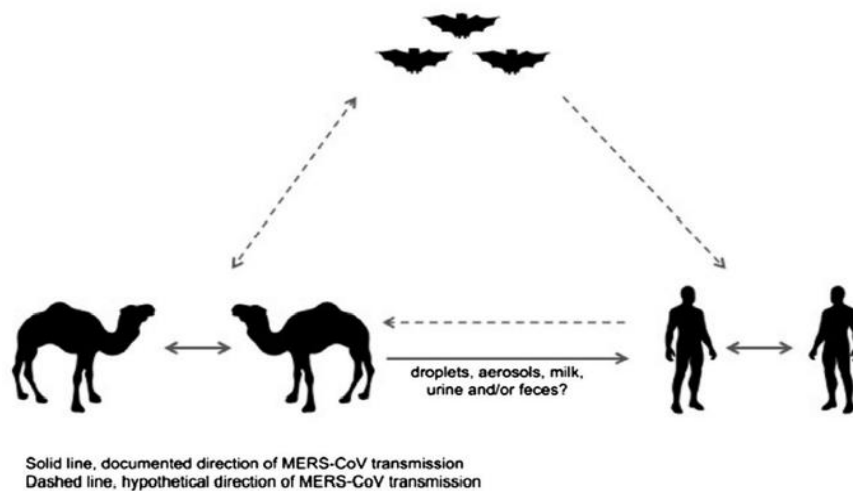
Figure 2. Confirmed and hypothetical transmission routes of MERS-CoV between humans, camels, and bats. The solid line represents the documented direction of MERS-CoV transmission. The dashed line represents the hypothetical direction of MERS-CoV transmission (290).

It is worth noting that consuming camels' unpasteurized milk, changes in camel farming practice, and direct contact with dromedary camels are likely the main routes of MERS-CoV transmission from camels to humans (15) (17). Nosocomial transmission of MERS-CoV has also been reported among health workers or patients sharing rooms in hospitals in KSA and South Korea (11).

1.3.2 MERS-CoV: Viral particle and genome organization

MERS-CoV is an enveloped, single-stranded, positive-sense RNA virus. Its virions are approximately 90 to 120 nm in diameter, and its morphology is characterized by a moderately pleomorphic or spherical shape with definite projections. It is one of the largest single-stranded RNA viruses with a genomic size of 30,119 nt in length, which acts as a viral messenger RNA (mRNA) that comprises a 5`-terminal cap structure and a poly 3` tail. (14)(17).
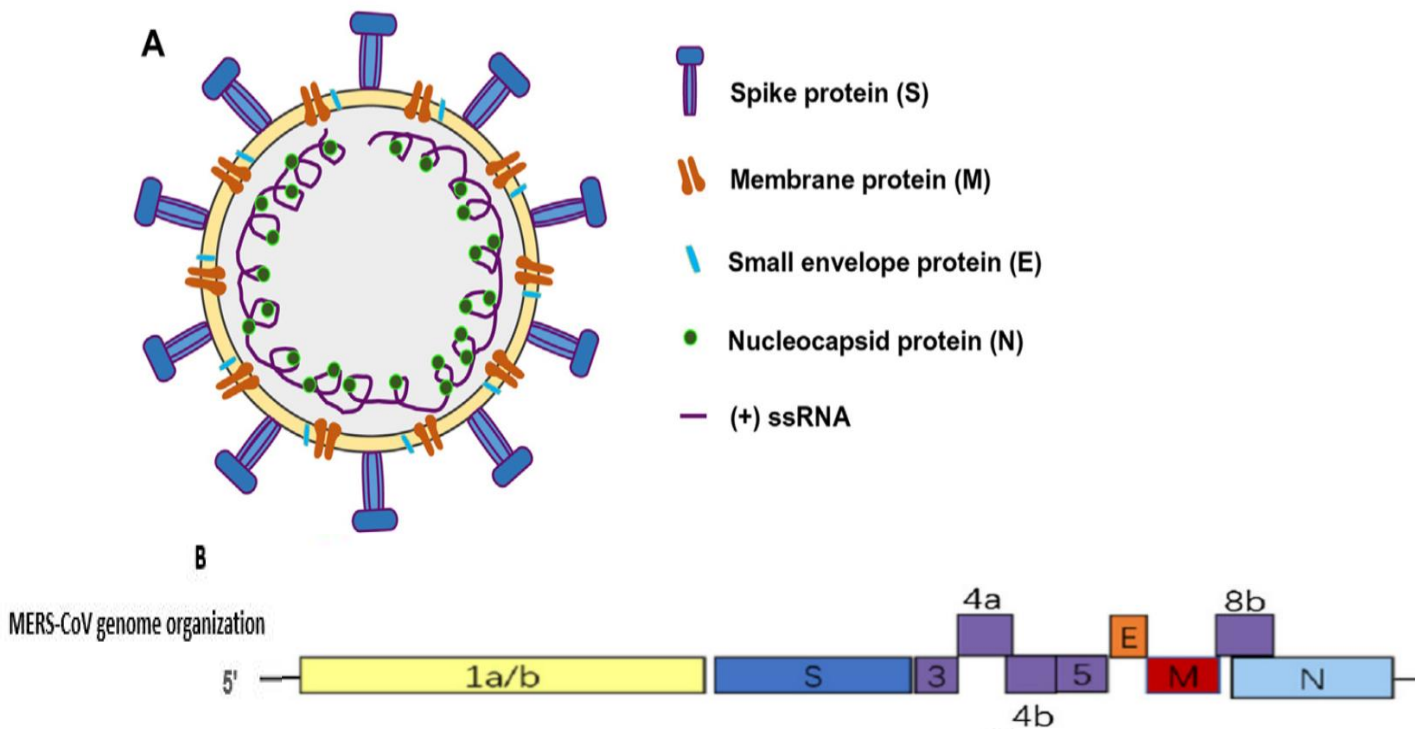
Figure 3. Schematic structure of MERS-CoV viral proteins and genome organization. (A) MERS-CoV virion contains a positive, single-stranded RNA and four structural proteins, including spike, nucleocapsid, envelope, and membrane (S, N, E, and M). **(B)** Around 11 kb of the MERS-CoV genome at the 3′ end constitutes structural genes (S, E, M, N) and five accessory proteins (ORF3, ORF4a, ORF4b, ORF5, ORF8). The figure adapted from ''Receptor-binding domain-based subunit vaccines against MERS-CoV'', Zang N, Virus Res, 2015 and from '' A comparison of COVID-19, SARS and MERS'', Hu T, Microbiology, 2020 (291).

MERS-CoV genome encodes for several structural and non-structural proteins. The 5'-proximal two-thirds of the viral genome contains the replicase-transcriptase gene, which codes for large polyproteins. This replicase-transcriptase gene is comprised of two overlapping open reading frames (ORF1a & ORF1b) and encodes 16 non-structural proteins (nsp1-16) that are highly conserved throughout coronaviruses and are required for viral RNA synthesis (19)(20). The remainder of the viral genome encodes structural proteins (S, E, M, and N) and five accessory proteins. Accessory genes are common in all coronaviruses and interspersed throughout the structural genes (Figure 3) (21).

1.3.3 MERS-CoV Structural proteins

1.3.3.1 S protein

Spike protein (S) is a MERS-CoV structural protein that plays a crucial role in virus replication. It mediates the virus attachment to host cells' receptors and facilitates viral entry (22). It is localized throughout the typical secretory pathway from the endoplasmic reticulum to the plasma membrane (16). It consists of two subunits which are S1, located at the N-terminus, and S2, located at the C-terminus. The S1 subunit contains the receptor-binding

domain (RBD), which binds the host's receptor dipeptidyl peptidase 4 (DPP4), enabling virus entry. Sialic acid and membrane-associated 78 kDa glucose-regulated protein (GRP78) have been identified as additional binding targets for the S1 subunit, thereby augmenting the virion attachment and entry (20–22).

1.3.3.2 N protein

Nucleocapsid protein (N) is one of the most abundant viral proteins in infected cells and is involved in nucleocapsid formation. It has a crucial role in virions assembly and RNA packing via its interaction with M protein and viral genome. It plays a role in immune evasion by suppressing type I and type III IFN signaling pathways (23) (24). Although it possesses two nuclear localization sequences, N protein has been shown to be localized predominately in cells' cytoplasm (19).

1.3.3.3 E protein

Envelope (E) is the smallest structural protein in MERS-CoV (31)-CoV (31). It forms pentameric ion channels in the lipid bilayer, allowing ions transport with more selectivity for Na+ and K+ (26). It is associated with internal cytoplasmic membranes, the endoplasmic reticulum, Golgi, and the endoplasmic reticulum-Golgi intermediate compartment. It is involved in assembling progeny virions and forming the viral envelope (25,27).

1.3.3.4 M protein

Membrane (M) protein is a component of the viral envelope. It is localized mainly in the Golgi apparatus and overlaps with the endoplasmic reticulum-Golgi intermediate compartment in infected cells. It interacts with all viral structural proteins, which makes it the central organizer of virus assembly (25)(19)(26). M protein has a crucial role in immune evasion by suppressing type I IFN expression (35).

1.3.4 MERS-CoV accessory proteins

The 3'- proximal one-third of the MERS-CoV genome encodes for five accessory proteins, including ORF3, ORF4a, ORF4b, ORF5, and ORF8. These proteins have different cellular localizations and functions. ORF3 is a 53 amino acid residues protein that is localized with the endoplasmic reticulum and the endoplasmic reticulum-Golgi intermediate compartment. ORF5 is the largest accessory protein, with 224 amino acid residues. It is mainly co-localized with the Golgi apparatus and the ER-Golgi intermediate compartment. ORF3 and ORF5 are suggested to have roles in virus replication and enhancing viral pathogenesis (12,17,26). ORF8b is a 93 amino acid residues long protein. It has a role in immune evasion by suppressing IRF3-mediated IFN-β expression.

ORF4a and ORF4b are 109 and 246 amino acid residues long, respectively. It has been shown that ORF4a and ORF4b suppress the innate immune response by disrupting IRF-3 phosphorylation, thereby inhibiting the synthesis of IFN-β (29) (16). Further studies are needed to elucidate the functional roles of ORF4a and ORF4b in MERS-CoV pathogenesis.

1.3.5 MERS-CoV: Replication cycle

MERS-CoV replication cycle starts with the binding of the S glycoprotein to the host cellular receptor Dipeptidyl peptidase-4 (DPP4) (27) (20). DPP4 is the primary receptor of MERS-CoV and is highly expressed in several human tissues, e.g., kidney, alveoli, liver, prostate, and lower respiratory tract cells, which explains the ability of MERS-CoV to infect multiple organs. MERS-CoV can infect many non-human species, such as horses, rabbits, bats, and camels. All of these non-human species express DPP4 receptors on various organs (28)(27)(29).

S glycoprotein consists of two subunits, S1, which contains the receptor-binding domain that binds DPP4, and S2, which possesses membrane-fusing mediators to facilitate virus-cell fusion and release viral genome into the cytoplasm (13) (14) (27).
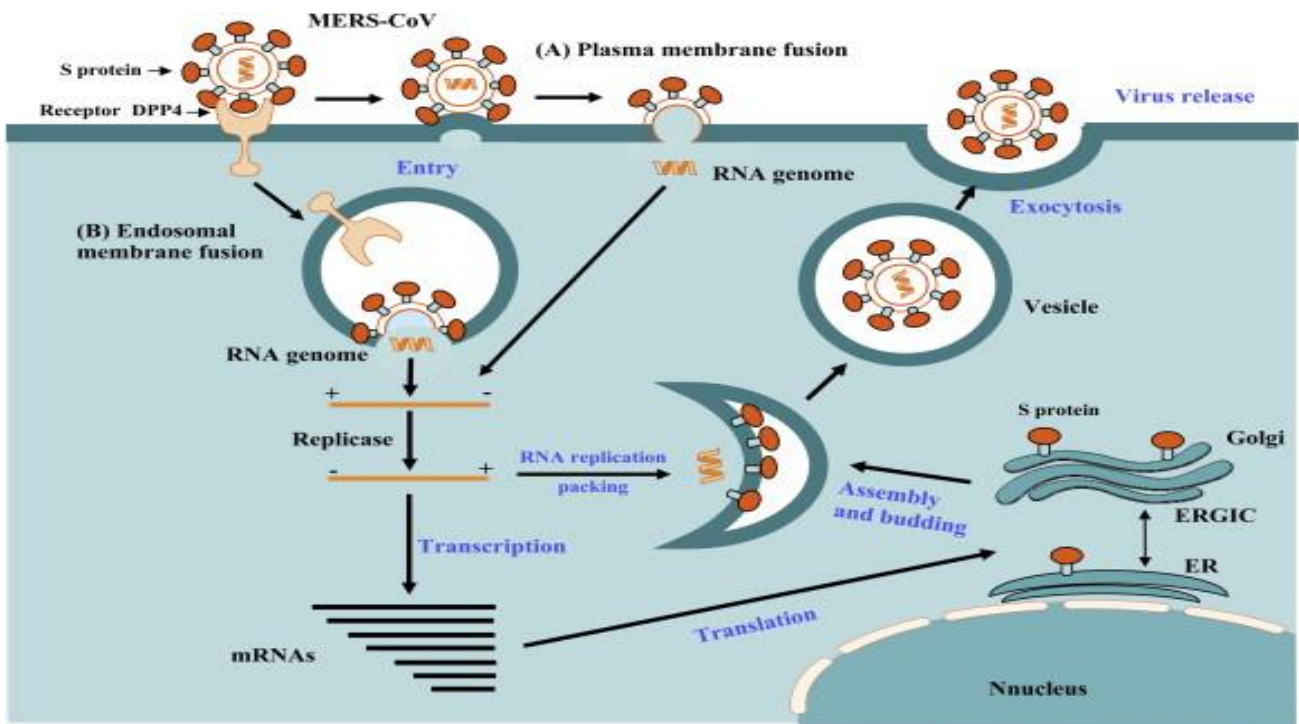
Figure 4. schematic overview of MERS-CoV replication cycle. Once the viral genome is released in the cytoplasm, ORF1a and ORF1b get translated, generating pp1a and pp1ab polyproteins. The pp1a and pp1ab are then cleaved at different sites yielding 16 non-structural proteins that form (RTCs). The RTC complex drives the production of full-length -ve RNA, which is used as a template to make full-length +ve RNA and overlapping subgenomic -ve RNAs. Subgenomic -ve RNAs are then transcribed to produce subgenomic mRNAs, which are then translated to produce viral structural and accessory proteins. Viral genomic RNA and structural proteins are assembled, and newly formed Virions are then released from the infected cells. The figure adapter from Middle East respiratory syndrome coronavirus (MERS-CoV): challenges in identifying its source and controlling its spread, Lu L, Microbes Infect, 2013 (33).

Once the viral genome is released in the cytoplasm, the host's ribosomes translate open reading frames ORF1a and ORF1b to generate pp1a and pp1ab polyproteins (30). The pp1a and pp1ab polyproteins are then cleaved by viral-encoded proteases, papain-like protease (PLpro) and 3C-like protease (3CLpro), at different sites generating 16 non-structural proteins, which assemble and form replication-transcription complexes (RTCs) (28) (14)(31).

The RTC initiates the viral RNA replication and transcription process, producing full-length complementary (-ve) RNA, which is used as a template to make more full-length (+ve) genomic RNA and overlapping subgenomic -ve RNAs. Subgenomic -ve RNA are then transcribed to produce subgenomic mRNA. Cellular ribosomes translate subgenomic mRNA to produce viral structural and accessory proteins (28)(14)(30).

As new viral genomic RNA accumulates, the N protein binds to newly synthesized viral RNA in the cytoplasm to form a helical nucleocapsid. Structural proteins E, S, and M are inserted into ER membranes before they are transported to the ER–Golgi intermediate compartment.

The newly formed nucleocapsid then buds to ER-Golgi intermediate compartment to interact with E, M, and S proteins and form new virions (Figure 4) (28)(31)(30).

1.3.6 MERS-CoV vaccine and treatment

There is no commercially licensed vaccine or antiviral drugs to treat MERS-CoV. Supportive care to alleviate symptoms is the only treatment option for MERS-CoV patients (13). Some anti-viral drugs have been tested as a potential treatment for MERS-CoV. One of the best anti-viral candidates to treat MERS-CoV is resveratrol (32). Resveratrol is a potent antiviral drug that inhibits several viral infections, including MERS-CoV *in vitro*. However, some studies showed that resveratrol has multiple side effects, such as strong cytotoxicity and enhancing HCV & HBV replication (33) (34). Therefore, there is an urgent need to develop safe and effective anti-viral drugs to treat MERS-CoV with minimal side effects. Identifying and understanding viral-host protein-protein interactions is one of the critical steps for developing an anti-viral treatment for MERS-CoV.

1.4 Tandem Mass Tag (TMT)-based quantitative proteomics

TMT-based quantitative proteomics analysis is a valuable tool for proteins identification and quantification. Protein identification relies on two factors, the correct matching of the peptide fragments to their proteins of origin and providing a comprehensive list of 'possible' proteins in the sample by the user for the proteomics data analysis program to compare the spectra. In the TMT approach, 11 samples can be analyzed in only a single run. Protein samples are proteolytically digested and labelled with distinct tandem mass tags. These tags have a specific 'cleavage linker' that breaks during a particular stage of the MS/MS analysis of peptide fragments allowing for the release of the mass reporters. The peptides from every sample are then combined equally and fractionated using liquid chromatography before being analyzed by LC-MS/MS to determine the identity of the peptides. Labelled peptides are first identified as single peaks before they are fragmented and allow the release of the mass reporters. The released mass reporters reflect the abundance of each peptide in every sample (Figure 5). A variety of proteomic analysis programs can be used to analyze the raw data to match the peptide fragments to their potential proteins. As mentioned earlier, these programs use protein databases specific to species of organism the samples were derived from to provide a final readout of the predicted proteins that have been detected and the relative quantities at which they are present in each sample.

Bats and camels are the natural animal hosts of MERS-CoV. However, MERS-CoV doesn't cause symptomatic disease in bats or camels, while it causes severe illness in humans. The

exact reasons for the lack of MERS-CoV symptomatic disease in bats and camels are still unknown. It is expected that the innate immune response of bats and camels to MERS-CoV behave differently from the human innate immune system and that these differences may underpin the differences in pathogenicity. Recent advances in TMT-based quantitative proteomics make this approach attractive for analyzing the difference in the innate immune response between bats, camels, and humans, which would contribute to our understanding of why MES-CoV is so lethal to humans but not to their animal hosts.
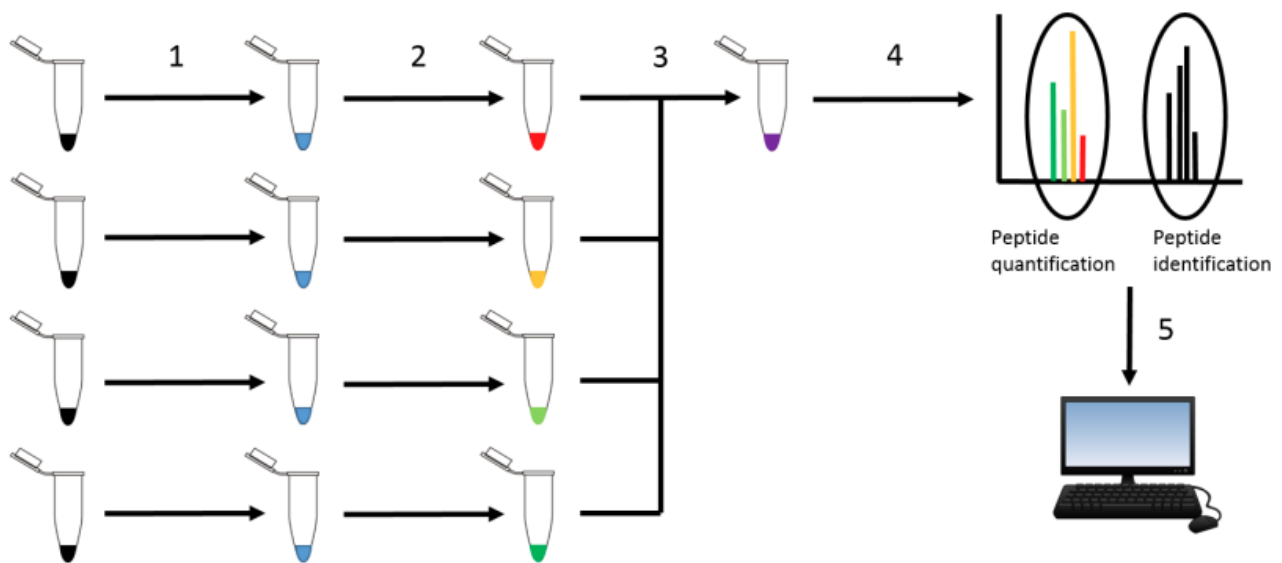
Figure 5. Sample preparation and data generation for TMT-Ms/MS proteomics. Proteins are digested using Trypsin to generate peptides. TMT labelling tags are added to label each peptide with a unique tag for that sample. Eleven samples can be run at one time as there are 11 unique identifiable tags commercially available. Samples are mixed and run through LC-MS-MS. The resulted peaks are passed through a proteomics program to identify which proteins are present and how their quantities are varied between samples. The figure adapter from Investigation and comparison of the human interactions of flaviviral NS5 protein, Hales J, 2019 (292).

1.5 SARS-CoV-2: General introduction

1.5.1 History and Epidemiology

In December 2019, several cases of patients with pneumonia-like symptoms of unknown causes were reported in local hospitals in Wuhan city, China. Most of the patients were linked to the local sea/wet food market. Using real-time RT-PCR, the new pathogen was confirmed as a virus (39). The newly identified virus was then rapidly sequenced, and its genome shared 79% similarity with the SARS genome and 50% with the MERS-CoV

genome. The genome of the newly identified virus shared 88% similarity to multiple bat-derived coronaviruses genomes, indicating that the world had encountered a new coronavirus spill-over event after MERS-CoV (40).

The novel coronavirus was isolated using human epithelial cells and examined under an electron microscope. The virus was 60 to 140 nm in diameter with characteristic projections of 9 to 12 nm, similar to the other coronaviruses (56). On 11 Feb 2020, the International Committee on Taxonomy of Viruses named this novel virus SARS-CoV-2. The disease caused by SARS-CoV-2 was named as Coronavirus disease-19 (COVID-19) (42,43).

1.5.2 SARS-CoV-2. Symptom and clinical manifestation

SARS-CoV-2 mainly affects the upper and lower respiratory tract systems. It is manifested by several symptoms ranging from asymptomatic to mild such as cough, fever, fatigue, nausea, and muscle aches. It also causes more severe symptoms like difficulty breathing, acute respiratory distress syndrome (ARDS), multi-organ failure, and septic shock that could lead to death (58,59).

The most prevalent symptoms among COVID-19 patients are fever (43.8% on admission and 88.7% during hospitalization) and cough (67.8%) (60). The mortality rate is generally higher in patients over 60 years old and with various chronic conditions, such as diabetes (type 1 or type 2), cancer, Tuberculosis, heart diseases, or HIV infection (61).The median incubation period of the SARS-CoV-2 infection is six days (51).

Covid-19 spread rapidly worldwide, causing the worst pandemic since the Spanish flu in 1918. COVID-19 was declared a pandemic on March 11, 2020, causing hundreds of millions of confirmed infections and several million deaths and has overwhelmed most healthcare systems worldwide.

Most countries implemented some forms of "lockdown" legislation to reduce human-human interactions and virus transmission, which also resulted in a devastating economic effect. As of January 20, 2022, SARS-CoV-2 had caused more than 332,617,707 reported infections and 5,551,314 deaths worldwide (64).

1.5.3 SARS-CoV-2 Transmission

Droplets inhalation is the primary transmission route of the SARS-CoV-2, with proximity and ventilation being key determinants of the transmission risk. The virus can also be transmitted to healthy individuals if they use the personal items of infected people, such as clothing, bedding, etc. (59).

It has been shown that SARS-CoV-2 virus particles were able to be detected up to 3 days post-inoculation on nonporous surfaces like glass or stainless steel (49). More interestingly, another study noted that viable SARS-CoV-2 particles were isolated for almost one-month post-inoculation at ambient temperature and humidity (20 °C and 50% RH) from these surfaces (50). These findings could explain why SARS-CoV-2 spreads faster than other respiratory viruses through populations.

1.5.4 Structural organization of SARS-CoV-2 genome

The SARS-CoV-2 genome is made up of a single-stranded positive-sense RNA packed in a protein envelope. Like other coronaviruses, the SARS-CoV-2 envelope possesses spike-like projections of surface glycoprotein. The genome of SARS-CoV-2 is slightly smaller than MERS-CoV, with an approximate length of 29,891 nt (66). There are 11 protein-coding genes in the viral genome that express 12 viral proteins. The GC content is only about 38%, and the genomic organization is similar to other coronaviruses (Figure 6) (67).
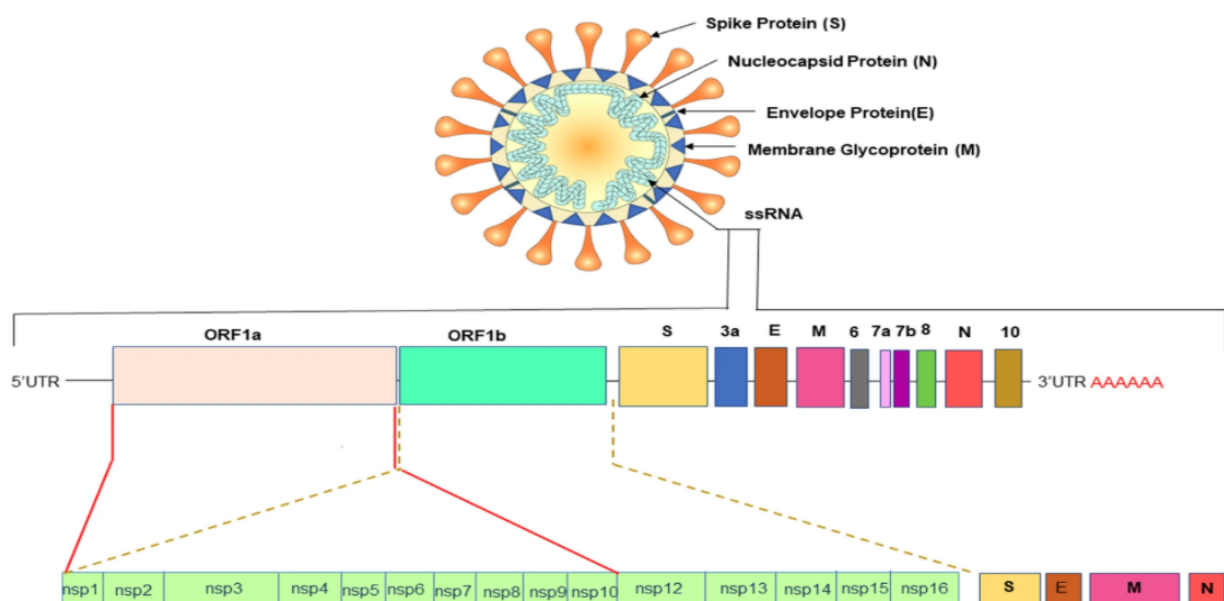
Figure 6. Structural organization of SARS-CoV-2 genome. The full-length RNA genome consists of 29,891 nucleotides containing a replicase complex (consisting of ORF1a and ORF1b) at the 5′UTR end. the 3′UTR encodes for four structural genes: Spike, Envelope, Membrane , and Nucleocapsid. The accessory genes are distributed in between the structural genes. The figure adapter from SARS coronavirus 2: from genome to infectome, Rastogi M, Respiratory Research,2020 (293).

The viral genome contains a 5'-cap and 3'poly-(A) tail structures flanking six functional open reading frames (ORFs). These ORFs are arranged as replicase (ORF1a/ORF1b), spike (S), envelope (E), membrane (M), and nucleocapsid (N). Multiple ORFs encoding accessory proteins are interspersed between structural genes, including 3a, 6, 7a, 7b, 8, and 10 ORFs (52) (55).

1.5.5 SARS-CoV-2 structural proteins

1.7.5.1 SARS-CoV-2 S protein

SARS-CoV-2 spike glycoprotein (S) is a class I transmembrane protein that protrudes from the virion's envelope. It is indispensable in initiating the viral replication cycle by binding the primary receptor, Angiotensin-converting enzyme 2 (ACE-2), and mediating viral entry. It consists of 1273 amino acid residues, making it longer than the S glycoprotein of SARS-CoV with a sequence homology of nearly 77.0% (55).

SARS-CoV-2 S glycoprotein comprises three domains: the intracellular domain, which shows an intracellular tail, the transmembrane domain, and the ectodomain (53).

The ectodomain consists of two subdomains: S1 and S2 subdomains. S1 is located at the top of the spike protein and is made up of two subunits, the N-terminal domain (NTD) and the C-terminal domain (CTD)(54)(53). The C-terminal domain (CTD) contains the receptor-binding domain (RBD), making it the major determent of virus tropism and an important target for the host's neutralizing antibodies. The RBD mediates the initial attachment of virion with the host cell receptor ACE-2 and subsequently initiates the infection process (71).

The S2 subdomain plays a central role in viral fusion. It is composed of fusion peptide (FP), heptad repeat 1 (HR1), central helix (CH), connector domain (CD), heptad repeat 2 (HR2), and transmembrane domain (TM)(55)(56). Once RBD- ACE2 binding takes place, the S2 subdomain undergoes conformational changes by inserting FP into the host cell's membrane, exposing HRs and stimulating their trimerization to form a coiled-coil structure, which drags the virus's envelope and the host cell's membrane into proximity to mediate viral fusion and entry (62).

One of the unique genomic features of the SARS-CoV-2 genome is the presence of four amino acid residues (PRRA) at the boundary of S1 and S2 subdomains, creating an effective furin cleavage site that has a crucial role in viral fusion (74).

1.5.5.2 SARS-CoV-2 E protein

SARS-CoV-2 E gene encodes to a small protein E with a size of 8.4-12 kDa (58). It is highly expressed during virus replication, but only a small amount is incorporated into the newly formed viral particles. The amino acid sequence of the SARS-CoV-2 E protein is almost identical to the SARS-CoV E protein except for only four variations. Therefore, it is presumed that the E proteins of both viruses function similarly (56). It has been shown that the E protein of coronaviruses acts as viroporins, allowing irons transport and facilitating the assembly and budding of new progeny from infected cells (71). Further studies are needed to precisely characterize the function of SARS-2-CoV E protein in the virus replication.

1.5.5.3 SARS-CoV-2 M

M protein is one of the most abundant viral proteins expressed during coronavirus replication. The conserved amino acid residues in the SARS-CoV-2 M protein and other coronaviruses suggest that M protein has similar roles in viral assembly and replication (70). Recently, it has been shown that the SARS-CoV-2 M protein has a crucial role in suppressing the host's innate immune response to facilitate virus replication by targeting RIG-I/MDA-5 signaling pathway. It disrupts RIG-I, MAVS, TRAF3, and TBK1 complex formation, which is required for IRF3 activation and IFN production (72).

1.5.5.4 SARS-CoV-2 N protein

SARS-CoV-2 N protein consists of 419 amino acid residues that are approximately 90% identical to the N protein of SARS-CoV (73). Therefore, It is suggested that SARS-CoV-2 N protein maintains the same primary functions as SARS-CoV N protein. These functions include packaging the viral RNA to form ribonucleocapsid (RNP) complex, interacting with M protein to mediate viral assembly, and participating in viral RNA transcription and replication processes (74). Interestingly, a study pointed out that N protein could be implicated as a molecular basis for the observed relations between SARS-CoV-2 and Parkinsonism. In that study, SARS-CoV-2 N protein but not S protein was found to accelerate the aggregation of α-synuclein into amyloid fibril, which is one of Parkinson's disease characteristics (75).

1.5.6 SARS-CoV-2 non-structural proteins

Following the entry and the release of viral genomic RNA, ORF1a and ORF1b open reading frames get translated to produce pp1a and pp1ab polyproteins. pp1a and pp1ab are then cleaved to generate 16 non-structural proteins (NSPs), forming the replication and transcription complex (64).

Non-structural protein	Function
NSP 1	Leader protein that inhibits host translation processes and is involved in host mRNA degradation (76).
NSP 2	Has a role in proofreading RNA synthesis. Also, it binds to prohibitin 1 and prohibitin 2 (PHB1 and PHB2) to modulate the survival signaling pathway of the host cells (77).
NSP3	Act as a viral protease that separates NSP1, NSP2, and NSP3 from pp1a and 1ab polyprotein (78). Also, it has a role in inhibiting host translation and suppressing innate immune response (95).
NSP4	It is needed to form a viral replication transcription complex (RTC). It anchors RTC to modified ER membranes (79).
NSP5	Involved in the cleavage of pp1a and pp1ab polyproteins to produce intermediate or mature non-structural proteins (80).
NSP6	helps in forming autophagosomes from ER, which can promote infection by facilitating the assembly of replicase proteins (81).
NSP7 & NSP8	Associated with NSP12 to facilitate viral replication (82).
NSP9	An RNA-binding molecule plays a role in viral replication (73).
NSP10 & NSP11	The exact role of these proteins is not clear yet.
NSP12	Has a role in the transcription, replication, and methylation of viral RNA (84).
NSP13	It is a superfamily I helicase that plays a role in RNA replication through unwinding duplex RNA (85).
NSP14	Encodes for proofreading exoribonuclease (ExoN) that is required for high-fidelity replication(76) (86).

NSP15	It possesses endoribonuclease activity that targets viral RNA to halt its accumulation, thereby preventing the host cell's dsRNA sensors from detecting accumulated viral genomes (101).
NSP16	Involved in immune response evasion (88).

1.5.7 SARS-CoV-2 accessory proteins

SARS-CoV-2 genome encodes for multiple accessory proteins during the replication cycle. These proteins include ORF3a, ORF6, ORF7a, ORF7b, ORF8, and ORF10 (80). It has been shown that coronaviruses' accessory proteins are not essential in the virus replication but contribute to viral pathogenesis (90). However, the roles of the SARS-CoV-2 accessory proteins haven't been thoroughly investigated.

1.5.7.1 ORF3a

ORF3a is a polymorphic, multifunctional protein with 275 amino acid residues, making it the largest accessory protein among the others. It is a glycosylated O-linked protein with three transmembrane domains and shares a sequence homology of nearly 73% with the ORF3a protein of SARS-CoV. ORF3a has a role in suppressing cellular antiviral responses. It has been shown that ORF3a mediates escaping the virus from autophagy clearance by inhibiting autophagic flux and preventing the fusion of autophagosomes with lysosomes (82). Although SARS-CoV does not depend on ORF3 for its reproduction, ORF3 deletion causes significant reduction of viral replication. Notably, the presence of ORF3a is critical for the SARS-CoV-2 and SARS-CoV replication when the E protein is absent, as virus missing E and 3a proteins is not viable in Vero E6 cells or infected animal models(83) (84) . Thus, ORF3a is required for maximizing virus replication. ORF3a is a viroporin, and could have a similar effect to viroporin on virion morphogenesis, viral entry, viral replication, and release (85).

1.5.7.2 ORF6

ORF6 is a 61 amino acid residues long protein. It's a shared protein with SARS-CoV but not with MERS-CoV and has a 67% similarity to the codon sequence of the SARS-CoV ORF6. ORF6 of SARS-CoV-2 has been shown to play an important role in immune response evasion by blocking the IFN signaling pathway. It localizes in the endoplasmic reticulum and Golgi compartments and disrupts nuclear import complex formation, preventing STAT1 translocation to the cell's nucleus and, thereby, inhibiting the expression of STAT1-activated genes (92,93). It has been shown that SARS-CoV-2 ORF6 protein interacts with several nucleopore proteins and nucleoporins to disrupt nucleocytoplasmic trafficking, thereby inhibiting cellular mRNA nuclear export and enhancing viral replication and pathogenesis (88,89).

1.5.7.3 ORF7a & ORF7b

SARS-CoV-2 bicistronic subgenomic RNA 7 generates two accessory proteins, ORF7a and ORF7b. The ORF7b start codon overlaps the ORF7a terminal codon in a -1 shifted ORF(90). ORF7a protein is 121 amino acid residues long and shares nearly 86% identity with ORF7a protein from SARS-CoV (94) (92). It plays an essential role in immune response evasion. ORF7a protein is ubiquitinated at position Lys 119 (K119), and such ubiquitination enhances ORF7a to inhibit type-I interferon (IFN-I) signaling by blocking STAT-2 phosphorylation (95,96). ORF7b protein is an integral membrane protein that is made up of 43 amino acid residues. It is localized o the Golgi compartment and shares 85.4% identity with SARS-CoV ORF7b (94). It has been shown that ORF7b promotes the type-I IFN signaling pathways and subsequently enhances Tumor Necrosis Factor-α-Induced Apoptosis in infected cells (97). Further studies are needed to elucidate the role of ORF7b in viral pathogenesis.

1.5.7.4 2 ORF8

ORF8 is 121 amino acid residues long protein. It shares the least similarity with SARS-CoV among the other viral proteins and has a role in antiviral immune evasion (94). The 1-17 residues contain an N-terminal sequence for Endoplasmic Reticulum import. The 18–121 residues are predicted to resemble immunoglobulin (Ig)-like folds to interact with host proteins (96). It antagonizes IFN production by targeting HSP90B1. Moreover, it has been shown that ORF8 interacts with class I major histocompatibility complex molecules (MHC-I

molecules) and mediates their down-regulation by targeting them for lysosomal degradation, and, therefore, disrupts antigen presentation and reduces the elimination of virus-infected cells by cytotoxic T lymphocytes (CTLs) (96,97,99). Because it is part of a hypervariable genomic region, ORF8 is susceptible to deletions and nucleotides substitution. SARS-CoV-2 isolates deleted from the ORF8 have been associated with milder symptoms and lower disease severity (96).

1.5.7.5 ORF10

ORF10 is a unique feature that distinguishes SARS-CoV-2 from SARS-CoV and MERS-CoV (100). Genome annotation of SARS-CoV-2 shows that ORF10 is an open reading frame, 117nt long, located downstream of the structural gene N. It encodes for a small accessory protein, 38 amino acid residues, that does not share sequence homology with any known protein (97) (98). It is predicted to be a hydrophobic, thermally stable, highly ordered protein. It contains at least one transmembrane region and a β-α-β motif, with a β-molecular recognition feature in the first β-strand (100). It is speculated that ORF10 protein might have a role in SARS-2-CoV immunogenicity and pathogenicity.

A study suggested that ORF10 suppresses the IFN-signalling pathway to enhance viral replication and pathogenesis by inducing mitophagy-mediated mitochondrial antiviral signaling protein (MAVS) degradation. (100). Also, it has been shown that ORF10 transcripts were markedly more expressed in Covid-19 severe cases than moderate cases, suggesting that ORF10 plays a role in maximal viral replication and pathogenesis (101).

On the other hand, a study reported that two individuals were infected with SARS-CoV-2, where the ORF10 gene was prematurely terminated with a stop codon. The disease in both cases was not attenuated, and both mutant viruses were isolated and cultured in VeroE6 cells. The replication curve of both mutants was similar to the intact ORF10 gene SARS-CoV-2. Furthermore, some studies suggested that ORF10 has no role in virus replication and pathogenicity and should not be treated as a protein-encoding gene; therefore, the SARS-CoV-2 genome should be altered (102) (103). Nevertheless, our lab showed that ORF10 transcripts exist using Nanopore ReCappable Sequencing (NRCeq) technology. NRCeq is a novel approach that can identify capped full-length sub-genomic RNAs (sgRNAs). In this approach, the native 5′ cap of viral sgRNAs is replaced by a 5′- linked RNA sequencing adapter, allowing for the differentiation of full-length, capped RNAs from fragmented RNAs and truncated sequencing artifacts. m7G cap sgRNA transcripts are then sequenced using direct nanopore sequencing. sgRNAs transcripts encoding ORF10 were

detected using NRCeq technology (104). One aim of this thesis is to shed light on the possible role of ORF10 in SARS-CoV-2 infection.

1.5.8 SARS-CoV-2 replication cycle

SARS-CoV-2 replication starts with the binding of RBD in the S1 subunit to 18 residues of the host cell's receptor ACE-2. ACE-2 is the primary receptor of SARS-CoV-2 and is highly expressed in multiple human organs, e.g., Lung, heart, intestine, kidney, etc. The RBD of SARS-CoV-2 binds ACE-2 with a higher affinity than SARS-CoV may be because of the variations in RBD of SARS-CoV-2 compared with SARS-CoV RBD (70).

Once the S1 subunit binds to the ACE-2 receptor, a cellular protease transmembrane serine protease 2 (TMPRSS2) mediates proteolytic cleavage at the boundary of S1-S2 subunits to initiate viral fusion (107). TMPRSS2 is 492 amino acid residues type II transmembrane serine protease. It is critical for SARS-CoV-2 S protein activation and facilitating virus fusion. (105–108). One of the marked differences between SARS-CoV-2 and SARS-CoV S glycoproteins is the presence of a polybasic sequence motif, Arg-Arg-Ala-Arg (RRAR), in SARS-CoV-2 S glycoprotein, which is cleaved by furin, a serine protease that is widely expressed in host cells.

It has been shown that cleaving (PRRAR) by furin increases the priming of the S protein and exposes more cell surface receptor binding sites, such as neuropilin-1 and neuropilin-2 (NRP1 and NRP2). It has been shown that SARS-CoV-2 can use NRP1 and NRP2 to promote its entry and infectivity (113,114). After the furin cleavage occurs, the S2 subunit undergoes conformational changes and inserts the fusion peptide to mediate virus-host membrane fusion and release the viral genome into the cytoplasm (60). Once the viral genome gets released in the cytoplasm, it recruits host-cell ribosomes to translate pp1a and pp1ab polyproteins from ORF1a and ORF1b. (111). pp1a and pp1ab polyproteins are then get cleaved by viral-encoded proteases, papain-like protease (PLpro), which is embedded in non-structural protein 3 (nsp3), and chymotrypsin-like or main protease (Mpro), that is embedded in non-structural protein 5 (nsp5), yielding to 16 non-structural proteins. These 16 non-structural proteins assemble and form viral replication–transcription complexes (RTCs) (120,121).

The RTC initiates the viral RNA replication, producing full-length -ve RNA and subgenomic -ve RNAs (-ve sgRNA). Full-length -ve RNA is used as a template for genome replication. Subgenomic negative-sense RNAs (-ve sgRNA) are used as templates to synthesize a set of +ve subgenomic RNA, which are then translated to generate viral structural and accessory proteins (Figure 7) (117,118).
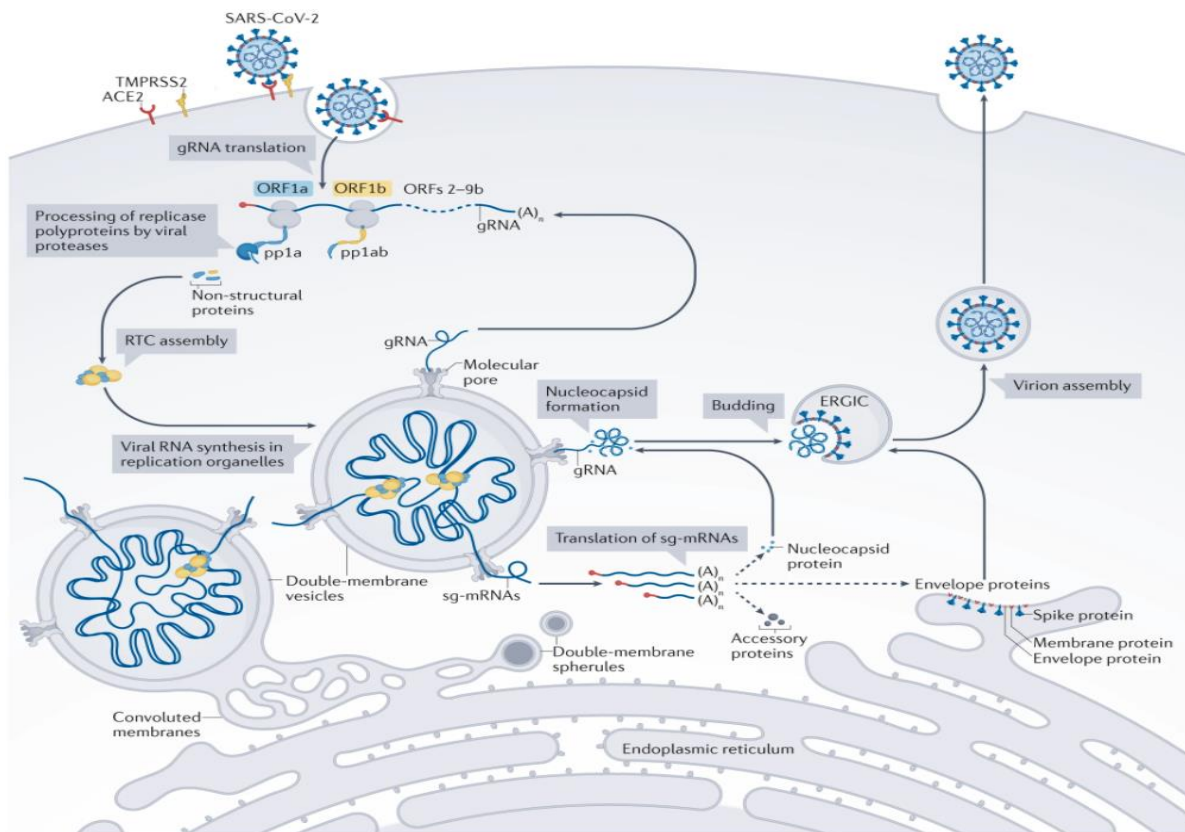
Figure 7. A schematic overview of the SARS-CoV-2 replication cycle. The S protein of SARS-CoV-2 binds to the host receptor ACE-2. Following the viral entry and releasing the viral genome to the cytoplasm, ORF1a and ORF1b are translated generating pp1a and pp1ab polyproteins. The pp1a and pp1ab are then cleaved at different sites yielding 16 non-structural proteins that form (RTCs). The RTC complex drives the production of full-length -ve RNA, which is used as a template to make full-length +ve RNA and overlapping subgenomic -ve RNAs. Subgenomic -ve RNAs are then transcribed to produce subgenomic mRNAs, which are then translated to produce viral structural and accessory proteins. Viral genomic RNA and structural proteins are assembled, and newly formed virions are then released from the infected cells. The figure adapted from Structures and functions of coronavirus replication–transcription complexes and their relevance for SARS-CoV-2 drug design,Malone B, nature reviews molecular cell biology, 2021 (111).

1.5.9 RNA synthesis of coronaviruses

The discontinuous viral transcription is one of the marked features of coronaviruses. This process occurs during -ve strand RNA synthesis, producing full-length -ve RNAs and a nested set of -ve sgRNAs. The -ve sgRNAs are then transcribed to produce sg-mRNA templates, which are translated to produce viral structural and accessory proteins. The 3′ ends of the nested set of the sg-mRNAs are identical and share a 5′ leader sequence, representing the 75 nucleotides at the 5′ end of the viral genomic RNA(115). The presence of the 5′ leader sequence in viral full-length -ve RNA and subgenomic -ve RNAs (-ve sgRNA) has several essential biological functions. For example, it provides a conserved starting point for +ve RNA synthesis of gRNA and all sg-mRNAs, acts as a recognition signal for the viral mRNA capping machinery, and enables all viral mRNA to escape from the translation shut-off mediated by NSP1(64,116).

During negative-strand RNA synthesis, the replication transcription complexes halt the transcription process when it comes into contact with transcription regulatory sequences 5′-ACGAAC-3 (TRSs), which are found upstream of most open reading frames in the 3′ one-third of the viral genome that encode the structural and accessory proteins. At these TRSs, the synthesis of the negative-strand RNA stalls and is re-initiated at the leader sequence (TRS-L), which is located near the 5′ end of the viral genome, producing a -ve strand copy of the leader sequence. This process is enhanced by base pairing interactions between +ve genomic RNA (+ve TRS-L) and the nascent -ve sgRNA (-ve TRS-B or TRS-body). The -ve strand copy of the leader sequence is then added to the nascent RNA to complete the synthesis of -ve sgRNAs. The -ve sgRNAs templates are then used to generate +ve sg RNAs, which are eventually translated to produce viral proteins (111,116).
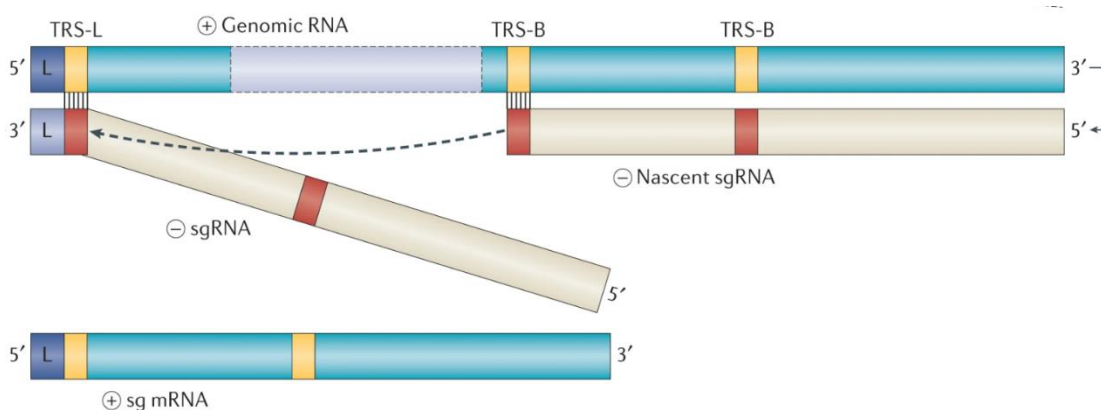
Figure 8. Schematic description of RNA synthesis in coronavirus. The synthesis of -ve sg RNA in coronaviruses is mediated by discontinuous transcription. In this process, the RTC pauses RNA synthesis following the encounter of the body transcription regulatory sequences (TRS-B) and relocates to a position adjacent to a leader sequence of the genomic RNA leading to the production and addition of a -ve copy of the leader sequence to each -ve sg RNA template. These sg -ve RNA templates are transcribed to produce +ve sg mRNAs. The +ve sg mRNAs are translated to viral structural and accessory proteins. The figure adapter from "Coronavirus biology and replication: implications for SARS-CoV-2", V'kovski P, Nature Reviews Microbiology, 2020 (64).

1.5.10 SARS-CoV-2 variants

SARS-CoV-2 has a high mutation rate, resulting in new variants with different genomic features than the ancestral strain. The new variants could be more virulent than their ancestors, e.g., exhibit a higher ability to evade the immune system, associated with more severe disease or increased transmission (123).

Therefore, frequent sequencing of SARS-CoV-2 samples is important to monitor Variants Under Investigation (VUI) and Variants of Concern (VOC). VUI is characterized by genetic changes affecting virus transmission, vaccine effectiveness, disease severity, and being more

frequent than the other variants. VOC is a dominant variant characterized by concerning abilities, such as causing more severe disease, increased transmissibility, evading conventional diagnostic detection methods, and reducing antibodies neutralization obtained from previous infection or vaccination (120). World Health Organization announced that VOCs would be labeled using the Greek alphabet letters (118).

The D614G variant was the first VOC discovered. It became the dominant variant and was associated with increased transmissibility but didn't cause more severe illness than the wild-type (Wuhan-Hu-1 strain) virus (119)(125).

1.5.10.1 *Alpha* (B.1.1.7 lineage)

The alpha variant was the first VOC reported in the UK in December 2020. The genome of the alpha variant contains seventeen mutations, of which eight were found in the S gene, including (Δ69-70 deletion, Δ144 deletion, N501Y, A570D, P681H, T716I, S982A, D1118H). Alpha variant showed a higher transmission rate and increased illness, hospitalization, and mortality than pre-existing variants (126,127).

1.5.10.2 Beta (B.1.351 lineage)

The beta variant was first reported in South Africa, causing the second wave of COVID-19 in different countries (124). This variant contains eight mutations in the S gene. Three of these mutations are found in the region of RBD (K417N, E484K, and N501Y), which enhances the binding of S protein to the ACE-2 receptor (128). The beta variant has been reported with increased transmissibility and reduced antibody neutralization by post-vaccination and convalescent sera (129).

1.5.10.3 *Gamma* (P.1 lineage)

The gamma variant was first detected in Brazil in December 2020. Its genome possesses 13 mutations in the S gene, three of which were found in the RBD region (L18F, K417N, E484K) (130). The gamma variant was associated with increased transmissibility and reduced antibody neutralization by post-vaccination and convalescent sera (131).

1.5.10.4 *Delta* (B.1.617.2 lineage)

The delta variant was first identified in India in 2020, causing a deadly second wave of Covid-19 in India and other countries. The spike gene of the delta variant contains ten mutations (T19R, G142D, 156del, 157del, R158G, L452R, T478K, D614G, P681R, D950N) (127). These mutations were associated with increased transmissibility and reduced antibody neutralization from convalescent sera by six-fold. Delta variant was eightfold less sensitive to vaccine-elicited antibodies (132).

1.5.10.5 Omicron (B.1.1.529 lineage)

The Omicron variant was first identified in South Africa in November 2021. It contains genomic mutations more than other known VOC, with more than 30 mutations in the S gene only. The RBD region of the Omicron variant harbors fifteen mutations, including Y505H, N501Y, Q498R, G496S, Q493R, E484A, T478K, S477N, G446S, N440K, K417N, S375F, S373P, S371L, G339D (124). The conventional RT-PCR test targeting the S gene failed to detect this variant due to these heavy mutations, specifically due to the deletion in positions 69–70 of S protein (128). It spreads quicker than other known VOCs and is associated with reduced neutralization by multiple therapeutic antibodies. The vaccine effectiveness against the Omicron variant is lower than the other variants. (134). (135,146).

1.5.11 drugs to treat COVID-19

Remdesivir is the only FDA-approved antiviral drug to treat Covid-19 disease (137). It is a nucleoside analog that inhibits viral replication by targeting RNA-dependent RNA polymerase (RdRp) to terminate RNA transcription prematurely (129). Favipiravir is a licensed antiviral drug in Japan used to treat resistant cases of influenza (139). An initial study has shown that Favipiravir effectively treats Covid-19 disease, especially in patients with mild or moderate illness. In that study, Favipiravir induced viral clearance in patients within one week and improved clinical symptoms (131). However, further studies are needed to determine the required dose and duration of treatment to confirm the efficiency of Favipiravir in COVID-19 treatment. Sotrovimab is a monoclonal antibody (nMAb) that neutralizes SARS-CoV 1. The parental form of this monoclonal was isolated from a patient with SARS-CoV 1 disease. Sotrovimab showed antiviral activity against multiple VOCs, including the alpha, beta, and

gamma, *in vitro*. A study has demonstrated that Sotrovimab reduced the disease progression among high-risk patients with mild and moderate Covid-19 (132).

1.7.11 SARS-CoV-2 Vaccination development

Vaccines are the most powerful tool to prevent and control infectious diseases. Many research organizations and academic institutions have made great efforts to develop the COVID-19 vaccine using different vaccine platforms, e.g., live attenuated virus, inactivated (killed) virus, subunit/peptide vaccines, vectored vaccines, and DNA/RNA vaccines (136). Some of these vaccines are currently in use. Most COVID-19 vaccine candidates utilize S protein as the main target to generate a sufficient titer of S antibodies to block viral-host receptor attachment and entry (137).

1.7.11.1 Pfizer/BioNTech and Moderna vaccines

Pfizer/BioNTech and Moderna are nucleic acid vaccines approved for use in the UK and other countries. They are based on a modified mRNA molecule with a non-natural RNA nucleobase N1-methylpseudouridin encodes for the S protein (135).

mRNA is fragile and less stable than DNA molecules. It is negatively charged, hard to penetrate the plasma membrane, and can easily be degraded by the host enzymes before synthesizing the target protein. Because of these reasons, the mRNA molecule gets encapsulated in a lipid nanoparticle (LNP) to facilitate its delivery (136,138). Pfizer/BioNTech and Moderna vaccines substantially protect against COVID-19 illness with very mild side effects.

1.7.11.2 Replication-defective viral vector vaccines

Due to its biological properties, adenovirus is widely used in vaccine and gene therapy research. These properties include a large capacity for foreign gene insertion in the virus backbone, the ability to accommodate multiple large transgenes easily, targeting a wide variety of dividing and non-dividing cells, and large-scale production (137) (140).

Human adenovirus-5 (HAdV-5) and (HAdV-2) are the most studied viruses as vectors for gene therapy and vaccine development (139). However, some problems hinder the progress of developing human adenovirus as gene therapy and vaccine vector, such as pre-existing vector

immunity as the result of the endemic human adenovirus among many populations, which could neutralize the virus thereby reducing the therapeutic gene delivery. Another problem is the possibility of spontaneous recombination between the recombinant virus and wild-type virus due to the ubiquitously of wild-type virus among human populations (141–143).

ChAdOx1 nCoV-19 is one of the Covid-19 vaccines approved in the UK and other countries. It is derived from chimpanzee adenovirus Y25 and deleted for E1 and E3 genes. E1 contains early genes required for transcription cascades; removing this region would prevent viral replication. Therefore, to enhance the efficiency of vaccine production, the E1 genes need to be provided in trans, like growing in HEK293 cells because E1 region is inserted in the genome in this cells line (134). E3 region contains genes involved in suppressing the immune response to enhance adenovirus replication; therefore, removing these genes would improve the vaccine's safety profile and increase packaging capacity for transgene sequences (142) (143). In the ChAdOx1 nCoV-19 vaccine, S protein was the main target to generate a sufficient titer of S antibodies, thereby blocking virus attachment and entry (144).

The specific aims of the project are:

1- Conduct high-throughput quantitative proteomics to analyze the expression of proteins involved in the innate immune response in bat, camel, and human cells to provide potential answers of why SARS-CoV-2 and MERS-CoV are so lethal to humans but not to their natural reservoirs.

2- Validate the interactions of MERS-CoV ORF4A & ORF4B proteins with the selected human cellular partners (and with bat and camel equivalent proteins) based on the proteomics dataset provided by our lab.

3- Elucidating the functional roles of the ORF10 gene in SARS-Co-2 replication using high-throughput quantitative proteomics and reverse genetics approaches.

CHAPTER 2. MATERIALS AND METHODS

2.1 Cells and culture conditions

MRC-5 cells (a genetically normal male human lung fibroblast-like), A549 cells (a human male lung epithelial-like derived from carcinomatous tissue), HEK293 cells (human embryonic kidney epithelial cell line immortalized by human adenovirus E1 region), Huh-7 cells (Human hepatocellular carcinoma cells), Dubca cells (Camelus dromedaries skin fibroblast), PaKiT cells (Black flying fox kidney tissue-derived cell line), BAN cells (Baby Hamster Kidney fibroblasts stably transfected with hACE2 and SARS-CoV2-N), VTN cells (Stable Vero E6 cell line constitutively expressing full-length human TMPRSS2), and A549-ACE2 cells (A549 lung carcinoma cells expressing ACE-2 receptors) were cultured in DMEM (Dulbecco's modified Eagle's medium) supplemented with 10% or 2% fetal bovine serum (FBS), 0.1 mM NEAAs, 2 mM L-glutamine, 100 µg/ml with or without 100 U/ml penicillin and 100 µg/ml streptomycin. Cells were maintained in a humidified incubator at 37 °C with 5% CO_2 and were passaged as follows: the growth medium was removed, and cells were washed with warm Dulbecco's phosphate-buffered saline (PBS) (Lonza). The PBS was removed, and a sufficient amount of 0.05% trypsin/EDTA (Life Technologies) was added to cover the cells monolayer. The cells were then incubated at 37°C with 5% CO_2 until detached from the surface of the cell culture vessel. Then, an appropriate volume of media was added to inactivate the trypsin, and cells were collected by centrifugation at 160 g for 4 min. Finally, the cells pellet was resuspended in the appropriate media volume, and the desired proportion of cell suspension was seeded to a new flask. Where necessary, the cell number was counted using a hemocytometer before passaging a defined number of cells into a new culture vessel.

2.2 Viral growth and assay

2.2.1 Viral infection

Viral infection was kindly performed by Dr. Rachel Milligan in Biosafety Level 3 (BSL-3) lab. Briefly, A549-ACE2 or VTN cells were detached with trypsin-EDTA, counted, and seeded in culture vessels a day before the experiment. The virus inoculum was diluted in the infection medium (Minimum Essential Medium containing 25 mM HEPES, 0.1 mM NEAAs, 2 mM L-glutamine, 100 µg/ml streptomycin 100 U/ml penicillin, and 2% FBS) to the required multiplicity of infection (MOI). On the day of the experiment, the virus inoculum was added for one hour

before it was removed. Infected cells were then incubated with fresh culture media in a humidified incubator for 18 hrs at 37 °C. After that, cells were harvested and prepared for LC-MS/MS analysis at the University of Bristol Proteomics Facility. Viral RNA was extracted from the culture supernatant, and RT-PCR was performed to confirm virus infection.

For growth kinetics experiments, A549-ACE2 or VTN cells were seeded in T-25 culture flasks one day before the experiment. On the day of the experiment, the virus inoculum was added. After one hr, the virus inoculum was removed, and cells were washed once with fresh media (same as infection media) before incubating for 48 hrs. Small aliquots of cell culture supernatant were taken to perform RT-qPCR at different time points. The experiments were performed in triplicates.

2.2 Viral stock production

SARS-CoV-2 ORF10 KO and SARS-CoV-2 W.T viral stocks were kindly produced by Dr. Rachel Milligan in BSL-3. In short, BAN cells were electroporated with the Vitro transcription reaction products (IVT) described below. Electroporated cells were resuspended in 30 ml of MEM 2% FBS media and plated in a T-25 flask. Cells were incubated at 37 °C for 72 hrs or until cytopathic effects (CPEs) were observed. After that, the culture supernatant was transferred into new culture vessels containing VTN cells and incubated for 48 hrs or until the observation of CPEs. Finally, the culture supernatant was collected, centrifuged at 4500 g for 10 min, aliquoted, and stored at –80 °C.

2.3 Virus stock titration

Viral stocks were kindly titred by Dr. Rachel Milligan in BSL-3. In brief, VTN cells were seeded in a 96-wells plate and grown until they reached ~ 90-95% confluent. Ten-fold serial dilutions of viral stocks were prepared in the 2% FBS MEM media. On the day of infection, the growth medium was removed, and the cell monolayer was washed with 2% FBS MEM media before adding the virus diluent. Cells were then incubated in a humidified incubator at 37°C with 5% CO_2 for 24 hrs. After that, the cell culture media was removed, and cells were then fixed with 4% Paraformaldehyde (PFA) in PBS for 60 min before they were washed twice with PBS and permeabilized with 0.1% Triton X-100 PBS for 10 min. Then, cells were washed with PBS and blocked for 30 min using 1% BSA-PBS 0.02% NaN3 blocking solution for 30 min. The blocking solution was then removed, and cells were incubated with SARS-CoV-2 anti N primary antibody diluted in blocking solution at room temperature for 45min. After that, cells were

washed twice with PBS before they were incubated with horseradish peroxidase (HRP) conjugated secondary antibody in a blocking solution. Cells' nucleus stained with DAPI at 1:2000 in 1% BSA-PBS 0.02% NaN3 for 10 min. Finally, cells were washed with PBS 0.02% NaN3 twice before they were imaged on the pico (Molecular Devices). The virus titer was quantified by counting total cells (positive for DAPI) and N-stained cells (positive for N) at each dilution.

2.3 Protein samples preparation

2.3.1 Sample preparation for western blotting analysis

Culture media were removed, and cells were washed with PBS. After that, an appropriate volume of 2X sample buffer (Appendix A) was added to cover the cells monolayer, and cells were collected using a sterile cell scraper. The DNA of cell lysates was shredded by ten passes through a 23-gauge needle before being heated at 95 °C for 5 minutes. Protein samples were stored at – 20 °C until the analysis day.

2.3.2 Sample preparation for LC-MS/MS analysis

Samples were prepared to perform LC-MS/MS analysis as follows: Culture media was removed, and cells were washed twice with PBS. Then, an appropriate volume of RIPA buffer (Appendix A) was added to the cell's monolayer. Cells were then collected using a cell scraper and transferred into a pre-chilled 1.5 ml Eppendorf tube. Protein samples were then stored at – 20 °C until the day of analysis.

2.3.3 Sample preparation for immunoprecipitation (co-IP)

The growth medium was removed, and cells were washed twice with PBS. Then, 3 ml of 0.05% trypsin/EDTA was added to the cells monolayer and incubated at 37°C for a few minutes until the cells detached. 8 ml of growth media were then added to deactivate trypsin/EDTA function, and the cell suspension was centrifuged at 200 x g for 7 minutes at 4 °C. The growth media was discarded, and the cells pellet was washed twice with ice-cooled PBS. After that, the cells pellet was lysed using Immunoprecipitation lysis buffer (Appendix A) for 30 min on ice with pipetting vigorously every 10 min, followed by sonication (4X –

Pulse 5-sec on, 10-sec pause, Amplitude 60%). The protein lysate was then centrifuged at 17,000 x g for 20 minutes at 4 °C, and 50 µl of the resulting supernatant was removed and stored at -20 °C as (an input sample). The rest volume of supernatant was incubated with FLAG-tagged magnetic beads, equilibrated with equilibration buffer (Appendix A) at 4 ˚C with rotation overnight. The beads were separated in a magnetic rack, and the supernatant was collected (unbound sample) and stored at -20 °C. The bead pellet was then washed twice using wash buffer (Appendix A) before resuspending it with 50 µl of 2X sample buffer. The beads were then heated at 95 °C for 3 min before they were separated in a magnetic rack, and the supernatant was collected (pull-down sample) and stored at -20°C until the day of analysis.

2.3.4 Protein quantification (BCA Protein Assay)

The protein concentration was determined using a Pierce™ B.C.A. Protein Assay Kit (Thermo Fisher Scientific), following the manufacturer's instructions. In short, BSA standards of known protein concentration (Diluted in 2X samples buffer in the range 0 - 2000 µg/ml) and samples of unknown protein concentration were prepared in 96 wells plate. The working Reagent A and Reagent B were made up and added to all wells containing BSA standards and protein samples. The BSA standards and protein samples were then transferred into a 37 °C incubator for 30 min. The standard curve was produced using the BSA standards and used to calculate the protein concentration of each sample.

2.3.5 Sodium Dodecyl Sulphate-Polyacrylamide Gel Electrophoresis (SDS-PAGE)

Sodium dodecyl sulfate-polyacrylamide gel electrophoresis (SDS-PAGE) was used throughout the study using a Bio-Rad mini-protein apparatus and power pack (Bio-Rad, CA, USA). 10% SDS resolving gels and 5% SDS stacking gels were prepared as described in (Appendix A). The protein lysates were mixed with an appropriate volume of 4X Laemmli containing 10% β-mercaptoethanol as a reducing agent. Separation of proteins by SDS-PAGE was performed using 1X SDS-PAGE running buffer (Appendix A) at 80-120 V. The PageRuler™ Plus Prestained Protein Ladder (Thermo Fisher Scientific, MA) was used as a protein molecular weight marker.

2.3.6 Western Blotting analysis

During the separation of proteins by SDS-PAGE, the polyvinylidene difluoride (PVDF) membrane was soaked in methanol for 1 min, washed with d H_2O for 2 min, and then soaked in transfer buffer for 5-15 min. After the separation of proteins by SDS-PAGE was completed, the protein samples were transferred into a (PVDF) membrane (GE Healthcare) using Semi-Dry Electrophoretic Transfer Cell (Bio-Rad) for 60 min at 15 V. The PVDF membrane was then blocked for 1 hr at room temperature in blocking solution (appendix A). The PVDF membrane was then washed PBST (appendix A) before it was incubated with the appropriate primary antibodies (Table 1) for 1 hr at room temperature or at 4 °C overnight. Then, the membrane was washed three times with 1 X TPBS for 5 min before it was incubated with the appropriate HRP-conjugated secondary antibody (Table 2) for 1 hour at room temperature. Finally, the PVDF membrane was washed three times for 5 min with 1 X TPBS and covered with LumiGLO® Chemiluminescent Substrate (Kirkegaard & Perry Laboratories, Inc, Maryland, USA) for 1-3 min. Finally, the membrane was drained before it was exposed to X-ray film (Amersham HyperfilmTM ECL, GE Healthcare Life Sciences, Buckinghamshire, UK). The film was developed using a Compact X4 Automatic X-ray Film Processor (Xograph Healthcare, Gloucestershire, UK).

Table 1. Primary antibodies used for Western Blotting analysis in this study

Name	Source	Working dilution	Catalog number	manufacturer
Anti-Phospho-STAT1 (p-STAT1)	Rabbit	1:1000	# 9167S	Cell signalling
Anti-Stat1 Antibody	Rabbit	1:1000	#9172	Cell signalling
β-Tubulin Antibody	Rabbit	1:5000	#2146	Cell signalling
hnRNP C1/C2 Antibody	Mouse	1:500	sc-32308	Santa Cruz
hnRNP A2/B1 Antibody	Mouse	1:500	sc-53531	Santa Cruz
anti-FLAG Antibody	Mouse	1:1000	F3165	Segma-Aldrich
hnRNPAB Antibody	Mouse	1:500	sc-376411	Santa Cruz
NDHII Antibody	Mouse	1:500	sc-137232	Santa Cruz
IFIT1 Antibody	Mouse	1:1000	ab236256	Abcam

Name	Source	Working dilution	Catalog number	manufacturer
NF45 Antibody	Mouse	1:500	sc-365068	Santa Cruz
OAS-2 Antibody	Mouse	1:1000	ab197655	Abcam
MX1 Antibody	Mouse	1:1000	ab207414	Abcam
KPNA4 Antibody	Mouse	1:500	sc-101547	Santa Cruz
SARS-CoV-2 anti-N antibody	Mouse	1:1000	GTX632269	GeneTex

Table 2.Secondary antibodies used for Western Blotting analysis

Name	Source	Working dilution	Catalog number	manufacturer
Mouse IgG HRP-conjugated Antibody	Mouse	1:1000	HAF007	R&D
mouse anti-rabbit IgG-HRP	Rabbit	1:5000	sc-2357	Santa Cruz

2.3.7 Immunofluorescence assay (IFA)

Cells were seeded in 96 wells plate one day before the experiment. On the day of the experiment, the cell culture was removed, and cells were washed with Opti-MEM reduced serum media before they were transfected with an appropriate volume of DNA plasmid using lipofectamine 2000, following the manufacturer's instructions. Transfected cells were then incubated in a humidified incubator at 37°C with 5% CO2 for 18 hr. After that, cells were fixed in 4% PFA-PBS for 5 min before they were washed twice with PBS and permeabilized with 0.1% Triton X-100 PBS for 10 min. After that, cells were washed with PBS and blocked for 30 min using 1% BSA-PBS 0.02% NaN3 blocking solution. The blocking solution was then removed, and cells were incubated with the appropriate primary antibody for 45 min. After that, cells were washed twice with PBS before they were further incubated with horseradish peroxidase (HRP) conjugated secondary antibody in a blocking solution. Cells nucleus stained with DAPI at 1:2000 in 1% BSA-PBS 0.02% NaN3 for 10 min. Finally, cells were washed with PBS 0.02% NaN3 twice and stored at 4 °C until the day of analysis. The cells labeled with immunofluorescence were analyzed using image Xpress Pico (Molecular Devices).

Table 3. Primary and secondary antibodies for IFA used in this study

Name	Source	Working dilution	Catalog number	manufacturer
SARS-CoV-2 (COVID-19) nucleocapsid antibody [6H3] (primary abs)	Mouse	1:1000	GTX632269	GeneTex
anti-FLAG Antibody (primary abs)	Mouse	1:1000	F3165	Segma-Aldrich
Mouse IgG HRP-conjugated Antibody(Secondary abs)	Mouse	1:1000	HAF007	R&D

2.4 RNA methods

2.4.1Total RNA extraction from adherent cells

TRIzol® (Thermo Fisher Scientific) was used to extract total RNA from Infected and mock cells. Briefly, culture media was removed, and 1 ml of TRIzol® was added to cover the cells' monolayer. The cell lysate was then collected and transferred into a 1.5 ml Eppendorf tube and incubated for 5 min at room temperature. 200 µl of chloroform was then added to the cell lysate, mixed, and incubated for 3 min before it was centrifugated for 15 minutes x12,000 g at 4 °C. After that, the resulted aqueous phase was transferred into a new Eppendorf tube and combined with 0.5 ml of isopropanol. The mixture was incubated for 10 minutes at RT before being centrifugated for 10 minutes x12,000 g at 4 °C. The resulting RNA pellet was washed with 1 ml of freshly prepared 75 % ethanol three times. Finally, the RNA pellet was air-dried before resuspending with 100-150 ul of DEPC-treated RNase-free water.

2.4.2 polyadenylated RNA enrichment, library preparation, and RNA Sequencing

mRNA was isolated from total RNA using Dynabeads® mRNA Purification Kit (Thermo Fisher Scientific), following the manufacturer's instructions. Briefly, 45 - 50 micro g of total RNA was adjusted to 100 µL of distilled DEPC-treated water. The RNA sample was heated for 2 min at 65 °C to disrupt secondary structures. Afterward, the sample was resuspended in 100 µl of

equilibrated Dynabeads™ and rotated on a roller or mixer for 5 minutes at room temperature. The beads were washed twice with 200 µL of washing buffer before resuspending with an appropriate volume of elution buffer. The sample was then heated at 70°C for 2 minutes, and eluted mRNA was transferred into a new Eppendorf tube. The quantity and quality of eluted mRNA were assessed using NanoDrop™ 2000/2000c Spectrophotometer (Thermo Fisher Scientific). 300-400 ng of mRNA was carried out for RNA library preparation. The SQK-RNA002 kits and MIN106D R9 version flow cells (Oxford Nanopore Technologies) were used to sequence the RNA library following the manufacturer's protocols. 0.8 to 2.6 million QC-passed reads were typically obtained per flow cell over 48 h. Data analysis was conducted by Prof. David Matthews.

2.4.3 Viral RNA extraction from cell culture supernatant

The culture supernatant of SARS-CoV-2 ORF10 KO transfected or infected cells and SARS-CoV-2 W.T infected cells were collected. 140 µl of the culture supernatant was used to extract viral RNA using Viral RNA Mini Kit (Qiagen, Hilden, Germany), following the manufacturer's instructions. The eluted viral RNA was then stored at -80 °C until the day of analysis.

2.4.4 Reverse transcription (RT) reaction

The cDNA was synthesized from viral RNA using the Invitrogen™ SuperScript™ IV One-Step RT-PCR System, following the manufacturer's procedures. Briefly, 50 ng of viral RNA was mixed with 2.5 µL of forward and reverse primers (final concentration 0.5 µM), 0.5 µL of SuperScript™ IV RT Mix, and 25 µL of 2X Platinum™ SuperFi™ RT-PCR Master. Nuclease-free water was added to the reaction mixture to a final volume of 50 µL. The reaction tubes were placed in a GS1 thermocycler machine (G-Storm, UK) with a heated lid set to 100 °C and incubated as follows:

Table 4. RT-PCR cycling and running parameters

Step	Temp	Time	No. cycle
Reverse transcription	45-60 °C	10 min	1
RT inactivation/initial denaturation	98°C	2 min	
Amplification	98°C	10 S	35-40
	55-72°C	10 S	
	72°C	30 S/kb	
Final extension	72°C	5 min	1

2.4.5 In vitro transcription (*IVT*)

RiboMAX™ Large Scale RNA. Production System-T7 (Promega) was used to perform In vitro transcription of a DNA template, following the manufacturer's instructions. Briefly, 1.5 µg of linearized DNA template was added to a mixture containing 10 µl of T7 Transfer buffer, 3.75 µl of UTP, 3.75 µl of CTP, 3.75 µl of ATP, and 0.75 µl of 100mM GTP. 5 µl of Cap Analog (NewEngland BioLabs) and 0.5 µl (1 unit µg of DNA template) of RNasin® Ribonuclease Inhibitor (Promega) were added to IVT reaction mixture to help in stabilizing the produced RNA and minimizing the risk of RNA degradation. Finally, 5µl of T7 Enzyme Mix was added, and the reaction mix was incubated at 30 ⁰C for 3 hrs. After that, RQ1 RNase-Free DNase was added to the raction mixture and incubated at 37 °C for 15 min to degrade the DNA template. The RNA quality was checked by running 1-2 µl on denaturing agarose gel, and NanoDrop™ 2000/2000c Spectrophotometer was used to determine the quantity.

2.4.6 Denaturing agarose gel electrophoresis

1 g agarose was dissolved in 72 ml nuclease-free water. 10 ml of 3-(N-morpholino) propane sulfonic acid (MOPS) buffer (10x; Thermo-Fisher), 18 ml of 37% formaldehyde (Sigma-Aldrich), and 25 µg ethidium bromide were added to the melted agarose gel to make the denaturing agarose gel. The gel was submerged in 1X MESA (Appendix). one volume of Formaldehyde Load Dye (Thermo-Fisher) was added to RNA samples, incubated at 70°C for 2 min and cooled in ice before loading into denaturing agarose gel.

2.4.7 Quantitative real-time RT-PCR (qRT-PCR)

Quantitative real-time PCR was performed using Langford N6//E/MS2 RT-qPCR, following the manufacturer's instructions. Briefly, 100-fold serial dilutions of MS2 phage, provided by the manufacturer, were prepared in nuclease-free water to generate the standard curves. 5 µl of viral RNA sample or diluted MS2 phage were mixed with 15 µl of the qRT-PCR reaction mixture. The qRT-PCR reaction mixture consists of 6.25 µl of 4X TaqPath 1-Step RT-qPCR Master Mix, 1 µl of Langford N6//E/MS2 25XPPM (containing the forward and reverse primers of the target gene N), 7.75 µl nuclease-free water. Target gene amplification was carried out as follows: initial denaturation for 2 min at 25°C, reverse transcription (RT) for 15 min at 50°C, RT inactivation for 2 min at 95 °C, followed by 40 cycles of denaturation for 10 s at 95 °C and annealing for 30 s at 60 °C. mRNA quantitation was determined by comparing the CT values of the samples with the standards using MxPro software (Agilent Technologies, CA, USA). qRT-PCR reactions were performed in duplicate.

2.5 Universal Type I Interferon treatment

MRC-5, Dubca, and Paki cells were seeded in a six-well plate or T-75 flasks a day before the experiment. On the day of the experiment, growth media were removed, and new fresh media containing an appropriate concentration of Universal type I interferon was added and incubated at 37°C for 4 or 8 hrs. Finally, cells were harvested for LC-MS/MS analysis or treated with TRIzol® to extract cellular RNA and perform nanopore sequencing.

2.6 Poly: IC transfection condition

MRC-5, Dubca, and Paki cells were seeded in a six-well plate or T-75 flasks a day before the experiment. On the day of the experiment, growth media were removed, and cells were washed with PBS and transfected with Poly: IC at a final concentration of 750ng/ml using RNAiMAX (Thermo Fisher Scientific), following the manufacturer's protocol. Transfected cells were incubated at 37°C for 4 or 8 hrs. Finally, cells were harvested for LC-MS/MS analysis or treated with TRIzol® to extract cellular RNA and perform nanopore sequencing.

2.7 DNA plasmid transfection using Polyethyleneimine

A549 cells were seeded in a six-well plate or T-75 flask a day before the experiment. On the day of the experiment, cells were washed with PBS before they were transfected with DNA plasmid using appropriate volumes of DNA and Polyethyleneimine (PEI) reagent. Finally, the cells were incubated at 37°C for 24 hrs before they were harvested for downstream analysis.

2.8 DNA plasmid transfection using Lipofectamine 300 transfection

A549 cells were transfected with DNA plasmids using Lipofectamine 300 transfection (Thermo Fisher Scientific), following the manufacturer's instructions. Briefly, cells were seeded at an appropriate density in a 96-wells plate a day before the experiment. On the day of the experiment, 5 µl of opti-medium was mixed with 100ng of DNA plasmid and 0.2 µl of P3000™ Reagent. In another tube, 5 µl of opt-medium was mixed with 0.2 µl of Lipofectamine™ 3000 Reagent. Afterward, both tubes were combined, and the resulting mixture was incubated at room temperature for 15 minutes to form the DNA-lipid complex. Finally, DNA-lipid complex was diluted in serum and antibiotic-free growth media and added to cells.

2.9 Nucleic acid methods

2.9.1 Bacterial transformation

10 ng of plasmid DNA was transformed into One Shot™ TOP10 Chemically Competent E. coli (Thermo Fisher Scientific), following the manufacturer's instructions. In short, 10 ng of plasmid DNA was added to 50 µL of DH5α Competent Cells. Bacterial cells were heat-shocked at 42 °C for 20 seconds before incubating in ice for 3 min. 1 ml of warmed LB broth was then added to the cells, followed by incubation at 37 °C for 1 h with shaking at 225 rpm. Cells were then plated on an agar plate containing ampicillin or kanamycin and incubated at 37 °C overnight. Afterward, a single colony was selected and grew in 50ml of LB containing ampicillin or kanamycin with a final concentration between 50-100 µg/mL overnight. Then, plasmid DNA was isolated from bacterial cultures using QIAGEN® Plasmid Plus Midi Kit, following the manufacturer's instructions. Plasmid DNA was screened and confirmed using appropriate restriction enzymes.

2.9.2 Restriction endonuclease reactions

One μg of plasmid DNA was digested with 5 U of appropriate restriction enzymes (NEB) for 1 hr at 37 °C in the buffer supplied by the manufacturer. To linearize the BAC DNA, 15 μg of DNA was digested with 75 U of appropriate restriction enzyme for 3 hr at 37 °C in the buffer supplied by the manufacturer.

Table 5. Restriction enzymes were used in this study

Restriction Enzymes used in this study	
Restriction endonuclease	**Source**
AVRII	New England Biolabs
PacI	New England Biolabs
XhoI	New England Biolabs
BamHI	New England Biolabs
StuI	New England Biolabs
AscI	New England Biolabs

2.9.3 PCR amplification

The PCR reactions were performed using Invitrogen™ Platinum™ SuperFi™ II DNA Polymerase, following the manufacturer's protocols. Briefly, the cDNA template or plasmid DNA was diluted to a final concentration of 5 ng/μl or one ng/μl, respectively. PCR reaction mixtures containing 10 μL of 5X SuperFi™ II Buffer, forward and reverse primers (final concentration 0.5 μM), 1 μL of 10 mM dNTPs, and 1 μL of Platinum™ SuperFi™ II DNA Polymerase were prepared and added to 5 ng of cDNA template or 1 ng to plasmid DNA. Nuclease-free water was added to the reaction mixture to a final volume of 50 μL. The reaction tubes were placed in a GS1 thermocycler machine (G-Storm, UK) with a heated lid set to 100 °C and incubated as follows:

Table 6.Conventional PCR cycling and running parameters:

Step	Temp	Time	No. cycle
Initial denaturation	98°C	30 sec	1
Denaturation	98°C	5-10 sec	
Annealing	60°C	10 sec	25-35
Extension	72°C	15-30 sec per 1 kb	
Final extension	72°C	5 min	1
	4°C	Hold	-

The final cDNA products were stored at -20 °C for further analysis.

Table 7. PCR primers list used in this study

Primers used in this study	
Primer Name	**Sequence (5′→3´)**
AVRIIFW	AAACCTAGG AACTGGGCCAGAAGCTGGAC-
ORF10FW	CACACAAGGCAGTAAGGCTATATAAACGTTTTCGCTTTTCCGTTTACGATAT ATAGTCTACTCTTGTGCA GATAGAATTCTCGTAAC
ORF10Rev	GTTACGAGAATTCTATCTGCACAAGAGTAGACTATATATCGTAAACGGA AAAGCGAAAACGTTTATATAGCCTTACTGCCTTGTGTG
PacI Rev	AAATTAATTAACTGCGGCGAGGGGCGCGCC
F1newF	CGCTAGGGATAACAGGGTAATATAGAAC
F1newR	TTACTTCTGTACCGAGTTCAACTG
F2newF	GATGAAAGGATTGATAAAGTACTTAATG
F2newR	ACTAGCACAAGTAAATGTACCATGC
F3newF	ACCTTTTGTTATGATGTCAGCACC
F3newR	GGAACACAAGTGTAACTTTAATTAAC
F4newF	CACTTAAGGGTGGTAAAATTGTTAATAATTG
F4newR	AGATTATAAGAGCCCACATGGAAATGG
F5newF	ACACTCGTTTATAAAGTTTATTATGGTAATG
F5newR	CATCCAAACAGTTAACACAATTTGGGTGG
F6newF	AAACTCTTTGACCGTTATTTTAAATATTGGG
F6newR	ATCTATAGGCAAATATTTTAATGCCTTCTC
F7newF	GTATACAGCTTGCTCTCATGCCGC
F7newR	GGACCTACAGATGGTTGTAAACCTTTAAC
F8newF	TTAGAAATGCCCGTAATGGTGTTC
F8newR	TCTCTCAAAAGGTTTGAGATTAGACTTC

F9newF	TAAGGTTGGTGGTAATTATAATTACCTG
F9newR	AAAATAGTTGGCATCATAAAGTAATGGG
F10newF	AATAATGAGGCTTTGGCTTTGCTGG
F10newR	TTGGTGTATTCAAGGCTCCCTCAG
F11newF	GGACTTCCCTATGGTGCTAACAAAG
F11newR	GATTCGCTACCTTAGGACCGTTATAG
OL1-F	CGGTGCGTCCCTGTTTGCATTATGAATTAG
OL1-R	AGCCACACAGATTTTAAAGTTCGTTTAGAG
OL2-F	CCAGTTTGTATTAACGGGCTTATGTTGCTCG
OL2-R	CTCATCAAATAAGTAGTATGTAGCCATACTCC
OL3-F	AGGTGATGTTAGAGAAACAATGAGTTACTTG
OL3-R	TGTAACTGTTTTCTTTGTAGAAAACATCCG
OL4-F	GACACCCCGTGACCTTGGTGCTTGTATTGAC
OL4-R	GACTGCAGCAATCAATGGGCAAGCTTTGTC
OL5-F	CCTTTTGCTATGGGTATTATTGCTATGTCTGC
OL5-R	CTGTGTAGAAACTAAGTAATCATAAACACC
OL6-F	GATGATGATTATTTCAATAAAAAGGACTGG
OL6-R	GTAATAGATTACCAGAAGCAGCGTGCATAGC
OL7-F	AGAGTACACCTTTGAAAAAGGTGACTATGG
OL7-R	CAAAGCACTCACAGTGTCAACAATTTCAGC
OL8-F	AACCTCTGGAACACTTTTACAAGACTTCAG
OL8-R	GTTATGAAATAGTTTTTAACTGTACTGTCC
OL9-F	AGGTGATGAAGTCAGACAAATCGCTCCAGG
OL9-R	GTAACCAACACCATTAGTGGGTTGGAAACC
OL10-F	TAGTTGTCTCAAGGGCTGTTGTTCTTGTGG
OL10-R	TATTAACTATTAACGTACCTGTCTCTTCCG
OL11-F	CTTTGCTGCTGCTTGACAGATTGAACCAGC
OL11-R	CACTTGCCGATCTATGCGGTGTGAAATACC

2.9.4 PCR product purification

GeneJET PCR Purification Kit (Thermo Scientific™) was used following the manufacturer's protocol to purify PCR products.

2.9.5 Agarose gel electrophoresis

The agarose gel was prepared by dissolving (0.8-1) g of agarose (Bioline, UK) in 100 ml of
1X TBE buffer containing 0.5 µg/ml ethidium bromide. The gel was then poured and set in a
tray. DNA samples were prepared by mixing 5 µL of DNA with 1 µL of 6 X DNA loading
buffer (appendix) and resolved by electrophoresis. a GeneRuler 1kb Plus DNA Ladder (Life
45 Technologies, CA, USA) was included on each gel to estimate the size of DNA. The
purity and quantity of DNA samples were determined by NanoDrop™ 2000/2000c
Spectrophotometer (Thermo Fisher Scientific, MA, USA).

2.9.6 Sanger sequencing

Plasmid DNA and RT-PCR products were sequenced by Eurofins Genomics (Germany).
DNA samples were prepared at a concentration of 2 ng/ µl. Primers were prepared at a
concentration of 2 pmol/µl. LaserGene software package version 2.9 (DNASTAR, Madison,
U.S.A.) was used to analyze the resulting sequences.

2.9.7 DNA Phenol/chloroform extraction and ethanol precipitation

BAC linearized DNA sample combined with an equal volume of phenol: chloroform. The
sample was mixed gently for 1 min before it was centrifuged at 13,000 g for 5 min. The
aqueous phase containing DNA was transferred into a new Eppendorf tube. 0.1 volume of 3
M NaOAc (pH 5.2) and 2.5 volumes of cold 100% ethanol were added to the aqueous phase
containing DNA, and the sample was gently mixed and incubated at -20°C for 30-60 min.
After that, the sample was centrifugated at 13,000 g for 20 min at 4 °. The DNA pellet was
washed with cold 70% ethanol before being centrifugated again at 13,000 g for 20 min at 4
°C. The DNA pellet was then air-dried and resuspended in ultra-pure sterile nuclease-free
water. DNA was aliquoted and stored at -20 °C. The purity and quantity of DNA samples
were determined by NanoDrop™ 2000/2000c Spectrophotometer (Thermo Fisher Scientific,
MA, USA).

2.10 Construction of virus mutants

2.10.1 Yeast Assembly

cDNA fragments were amplified from Plasmids DNA using Platinum™ SuperFi II PCR Master Mix (Invitrogen). The assembly of cDNA fragments was performed using the GeneArt™ High-Order Genetic Assembly System (Invitrogen). In brief, 100 ng of the GeneArt™ pYES1L Vector combined with 200 ng of cDNA fragments prepared by PCR synthesis to make a pYES1L Vector / cDNA fragments mixture. Saccharomyces cerevisiae strain (MaV203 cells) were transformed with pYES1L Vector/cDNA mixture, following the manufacturer's instructions. MaV203 cells pellet was resuspended in sterile saline and streaked on tryptophan-free yeast agar plates. Plates were incubated at 30ºC for 2-3 days.

2.10.2 Yeast colonies screening

Multiple yeast colonies were selected, re-spread on a grid plate, and incubated overnight at 30 ºC. After that, each yeast colony was collected using a sterile loop, resuspended in 100uL of 5% w/v Chelex-100, and mixed with the half volume of acid-washed glass beads. The samples were then vortexed at room temperature for 4 min at the highest speed. The cell lysates were heated for 2 min at 99 ºC before they were centrifugated for 2 min at 14,800 rpm. 1 uL from the supernatant of each cell lysates was used for initial screening using standard PCR to amplify the recombinant junction between cDNA fragment and vector pYES1L. Positive clones were then further screened for the rest of the fragments' recombinant junctions using multiplex PCR in 2 sets. Set A screens for the recombinant junctions between fragments 1, 2, 3, 4, 5, and 9 using OL-1, OL-2, OL-3, OL-4, OL-5, and OL-9 forward and reverse primers. Set B screens for the recombinant junctions between fragments 6, 7, 8, 10 +11 using OL-6, OL-7, OL-8, OL-10, and OL-11 forward and reverse primers.

Table 8. List of plasmids used in this study

Plasmid	Selection marker	Source
ORF4A pcDNA™3.3-TOPO plasmid	Ampicillin	Invitrogen by ThermoFisher Scientific
ORF4B pcDNA™3.3-TOPO plasmid	Ampicillin	Invitrogen by ThermoFisher Scientific
ORF10 pcDNA™3.3-TOPO plasmid	Ampicillin	Invitrogen by ThermoFisher Scientific
GFP pcDNA™3.3-TOPO plasmid	Kanamycin	Invitrogen by ThermoFisher Scientific
Fragment 1 pJet1.2 plasmid	Ampicillin	Invitrogen by ThermoFisher Scientific
Fragment 2 pJet1.2 plasmid	Ampicillin	Invitrogen by ThermoFisher Scientific
Fragment 3 pJet1.2 plasmid	Ampicillin	Invitrogen by ThermoFisher Scientific
Fragment 4 pJet1.2 plasmid	Ampicillin	Invitrogen by ThermoFisher Scientific
Fragment 5 pJet1.2 plasmid	Ampicillin	Invitrogen by ThermoFisher Scientific
Fragment 6 pJet1.2 plasmid	Ampicillin	Invitrogen by ThermoFisher Scientific
Fragment 7 pJet1.2 plasmid	Ampicillin	Invitrogen by ThermoFisher Scientific
Fragment 8 pJet1.2 plasmid	Ampicillin	Invitrogen by ThermoFisher Scientific
Fragment 9 pJet1.2 plasmid	Ampicillin	Invitrogen by ThermoFisher Scientific
Fragment 10+11 in pJet1.2 plasmid	Ampicillin	Invitrogen by ThermoFisher Scientific
mNeongreen pJet1.2 plasmid	Ampicillin	Invitrogen by ThermoFisher Scientific
mScarlet pJet1.2 plasmid	Ampicillin	Invitrogen by ThermoFisher Scientific
Fragment 10 +11 ORF10 KO pJet1.2 plasmid.	Ampicillin	Invitrogen by ThermoFisher Scientific
Fragment 10 +11 mNeonGreen pJet1.2 plasmid	Ampicillin	Invitrogen by ThermoFisher Scientific
Fragment 10 +11 ΔORF10mScarlet pJet1.2 plasmid	Ampicillin	Invitrogen by ThermoFisher Scientific

2.10.3 Transferred the assembled structure from yeast to *E. coli*

1-2 uL from yeast-prepared lysate was transformed into One Shot™ TOP10 Electrocomp™ E.coli (Invitrogen, ThermoFisher) in a chilled 0.2cm cuvette, following the manufacturer's protocol. The E. coli Pulser™ Transformation Apparatus (BioRad) was used to electroporate E. coli under the condition of 2.5kV; 200Ω and 25μFd. 0.5 ml of SOC Medium (Invitrogen, ThermoFisher) was immediately added to electroporated cells, and the cell suspension was incubated at 37 ⁰C for 60 min with shaking at 225 rpm. Finally, different volumes of transformed bacteria were plated on LB-Spectinomycin (100μg/ml) plate overnight.

2.10.4 Amplification and isolation of BAC/YAC construct

NucleoBond® Xtra BAC (Macherey-Nagel) was used for DNA purification following the manufacturer's instructions. Briefly, a single colony was picked and resuspended in 250 ml of LB-media containing 50µg/ml Spectinomycin and incubated overnight at 37 ⁰C with shaking at 220 rpm. Cells were harvested by centrifugation at 4500 x g for 30 min at 4 ⁰C. Cells pellets were then resuspended vigorously using the provided resuspension buffer (RES-BAC) before adding a lysis buffer followed by a neutralization buffer. The cell suspension was then loaded into the equilibrated filter column to elute DNA using a heated elution buffer provided by the manufacturer. 0.4 volume of isopropanol was added to participate DNA, DNA / isopropanol mixture was incubated for 2 min and centrifugated at 30,000g for 30 min at 4 ⁰C. After that, the DNA pellet was washed with 70% ethanol and centrifugated at 30,000g for 15 mins. The purified DNA pellet was dissolved in sterile water on a platform shaker overnight at 4 ⁰C. DNA quantity and purity were determined by NanoDrop™ 2000/2000c Spectrophotometer (Thermo Fisher Scientific, MA, USA).

2.10.5 BAC DNA digest and linearization

The isolated BAC DNA was validated using EcoRI and StuI restriction enzymes (NewEngland BioLabs). After confirming the DNA construct, 15 µg of the DNA was incubated with the Asc1 (NewEngland BioLabs) restriction enzyme in CutSmart buffer for 2hrs at 37⁰C to linearize the DNA template. The linearized DNA was then extracted using the conventional Phenol-Chloroform extraction protocol described before and stored at -20 ⁰C until the day of In Vitro transcription.

2.11 Recover mutant viruses

BAN cells were transfected with *IVT* products using the Neon® Transfection System (Invitrogen, ThermoFisher), following the workflow described for adhering cell lines. Briefly, ~85-90% of confluent cells were trypsinized, counted, and resuspended at 1x106 cells/100µL in DPBS without Mg2+ and Ca2+. 110µl of cells suspension was then mixed with different volumes (5 µl or 10µl) of *IVT* products and electroporated using the Neon® Transfection system. Electroporated cells were immediately resuspended in 6ml of 2% FBS antibiotic-free medium and incubated at 37 ⁰C for 48-72 hrs or until the appearance of CPEs. Afterward, cell culture supernatant was transferred to VTN (VeroE6 TMPRSS2) cells to propagate the mutant

virus. Viral RNA was extracted from the culture supernatant to confirm virus infection using RT-PCR.

2.12 Quantitative mass spectrometry analysis

2.12.1 TMT labeling and high pH reversed-phase chromatography

The protein concentration in (co-IP) samples and cell lysates were determined by the BCA assay. 50 μg of protein were prepared and sent to the University of Bristol Proteomics Facility to conduct LC-MS/MS analysis.

2.12.2 TMT labeling and high pH reversed-phase chromatography

Co-Immunoprecipitation (co-IP) samples were reduced by adding 5 μl of 200 mM Tris (2-Carboxyethyl) phosphine Hydrochloride (TCEP) and incubated for 1 hr at 55 °C. Samples were then alkylated by adding 5 μl of 375mM iodoacetamide and incubated for 30 min at room temperature. The samples were digested with 2.5μg trypsin overnight at 37 ⁰C. The resulting peptides were then labeled with TMT ten-plex reagents according to the manufacturer's protocol (Thermo Fisher Scientific, Loughborough, LE11 5RG, UK). Labeled samples were then pooled and desalted using a SepPak cartridge according to the manufacturer's instructions. The eluate from the SepPak cartridge was evaporated to dryness and resuspended in buffer A (20 mM ammonium hydroxide, pH 10), then fractioned by high pH reversed-phase chromatography using an Ultimate 3000 liquid chromatography system (Thermo Scientific). In short, The sample was loaded onto an XBridge BEH C18 Column (130Å, 3.5 μm, 2.1 mm x 150 mm, Waters) in buffer A and ran in a gradient of buffer B (20 mM Ammonium Hydroxide in acetonitrile, (pH 10) from 0-95% over 1 hr. The resulting fractions were evaporated to dryness and resuspended in 1% formic acid before analysis by nano-LC MSMS using an Orbitrap Fusion Lumos mass spectrometer.

2.12.3 Nano-LC Mass Spectrometry

High pH RP fractions were further fractionated using an Ultimate 3000 nano-LC system in line with an Orbitrap Fusion Lumos mass spectrometer. Briefly, peptides in 1% formic acid were injected onto an Acclaim PepMap C18 nano-trap column (Thermo Scientific). After washing with 0.5% acetonitrile, and 0.1% formic acid, peptides were resolved on a 250 mm × 75 μm

Acclaim PepMap C18 RP analytical column (Thermo Scientific) over a 150 min organic gradient, using seven gradient segments (1-6% solvent B over 1min, 6-15% B over 58min, 15-32%B over 58min, 32-40%B over 5min, 40-90%B over 1 min, held at 90%B for 6 min and then reduced to 1%B over 1 min) with a flow rate of 300 nl/min. Solvent A was 0.1% formic acid, and Solvent B was aqueous 80% acetonitrile in 0.1% formic acid. Peptides were ionized by nano-electrospray ionization at 2.0 kV and a temperature of 300°C.

All acquired spectra from the Orbitrap MS controlled by Xcalibur 4 software (Thermo Scientific) were operated in data-dependent acquisition mode using a Synchronous Precursor Selection (SPS)-MS3 workflow. FTMS1 spectra were collected at a resolution of 120,000 with automatic gain control (AGC) target of 200,000 and a max injection time of 50 ms. Precursors were filtered with an intensity threshold of 5,000 according to charge state (to include charge states 2-7) and with monoisotopic peak determination set to Peptide. Previously interrogated precursors were excluded using a dynamic window (60s +/-10ppm). The MS2 precursors were isolated with a quadrupole isolation window of 0.7 m/z. Then the ITMS2 spectra were collected with an AGC target of 10,000 max injection time of 70 ms and CID collision energy of 35%.

The Orbitrap was used for FTMS3 analysis at 50,000 resolution, with an AGC target of 50,000 and a maximum injection time of 105 ms. To achieve maximum TMT reporter ion yield, precursors were fragmented by high-energy collision dissociation (HCD) at a normalized collision energy of 60%. In the FTMS3 scan, Synchronous Precursor Selection (SPS) was able to include up to five MS2 fragment ions.

2.12.4 Data analysis

The raw data files were processed and quantified using Proteome Discoverer software v2.1 (Thermo Scientific) and searched against Uniprot/SwissProt human database and FASTA files containing the SARS-CoV-2 ORF10 (GenBank Protein Identification: QQD86937.1) and SARS-CoV-2 (GenBank accession number: NC_045512). Peptide precursor mass tolerance was set at 10ppm, and MS/MS tolerance was set at 0.6Da. Search criteria included oxidation of methionine (+15.995Da), acetylation of the protein N-terminus (+42.011Da), and Methionine loss plus acetylation of the protein N-terminus (-89.03Da) as variable modifications and carbamidomethylation of cysteine (+57.021Da) and the addition of the TMT mass tag (+229.163Da) to peptide N-termini and lysine as fixed modifications. Full tryptic digestion was used throughout searches, and a maximum of two missed cleavages were permitted. All data were filtered to meet a false discovery rate (FDR) of 5% with the reverse database search option enabled. The main search was conducted by Dr.Kate Heesom, and the ThermoFischer .msf file and excel spreadsheet were produced for further analysis. The above

proteomics analysis and the protocols are provided as a service from the faculty proteomics facility.

2.12.5 Data analysis

The statistical computing and graphics program R was used by Dr. Philip A Lewis to perform bioinformatics and statistical analysis. The ratios were log2 transformed and normalized by subtraction of the median ratio in each comparison from the other ratios. An unpaired two-sample student t-test with the permutation-based FDR 0.05 was performed to determine the statistical significance of the conditions of interest. An online version of the Search Tool for the Retrieval of Interacting Genes/Proteins (STRING) (von Mering et al., 2003) was used to annotate the Pakit cells database, while Dubca cells data was annotated manually using Uniport Database. Proteins that increased or decreased in amount (≥ 1 fold, ≥ 1.5 fold, and ≥ 1.7 fold) in the condition under investigation compared to the control condition were analyzed using a search tool for the retrieval of interacting genes (STRING) to identify groups of functional enriched proteins corresponding to specific gene ontology terms and identify protein networks and processes over-presented in SARS-CoV-2 and SARS-CoV-2 ORF10 KO infected cells or ORF10 transfected cells. Functional Enrichment analysis program (FunRich) version 3.1.3 (Pathan et al., 2015) was used to compare data sets, identify overlapping proteins, and produce Venn diagrams.

CHAPTER 3. High-throughput proteomics analysis of host innate immune response in bat, camel, and human cells

3.1 Introduction

Several zoonotic viral outbreaks have emerged during the last three decades, including Ebola, Marburg, Zika, Henda, SARS-CoV, MERS-CoV, and the ongoing SARS-CoV-2 pandemic. All those zoonotic outbreaks are the result of the transmission of viruses from their primary or intermediate animal hosts to humans (144).

Bats are the primary animal host of MERS-CoV and SARS-CoV-2, and camels serve as an intermediate host for MERS-CoV and are responsible for the spillover infections (145). It is suggested that bats and camels are better than humans at generating appropriate immune responses against MERS-CoV and SARS-CoV-2, thereby minimizing the damage resulting from viral replication (167).

Host innate immune system act as the first line of defense against invading pathogens (168). It can detect the conserved pathogen-associated molecular patterns (PAMPs) of invading pathogens using host pattern recognition receptors (PRRs) and initiates diverse cellular signaling pathways to elicit an effective anti-viral immune response (168).

Toll-like receptors (TLRs), RIG-I (retinoic acid-inducible gene I), and melanoma differentiation-associated protein 5 (MDA5) function as pattern recognition receptors (PRRs) that can detect the presence of invading viruses (169). PRRs have been shown to activate the IFN production upon detecting viral double-strand RNA (dsRNA) (168,169).

Once it binds viral dsRNA, TLR3 initiates the IFN signaling pathway to induce a wide array of interferon-stimulated genes (ISGs) that inhibit viral replication. Briefly, when TLR3 is activated, it signals through TRIF (TIR-domain-containing adapter-inducing interferon-β) to activate the transcription factor nuclear factor kappa-light-chain-enhancer of activated B cells (NF-κB) and interferon regulator factors 3 and 7 (IRF3 and IRF7) (171). The activation of the transcription factor NF-κB is achieved via the recruitment of TNF receptor-associated factors 6 (TRAF6), which eventually lead to the release of NF-κB by degrading its inhibitor molecule (IκB). The released NF-κB then translocates into the nucleus to induce pro-inflammatory cytokines and chemokines, such as IL-6, IL-8, tumor necrosis factor α (TNF-α), C–C motif chemokine ligand 2 (CCL2), and C–X–C motif chemokine 10 (CXCL10). These cytokines and chemokines have essential roles in regulating the expression of several genes involved in immune cells' recruitment (170, 171,172) (174).

The activation of IRF3 and IRF7 is mediated by TRAF3 (TNF Receptor Associated Factor 3), which ultimately activates inducible IκB kinase ε (IKKε) and NF-κB activator binding kinase 1 (TBK1) to phosphorylate IRF3 and IRF7. Once IRF3 and IRF7 get phosphorylated, they translocate into the nucleus to initiate IFN production (170,172).

MDA5 and RIG-I are cytoplasmic receptors that can detect long and short viral dsRNA, respectively, and activate the same signaling pathway of TLR3. Once MDA5 or RIG-I bind viral dsRNA, their caspase activation and recruitment domains (CARD) become exposed and bind to the adaptor protein mitochondrial antiviral signaling (MAVS) to trigger a similar signaling pathway of TLR3 (175). MAVS interacts with TRAF2/6 and TRAF2/3 leading to phosphorylation and activation of NF-κB and (IRF3&IRF7). Once IRF3 and IRF7 get phosphorylated, they translocate to the nucleus and initiate the production of IFNα/β and IFNλ (Figure 8).
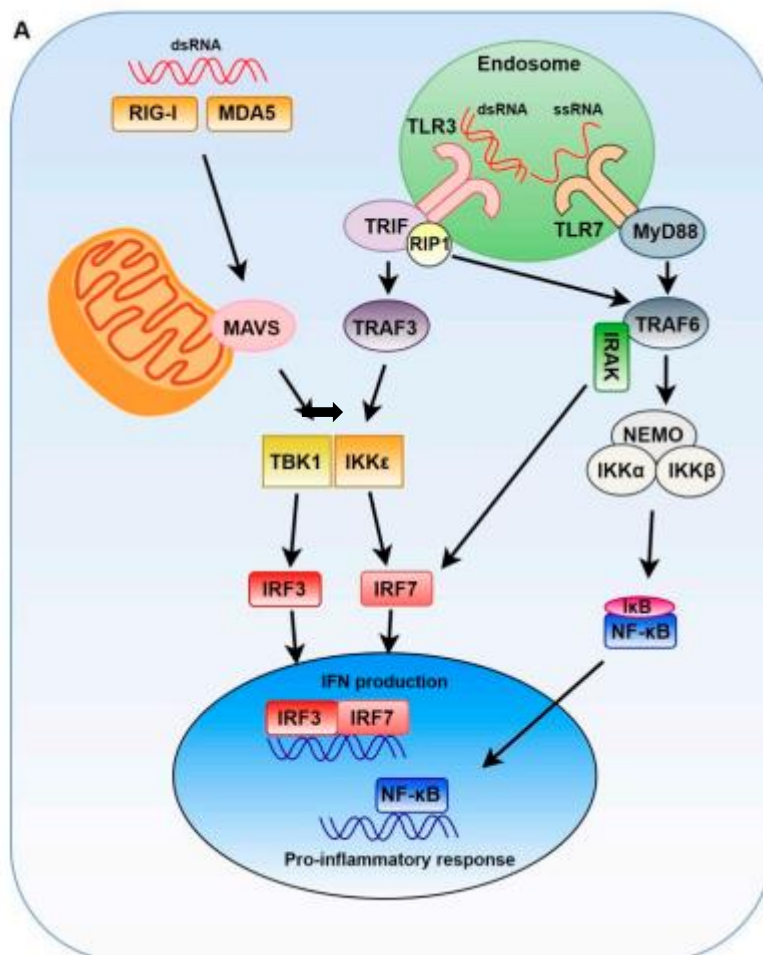
Figure 9. Host innate immune response to virus infection. Once TLRs, MDA5, or RIG-I (PRRs) detect viral dsRNA, they trigger signaling cascades that eventually lead to activation of NF-κB, IRF3, and IRF7 to induce the production of IFNs and pro-inflammatory cytokines. The figure adapted from " Viral Innate Immune Evasion and the Pathogenesis of Emerging RNA Virus Infections ", Nelemans, T, Viruses, 2019 (150).

When IFNα/β molecules get expressed, they bind to their heterodimeric receptors, which are made up of the IFNAR1 and IFNAR2 subunits. IFNλ binds to its heterodimeric receptors, consisting of IFNLR1 and IL-10 receptor β (174). Binding IFNs to their receptors phosphorylates Janus kinase 1 (JAK1) and tyrosine kinase 2 (TYK2), which initiates heterodimerization and phosphorylation of STAT1 and STAT2 and mediates the formation of canonical (ISGF3 complex) that made up of phospho-Stat 1, phospho-Stat 2 and IRF9. Once ISGF3 is formed, it translocates to the nucleus to activate a wide range of interferon-stimulated genes (ISGs) needed for the induction of the antiviral state (Figure 9) (174,175).
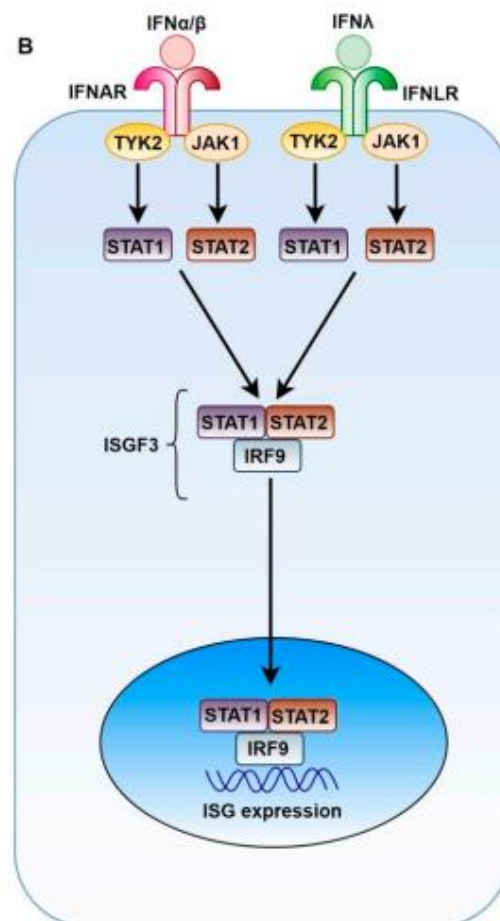
Figure 10. Interferon (IFN) signaling pathway. IFNα/β binds to IFNAR1 and IFNAR2 receptors, while IFNλ binds to IFNLR1 and IL10RB. Once bound to their receptors, IFNα/β and IFNλ initiate two types of signaling pathways that eventually converge, resulting in ISGs expression. The figure adapted from " Viral Innate Immune Evasion and the Pathogenesis of Emerging RNA Virus Infections ", Nelemans, T, Viruses, 2019 (150).

It is believed that viruses evade the host's innate immune response by modulating the cellular environment to replicate optimally. This modulation causes alterations in the host cell's proteome, which could be one of the main determinants of disease severity. In contrast to humans, the animal reservoirs of MERS-CoV & SARS-CoV-2 can carry the viruses without becoming severely ill. One possibility could be the difference in proteome changes between human and animal cells in the early stages of the innate response to viral infection (176) (167).

TMT-MS/MS is a powerful tool to identify and quantify proteins in a cellular sample, allowing comparative analysis of the proteome's changes between different cell populations.

In this chapter, a comparative quantitative proteomic analysis was conducted on proteins contained in total cell lysates from Universal IFN or Poly: IC treated cells compared to mock-treated cells. IFNs are a group of indispensable cytokines for inducing an appropriate immune response to viral infections. They bind to their cell surface receptors to initiate signaling pathways that eventually activate the transcription of many ISGs to inhibit virus replication (Figure 10) (177).

Polyinosinic: polycytidylic acid [Poly(I: C)] is a synthetic dsRNA analog that has been shown to have a similar innate immune stimulatory effect to viral dsRNA (178). Poly(I:C) is recognized by the host cell's PRRs to initiate the IFN signaling pathway (Figure 10) (179).

By comparing the proteome of IFN or Poly: IC treated cells with mock-treated cells, it is possible to identify the difference in modulated host proteins in humans and (SARS-CoV-2 & MERS-CoV) animal hosts in response to external signals, like interferon, and in detecting an internal pathogen. Three replicates of MRC-5, Dubca, and PaKiT cells were grown in a T-25 flask and were either treated with IFN or transfected with Poly: IC for 4 hrs before being harvested and used to prepare total cell lysate. The induction of innate immune response was confirmed by western blotting before sending the samples to the proteomics core facility at the University of Bristol.
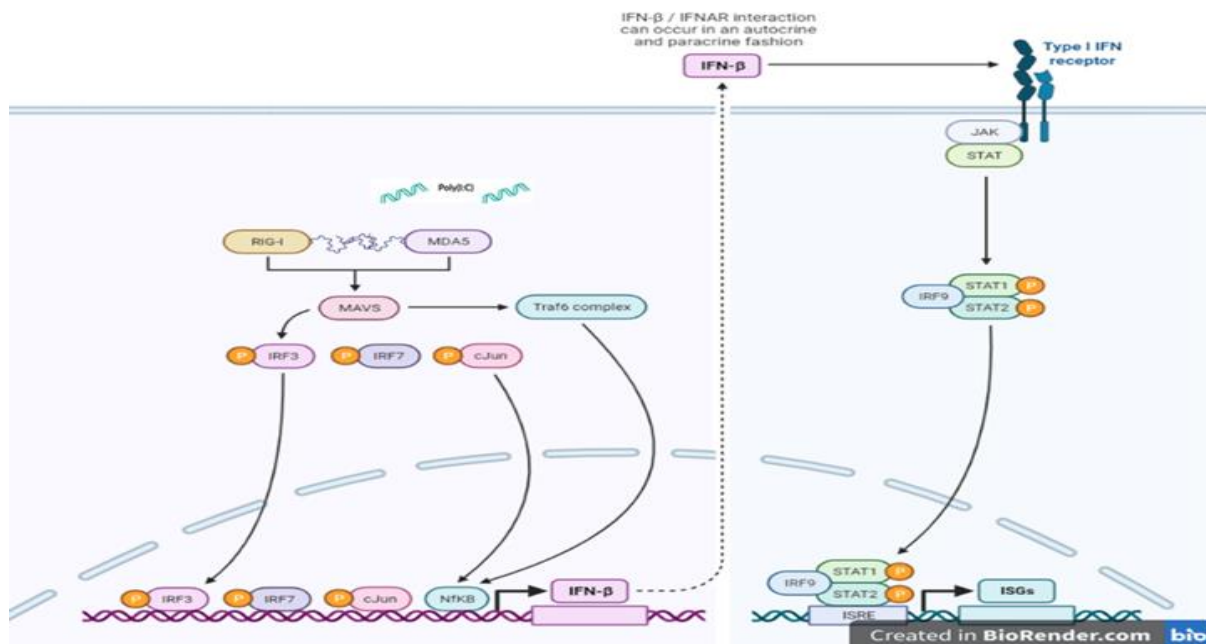
Figure 11. Stimulating the innate immune response of human, bat, and camel cell lines using Poly: IC or universal type I interferon. Cells were transfected with poly: IC to activate cytoplasmic dsRNA sensors downstream signaling pathways, or treated with universal type I interferon to stimulate the interferon JAK-STAT signaling pathway.

3.2 Results

3.2.1 Stimulating the innate immune response of MRC-5, PaKiT, and Dubca cells using universal type I IFN and Poly: IC treatments

Dubca (camel), MRC-5 (human), and PaKiT (bat) cells were treated with IFN or Poly: IC to stimulate the interferon JAK/STAT signaling pathway before analyzing the innate immune response by Western blot analysis (Figure 11, Figure12).
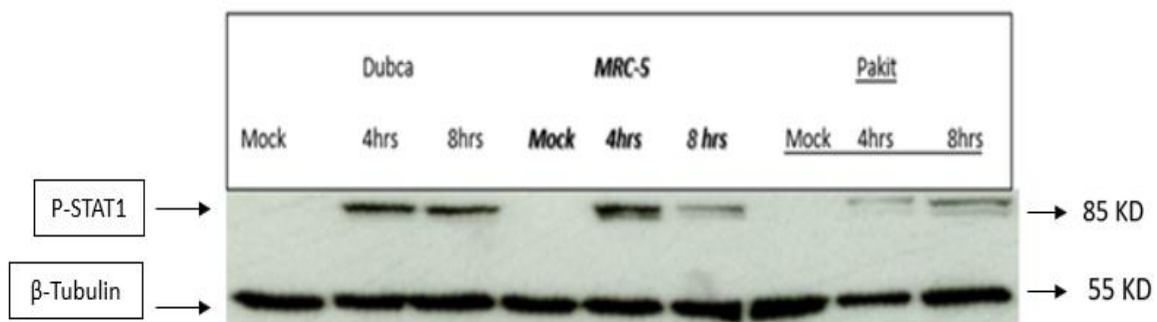
Figure 12. Innate immune response induction via JAK/STAT signaling pathway. Dubca, MRC-5, and PaKiT cells were treated with IFN (1000 IU/mL) for 4 hrs or 8hrs. The induction of innate immune response was confirmed by western blotting analysis using anti phospho-STAT1 antibody. The molecular weight of P-STAT1 protein is 85 KDa.
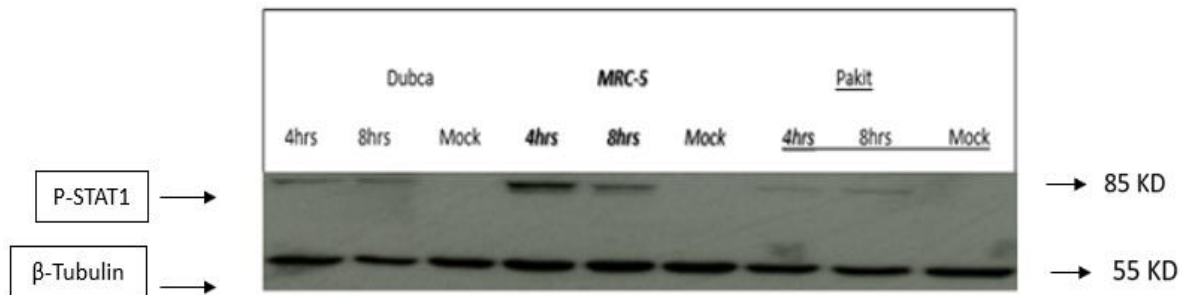
Figure 13. Stimulation of the innate immune response via cytoplasmic dsRNA sensors. Dubca, MRC-5, and PaKiT cells were transfected with 750ng/ml of Poly: IC (a synthetic analog of double-stranded RNA that stimulates the innate immune response signaling pathway via different cytoplasmic dsRNA sensors) for 4hrs or 8 hrs. The induction of innate immune response was confirmed by western blotting analysis using anti phospho- STAT1 antibody. The molecular weight of P-STAT1 protein is 85 KDa.

3.2.2 Examining the expression levels of STAT 1 in MRC-5, Pakit and Dubca cells following the IFN or Poly: IC treatment

MRC-5, Dubca, and PaKit cells were treated with IFN or Poly: IC to stimulate the interferon JAK/STAT signaling pathway. The amount of STAT 1 protein in IFN or Poly: IC treated cells and mock cells were examined by western blot analysis. The analysis showed similar expression levels of STAT1 protein in the Poly: IC treatment condition and mock in the three cell lines (Figure 13). These results are consistent with our phosphoproteomic and proteomic dataset, which reveals a predominance of STAT1 phosphorylation in Poly: IC treatment condition compared to mock, with a similar appendance of STAT1 protein in all cell lines.

Furthermore, the western blot analysis showed similar expression levels of STAT 1 protein in the IFN treatment condition and mock in MRC-5 and Dubca cells (Figure 13). These results are also consistent with our phosphoproteomic and proteomic dataset, which reveals a predominance of STAT1 phosphorylation in IFN treatment conditions in MRC-5 and Dubca cells compared to their mocks, with similar appendance of STAT1 protein.

On the other hand, although the proteomic dataset of PaKit cells showed similar levels of STAT1 expression in mock and IFN-treated cells, the western blot analysis showed STAT 1 protein expression is slightly higher in PaKit IFN-treated cells compared to the mock (Figure 13).
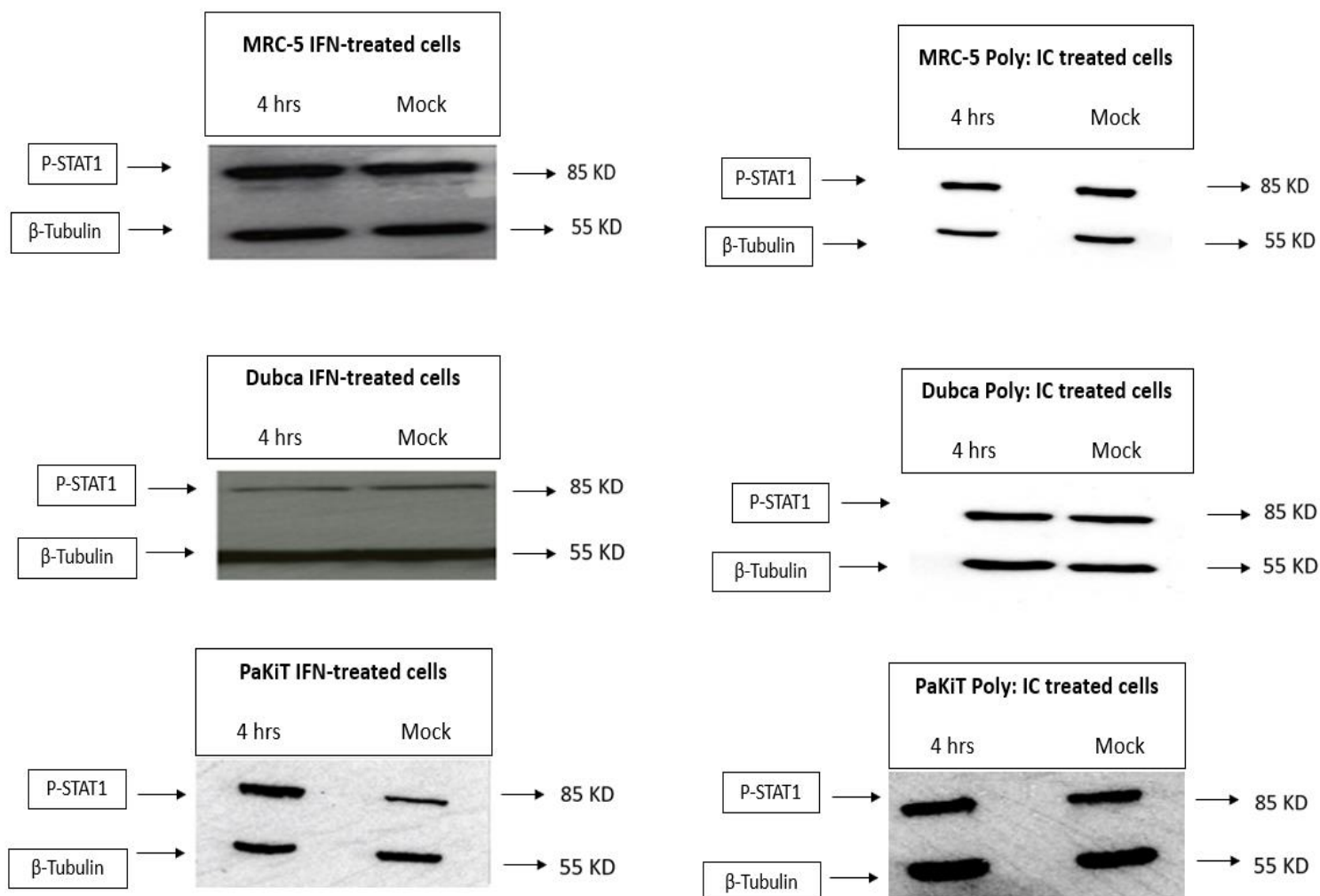
Figure 14. Examining the level of STAT1 expression upon stimulating the innate immune response of MRC-5, Dubca, and PaKit cells. MRC-5, Dubca, and PaKit cells were treated with IFN or transfected with Poly:IC for 4 hrs. Cells were harvested and the STAT1 expression was examined by western blotting analysis using anti-STAT1 antibody. The molecular weight of STAT1 protein is 85 KDa.

3.2.4 TMT-MS/MS analysis of total cell lysate from MRC-5, Duba, and PaKiT cells treated with either IFN or poly: IC

The innate immune response of MRC-5, Duba, and Pakit cells was successfully stimulated using either universal IFN or Poly: IC. Next, we used the same experimental conditions to conduct TMT-MS/MS and perform bioinformatic analysis on the resultant datasets to identify the host's modulated proteins in response to innate immune stimuli in all three species.

MRC-5, Dubca, and Pakit cells were grown in a T-25 flask and were either treated with either IFN or transfected with Poly: IC for 4 hrs to stimulate the innate immune response. The induction of innate immune response was confirmed by western blotting analysis before sending the samples to the proteomics core facility at the University of Bristol. The experiment was performed in triplicate (Figure 14).
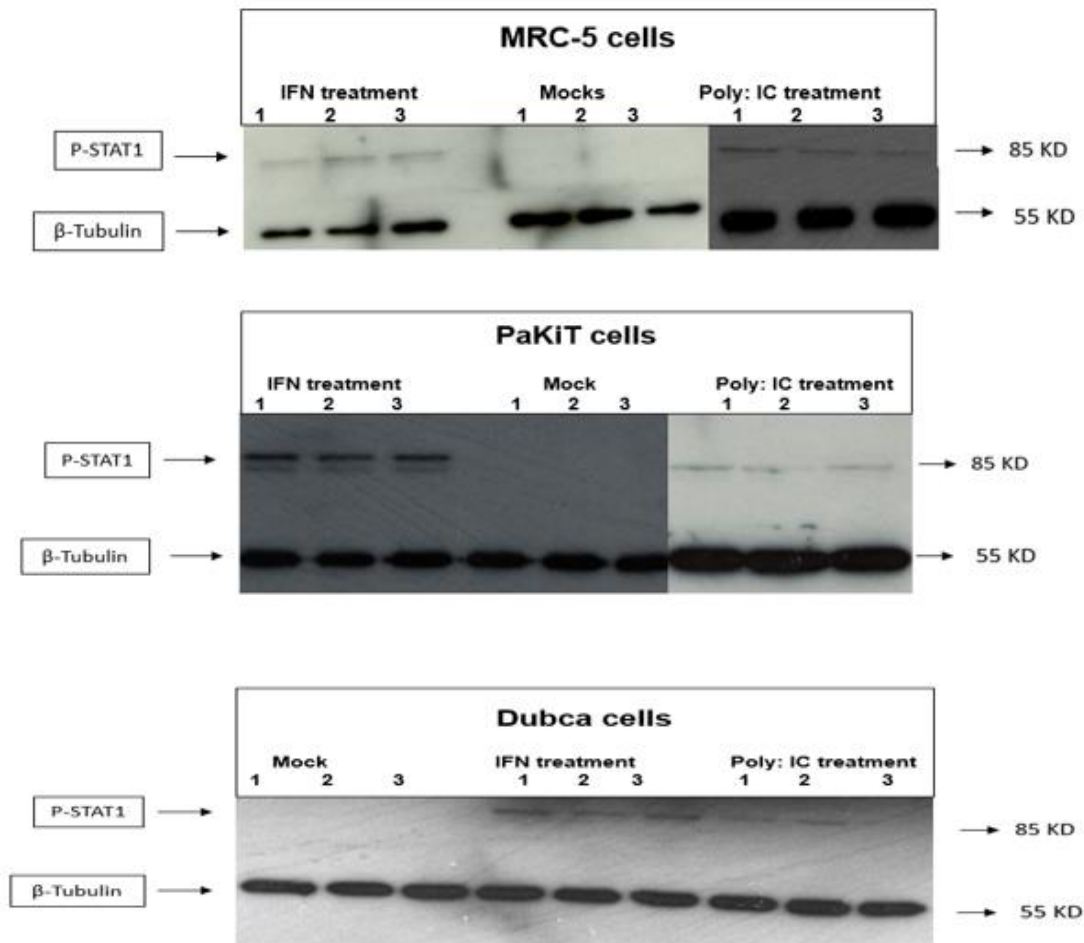
Figure 15. Confirming the induction of innate immune response in cells before sending samples for TMT-MS/MS analysis. PaKiT , MRC-5, and Dubca were grown in T-25 flasks and were either treated with 1000IU/mL of IFN or transfected with 750ng/mL of Poly: IC for 4 hrs. Cells were harvested and lysed using RIPA buffer. The induction of innate immune response was confirmed using anti-phospho STAT1 antibody before conducting TMT-MS/MS Analysis. The molecular weight of P-STAT1 protein is 85 KDa.

3.2.4.1 Host proteins increased in MRC-5 IFN-treated cells compared to mock cells

Thirty-nine host proteins were ≥ 1 log2 fold upregulated in MRC-5 IFN treated cells compared to mock cells (Table 9). These proteins were analyzed by STRING analysis to reveal their specific host pathways (Figure 15). The analysis showed significant enrichment of proteins involved in the antiviral immune response (Table 10).

Table 9. Host proteins increased ≥ 1 log2 fold in MRC-5 IFN treated cells compared to mock cells. Proteins' IDs and names are obtained from UniProt: the universal protein knowledgebase in 2021.

Uniport ID	Protein name & Gene symbol	IFN-treated cells /Mock log2-fold change average
A0A024RDA4	C-X-C motif chemokine. GN=CXCL10	4.86
Q15646	2'-5'-oligoadenylate synthetase-like protein. GN= OASL	4.36
P09913	Interferon-induced protein with tetratricopeptide repeats 2. GN=IFIT2	3.66
Q5T765	Interferon-induced protein with tetratricopeptide repeats 3. GN=IFIT3	3.22
P20591	Interferon-induced GTP-binding protein Mx1. GN=MX1	3.18
P09914	Interferon-induced protein with tetratricopeptide repeats 1. GN=IFIT1	3.07
Q8NG68	Tubulin--tyrosine ligase. GN=TTL	2.56
Q96AZ6	Interferon-stimulated gene 20 kDa protein. GN=ISG20	2.39
P02458	Collagen alpha 1(II) chain. GN=COL2A1	2.03
Q9BYX4	Interferon-induced helicase C domain-containing protein 1. GN= IFIH1	2
Q9C0A0	Contactin-associated protein-like 4 GN=CNTNAP4	1.94
O95786	Probable ATP-dependent RNA helicase DDX58 GN=DDX58	1.77
Q9UMW8	Ubl carboxyl-terminal hydrolase 18 GN=USP18	1.76
Q5TF85	Family with sequence similarity 46, member A, isoform CRA_a GN=TENT5A	1.75
Q9BWW8	Apolipoprotein L6. GN=APOL6	1.65
Q5U079	Jun B proto-oncogene, GN=JUNB	1.47
Q96A46	Mitoferrin-2. GN=SLC25A28	1.45
Q15021	Condensin complex subunit 1. GN=NCAPD2	1.32
P05161	Ubiquitin-like protein ISG15. GN=ISG15	1.3
Q8IWD4	Coiled-coil domain-containing protein 117. GN=CCDC117	1.3
A5D8V7	Coiled-coil domain-containing protein 151. GN=CCDC151	1.25
Q5TEJ8	Protein THEMIS2. GN=THEMIS2	1.22
O75665	Oral-facial-digital syndrome 1 protein. GN=OFD1	1.22
O95837	Guanine nucleotide-binding protein subunit alpha-14. GN=GNA14	1.2
Q68DH5	G-protein coupled receptor-associated protein LMBRD2. GN=LMBRD2	1.2
A0A024QYT5	Serpin peptidase inhibitor, clade E (Nexin, plasminogen activator inhibitor type 1), member 1, isoform CRA_b .GN=SERPINE1	1.18
Q9NZQ7	Programmed cell death 1 ligand 1. GN=CD274	1.15

Q96B49	Mitochondrial import receptor subunit TOM6 homolog. GN=TOMM6	1.14
A0A1S6YJG6	Catechol-O-methyltransferase. GN=COMT	1.12
Q9H8M9	Protein eva-1 homolog A. GN=EVA1A	1.12
P13164	Interferon-induced transmembrane protein 1. GN=IFITM1	1.11
Q96RP9	Elongation factor G, mitochondrial. GN= GFM1	1.1
Q99766	ATP synthase subunit s, mitochondrial. GN=DMAC2L	1.1
P13747	HLA class I histocompatibility antigen, alpha chain E.GN=HLA-E	1.09
Q8N883	Zinc finger protein 614. GN=ZNF614	1.09
Q07820	Induced myeloid leukemia cell differentiation protein Mcl-1 .GN=MCL1	1.08
O95497	Pantetheinase. GN=VNN1	1.07
P49407	Beta-arrestin-1. GN= ARRB1	1.06
K7EJB5	Small nuclear ribonucleoprotein Sm D2. GN=SNRPD2	1

Table 10. Host innate immune proteins increased ≥ 1 log2 fold in MRC-5 universal IFN treated cells compared to mock cells and their functions.

Host innate immune proteins	
Protein symbol	**Protein name and function**
OASL	2'-5'-oligoadenylate synthase-like protein enhances IFN signaling and has a role in suppressing the replication of RNA viruses. (180,181).
IFIT2	IFN-induced protein with tetratricopeptide repeats 2. It exhibits antiviral activity by inhibiting the expression of viral mRNA (182).
IFIT3	IFN-induced protein with tetratricopeptide repeats 3. It activates Mitochondrial antiviral signaling protein (MAVS) to promote IFN production (178).
MX1	Interferon-induced GTP-binding protein Mx1. It possesses antiviral activity against many RNA viruses and some DNA viruses by targeting viral ribonucleocapsid (183) (184) .
IFIT1	IFN-induced protein with tetratricopeptide repeats 1. It possesses anti-viral activities such as sensing viral RNA and inhibiting the expression of viral mRNA (185).
ISG20	Interferon-stimulated gene 20 kDa protein exhibits antiviral activity against RNA viruses by targeting viral replication and translation processes (186)

IFIH1	Interferon-induced helicase C domain-containing protein 1. It is also known as MDA-5. It acts as a cytoplasmic sensor of viral dsRNA and plays an essential role in activating IFNs and proinflammatory cytokines signaling pathways. It has been shown to detect RNA viruses such as dengue virus (DENV), and West Nile virus (WNV)(187).
DDX58	Antiviral innate immune response receptor RIG-I. It is also known as RIG-I. Like MDA-5, It acts as a cytoplasmic sensor of viral dsRNA and plays a vital role in activating IFNs and proinflammatory cytokines signaling pathways (188).
ISG15	Ubiquitin-like protein ISG15. It plays a vital role in the innate immune response to a viral infection either via its conjugation to a target protein such as IFIT1, MX1/MxA (ISGylation) or as an unconjugated protein(189) ISGylation of viral sensors stimulates the innate immune response against a wide range of RNA viruses (190).
IFITM1	Interferon-induced transmembrane protein 1. It displays antiviral activity by preventing releasing the viral genome into the host's cytoplasm (191). It has been shown to inhibit SARS-CoV-2 S protein-mediated syncytia formation(192)
CXCL10	C-X-C motif chemokine 10 is a pro-inflammatory cytokine. It is expressed within tissues following viral infection. It is produced mainly by T cells and monocytes in response to IFN and contributes inactivation and migration of immune cells toward the sites of infection (193).
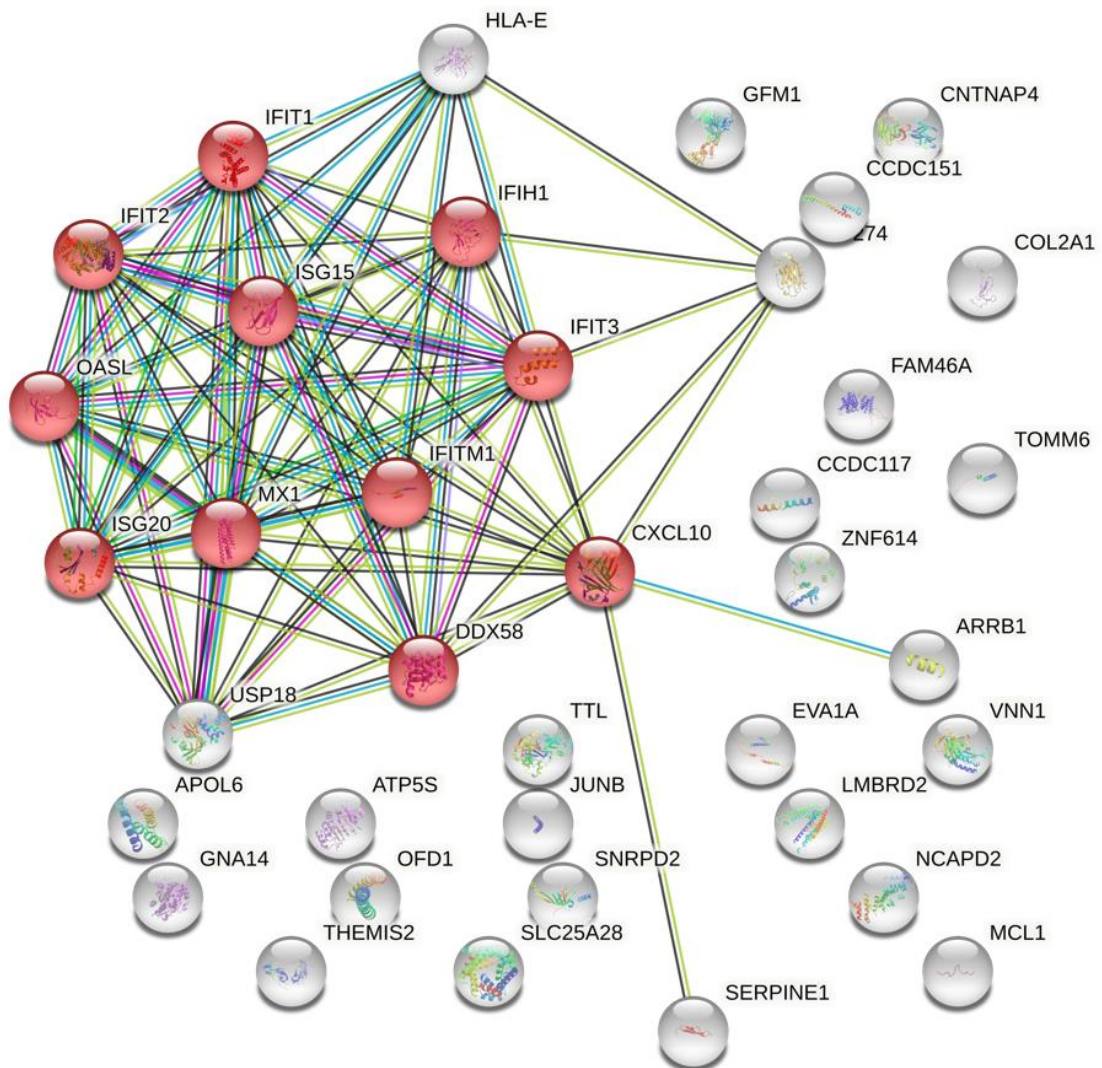
Figure 16. STRING analysis of proteins increased ≥ 1 log2 fold in MRC-5 IFN treated cells. The STRING database was searched to analyze host proteins that showed a ≥ 1 log2 fold enrichment in MRC-5 IFN treated cells compared to mock cells. Nodes representing proteins that most significantly enriched the GO term. Proteins involved in the antiviral immune response process are shaded in red.

3.2.3.2 Host proteins that decreased in MRC-5 IFN-treated cells compared to mock cells.

Sixteen host proteins were ≥ 1 log2 fold downregulated in MRC-5 IFN treated cells compared to mock cells (Table 11). These proteins were analyzed by STRING analysis to reveal their specific host pathways. The analysis showed enrichment of proteins involved in Collagen fibril organization (Figure 16).

Table 11. Cellular proteins decreased ≥ 1 log2 fold in MRC-5 universal IFN treated cells compared to mock cells. Proteins' IDs and names are obtained from UniProt: the universal protein knowledgebase in 2021.

Uniport ID	Protein name & Gene symbol	IFN-treated cells /Mock log2-fold change average
A0A024R2B6	Serpin B5. GN= SERPINB5	-2.66
P08123	Collagen alpha 2(I) chain. GN=COL1A2	-1.86
D3DTX7	Collagen, type I, alpha 1, isoform CRA_a. GN=COL1A1	-1.71
P02452	Collagen alpha 1(I) chain. GN=COL1A1	-1.63
P09471	Guanine nucleotide-binding protein G(o) subunit alpha. GN= GNAO1	-1.62
Q1MSJ5	Centrosome and spindle pole-associated protein 1 GN=CSPP1	-1.55
Q8IUG5	Unconventional myosin-XVIIIb. GN=MYO18B	-1.41
Q15113	Procollagen C-endopeptidase enhancer 1. GN=PCOLCE	-1.35
Q99952	Tyrosine-protein phosphatase non-receptor type 18. GN=PTPN18	-1.29
Q16236	Nuclear factor erythroid 2-related factor 2. GN=NFE2L2	-1.29
P05997	Collagen alpha 2(V) chain. GN=COL5A2	-1.16
Q68DK2	Zinc finger FYVE domain-containing protein 26. GN=ZFYVE26	-1.15
Q9UE24	Menin OS=Homo sapiens. GN=MEN1	-1.09
Q8IZU8	Dermatan-sulfate epimerase-like protein. GN=DSEL	-1.08
J3KPJ3	Calcium/calmodulin-dependent protein kinase. GN=CAMKK1	-1.07
Q96G01	Protein bicaudal D homolog 1. GN=BICD1	-1.02
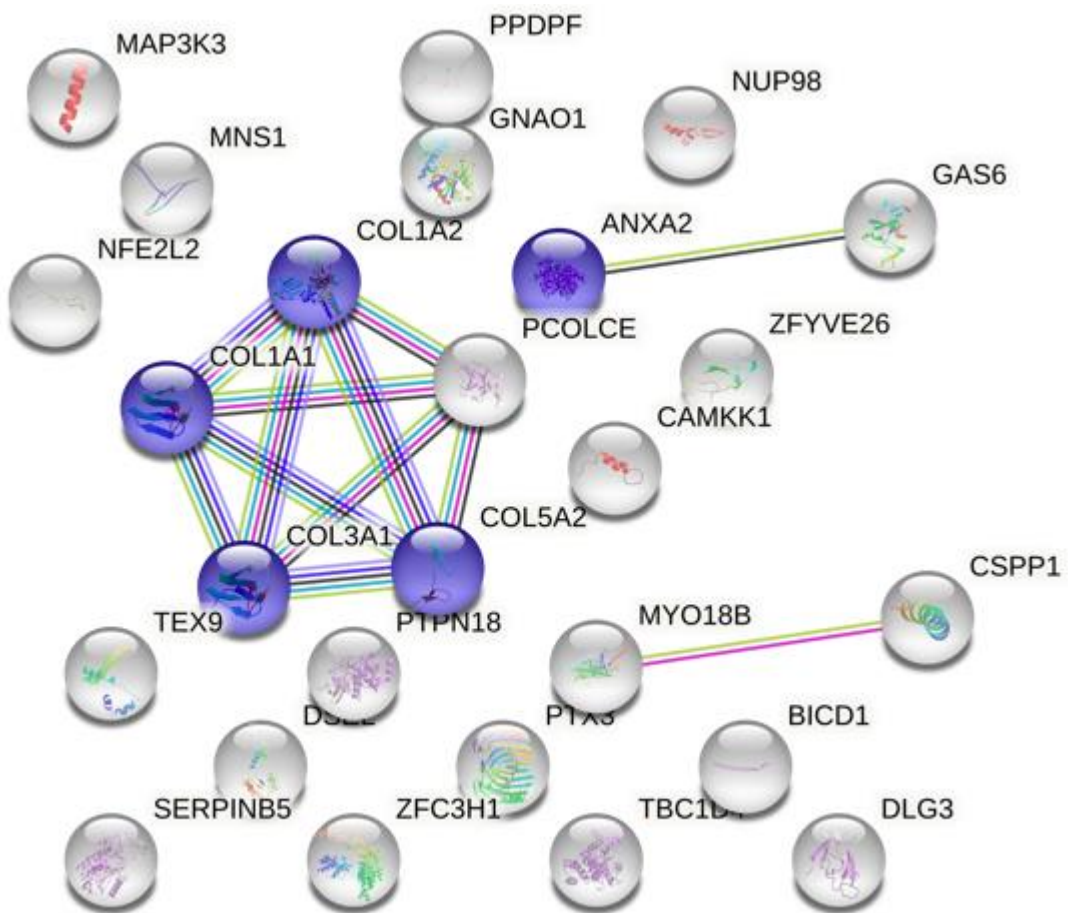
Figure 17.STRING analysis of proteins that decreased ≥ 1 log2 in MRC-5 IFN treated cells. The STRING database was searched to analyze host proteins that showed a ≥ 1 log2 decrease in MRC-5 IFN treated cells compared to mock cells. Nodes representing proteins that most significantly enriched the GO term. Proteins involved in the Collagen fibril organization process are shaded in blue.

3.2.3.3 Host proteins increased in MRC-5 Poly: IC treated cells compared to mock cells.

Twenty-nine proteins were ≥ 1 log2 fold upregulated in MRC-5 Poly: IC transfected cells compared to mock cells (Table 12). These proteins were analyzed by STRING analysis to reveal their specific host pathways (Figure 17). The analysis showed significant enrichment of proteins involved in the innate immune response process (Table 13).

CXCL10, OASL, IFIT2, IFIT3, and IFIT1 were common up-regulated proteins among MRC-5 IFN and Poly: IC treated cells.

Table 12. Cellular proteins increased ≥ 1 log2 fold in MRC-5 Poly: IC transfected cells compared to mock cells. Proteins' IDs and names are obtained from UniProt: the universal protein knowledgebase in 2021.

Uniport ID	Protein name & Gene ID	Poly: IC - treated cells /Mock log2-fold change average
A0A024RDA4	C-X-C motif chemokine. GN=CXCL10	5.86
Q15646	2'-5'-oligoadenylate synthase-like protein. GN= OASL	4.48
P02787	Serotransferrin. GN= TF	3.36
P02790	Hemopexin. GN=HPX	3.11
A6XGL2	Insulin. GN=INS	2.97
P01619	Immunoglobulin kappa variable 3-20 . GN= IGKV3-20	2.91
I3L2C0	Active breakpoint cluster region-related protein. GN=ABR	2.76
Q8N6V9	Testis-expressed protein 9. GN=TEX9	2.27
P09913	Interferon-induced protein with tetratricopeptide repeats 2. GN=IFIT2	2.26
O75807	Protein phosphatase 1 regulatory subunit 15A. GN=PPP1R15A	2.06
P55201	Peregrin. GN=BRPF1	1.84
Q9HB40	Retinoid-inducible serine carboxypeptidase.GN= SCPEP1	1.65
Q5T765	Interferon-induced protein with tetratricopeptide repeats 3, isoform CRA_a. GN=IFIT3	1.61
P09914	Interferon-induced protein with tetratricopeptide repeats 1. GN=IFIT1	1.43
Q08554	Desmocollin-1. GN=DSC1	1.39

Q14520	Hyaluronan-binding protein 2. GN=HABP2	1.37
P17936	Insulin-like growth factor-binding protein 3.GN= IGFBP3	1.37
P07358	Complement component C8 beta chain	1.28
E9PN66	Tumor protein p53-inducible protein 11	1.24
Q15652	Probable JmjC domain-containing histone demethylation protein 2C. GN=JMJD1C	1.19
J3KNF5	Centrosomal protein of 290 kDa. GN=CEP290	1.13
Q9ULV0	Unconventional myosin-Vb. GN=MYO5B	1.12
Q6AI12	Ankyrin repeat domain-containing protein 40. GN=ANKRD40	1.1
G5E9G6	E3 ubiquitin-protein ligase TRIP12. GN=TRIP12	1.1
Q5VT06	Centrosome-associated protein 350 GN=CEP350	1.07
Q5TF85	Family with sequence similarity 46, member A, isoform CRA_a GN=TENT5A	1.04
Q96T17	MAP7 domain-containing protein 2. GN=MAP7D2	1.03
B4E1B2	Beta-1 metal-binding globulin.	1
Q8N8Z6	Discoidin, CUB and LCCL domain-containing protein 1. GN=DCBLD1	1

Table 13. Cellular innate immune proteins increased ≥ 1 log2 fold in MRC-5 Poly: IC transfected cells compared to mock cells and their functions.

Host innate immune proteins	
Protein symbol	**Protein name and function**
OASL	2'-5'-oligoadenylate synthase-like protein enhances IFN signaling and has a role in suppressing the replication of RNA viruses. (180,181).
IFIT2	IFN-induced protein with tetratricopeptide repeats 2. It exhibits antiviral activity by inhibiting the expression of viral mRNA (182).
IFIT3	IFN-induced protein with tetratricopeptide repeats 3. It activates Mitochondrial antiviral signaling protein (MAVS) to promote IFN production (178).

IFIT1	IFN-induced protein with tetratricopeptide repeats 1. It possesses anti-viral activities such as sensing viral RNA and inhibiting the expression of viral mRNA (185).
CXCL10	C-X-C motif chemokine 10 is a pro-inflammatory cytokine that is expressed within tissues following viral infection. It contributes to lymphocyte activation, extravasation, and accumulation of virus-specific T cells within sites of infection(193).
C8B	Complement component C8 beta chain is a member of membrane attack complex (MAC), which mediates innate and adaptive immune responses (194).
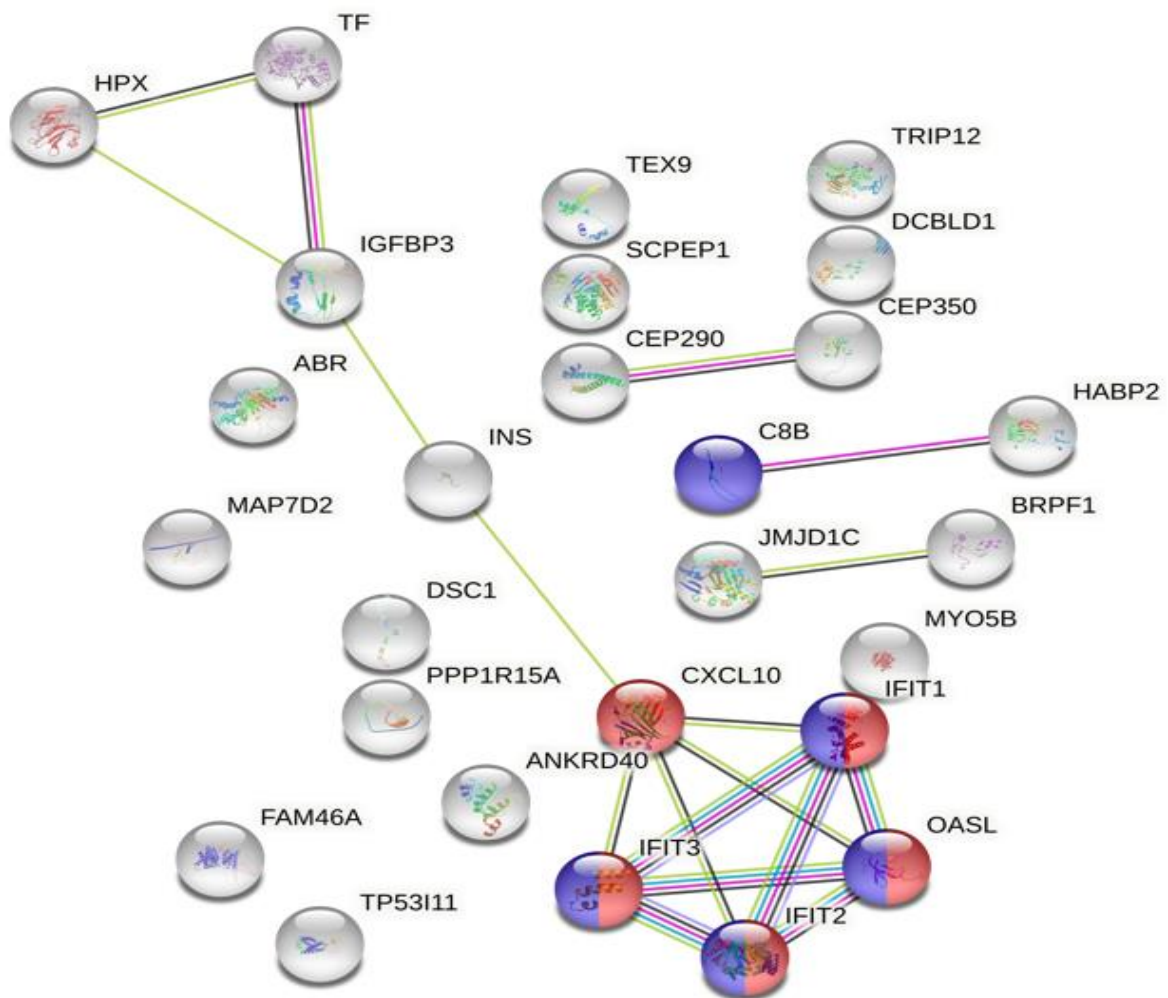
Figure 18. STRING analysis of proteins that increased ≥ 1 log2 fold in MRC-5 Poly: IC transfected cells. The STRING database was searched to analyze host proteins that showed a ≥ 1 log2 increase in MRC-5 IFN treated cells compared to mock cells. Nodes representing proteins that most significantly enriched the GO term. Proteins involved in the defense response to viral infection are shaded in red. Proteins involved in the innate immune response are colored in blue.

3.2.3.4 Host proteins decreased in MRC-5 Poly: IC treated cells compared to mock cells

Compared to mock cells, one hundred seventeen proteins were down-regulated ≥ 1 log2 fold in MRC-5 Poly: IC transfected cells (Table 14). These proteins were analyzed by STRING analysis to reveal their specific host pathways. The analysis showed significant enrichment of proteins involved in the extracellular matrix organization process (Figure 18).

Table 14. Cellular proteins decreased ≥ 1 log2 fold in MRC-5 Poly: IC transfected cells compared to mock cells. Proteins' IDs and names are obtained from UniProt: the universal protein knowledgebase in 2021.

Uniport ID	Protein name & Gene ID	Poly:IC -treated cells /Mock log2-fold change average
A0A1B0GTI3	Alpha-ketoglutarate-dependent dioxygenase. GN=FTO	-5.17
O95837	Guanine nucleotide-binding protein subunit alpha-14. GN=GNA14	-4.94
Q9H8M9	Protein eva-1 homolog A. GN=EVA1A	-4.31
Q5JXB2	Putative ubiquitin-conjugating enzyme E2 N-like. GN=UBE2NL	-4.11
Q96RP9	ELONGATION FACTOR G, MITOCHONDRIAL. GN= GFM1	-3.7
Q68DH5	G-protein coupled receptor-associated protein LMBRD2. GN=LMBRD2	-3.45
Q8N883	Zinc finger protein 614. GN=ZNF614	-3.01
Q16720	Plasma membrane calcium-transporting ATPase 3. GN=ATP2B3	-2.98
O75665	Oral-facial-digital syndrome 1 protein. GN=OFD1	-2.98
Q15021	Condensin complex subunit 1. GN=NCAPD2	-2.87
O95497	Pantetheinase. GN= VNN1	-2.73
A5D8V7	Coiled-coil domain-containing protein 151. GN=CCDC151	-2.69
P49407	Beta-arrestin-1. GN= ARRB1	-2.68
J3KMX3	Alpha-fetoprotein. GN=AFP	-2.67
A0A481U987	Antithrombin (Fragment). GN=SERPINC1	-2.49
Q9P2H0	Centrosomal protein of 126 kDa. GN=CEP126	-2.44
Q59FY1	Synapse-associated protein 102 variant (Fragment) .	-2.25
A0A024R219	Zinc finger, A20 domain containing 2, isoform CRA_a. GN=ZA20D2	-2.17

B9A6K1	TBC1 domain family, member 5. GN=TBC1D5	-2.17
Q86TG7	Retrotransposon-derived protein PEG10. GN=PEG10	-2.16
O14965	Aurora kinase A. GN= AURKA	-2.13
P35443	Thrombospondin-4. GN=THBS4	-2.12
Q5T013	Putative hydroxypyruvate isomerase (Fragment). GN=HYI	-2.08
P49747	Cartilage oligomeric matrix protein. GN= COMP	-2.07
Q59EM7	NF-kappaB inhibitor beta variant (Fragment) GN= Q59EM7	-2.03
P01033	Metalloproteinase inhibitor 1 OS=Homo sapiens OX=9606 PE=2 SV=1	-2.01
O00481	Butyrophilin subfamily 3 member A1. GN=BTN3A1	-1.95
A0A024R2B6	Serpin peptidase inhibitor, clade B (Ovalbumin), member 5, isoform CRA_b. GN=SERPINB5	-1.94
A2RTY6	inter-alpha (Globulin) inhibitor H2 .GN=ITIH2	-1.91
P21964	Catechol-O-methyltransferase (Fragment). GN=COMT	-1.83
P08123	Collagen alpha-2(I) chain. GN=COL1A2	-1.81
Q12860	Contactin-1. GN=CNTN1	-1.81
B0YIW2	Apolipoprotein C-III. GN=APOC3	-1.8
Q07820	Induced myeloid leukemia cell differentiation protein Mcl-1. GN=MCL1	-1.8
Q06033	Inter-alpha-trypsin inhibitor heavy chain H3. GN=ITIH3	-1.79
Q68DK2	Zinc finger FYVE domain-containing protein 26. GN=ZFYVE26	-1.77
Q15113	Procollagen C-endopeptidase enhancer 1. GN=PCOLCE	-1.75
Q6FI00	CCND1 protein.GN=CCND1	-1.75
Q99983	Osteomodulin. GN= OMD	-1.72
Q99798	Aconitate hydratase, mitochondrial GN=ACON.	-1.69
Q5T011	KICSTOR complex protein SZT2. GN=SZT2	-1.68
Q2TAZ0	Autophagy-related protein 2 homolog A. GN=ATG2A	-1.68
P02452	Collagen alpha 1(I) chain. GN=COL1A1	-1.67
P04278	Sex hormone-binding globulin. GN=SHBG	-1.66
A0A024R1Y8	Follistatin-like 3 (Secreted glycoprotein), isoform CRA_a . GN=FSTL3	-1.61
A0A0G2JPD3	HLA class I histocompatibility antigen, A alpha chain. GN=HLA-A	-1.59
Q8ND90	Paraneoplastic antigen Ma1 (PNMA1) protein. GN=PNMA1	-1.52
Q16853	Membrane primary amine oxidase. GN=AOC3	-1.48
A0A384N669	Epididymis secretory sperm binding protein.	-1.46

A0A024R466	Integral membrane protein 2C, isoform CRA_a. GN=ITM2C	-1.45
H0YDF9	Protein scribble homolog (Fragment). GN=SCRIB	-1.44
P61587	Rho-related GTP-binding protein RhoE. GN=RND3	-1.43
P02458	Collagen alpha 1(II) chain. GN=COL2A1	-1.43
Q86YD1	Prostate tumor-overexpressed gene 1 protein. GN=PTOV1	-1.42
P29279	CCN family member 2. GN=CTGF	-1.41
P05997	Collagen alpha 2(V) chain. GN=COL5A2	-1.4
Q9NZV1	Cysteine-rich motor neuron 1 protein. GN=CRIM1	-1.4
H0YAC1	Plasma kallikrein (Fragment). GN=KLKB1	-1.39
Q16270	Insulin-like growth factor-binding protein 7. GN=IGFBP7	-1.38
P05067	Amyloid-beta precursor protein. GN= APP	-1.38
B4E1Z4	C3/C5 convertase	-1.36
D3DQH8	Secreted protein, acidic, cysteine rich (Osteonectin), isoform CRA_a. GN=SPARC	-1.34
Q9Y5F9	Protocadherin gamma-B6. GN=PCDHGB6	-1.34
A8K6K4	cDNA FLJ77565, highly similar to Homo sapiens interleukin 1 receptor accessory protein (IL1RAP), transcript variant 1, mRNA	-1.31
B4DPQ0	Complement C1r subcomponent. GN=C1R	-1.28
A0A0S2Z4F1	EGF containing fibulin-like extracellular matrix protein 1 isoform 1 (Fragment). GN=EFEMP1	-1.28
P07996	Thrombospondin-1. GN=THBS1	-1.27
P02461	Collagen alpha-1(III) chain. GN=COL3A1	-1.26
P07996	Thrombospondin 1. GN=THBS1	-1.26
Q59ED0	Cyclin-dependent kinase variant (Fragment).	-1.25
Q6ZN30	Zinc finger protein basonuclin-2. GN=BNC2	-1.25
D3DTX7	Collagen, type I, alpha 1, isoform CRA_a. GN=COL1A1	-1.24
Q9Y6H1	Coiled-coil-helix-coiled-coil-helix domain-containing protein 2. GN=CHCHD2	-1.24
Q13361	microfibrillar associated protein 5 (MFAP5). GN= MFAP5	-1.24
P30279	G1/S-specific cyclin-D2 OS=Homo sapiens OX=9606 GN=CCND2	-1.23
Q02224	Centromere-associated protein E. GN=CENPE	-1.22
Q7Z5N4	Protein sidekick 1. GN=SDK1	-1.21
Q92529	SHC-transforming protein 3. GN=SHC3	-1.2
Q9Y6T7	Diacylglycerol kinase beta. GN=DGKB	-1.2

Q13829	BTB/POZ domain-containing adapter for CUL3-mediated RhoA degradation protein 2. GN=TNFAIP1	-1.19
Q96P44	Collagen alpha 1(XXI) chain. GN=COL21A1	-1.18
Q99952	Tyrosine-protein phosphatase non-receptor type 18.GN=PTPN18	-1.17
P13591	Neural cell adhesion molecule 1. GN=NCAM1	-1.17
Q99766	ATP synthase subunit s, mitochondrial. GN=DMAC2L	-1.17
Q14596	Next to BRCA1 gene 1 protein. GN= NBR1	-1.16
Q12841	Follistatin-related protein 1. GN=FSTL1	-1.16
Q8NFZ5	TNFAIP3-interacting protein 2. GN=TNIP2	-1.16
Q7Z528	Integral membrane protein 2	-1.16
P07357	Complement component C8 alpha chain. GN=C8A	-1.16
C0JYY2	Apolipoprotein B (Including Ag(X) antigen), isoform CRA_a. GN=APOB	-1.15
Q5T3F8	CSC1-like protein 2. GN=TMEM63B	-1.14
Q14061	Cytochrome c oxidase copper chaperone. GN=COX17	-1.13
Q86TV4	Fibulin-5	-1.12
Q9Y666	Solute carrier family 12 member 7. GN=SLC12A7	-1.12
O75030	Microphthalmia-associated transcription factor. GN=MITF	-1.11
Q8TF21	Ankyrin repeat domain-containing protein 24. GN=ANKRD24	-1.1
P40189	Interleukin-6 receptor subunit beta. GN=IL6ST	-1.09
Q13332	Receptor-type tyrosine-protein phosphatase S. GN=PTPRS	-1.09
Q5TGL8	PX domain-containing protein 1. GN=PXDC1	-1.09
Q1MSJ5	Centrosome and spindle pole-associated protein 1. GN=CSPP1	-1.07
Q9UEG9	Cytochrome c oxidase subunit 6A, mitochondrial	-1.07
J3KPJ3	Calcium/calmodulin-dependent protein kinase kinase 1. GN=CAMKK1	-1.06
A8K2N0	cDNA FLJ77835, highly similar to Homo sapiens complement component 1, s subcomponent (C1S), transcript variant 2, mRNA	-1.06
Q76LX8	A disintegrin and metalloproteinase with thrombospondin motifs 13. GN=ADAMTS13	-1.06
K7EJB5	Small nuclear ribonucleoprotein Sm D2. GN=SNRPD2	-1.06
P19883	Follistatin. GN=FST	-1.05
O00391	Sulfhydryl oxidase 1. GN=QSOX1	-1.05
Q9NP84	Tumor necrosis factor receptor superfamily member 12A. GN=TNFRSF12A	-1.05

H0Y474	V-type proton ATPase subunit G (Fragment). GN=ATP6V1G2	-1.04
Q96DA6	Mitochondrial import inner membrane translocase subunit TIM14. GN=DNAJC19	-1.04
B7Z5R7	cDNA FLJ61355, highly similar to CLIP-associating protein 1.	-1.04
X6R7I6	Pancreatic progenitor cell differentiation and proliferation factor. GN=PPDPF	-1.03
Q9UBN6	Tumor necrosis factor receptor superfamily member 10D. GN=TNFRSF10D	-1.03
P16035	Metalloproteinase inhibitor 2. GN=TIMP2	-1.03
E7ET40	Urokinase-type plasminogen activator. GN=PLAU	-1
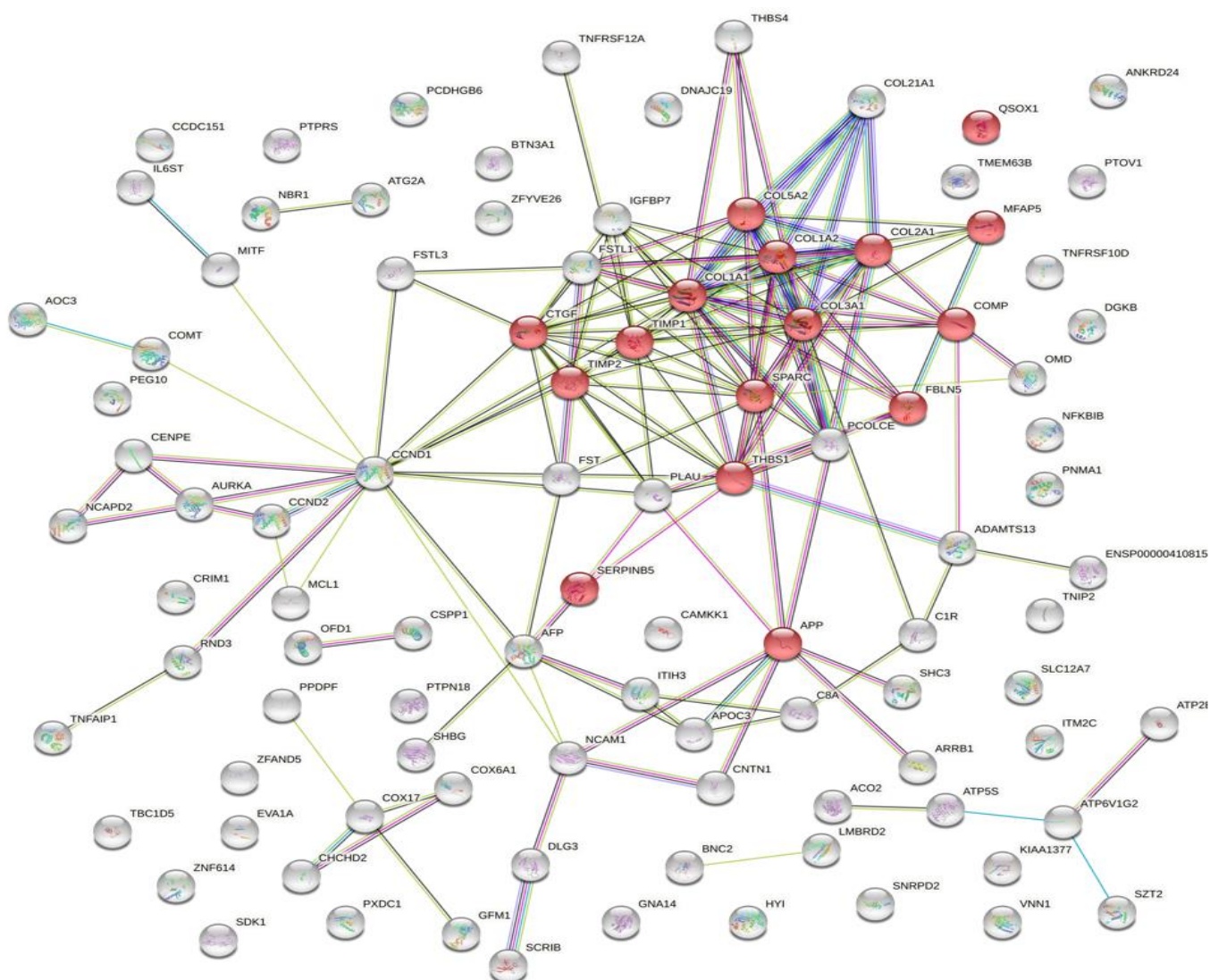
Figure 19. STRING analysis of proteins decreased ≥ 1 log2 fold in MRC-5 Poly: IC transfected cells. The STRING database was searched to analyze host proteins that showed a ≥ 1 log2 fold decrease in MRC-5 Poly: IC treated cells compared to mock cells. Nodes representing proteins that most significantly enriched the GO term. Proteins involved in the extracellular matrix organization process are shaded in red.

3.2.3.5 Host proteins increased in PaKiT IFN-treated cells compared to mock cells

Forty-eight proteins were ≥ 1 log2 fold upregulated in PaKiT IFN treated cells compared to mock cells (Table 15). These proteins were analyzed by STRING analysis to reveal their specific host pathways (Figure 19). The analysis showed significant enrichment of proteins involved in innate immune response (Table 16). Some of these proteins are shared between PaKiT and MRC-5 IFN-treated cells, including IFIT1, IFIT2, IFIT3, ISG15, and DDX58.

Interestingly, CXCL10 protein, which has a role in inflammasome activation and is associated with the severity of viral diseases, was the highest up-regulated in MRC-5 IFN-treated cells but wasn't up-regulated in PaKiT IFN-treated cells. The probable functions of bat proteins are based on homology to human proteins.

Table 15. Cellular proteins increased ≥ 1 log2 fold in PaKiT universal IFN treated cells compared to mock cells. Proteins' IDs and names are obtained from UniProt: the universal protein knowledgebase in 2021.

Uniport ID	Protein name & Gene symbol	IFN -treated cells /Mock log2-fold change average
L5KN80	Interferon regulatory factor 7. GN=PAL_GLEAN10011152	5
L5KCI3	Interferon-induced GTP-binding protein Mx2. GN=PAL_GLEAN10008393	4.23
L5JNL9	Interferon-induced protein with tetratricopeptide repeat 1. GN=PAL_GLEAN10018382	3.7
L5JQB4	Interferon-induced protein with tetratricopeptide repeat 3. GN=PAL_GLEAN10018383	2.99
L5JPT0	Interferon-induced protein with tetratricopeptide repeat 2. GN=PAL_GLEAN10018384	2.87
L5L3T4	Protein deltex-3-like protein. GN=PAL_GLEAN10006545	2.62
L5JYW2	Interferon-induced helicase C domain-containing protein 1. GN=PAL_GLEAN10025907	2.43
L5K4P7	Interferon-induced guanylate-binding protein 1. GN=PAL_GLEAN10023941	1.91
L5KLN7	Lymphocyte antigen 6H. GN=PAL_GLEAN10010433	1.89

L5K4S7	Spatacsin. GN=PAL_GLEAN10023533	1.82
L5L1H8	Sp110 nuclear body protein. GN=PAL_GLEAN10014326	1.78
L5K2E8	StAR-related lipid transfer protein 9. GN=PAL_GLEAN10023569	1.7
L5K8H1	ERC protein 2 .GN=PAL_GLEAN10022192	1.59
L5JXN7	Polyadenylate-binding protein. GN=PAL_GLEAN10024380 PE=3 SV=1	1.56
L5JTS7	Kinesin-like protein. GN=PAL_GLEAN10019747	1.54
L5L1R3	Ubiquitin carboxyl-terminal hydrolase. GN=PAL_GLEAN10014431	1.53
L5KAD8	Interferon-induced GTP-binding protein MX1. GN=PAL_GLEAN10008392	1.5
L5KS39	Tumor necrosis factor ligand superfamily member. GN=PAL_GLEAN10012872	1.47
L5JU10	Ribonuclease ZC3H12A. GN=PAL_GLEAN10014935	1.41
L5JVE3	Proheparin-binding EGF-like growth factor. GN=PAL_GLEAN10016791	1.4
L5L743	Ubiquitin cross-reactive protein. GN=PAL_GLEAN10001765	1.37
L5JUK2	Histone-lysine N-methyltransferase, H3 lysine-36 and H4 lysine-20 specific (Fragment). GN=PAL_GLEAN10016940	1.35
L5KF09	Thymosin beta 4. GN=PAL_GLEAN10007819	1.33
L5JMY5	Protein dopey-1. GN=PAL_GLEAN10025212	1.31
L5K1C2	Transcription initiation factor TFIID subunit 7. GN=PAL_GLEAN10002206	1.28
L5JYX0	NFX1-type zinc finger-containing protein 1. GN=PAL_GLEAN10024454 -	1.26
L5JML8	Vitamin K-dependent protein S. GN=PAL_GLEAN10016398	1.24
L5JSY7	Sestrin-2. GN=PAL_GLEAN10015062	1.22
L5L376	Poly [ADP-ribose] polymerase. GN=PAL_GLEAN10006547	1.21
L5KWZ6	Protein EURL like protein. GN=PAL_GLEAN10018491	1.21
L5KZZ3	FERM domain-containing protein 4A. GN=PAL_GLEAN10015805	1.2
L5KHT4	Disks large-associated protein 2. GN=PAL_GLEAN10015377	1.2
L5KUU1	MTSS1-like protein. GN=PAL_GLEAN10016319	1.18
L5K519	Septin-14. GN=PAL_GLEAN10011938	1.17
L5KYF7	Select seq ref|XP_024899739.1| axonemal dynein light chain domain-containing protein 1 isoform X3. GN= PAL_GLEAN10017721.	1.14
L5KC19	Putative ATP-dependent RNA helicase DDX58. GN=PAL_GLEAN10008309	1.13
L5KBE6	5'-nucleotidase domain-containing protein 2. GN=PAL_GLEAN10022223	1.13
L5JTD4	Tetraspanin. GN=PAL_GLEAN10022498	1.12
L5L2X8	Poly [ADP-ribose] polymerase 9. GN=PAL_GLEAN10006544	1.11
L5KN22	Zinc finger protein 234. GN=PAL_GLEAN10003982	1.1

L5K6D8	Tetratricopeptide repeat protein 5. GN=PAL_GLEAN10001582	1.1
L5KSD2	Lysine-specific demethylase 2B (Fragment). GN=PAL_GLEAN10008843	1.08
L5K588	Transcription factor jun-B. GN=PAL_GLEAN10002775	1.06
L5KMD9	Zinc finger protein 283. GN=PAL_GLEAN10003980	1.06
L5L5U5	Keratin, type II cytoskeletal 2 oral. GN=KRT76	1.05
L5KWQ5	Liprin-alpha-4. GN=PAL_GLEAN10000794	1.03
L5JXG9	60S ribosomal protein L7a. GN=PAL_GLEAN10024146	1.03
L5K8D1	Tyrosine-protein kinase. GN=PAL_GLEAN10021049	1

Table 16. Cellular innate immune proteins increased ≥ 1 log2 fold in PaKiT universal IFN treated cells compared to mock cells and their functions. The functional descriptions are based on human homologs.

Host innate immune proteins	
Protein symbol	**Protein name and function**
IFIT1	Interferon Induced Protein with Tetratricopeptide Repeats 1. The human counterpart of IFIT1 disrupts viral replication by inhibiting the expression of viral mRNAs (185).
IFIT2	IFN-induced protein with tetratricopeptide repeats 2. The human counterpart of IFIT2 exhibits antiviral activity by inhibiting the expression of viral mRNA (182).
IFIT3	IFN-induced protein with tetratricopeptide repeats 3. The human counterpart of IFIT3 activates Mitochondrial antiviral signaling protein (MAVS) to promote IFN production (178).
ISG20	Interferon-stimulated gene 20 kDa protein. The human counterpart of ISG20 exhibits antiviral activity against RNA viruses by targeting viral replication and translation processes (186).
DDX58	DExD/H-Box Helicase 58 (RIG-I). The human counterpart of DDX58 senses viral nucleic acids and initiates anti-viral signaling cascades leading to the production of interferons and proinflammatory cytokines (188).
ISG15	Ubiquitin-like protein ISG15. The human counterpart of ISG15 plays a vital role in the innate immune response to viral infections either via its conjugation to a target protein such as IFIT1, MX1/MxA (ISGylation) or as

	an unconjugated protein (189). ISGylation of viral sensors stimulates the innate immune response against a wide range of RNA viruses (190).
MX1	Interferon-induced GTP-binding protein Mx1. The human counterpart of Mx1 possesses a potent antiviral activity by targeting viral ribonucleocapsid or nucleoprotein synthesis (193).
ZNFX1	Zinc Finger NFX1-Type Containing 1. The human counterpart of ZNFX1 acts as a cellular sensor that sense viral dsRNA to initiate the antiviral response signaling cascades to restrict viral replication (194).
DTX3L	E3 ubiquitin-protein ligase DTX3L.The human counterpart of DTX3L plays a role in interferon-mediated antiviral responses in association with host protein PARP9 (195).
ZC3H12A	Zinc finger CCCH-type containing 12A. The human counterpart of ZC3H12A endoribonuclease is proposed to have a role in the suppression of viral infections in association with host protein MCPIP1(196).
TNFSF10	Tumor necrosis factor ligand superfamily member 10. The human counterpart of TNFSF10 is involved in immune surveillance against virus-infected cells by inducing apoptosis (197).
IRF7	Interferon Regulatory Factor 7. The human counterpart of IRF7 has an indispensable role in the innate immune response against viral infections. It regulates the transcription of type I IFN and IFN-stimulated genes (ISGs).
IFIH1	Interferon-induced helicase C domain-containing protein 1 (MDA-5). The human counterpart of (MDA-5) is a cytoplasmic sensor of viral dsRNA. It plays an essential role in activating IFNs and proinflammatory cytokines signaling pathways. (185)
IFIGBP	Interferon-induced guanylate-binding protein 1. The human counterpart of IFIGBP has anti-viral activities against multiple RNA viruses (174).
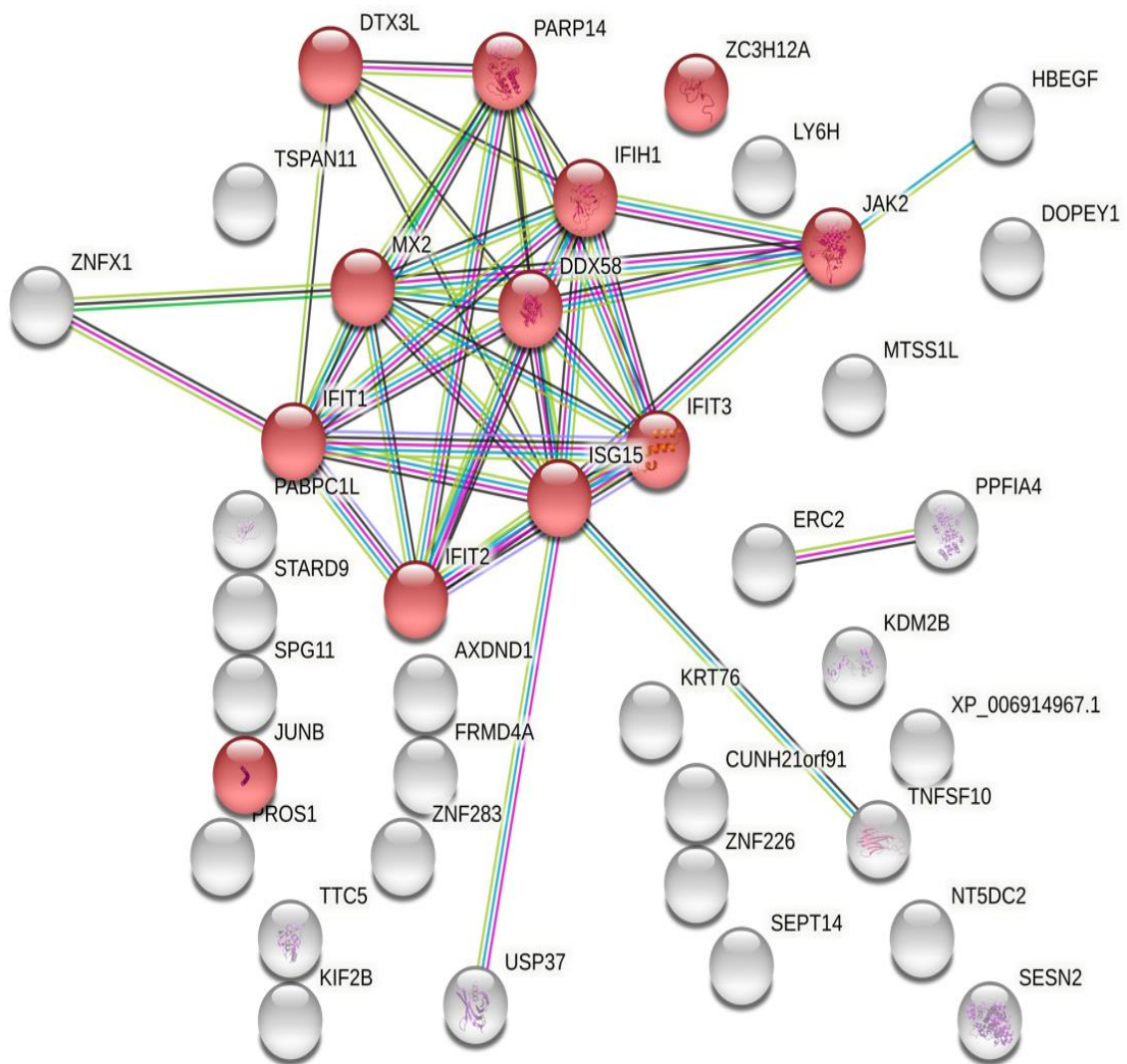
Figure 20.STRING analysis of proteins that increased ≥ 1 log2 fold in PaKiT IFN treated cells. The STRING database was searched to analyze host proteins that showed a ≥ 1 log2 fold increase in PaKiT IFN treated cells compared to mock cells. Nodes representing proteins that most significantly enriched the GO term. Proteins involved in innate immune response process are shaded in red.

3.2.3.6 Host proteins decreased in PaKiT IFN-treated cells compared to mock cells

Nineteen proteins were ≥ 1 log2 fold decreased in PaKiT IFN treated cells compared to mock cells (Table 17). These proteins were analyzed by STRING analysis to reveal their specific host pathways. The analysis showed significant enrichment of human-counterparts proteins expressed in the digestive gland and urinary system (Figure 20).

Table 17. Cellular proteins decreased ≥ 1 log2 fold in PaKiT universal IFN treated cells compared to mock cells. Proteins' IDs and names are obtained from UniProt: the universal protein knowledgebase in 2021.

Uniport ID	Protein name & Gene symbol	IFN-treated cells /Mock log2-fold change average
L5KGV6	V-type proton ATPase subunit S1. GN=PAL_GLEAN10001437	-2.11
L5KBY1	Elongation factor 1-alpha 1. GN=PAL_GLEAN10003084	-1.66
L5JYV3	60S ribosomal protein L27a.GN=PAL_GLEAN10016140	-1.62
L5K5Z4	Centromere protein R. GN=PAL_GLEAN10023825	-1.35
L5L1M5	Desmin. GN=PAL_GLEAN10014391	-1.32
L5L828	Guanine nucleotide-binding protein G(I)/G(S)/G(T) subunit beta-1. GN=PAL_GLEAN10001823	-1.29
L5KW95	Long-chain specific acyl-CoA dehydrogenase, mitochondrial. GN=PAL_GLEAN10008656	-1.21
L5JY72	Sequestosome-1. GN=PAL_GLEAN10016992	-1.19
L5KRQ2	Ferritin. GN=PAL_GLEAN10011491	-1.18
L5L6V3	FCH domain only protein 1 (Fragment). GN=PAL_GLEAN10006663	-1.13
L5KBJ8	Sigma 1-type opioid receptor. GN=PAL_GLEAN10008271	-1.13
L5KRT5	Annexin A2. GN=PAL_GLEAN10000955	-1.11
L5KC97	60S ribosomal protein L35a. GN=PAL_GLEAN10003467	-1.08
L5KFE6	Proteasome assembly chaperone 3. GN=PAL_GLEAN10002669	-1.07
L5L1L9	Mothers against decapentaplegic homolog. GN=PAL_GLEAN10016624	-1.05

L5L8D1	Solute carrier family 2, facilitated glucose transporter member 1. GN=PAL_GLEAN10004399	-1.05
L5JWV1	Protein YIPF. GN=PAL_GLEAN10016704	-1.04
L5JXC6	Protein S100. GN=PAL_GLEAN10005524	-1.02
L5JYI6	Centrosome-associated protein CEP250. GN=PAL_GLEAN10024274	-0.99
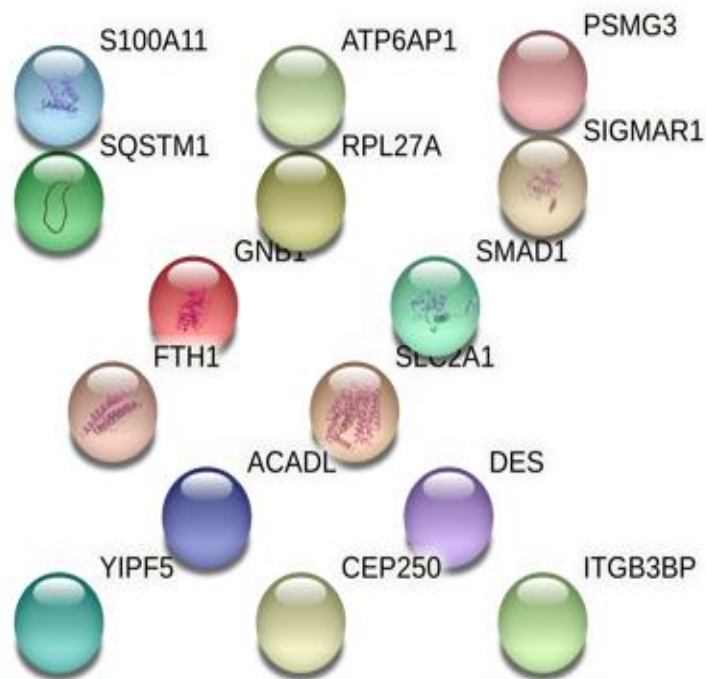
Figure 21. STRING analysis of proteins that decreased ≥ 1 log2 fold in PaKiT IFN cells. The STRING database was searched to analyze host proteins that showed a ≥ 1 log2 fold decrease in PaKiT IFN treated cells compared to mock cells. Nodes representing proteins that most significantly enriched the GO term.

3.2.3.7 Host proteins increased in PaKiT Poly: IC treated cells compared to mock cells

One hundred and two proteins were ≥ 1 log2 fold increased in PaKiT Poly: IC transfected cells compared to mock cells (Table 18). These proteins were analyzed by STRING analysis to reveal their specific host pathways (Figure 21). Interestingly, the analysis showed that very few (0.03%) of the up-regulated proteins are involved in innate immune response pathways, including only ISG15, IFIT2, and IFIT3 proteins (Table 19). The probable functions of bat proteins are based on homology to human proteins.

Table 18. **Cellular proteins increased ≥ 1 log2 fold in PaKiT Poly: IC transfected cells compared to mock cells. Proteins' IDs and names are obtained from UniProt: the universal protein knowledgebase in 2021.**

Uniport ID	Protein name & Gene ID	Poly: IC - treated cells /Mock log2-fold change average
L5KQL5	Annexin A2. GN=PAL_GLEAN10000956	6.64
L5K2K1	Thioredoxin. GN=PAL_GLEAN10017397	6.64
L5JR34	Zinc finger MYM-type protein 2. GN=PAL_GLEAN10000103	4.7
L5K642	AMP deaminase 1. GN=PAL_GLEAN10017431	4.44
L5L0Y4	60S ribosomal protein L28. GN=PAL_GLEAN10018798	4.25
L5KLA0	Purine nucleoside phosphorylase. GN=PAL_GLEAN10025016	3.93
L5KAE7	SH3 domain-binding glutamic acid-rich protein. GN=PAL_GLEAN10008411	3.79
L5KX02	Aldehyde dehydrogenase. GN=PAL_GLEAN10008598	3.64
L5L5U0	Keratin, type II cytoskeletal 78. GN=PAL_GLEAN10005078	3.48
L5KKC0	Phosphoenolpyruvate carboxykinase [GTP], mitochondrial. GN=PAL_GLEAN10002523	3.47
L5JWD3	Beta-enolase. GN=PAL_GLEAN10010127	3.34
L5L4I8	Neurofilament heavy polypeptide. GN=PAL_GLEAN10007920	3.28
L5KF09	Thymosin beta-4. GN=PAL_GLEAN10007819	2.98
L5JWH0	Heat shock protein HSP 90-alpha. GN=PAL_GLEAN10001135	2.82
L5L200	Paralemmin-2. GN=PAL_GLEAN10009411	2.82
L5KLW9	Protein dpy-19 like protein 1. GN=PAL_GLEAN10021914	2.73

L5K4S7	Spatacsin. GN=PAL_GLEAN10023533	2.64
L5JXG5	Myosin regulatory light polypeptide 9. GN=PAL_GLEAN10024294	2.3
L5KNK8	Fos-related antigen 1. GN=PAL_GLEAN10011352	2.24
L5L0T8	GrpE protein like protein 2, mitochondrial. GN=PAL_GLEAN10018738	2.21
L5JTA2	High mobility group nucleosome-binding domain-containing protein 4. GN=PAL_GLEAN10005249	2.19
L5KAX1	Cullin-associated NEDD8-dissociated protein 2. GN=PAL_GLEAN10022309	2.07
L5K588	Transcription factor jun-B.GN=PAL_GLEAN10002775	1.99
L5JRD4	Peptidylprolyl isomerase .GN=PAL_GLEAN10019546	1.93
L5K2H9	Nebulin-related-anchoring protein. GN=PAL_GLEAN10014175	1.86
L5KL54	Plastin-2 . GN=PAL_GLEAN10001106	1.85
L5JSA4	Latent-transforming growth factor beta-binding protein 2. GN=PAL_GLEAN10020649	1.8
L5KL89	Ras-related protein Rab-37. GN=PAL_GLEAN10014765	1.7
L5JNT3	Autophagy protein 5. GN=PAL_GLEAN10018553 =	1.65
L5KUU0	Lysine-specific histone demethylase 1B.GN=PAL_GLEAN10016417	1.63
L5JWI8	Protein S100-A7. GN=PAL_GLEAN10005499	1.61
L5K8H1	ERC protein 2. GN=PAL_GLEAN10022192	1.58
L5K2E8	StAR-related lipid transfer protein 9. GN=PAL_GLEAN10023569	1.54
L5JU57	Protein S100. GN=PAL_GLEAN10005505	1.54
L5KMD9	Zinc finger protein 283. GN=PAL_GLEAN10003980	1.53
L5JV97	Poly(A) RNA polymerase, mitochondrial. GN=PAL_GLEAN10005150	1.52
L5KZN8	Zinc transporter SLC39A7. GN=PAL_GLEAN10007109	1.52
L5KER5	Septin-5. GN=PAL_GLEAN10007698	1.51
L5KFB7	IQ domain-containing protein E. GN=PAL_GLEAN10002622	1.49
L5KTG2	DNA polymerase epsilon catalytic subunit. GN=PAL_GLEAN10008698	1.47
L5JPT0	Interferon-induced protein with tetratricopeptide repeat 2. GN=PAL_GLEAN10018384	1.45
L5KSY3	Elastin microfibril interfacer 1. GN=PAL_GLEAN10020247	1.45
L5JXN7	Polyadenylate-binding protein. GN=PAL_GLEAN10024380	1.43
L5JMY5	Protein dopey-1. GN=PAL_GLEAN10025212	1.43
L5K810	LIM and cysteine-rich domains protein 1. GN=PAL_GLEAN10022247	1.42
L5K5D6	Na(+)/H(+) exchange regulatory cofactor NHE-RF3. GN=PAL_GLEAN10017495	1.42

L5JQB4	Interferon-induced protein with tetratricopeptide repeat 3. GN=PAL_GLEAN10018383	1.41
L5JU10	Ribonuclease ZC3H12A GN=PAL_GLEAN10014935	1.41
L5K0G3	m-AAA protease-interacting protein 1, mitochondrial. GN=PAL_GLEAN10026101	1.41
L5KZH3	PDZ domain-containing protein 2.GN=PAL_GLEAN10014082	1.41
L5JW17	Histone H1.3 GN=PAL_GLEAN10005256	1.4
L5JTS7	Kinesin-like protein. GN=PAL_GLEAN10019747	1.36
L5JTZ2	Disintegrin and metalloproteinase domain-containing protein 15. GN=PAL_GLEAN10005429	1.36
L5KN22	Zinc finger protein 234. GN=PAL_GLEAN10003982	1.35
L5K7G3	Nuclear factor 1 X-type. GN=PAL_GLEAN10002793	1.35
L5K382	Histone H2B .GN=PAL_GLEAN10017518 PE=3 SV=1	1.31
L5L093	Retinol-binding protein 1. GN=PAL_GLEAN10015930	1.31
L5KYQ9	High mobility group protein HMG-I/HMG-Y. GN=PAL_GLEAN10007082	1.29
L5L743	Ubiquitin cross-reactive protein. GN=PAL_GLEAN10001765	1.26
L5JR19	Roundabout like protein 1. GN=PAL_GLEAN10016377	1.26
L5KWI0	5-aminolevulinate synthase. GN=PAL_GLEAN10009271	1.25
L5KR89	Fatty acid desaturase 3. GN=PAL_GLEAN10011494	1.25
L5JTD4	Tetraspanin. GN=PAL_GLEAN10022498	1.23
L5KUN8	Proteasome subunit beta. GN=PAL_GLEAN10016251	1.23
L5L851	Protein capicua like protein. GN=PAL_GLEAN10000970	1.23
L5KX82	Guanine nucleotide-binding protein G(O) subunit alpha. GN=PAL_GLEAN10011048	1.23
L5KQP0	PDZ and LIM domain protein 5. GN=PAL_GLEAN10010934	1.22
L5KWQ5	Liprin-alpha-4. GN=PAL_GLEAN10000794	1.21
L5KCG4	Tropomyosin beta chain. GN=PAL_GLEAN10008239	1.21
L5JL92	Protein tyrosine phosphatase type IVA 1. GN=PAL_GLEAN10025280	1.21
L5JR65	Cysteine-rich protein 1. GN=PAL_GLEAN10020979	1.2
L5K657	Nuclear factor 1. GN=PAL_GLEAN10021022	1.19
L5JVE3	Proheparin-binding EGF-like growth factor. GN=PAL_GLEAN10016791	1.17
L5KUU1	MTSS1-like protein. GN=PAL_GLEAN10016319	1.17
L5KEY8	Galectin .GN=PAL_GLEAN10002077 PE=4 SV=1	1.16
L5L3K6	Hepatoma-derived growth factor-related protein 3. GN=PAL_GLEAN10009544	1.14

L5JUK2	Histone-lysine N-methyltransferase, H3 lysine-36 and H4 lysine-20 specific (Fragment). GN=PAL_GLEAN10016940	1.13
L5L6X5	Single-stranded DNA-binding protein 4. GN=PAL_GLEAN10006688	1.12
L5JMU2	Connective tissue growth factor .GN=PAL_GLEAN10018714 PE=4 SV=1	1.12
L5KHT4	Disks large-associated protein 2. GN=PAL_GLEAN10015377	1.1
L5K8R0	Leucine-rich repeat serine/threonine-protein kinase 2. GN=PAL_GLEAN10002696	1.09
L5K1C2	Transcription initiation factor TFIID subunit 7. GN=PAL_GLEAN10002206	1.08
L5JU04	Pre-B-cell leukemia transcription factor-interacting protein 1. GN=PAL_GLEAN10005441	1.07
L5KYF7	axonemal dynein light chain domain-containing protein 1 isoform X3. GN=PAL_GLEAN10017721	1.06
L5JW28	Histone H1.3. GN=PAL_GLEAN10005266	1.06
L5KZJ7	Progressive ankylosis protein like protein. GN=PAL_GLEAN10014116	1.06
L5JWV6	Ubiquitin carboxyl-terminal hydrolase. GN=PAL_GLEAN10002727	1.05
L5KF03	Putative leucyl-tRNA synthetase, mitochondrial. GN=PAL_GLEAN10007813	1.05
L5JXG9	60S ribosomal protein L7a. GN=PAL_GLEAN10024146	1.04
L5JWU0	Ankyrin repeat domain-containing protein 13A. GN=PAL_GLEAN10002708	1.04
L5KYV4	Plastin-3. GN=PAL_GLEAN10000624	1.04
L5KLN7	Lymphocyte antigen 6H. GN=PAL_GLEAN10010433	1.03
L5K1L8	MHD domain-containing death-inducing protein. GN=PAL_GLEAN10023258	1.03
L5KY95	BMP-2-inducible protein kinase. GN=PAL_GLEAN10012273	1.03
L5JV72	Astrocytic phosphoprotein PEA-15. GN=PAL_GLEAN10006994	1.02
L5KD84	Syntaxin-11. GN=PAL_GLEAN10014008	1.02
L5KHJ9	Histone H1.0. GN=PAL_GLEAN10002073	1.02
L5KTF5	Butyrate response factor 2. GN=PAL_GLEAN10021302	1.02
L5KE13	Pleckstrin like proteiny domain-containing family A member 2. GN=PAL_GLEAN10021562	1.02
L5L6Y8	Zinc finger protein 324A. GN=PAL_GLEAN10000666	1.01
L5KCJ3	Lebercilin-like protein GN=PAL_GLEAN10008412	0.99
L5KKW4	Histone H2A GN=PAL_GLEAN10015638	0.99

Table 19. Host innate immune proteins increased ≥ 1 log2 fold in PaKiT Poly: IC transfected cells compared to mock cells and their functions. The functional descriptions are based on human homologs.

Host innate immune proteins	
Protein symbol	**Protein name and function**
ISG15	Ubiquitin-like protein ISG15. The human counterpart of ISG15 plays a vital role in the innate immune response to viral infections either via its conjugation to a target protein such as IFIT1, MX1/MxA (ISGylation) or as an unconjugated protein (189). ISGylation of viral sensors stimulates the innate immune response against a wide range of RNA viruses (190).
IFIT2	IFN-induced protein with tetratricopeptide repeats 2. The human counterpart of IFIT2 exhibits antiviral activity by inhibiting the expression of viral mRNA (182).
IFIT3	IFN-induced protein with tetratricopeptide repeats 3. The human counterpart of IFIT3 activates Mitochondrial antiviral signaling protein (MAVS) to promote IFN production (178).

Figure 22. STRING analysis of proteins that increased ≥ 1 log2 fold in PaKiT Poly: IC treated cells. The STRING database was searched to analyze host proteins that showed a ≥ 1 log2 fold increase in Pakit Poly: IC transfected cells compared to mock cells. Nodes representing proteins that most significantly enriched the GO term. Proteins involved in innate immune response process are shaded in red.

3.2.3.8 Host proteins decreased in PaKiT Poly: IC treated cells compared to mock cells

Seventy-nine proteins were ≥ 1 log2 fold decreased in Pakit Poly: IC transfected cells (Table 20). These proteins were analyzed by STRING analysis to reveal their specific host pathways (Figure. 22). The analysis showed significant enrichment of proteins involved in complement and coagulation cascades and complement activation process, e.g., complement factor B, Kininogen-1, Coagulation factor ix, ITIH2, and ITIH (196); and proteins involved in iron homeostases, e.g., Ferritin heavy chain, Ferritin light chain, Transmembrane protein 199, and V-type proton ATPase subunit S1 (197)(198). The probable functions of proteins are based on homology to human proteins.

Table 20. Cellular proteins decreased ≥ 1 log2 fold in PaKiT Poly: IC transfected cells compared to mock cells. Proteins' IDs and names are obtained from UniProt: the universal protein knowledgebase in 2021.

Uniport ID	Protein name & Gene ID	Poly: IC - treated cells /Mock log2-fold change average
L5JMI8	Sialomucin core protein 24 .GN=PAL_GLEAN10018586 .	-2.29
L5L1M5	Desmin .GN=PAL_GLEAN10014391 PE=3 SV=1	-2.24
L5L1J2	Apolipoprotein D .GN=PAL_GLEAN10007388 PE=3 SV=1	-2.18
L5KGV6	V-type proton ATPase subunit S1 .GN=PAL_GLEAN10001437 .	-2.03
L5K5B4	Transthyretin .GN=PAL_GLEAN10023130 .	-1.98
L5KSA3	ATP-binding cassette sub-family G member 2 .GN=PAL_GLEAN10010911 .	-1.88
L5JSS2	Protein phosphatase 1H .GN=PAL_GLEAN10022331 .	-1.82
L5KAM2	Inter-alpha-trypsin inhibitor heavy chain H3 .GN=PAL_GLEAN10022216 .	-1.8
L5KLZ9	Protein-lysine 6-oxidase .GN=PAL_GLEAN10025071 .	-1.78
L5KRQ2	Ferritin .GN=PAL_GLEAN10011491 .	-1.74
L5KZX2	Inter-alpha-trypsin inhibitor heavy chain H2 .GN=PAL_GLEAN10015769 .	-1.71
L5L473	Leucine-rich repeat-containing protein 58 .GN=PAL_GLEAN10006522 .	-1.7
L5KRQ1	Cysteine-rich motor neuron 1 protein .GN=PAL_GLEAN10020328 .	-1.68

L5KXA2	ADP-ribosylation factor-like protein 2-binding protein .GN=PAL_GLEAN10011075 .	-1.68
L5JU59	Transmembrane protein 199 .GN=PAL_GLEAN10019924 .	-1.64
L5JX46	Translation factor GUF1, mitochondrial .GN=GUF1 .	-1.61
L5KXB5	Kinesin-like protein .GN=PAL_GLEAN10011098 .	-1.59
L5JUP8	Coagulation factor IX .GN=PAL_GLEAN10007722 .	-1.58
L5L2R4	Suppressor of tumorigenicity protein 14 .GN=PAL_GLEAN10006573 .	-1.56
L5KVD7	Bardet-Biedl syndrome 2 protein homolog .GN=PAL_GLEAN10011059 .	-1.56
L5KIU0	Thrombospondin-4 .GN=PAL_GLEAN10024937 .	-1.55
L5K6K8	Nephronectin .GN=PAL_GLEAN10022589.	-1.54
L5K4R6	Protein Hook like protein 2 .GN=PAL_GLEAN10002774 .	-1.53
L5KVU4	Ileal sodium/bile acid cotransporter .GN=PAL_GLEAN10013739.	-1.53
L5KC34	Integral membrane protein 2B .GN=PAL_GLEAN10021708.	-1.44
L5JYV3	60S ribosomal protein L27a .GN=PAL_GLEAN10016140 .	-1.38
L5K5N7	Receptor-type tyrosine-protein phosphatase delta .GN=PAL_GLEAN10021030.	-1.36
L5JMZ8	Kininogen-1 .GN=PAL_GLEAN10018223.	-1.35
L5KV82	tRNA (guanine-N (7)-)-methyltransferase .GN=METTL1 .	-1.34
L5JUE3	Protein FAM101B .GN=PAL_GLEAN10019997.	-1.3
L5KD94	Amphoterin-induced protein 2 .GN=PAL_GLEAN10010033.	-1.29
L5KBY1	Elongation factor 1-alpha 1 .GN=PAL_GLEAN10003084.	-1.28
L5KZG9	Atrial natriuretic peptide clearance receptor .GN=PAL_GLEAN10014077.	-1.27
L5K5Z4	Centromere protein R .GN=PAL_GLEAN10023825.	-1.27
L5L5B8	Complement factor B .GN=PAL_GLEAN10001065.	-1.26
L5K5V2	Sortilin .GN=PAL_GLEAN10017351.	-1.26
L5KLR6	Sorting nexin-10 .GN=PAL_GLEAN10021846.	-1.25
L5K7A3	Keratin, type II cytoskeletal 8 .GN=PAL_GLEAN10023973.	-1.21
L5KDN2	Angiopoietin-1 .GN=PAL_GLEAN10021439.	-1.21
L5L4J6	Ferritin .GN=PAL_GLEAN10004572.	-1.2
L5L0M0	Secreted protein, acidic, cysteine-rich (Osteonectin) .GN=PAL_GLEAN10018783.	-1.19
L5KI66	Alpha-2-macroglobulin .GN=PAL_GLEAN10015609.	-1.18
L5KAY5	Tetratricopeptide repeat protein 3 .GN=PAL_GLEAN10008435.	-1.18
L5K157	WAP four-disulfide core domain protein 2 .GN=PAL_GLEAN10024395.	-1.18
L5JZK1	Interferon-alpha/beta receptor beta chain .GN=PAL_GLEAN10025736.	-1.18

L5K630	Phosphorylase b kinase gamma catalytic chain, skeletal muscle isoform .GN=PAL_GLEAN10011947.	-1.18
L5JVW8	U3 small nucleolar ribonucleoprotein IMP4 .GN=PAL_GLEAN10022551 .	-1.15
L5KC97	60S ribosomal protein L35a .GN=PAL_GLEAN10003467.	-1.14
L5JPL3	Ephrin type-A receptor 7 .GN=PAL_GLEAN10025158.	-1.12
L5JM97	G patch domain-containing protein 1 .GN=PAL_GLEAN10025691.	-1.11
L5K529	Sodium-dependent phosphate transport protein 2B .GN=PAL_GLEAN10022651.	-1.1
L5KW95	Long-chain specific acyl-CoA dehydrogenase, mitochondrial .GN=PAL_GLEAN10008656.	-1.1
L5L6E7	Keratin, type I cytoskeletal 18 .GN=PAL_GLEAN10005076.	-1.09
L5KA80	Angiopoietin-1 .GN=PAL_GLEAN10021440.	-1.08
L5KPB5	Neuropilin .GN=PAL_GLEAN10003729.	-1.08
L5KVU6	2-methoxy-6-polyprenyl-1,4-benzoquinol methylase, mitochondrial .GN=COQ5 .	-1.08
L5K3R7	Retinal dehydrogenase 2 .GN=PAL_GLEAN10023433 .	-1.08
L5KQA6	Autophagy-related protein 2 like protein A .GN=PAL_GLEAN10011403 .	-1.07
L5KCN5	E3 SUMO-protein ligase NSE2 .GN=PAL_GLEAN10021368 .	-1.07
L5KCI1	Melanoma-associated antigen D1 .GN=PAL_GLEAN10000503 .	-1.06
L5K106	Nidogen-2 .GN=PAL_GLEAN10023304 .	-1.06
L5K4C0	Alpha-adducin .GN=PAL_GLEAN10022890 .	-1.06
L5K9A5	Fibulin-1 .GN=PAL_GLEAN10007147 .	-1.06
L5KU39	Cadherin-5 .GN=PAL_GLEAN10016188 .	-1.05
L5JYJ2	Pituitary tumor-transforming protein 1 protein-interacting protein .GN=PAL_GLEAN10002937 .	-1.05
L5K8Y0	Inter-alpha-trypsin inhibitor heavy chain H1 .GN=PAL_GLEAN10022217 .	-1.04
L5KYL1	Elongation factor 1-alpha .GN=PAL_GLEAN10013774 .	-1.04
L5KJ12	E3 ubiquitin-protein ligase Praja2 .GN=PAL_GLEAN10025021 .	-1.04
L5KLU7	Zinc transporter ZIP4 .GN=PAL_GLEAN10010497 PE=1 SV=1	-1.04
L5KWP1	Chromodomain-helicase-DNA-binding protein 9 .GN=PAL_GLEAN10011027 .	-1.04
L5L6V6	Keratin, type II cytoskeletal 8 .GN=PAL_GLEAN10005077 .	-1.03
L5KXN3	Amyloid beta A4 protein .GN=PAL_GLEAN10018500 .	-1.03
L5KM74	Protein PTHB1 .GN=PAL_GLEAN10021909 .	-1.02
L5KKS0	Glyoxylate reductase .GN=PAL_GLEAN10017258 .	-1.02

L5K7J6	E3 ubiquitin-protein ligase RNF181 .GN=PAL_GLEAN10005181 .	-1.01
L5KVV9	Coiled-coil-helix-coiled-coil-helix domain-containing protein 10, mitochondrial .GN=PAL_GLEAN10010858 .	-1.01
L5JQE7	Metalloreductase STEAP2 .GN=PAL_GLEAN10013625 .	-1
L5KI65	Fibroblast growth factor receptor OS=Pteropus alecto OX=9402 GN=PAL_GLEAN10003442 PE=3 SV=1	-0.99
L5K637	Olfactomedin-like protein 3 OS=Pteropus alecto OX=9402 GN=PAL_GLEAN10017425 PE=4 SV=1	-0.99
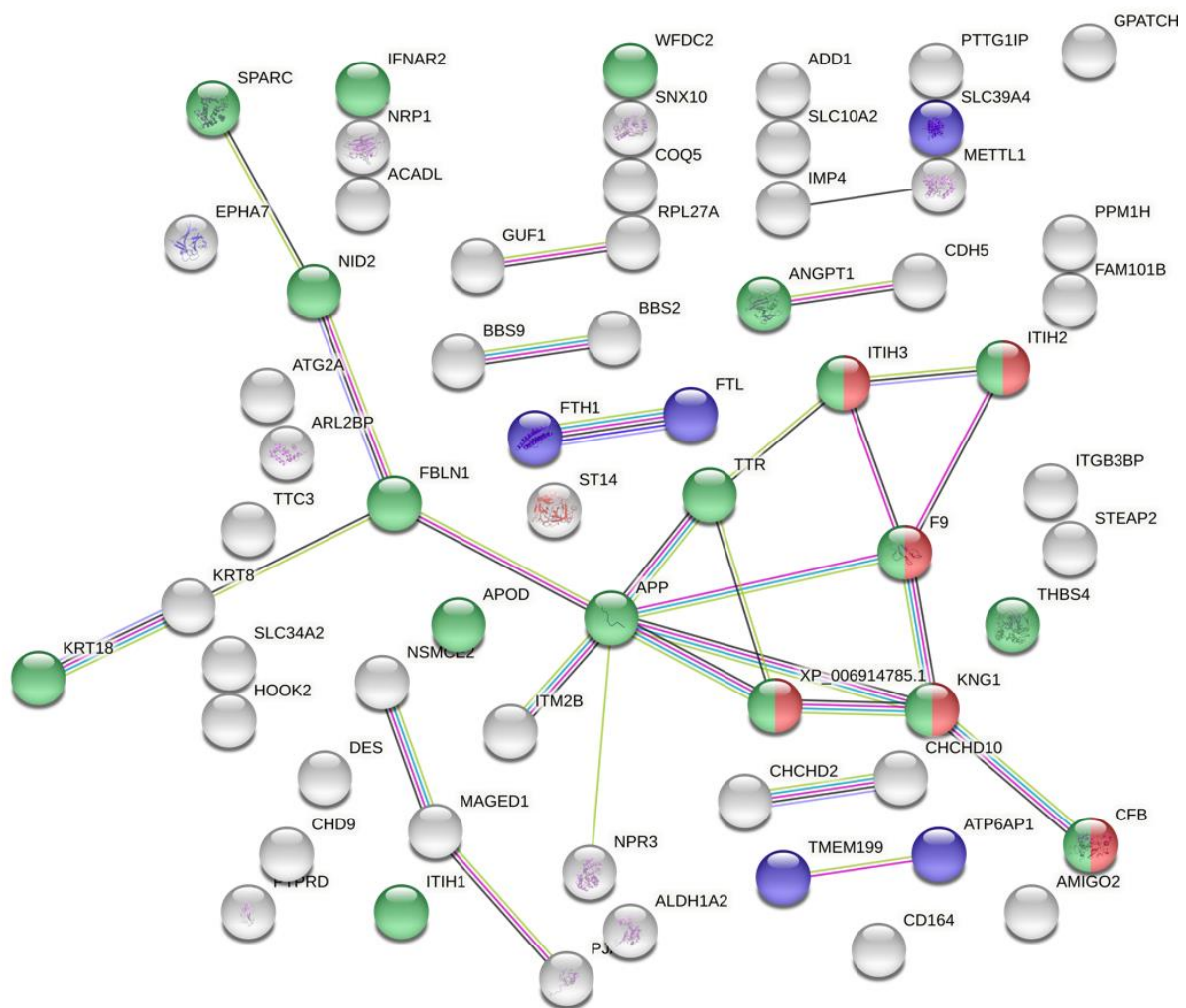
Figure 23. STRING analysis of proteins decreased ≥ 1 log2 fold in PaKiT Poly: IC transfected cells. The STRING database was searched to analyze host proteins that showed a ≥ 1 log2 fold decrease in Pakit Poly: IC transfected cells compared to mock cells. Nodes representing proteins that most significantly enriched the GO term. Proteins involved in regulating iron homeostasis are shaded in blue. Proteins involved in complement and coagulation cascades and complement activation are colored in red. Proteins localized in the cell's extracellular region are shaded in green.

3.2.3.9 Host protein increased in Duba IFN treated cells compared to mock cells

Forty-seven proteins were ≥ 1 log2 fold upregulated in Dubca IFN-treated cells compared to mock cells (Table 21). These proteins were analyzed by STRING analysis to reveal their specific host pathways (Figure 23). The analysis showed significant enrichment of proteins involved in the innate immune response (Table 22). The probable functions of proteins are based on homology to human proteins. Five up-regulated proteins in Dubca IFN-treated cells are shared with up-regulated proteins in MRC-5 and PaKiT IFN-treated cells (26 Figure). Surprisingly, no proteins were ≥ 1 log2 decreased in Dubca IFN-treated cells compared with mock cells.

Table 21. Cellular proteins increased ≥ 1 log2 fold in Dubca universal IFN treated cells compared to mock cells. Proteins' IDs and names are obtained from UniProt: the universal protein knowledgebase in 2021.

Uniport ID	Protein name & Gene ID	IFN-treated cells /Mock log2-fold change average
A0A4U5SAU6	C-C motif chemokine (CCL5) .GN=Cadr_00020015 .	6.64
A0A4U5SPV1	interferon-induced protein with tetratricopeptide repeats 3 .GN=Cadr_00009369 .	4.14
A0A4U5SFF6	Interferon-induced protein 44 .GN=Cadr_00015917 .	3.41
A0A5N4DJ57	Interferon-induced protein with tetratricopeptide repeats 2 .GN=Cadr_00009370 .	3.29
A0A4U5RYV5	Z-DNA-binding protein 1 .GN=Cadr_00021855 .	2.98
A0A4U5RV52	tumor necrosis factor ligand superfamily member 18 .GN=Cadr_00025204 .	2.56
A0A4U5TH50	Interferon regulatory factor 1 .GN=Cadr_00004357 .	2.47
A0A5N4DCR2	Interferon-induced protein 44-like .GN=Cadr_00015916 .	2.38
A0A4U5SFP6	Ubiquitin-like protein ISG15 .GN=Cadr_00014749 .	2.32
A0A4U5RH84	2'-5'-oligoadenylate synthase-like protein .GN=Cadr_00028519 .	2.24
A0A4U5RX67	Gamma-interferon-inducible protein 16 .GN=Cadr_00024995 .	2.23
A0A4U5TK63	Dynamin-type G domain-containing protein .GN=Cadr_00001216 .	2.2
A0A4U5SM34	Interferon-induced protein with tetratricopeptide repeats 1 .GN=Cadr_00009368 .	2.19
A0A4U5T9X3	interferon-induced helicase C domain-containing protein 1 .GN=Cadr_00006935 .	2.09

A0A4U5SKU1	Apolipoprotein L3 .GN=Cadr_00017877 .	2.09
A0A4V6XXS0	Elp3 domain-containing protein .GN=Cadr_00018225 .	2.07
A0A4U5TKB7	GED domain-containing protein .GN=Cadr_00001217 .	1.89
A0A5N4E949	ripartite motif-containing protein 14 .GN=Cadr_00016643 .	1.69
A0A4U5RE88	Helicase ATP-binding domain-containing protein .GN=Cadr_00029504 .	1.69
A0A4U5T2S9	SAM domain-containing protein .GN=Cadr_00008023 .	1.63
A0A4U5R7P2	probable ATP-dependent RNA helicase DDX58 .GN=Cadr_00030630 .	1.61
A0A4V6AJF8	IRF tryptophan pentad repeat domain-containing protein .GN=Cadr_00005833 .	1.61
A0A4U5THV8	HECT domain-containing protein .GN=Cadr_00002023 .	1.58
A0A4U5RSC8	bone marrow stromal antigen 2 .GN=Cadr_00026183 .	1.49
A0A4U5SG98	Inhibitor_Mig-6 domain-containing protein .GN=Cadr_00014904 .	1.47
A0A4U5RH50	25A_SYNTH_3 domain-containing protein .GN=Cadr_00028522 .	1.46
A0A4U5TL86	Poly [ADP-ribose] polymerase .GN=Cadr_00000740 .	1.38
A0A4U5SHU5	GB1/RHD3-type G domain-containing protein (Fragment) .GN=Cadr_00015995 .	1.29
A0A4U5SHB6	RBR-type E3 ubiquitin transferase .GN=Cadr_00015314 .	1.29
A0A4U5TLD0	RING-type domain-containing protein .GN=Cadr_00000742 .	1.24
A0A4V6ADR1	25A_SYNTH_3 domain-containing protein .GN=Cadr_00028520 .	1.22
A0A4U5SGW6	GBP_C domain-containing protein .GN=Cadr_00015997 .	1.2
A0A4U5TK96	GED domain-containing protein .GN=Cadr_00001218 .	1.18
A0A4U5SHT6	GB1/RHD3-type G domain-containing protein .GN=Cadr_00015999 .	1.16
A0A4U5RZN9	NFX1-type zinc finger-containing protein 1 .GN=Cadr_00021780 .	1.14
A0A4U5R7A3	Mab-21 domain-containing protein .GN=Cadr_00030966 .	1.14
A0A4U5SZY1	Macrophage colony-stimulating factor 1 .GN=Cadr_00012348 .	1.14
A0A4U5SGZ5	Uncharacterized protein .GN=Cadr_00016002 .	1.13
A0A4U5RJ94	OAS1_C domain-containing protein .GN=Cadr_00028521 .	1.13
A0A4U5RPG3	BZIP domain-containing protein .GN=Cadr_00023710 .	1.12
A0A4U5SS01	E3 ubiquitin-protein ligase TRIM21 isoform X2 .GN=Cadr_00013767 .	1.09
A0A4V6AIV9	terminal nucleotidyltransferase 5A isoform X1 .GN=Cadr_00010676 .	1.05
A0A4U5R995	BTB domain-containing protein .GN=Cadr_00003217 .	1.02
A0A4U5SXV7	terminal nucleotidyltransferase 5A isoform X1 .GN=Cadr_00011883 .	1.01
A0A4U5R7H0	XIAP-associated factor 1 .GN=Cadr_00031375 .	1
A0A4U5SS64	UBIQUITIN_CONJUGAT_2 domain-containing protein .GN=Cadr_00013097 .	0.99

A0A4U5RI45	Unconventional myosin-Vb isoform X3 .GN=Cadr_00028067 .	0.99

Table 22. Innate immune proteins increased ≥ 1 log2 fold in Dubca universal IFN treated cells compared to mock cells and their functions. The functional descriptions are based on human homologs.

Host innate immune proteins	
Protein symbol	**Protein name and function**
IFIT1	Interferon-Induced Protein with Tetratricopeptide Repeats 1. The human counterpart of IFIT1 disrupts viral replication by inhibiting the expression of viral mRNAs (185).
IFIT2	IFN-induced protein with tetratricopeptide repeats 2. The human counterpart of IFIT2 exhibits antiviral activity by inhibiting the expression of viral mRNA (182).
IFIT3	IFN-induced protein with tetratricopeptide repeats 3. The human counterpart of IFIT3 activates Mitochondrial antiviral signaling protein (MAVS) to promote IFN production (178).
DDX58	Antiviral innate immune response receptor RIG-I. It is also known as RIG-I. Like MDA-5, It acts as a cytoplasmic sensor of viral dsRNA and plays a vital role in activating IFNs and proinflammatory cytokines signaling pathways (188).
ISG15	Ubiquitin-like protein ISG15. The human counterpart of ISG15 plays a vital role in the innate immune response to viral infections either via its conjugation to a target protein such as IFIT1, MX1/MxA (ISGylation) or as an unconjugated protein (189). ISGylation of viral sensors stimulates the innate immune response against a wide range of RNA viruses (190).
IFI44L	Interferon Induced Protein 44 Like. The human counterpart of IFI44L has a role in suppressing viral replication (199).
PARP14	Poly (ADP-Ribose) Polymerase Family Member 14. The human counterpart of PARP14 has a crucial role in interferon response to the SARS-CoV-2 infection and helps balance the pro-inflammatory cytokines storm during viral infection (197). It is required to transcription primary antiviral response genes regulated by the IRF3 (200).

OAS1	2'-5'-Oligoadenylate Synthetase 1. The human counterpart of OAS1 is dsRNA-activated antiviral enzyme that has an essential role in the cellular innate immune response against viral infections. It has been shown that the expression of prenylated OAS1 is associated with a reduced risk of severe COVID-19 disease (201).
OASL	2'-5'-Oligoadenylate Synthetase Like. The human counterpart of OASL enhances IFN signaling cascades and has a role in suppressing the replication of RNA viruses. (202)
TNFSF18	TNF Superfamily Member 18. The human counterpart of TNFSF18 has an essential role in modulating host immune response by trigging increased phosphorylation of STAT1 and mediates activation of NF-kappa-B (203).
TRIM14	Tripartite Motif Containing 14. The human counterpart of TRIM14 has a vital role in the innate immune defense against pathogens. It mediates the type I IFN production by activating the IFN regulatory factor IRF3 and NF-kappa-B pathways (204).
IFI16	Interferon Gamma Inducible Protein 16. The human counterpart of IFI16 is involved in the innate immune response by recognizing the viral genome and triggering IFN-β signaling pathway (205).
IRF1	Interferon Regulatory Factor 1. The human counterpart of IRF1 has a crucial role in inducing an innate immune response. It regulates IFN and IFN-inducible genes transcription during viral or bacterial infections (206).
CCL5	C-C Motif Chemokine Ligand 5. The human counterpart of CCL5 is a proinflammatory chemokine generated by virus-infected cells and attracts monocytes, T lymphocytes, and eosinophils to the site of infection. It has been shown that increased levels of CCL5 are associated with disease severity of RSV (207)
IFI44	Interferon Induced Protein 44. The human counterpart of IFI44 has been shown to have a role in suppressing the replication of RSV, Bunyamwera virus, and HIV-1 (208).
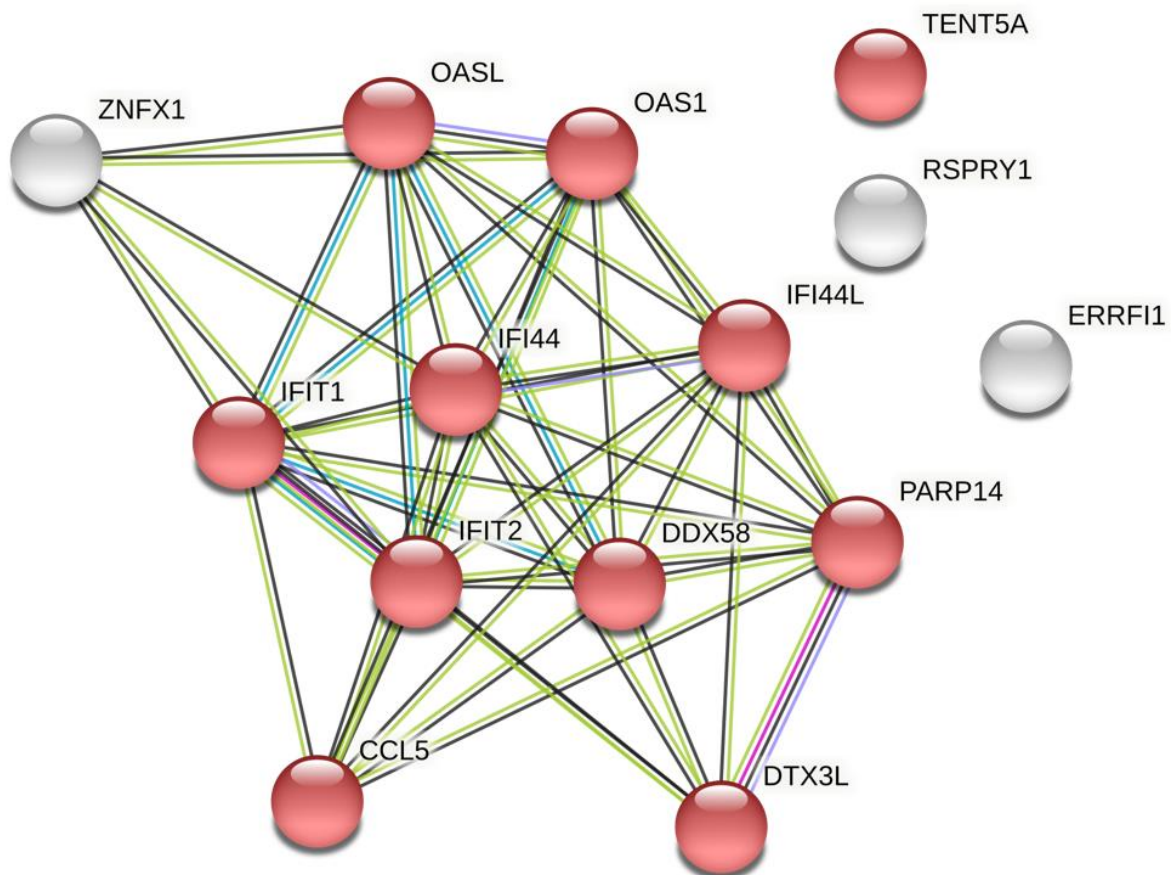
Figure 24. STRING analysis of proteins that increased ≥ 1 log2 fold in Dubca IFN treated cells. The STRING database was searched to analyze host proteins that showed a ≥ 1 log2 fold increase in Dubca IFN treated cells compared to mock cells. Nodes representing proteins that most significantly enriched the GO term. Proteins involved in innate immune response process are shaded in red.

3.2.3.10 Host proteins increased in Duba Poly: IC treated cells compared to mock cells

Fifty-two proteins were ≥ 1 log2 fold up-regulated In Dubca Poly: IC transfected cells compared to mock cells (Table 23). These proteins were analyzed by STRING analysis to reveal their specific host pathways (Figure 24). The analysis showed significant enrichment of proteins involved in the anti-viral innate immune response process (Table 24). The probable functions of bat proteins are based on homology to human proteins. Two up-regulated proteins are shared with up-regulated proteins in MRC-5 and PaKiT Poly: IC treated cells (27 Figure).

Table 23. Cellular proteins increased ≥ 1 log2 fold in Dubca Poly: IC transfected cells compared to mock cells. Proteins' IDs and names are obtained from UniProt: the universal protein knowledgebase in 2021.

Uniport ID	Protein name & Gene ID	Poly:IC treated cells /Mock log2-fold change average
A0A4U5SAU6	chemokine (C-C motif) ligand 5 (CCL5).GN=Cadr_00020015 .	6.64
A0A4U5S8U6	C-C motif chemokine 2 (CCL2).GN=Cadr_00019596 .	5.2
A0A4U5SPV1	interferon-induced protein with tetratricopeptide repeats 3 .GN=Cadr_00009369 PE=4 SV=1	4.57
A0A5N4DJ57	Interferon-induced protein with tetratricopeptide repeats 2 .GN=Cadr_00009370 PE=4 SV=1	4.49
A0A5N4EDC2	Interferon regulatory factor .GN=Cadr_00004357 .	3.78
A0A4U5SM34	Interferon-induced protein with tetratricopeptide repeats 1 .GN=Cadr_00009368 .	3.44
kab1260471	E-selectin .GN=Cadr_00025166 .	3.32
A0A4U5TJQ5	C-X-C motif chemokine 10 (CXCL10).GN=Cadr_00001916 .	2.88
A0A4U5T9X3	interferon-induced helicase C domain-containing protein 1 .GN=Cadr_00006935 .	2.82
A0A4U5SFP6	Ubiquitin-like protein ISG15 .GN=Cadr_00014749 .	2.82
A0A4U5RH84	2'-5'-oligoadenylate synthase-like protein .GN=Cadr_00028519 .	2.49
A0A4U5SFF6	Interferon-induced protein 44 .GN=Cadr_00015917 .	2.48
A0A4U5RGB8	Protein kinase domain-containing protein .GN=Cadr_00028539 .	2.28
A0A5N4EE58	Early growth response protein .GN=Cadr_00004264 .	2.28
A0A4U5SKR6	IF rod domain-containing protein .GN=Cadr_00017307 .	2.27
A0A4U5S3T0	TIP120 domain-containing protein .GN=Cadr_00021134 .	2.23

A0A4U5RYV5	Z-DNA-binding protein 1 .GN=Cadr_00021855 .	2.17
A0A4U5SHB6	RBR-type E3 ubiquitin transferase .GN=Cadr_00015314 .	2.11
A0A4U5RVJ1	Golgin-45 .GN=Cadr_00025159 .	2.08
A0A4U5S0B1	Syndecan .GN=Cadr_00021719 .	2.02
A0A4V6AKD8	3-hydroxy-3-methylglutaryl coenzyme A reductase .GN=Cadr_00004677 .	1.98
A0A4U5S7G8	DUF3338 domain-containing protein .GN=Cadr_00020993 .	1.95
A0A5N4CIV3	protein RD3 .GN=Cadr_00023725 .	1.83
A0A4U5RSC8	bone marrow stromal antigen 2 .GN=Cadr_00026183 .	1.79
A0A4U5TG89	EGF-like domain-containing protein .GN=Cadr_00004234 .	1.78
A0A4V6XXS0	Elp3 domain-containing protein .GN=Cadr_00018225 .	1.78
A0A4U5RJ25	CCAAT/enhancer-binding protein delta like .GN=Cadr_00027574 .	1.75
A0A4U5SXD0	mRNA decay activator protein ZFP36 .GN=Cadr_00010914 .	1.67
A0A4U5RS65	BZIP domain-containing protein .GN=Cadr_00026337 .	1.67
A0A4U5RCJ6	ADP-ribosylation factor-like protein 5B isoform X1 (Fragment) .GN=Cadr_00027172 .	1.66
A0A4U5SJP3	PH_15 domain-containing protein .GN=Cadr_00017794 .	1.56
A0A4U5SZ06	t-SNARE coiled-coil homology domain-containing protein .GN=Cadr_00010220 .	1.5
A0A4U5SKU1	Apolipoprotein L3 .GN=Cadr_00017877 .	1.49
A0A4U5SZY1	Macrophage colony-stimulating factor 1 .GN=Cadr_00012348 .	1.47
A0A4U5RS59	low-density lipoprotein receptor isoform X1 .GN=Cadr_00026430 .	1.44
A0A4U5RF58	PALP domain-containing protein .GN=Cadr_00028438 .	1.4
A0A4U5TJS4	Heat shock cognate 71 kDa protein .GN=Cadr_00001549 .	1.38
A0A4U5SCK5	mRNA decay activator protein ZFP36L2 .GN=Cadr_00018574 .	1.35
A0A4U5RPG3	BZIP domain-containing protein .GN=Cadr_00023710 .	1.33
A0A4U5SPU1	IF rod domain-containing protein .GN=Cadr_00009162 .	1.24
A0A4U5RKN5	Alpha-mann_mid domain-containing protein .GN=Cadr_00025770 .	1.17
A0A4U5RI31	BZIP domain-containing protein .GN=Cadr_00029918 .	1.16
A0A4U5SZD0	ensconsin isoform X5 .GN=Cadr_00010272 .	1.15
A0A4U5RE88	Helicase ATP-binding domain-containing protein .GN=Cadr_00029504 .	1.14
A0A4U5TK63	Dynamin-type G domain-containing protein .GN=Cadr_00001216 .	1.1
A0A4U5SFG1	TLDc domain-containing protein .GN=Cadr_00015916 .	1.09
A0A4U5THV8	HECT domain-containing protein .GN=Cadr_00002023 .	1.07

A0A4U5SHX1	IF rod domain-containing protein (Fragment) .GN=Cadr_00017292 .	1.06
A0A4U5RUX0	Protein kinase domain-containing protein .GN=Cadr_00024580 .	1.05
A0A4V6AJF8	IRF tryptophan pentad repeat domain-containing protein .GN=Cadr_00005833 .	1.05
A0A4U5RID8	BHLH domain-containing protein (Fragment) .GN=Cadr_00028028	1.02
A0A4U5RI45	Unconventional myosin-Vb isoform X3 .GN=Cadr_00028067 .	1

Table 24.Host innate immune proteins that were ≥ 1 log2 fold up-regulated in Dubca Poly: IC transfected cells compared to mock cells and their functions. The functional descriptions are based on human homologs.

Host innate immune proteins	
Protein symbol	**Protein name and function**
IFIT1	Interferon-Induced Protein with Tetratricopeptide Repeats 1. The human counterpart of IFIT1 disrupts viral replication by inhibiting the expression of viral mRNAs (185).
IFIT2	IFN-induced protein with tetratricopeptide repeats 2. The human counterpart of IFIT2 exhibits antiviral activity by inhibiting the expression of viral mRNA (182).
IFIT3	IFN-induced protein with tetratricopeptide repeats 3. The human counterpart of IFIT3 activates Mitochondrial antiviral signaling protein (MAVS) to promote IFN production (178).
ISG15	Ubiquitin-like protein ISG15. The human counterpart of ISG15 plays a vital role in the innate immune response to viral infections either via its conjugation to a target protein such as IFIT1, MX1/MxA (ISGylation) or as an unconjugated protein (189). ISGylation of viral sensors stimulates the innate immune response against a wide range of RNA viruses (190).
OASL	2'-5'-oligoadenylate synthase-like protein. The human counterpart of OASL functions in enhancing IFN signaling cascades and has a role in suppressing the replication of RNA viruses. (200)
IRF1	Interferon Regulatory Factor 1. The human counterpart of IRF1 has a crucial role in inducing innate immune responses. It regulates IFN and ISGs transcription during pathogens infections (206).

CCL5	Chemokine (C-C motif) ligand 5. The human counterpart of CCL5 is a proinflammatory chemokine generated by virus-infected cells and attracts monocytes, T lymphocytes, and eosinophils to the site of infection. It has been shown that increased levels of CCL5 are associated with disease severity of RSV infection (207)
CCL2	C-C Motif Chemokine Ligand 2. Elevated levels of CCL2 human counterpart are associated with higher viral load and increased severity of viral infections (209). Recently, it has been shown that the severity and high SARS-CoV-2 viral load were associated with low expression of CCL2 (210).
IFI44	Interferon Induced Protein 44. The human counterpart of IFI44 has been shown to have a role in suppressing the replication of RSV, Bunyamwera virus, and HIV-1 (208).
IFIH1	Interferon induced with helicase C domain 1. The human counterpart of IFIH1 (MDA-5) acts as a cytoplasmic sensor of viral dsRNA and plays a crucial role in activating IFNs and proinflammatory cytokines signaling pathways. (185)
CXCL10	C-X-C motif chemokine ligand 10. The human counterpart of CXCL10 is a pro-inflammatory cytokine that is expressed within tissues following viral infection. It contributes to lymphocyte activation, extravasation, and accumulation of virus-specific T cells within sites of infection (191)
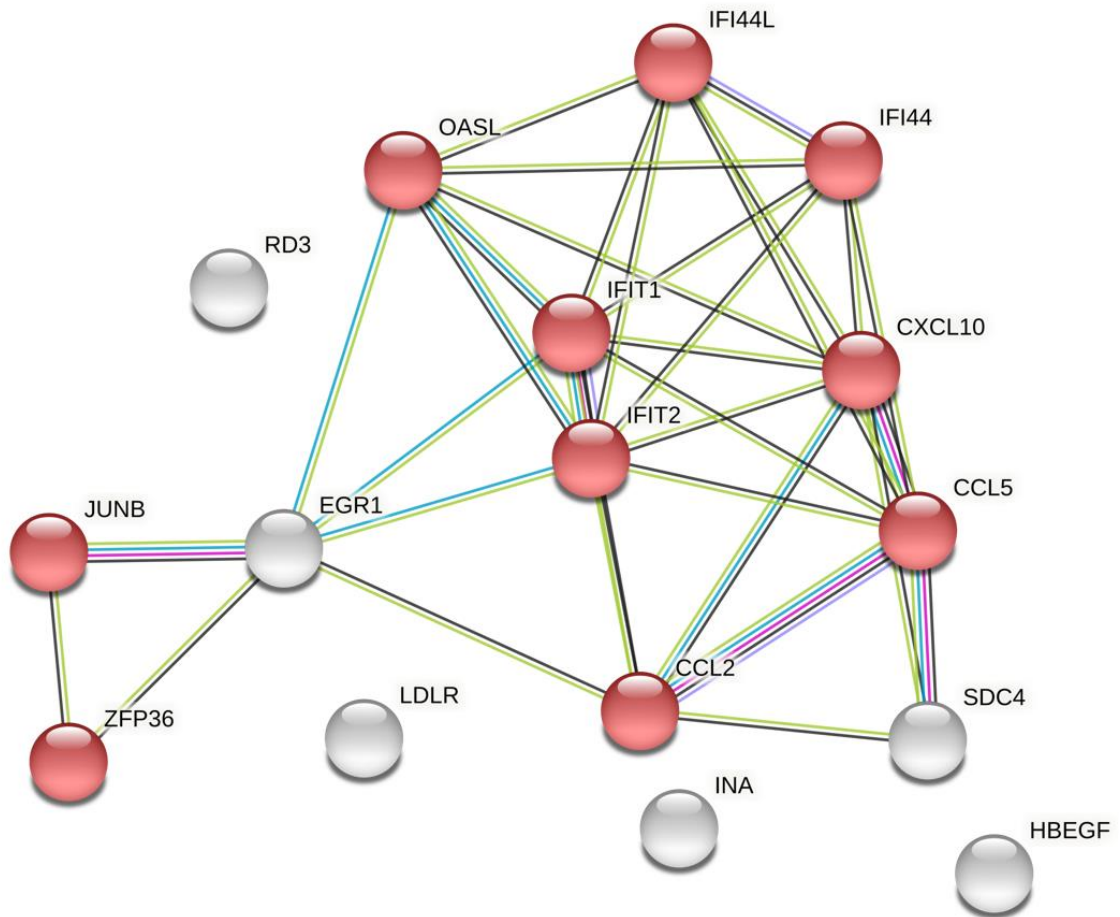
Figure 25.The STRING analysis of proteins increased ≥ 1 log2 fold in Dubca Poly: IC transfected cells. The STRING database was searched to analyze proteins that showed ≥ 1 log2 fold increase in Dubca Poly: IC transfected cells compared to mock cells. Nodes representing proteins that most significantly enriched the GO term. Proteins involved in innate immune response process are shaded in red.

3.2.3.11 Host protein decreased in Dubca Poly: IC treated cells compared to mock cells

Thirty-one proteins were ≥ 1 log2 fold down-regulated in Dubca Poly: IC transfected cells (Table 25). These proteins were analyzed by STRING analysis to reveal their specific host pathways. The analysis showed significant enrichment of proteins involved in the Complement System, such as C3/C5 convertase, complement C4-A, and complement component C6 (211) (Figure 25). The probable functions of proteins are based on homology to human proteins.

Table 25. Cellular proteins decreased ≥ 1 log2 fold in Dubca Poly: IC transfected cells compared to mock cells. Proteins' IDs and names are obtained from UniProt: the universal protein knowledgebase in 2021.

Uniport ID	Protein name & Gene ID	Poly:IC-treated cells /Mock log2-fold change average
A0A4U5SEV4	BHLH domain-containing protein.GN=Cadr_00015138 .	-1.99
A0A4U5TBP3	Fructose-bisphosphate aldolase.GN=Cadr_00016605 PE=3 SV=1	-1.68
A0A4U5RD60	protein TASOR 2 isoform X1.GN=Cadr_00027468 .	-1.62
A0A4U5RDN7	Pregnancy zone protein.GN=Cadr_00029632 .	-1.54
A0A4U5RQZ2	Transthyretin.GN=Cadr_00028823 .	-1.49
A0A4U5TIC2	Serum albumin protein.GN=Cadr_00001883 .	-1.38
A0A4V6AK78	ADAM_CR_2 domain-containing protein.GN=Cadr_00016105 .	-1.38
A0A4U5SDY8	Vitellogenin domain-containing protein.GN=Cadr_00018348 .	-1.35
A0A4U5TLC5	kininogen-1 isoform X2 protein.GN=Cadr_00000557 .	-1.34
A0A4U5SN52	SERPIN domain-containing protein.GN=Cadr_00009891 .	-1.34
A0A4U5RS00	Cartilage oligomeric matrix protein.GN=Cadr_00026133 .	-1.29
A0A4U5RW40	apolipoprotein M isoform X1.GN=Cadr_00022413 .	-1.27
A0A5N4CRK0	C3/C5 convertase.GN=Cadr_00022439 .	-1.27
A0A4V6AD17	Phosphorylase b kinase regulatory subunit.GN=Cadr_00003131 .	-1.25
A0A4U5RY11	Complement C4-A .GN=Cadr_00022444 .	-1.25
A0A4U5SGT3	MACPF domain-containing protein.GN=Cadr_00015728 .	-1.25
A0A4U5SV19	Vascular cell adhesion protein 1.GN=Cadr_00012426 .	-1.25

A0A4U5RWW0	Transcription factor SOX.GN=Cadr_00022162 .	-1.23
A0A4U5SV14	cadherin-5 isoform X1.GN=Cadr_00011933 .	-1.19
A0A4U5SWF7	ANK_REP_REGION domain-containing protein.GN=Cadr_00010887 .	-1.19
A0A4U5TLQ4	fetuin-B like protein.GN=Cadr_00000554 .	-1.16
A0A4U5T516	WD_REPEATS_REGION domain-containing protein.GN=Cadr_00006540 .	-1.15
A0A4U5RC91	Inter-alpha-trypsin inhibitor heavy chain H2.GN=Cadr_00027450 .	-1.11
A0A4U5RQP6	follistatin-related protein 3 (Fragment).GN=Cadr_00026724 .	-1.1
A0A4U5RU68	SERPIN domain-containing protein.GN=Cadr_00025218 .	-1.1
A0A4U5TGE9	complement component C6 (Fragment).GN=Cadr_00004885 .	-1.1
A0A4U5TJK9	Circadian locomoter output cycles protein kaput.GN=Cadr_00002050 .	-1.07
A0A4U5SBM4	dynein regulatory complex protein 1 isoform X1.GN=Cadr_00018405 .	-1.07
A0A4U5SI34	Aa_trans domain-containing protein.GN=Cadr_00017452 .	-1.05
A0A4U5T607	Thrombospondin-1.GN=Cadr_00005571 .	-1.02
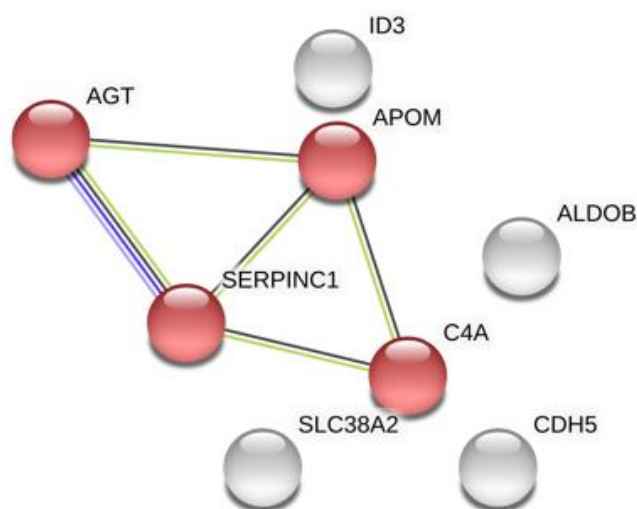
Figure 26. STRING analysis of proteins decreased ≥ 1 log2 fold in Dubca Poly: IC transfected cells. The STRING database was searched to analyze host proteins that showed ≥ 1 log2 fold decrease in Dubca Poly:IC transfected cells compared to mock cells. Nodes representing proteins that most significantly enriched the GO term. Proteins (Shaded in red) are localized in cells' extracellular space.
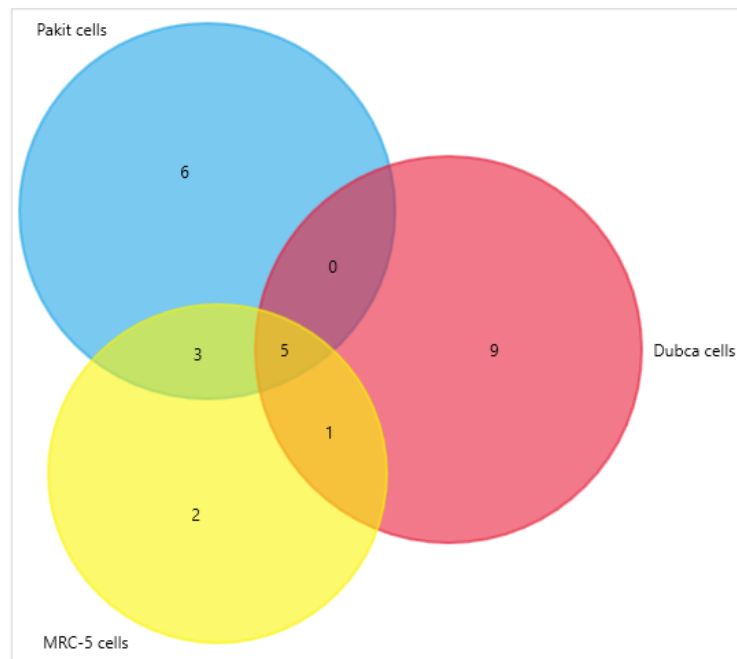
Figure 27. The Venn diagram shows the number of unique and overlapping innate immune proteins that increased ≥ 1 log2 fold in the IFN treatment condition of all three species.

.
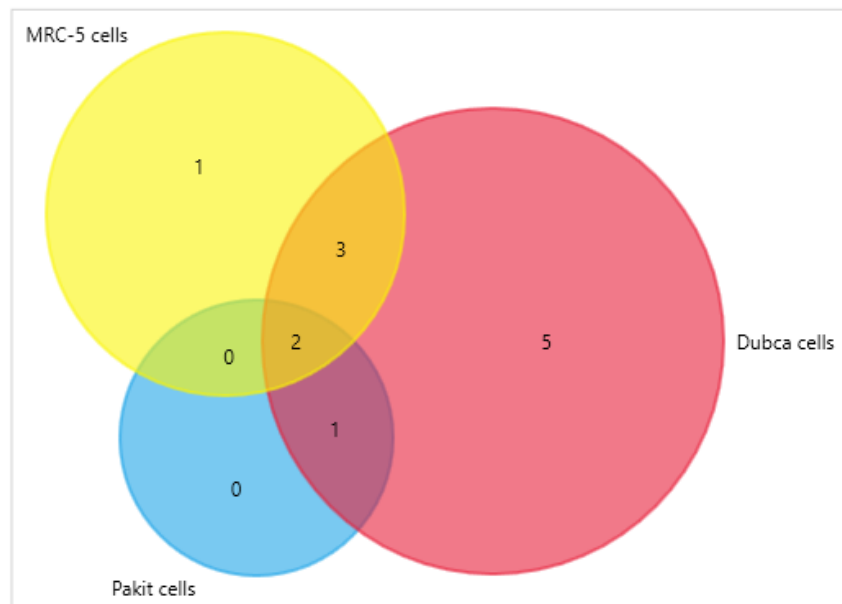
Figure 28. The Venn diagram shows the number of unique and overlapping innate immune proteins that increased ≥ 1 log2 fold in the Poly: IC treatment condition of all three species.

3.3 Discussion

Bats are the primary host of several human viruses with a marked lethality, such as Ebola, MERS-CoV, Marburg, SARS-CoV, and SARS-CoV-2. Other animals could serve as an intermediate host for viruses that originated from bats before being transmitted to humans. For example, it is suggested that the Egyptian tomb bat was the primary source of MERS-CoV before it transmitted to the dromedary camel and subsequently infected humans. Another example is the Nipah (NiV) virus which originated in fruit bats and then transmitted to swine before infecting humans (212).

The MERS-CoV epidemic and SARS-CoV-2 pandemic prompt the question of why bat-borne viruses are so lethal when they adapt to cause human disease but not in their animal hosts. It is proposed that the immune system of animal hosts responds to MERS-CoV and SARS-CoV-2 infections differently than humans, allowing them to be persistently infected without clinical symptoms (192,193). Therefore, a comprehensive analysis of the innate host response in bats, camels, and human cells could help in explaining why MES-CoV and SARS-CoV-2 are so lethal to humans but not in their animal hosts.

In this chapter, I used a high-throughput proteomic analysis to investigate the alteration of host proteins' expression in bat, human, and camel cells in response to innate immune system stimuli IFN and Poly: IC.

Compared to the mock, bioinformatic analysis of the IFN treatment condition showed that most induced alterations were common in all three species. Thirty-nine host proteins were ≥ 1 log2 fold up-regulated in MRC-5 IFN-treated cells. 28% of them have different roles in the anti-viral immune response. Forty-eight host proteins were ≥ 1 log2 fold increased in PaKiT IFN treated cells. 30% of them are involved in regulating the host's innate immune response. Forty-five host proteins were ≥ 1 log2 fold up-regulated in Dubca IFN-treated cells, and 33% of these proteins have roles in the innate immune response process. IFIT1, IFIT2, IFIT3, DDX58, and ISG15 proteins are commonly increased in the IFN treatment condition of the three species.

Overexpression of pro-inflammatory cytokines resulting from MERS-CoV or Covid-19 has been associated with the diseases' severity and mortality. Inflammatory reactions must be controlled to prevent severe tissue damage during viral infections (213). Bats have evolved unique methods to decrease severe virus-induced pro-inflammatory responses while maintaining high levels of type I IFN production to control virus replication. For example, Bats show a dramatic decrease in NLRP3 inflammasome activation compared to their human or mouse counterparts. NLRP3 is an intracellular sensor that recognizes viral infection and promotes IL-1β and IL-18 secretion. Higher levels of IL-18 have been shown to be associated

with Covid-19 disease severity (195,196). This is one reason why bats can host many deadly viruses without clinical symptoms (214).

CXCL10 is a pro-inflammatory cytokine that is expressed within tissues following viral infection. It is produced by a wide range of cell types, such as monocytes, epithelial cells, neutrophils, and fibroblasts in response to IFNs. It stimulates the CXCR3 receptor on the macrophages, dendritic cells, and activated B & T cells to recruit them to the site of infection (215). CXCL10 levels have been found to be abnormal in patients infected with viral diseases (216). Increased levels of CXCL10 were associated with acute lung injury (ALI) or acute respiratory distress syndrome (ARDS) in Covid-19 patients (217). Our proteomics analysis showed that CXCL10 was the most up-regulated protein in MRC-5 IFN treated cells. Notably, CXCL10 and other pro-inflammatory chemokines were not up-regulated in IFN-treated PaKiT cells. This data supports the previous reports concluding that while bats produce a high level of IFN, they suppress an overactive pro-inflammatory response limiting the virus-induced immunopathology introduced in people infected with the same viruses (218).

CXCL10 wasn't up-regulated in Dubca IFN-treated cells, while CCL5 was the most up-regulated protein. In humans, CCL5 is one of the host's chemokines produced by virus-infected cells that attract monocytes and T cells to the site of infection. Following cell death after virus infection, it's critical to remove virus-infected, apoptotic cells from the tissue. The tissue macrophage is the cell type responsible for debris removal. The remaining apoptotic cells can cause more tissue injury through proinflammatory cytokines if this process is disrupted. It has been shown that CCL5 plays an essential role in host survival during viral infection by protecting macrophages from virus-induced apoptosis, allowing for adequate clearance of cellular debris that would cause severe inflammation (219)(220). Our proteomic data demonstrate that camel cells could suppress overactive pro-inflammatory chemokines, such as CXCL10, and recruit CCL5 chemokine to control virus replication with minimal tissue damage. Increasing the expression level of CXCL10 in MRC-5 but not in PaKiT and Dubca IFN-treated cells could help understand why bats and camels survive pathogenic viruses without severe illness.

Bioinformatic analysis of the Poly: IC treatment condition showed a difference in the expression of proteins involved in the immune system between the three species.

Twenty-nine proteins were ≥ 1 log2 fold increase in MRC-5 Poly: IC treated cells. 20% of them are involved in the innate immune response process, with CXCL10 being the highest up-regulated protein on the list. As mentioned before, it has been shown that high levels of CXCL10 are associated with the severity of respiratory viral diseases (221).

One hundred proteins were ≥ 1 log2 fold increased in PaKiT Poly: IC treated cells. Interestingly, only 0.03% of the human homologs of these proteins have roles in the innate immune response process. Up-regulating only a small number of proteins involved in the host innate immune response could be attributed to PaKiT cells showing a delayed reaction to Poly: IC treatment, and a prolonged treatment might be needed to stimulate ISGs protein production. Another possibility could be that PRRs in PaKiT cells are already activated with high baseline expression, and the increased PRRs RNA transcripts post-poly I: C treatment were insufficient to induce ISGs protein production. It's worth mentioning that the western blotting analysis of PaKit IFN-treated cells showed increased expression of STAT 1 protein compared to Poly: IC treated cells. This increase in STAT 1 expression could increase the proportion of protein phosphorylation, thus stimulating a more robust innate immune response.

Fifty-two proteins were ≥ 1 log2 fold increased in Dubca Poly: IC treated cells. About a quarter of them have human homologs that have roles in the anti-viral immune response process, including CCL5, CCL2, IFIT2, IFIT3, IFIT1, IRF1, CXCL10, OASL, IFIH1, ISG15, IFI44, and IFI44L. CCL2 is a potent pro-inflammatory chemokine that is expressed within tissues following microbial infection. It recruits monocytes, memory T cells, and dendritic cells to the sites of infection or inflammation. Increased levels of CCL2 were associated with disease severity in patients infected with H7N9 (222). However, CCL5 was the highest-regulated protein on the list. This chemokine is required for host survival during viral infections due to its role in clearing cellular corpses and preventing severe inflammation (223).

Our high-throughput proteomics data showed CXCL10 was up-regulated in MRC-5 Poly: IC and Dubca Poly: IC treated cells. However, compared to humans, camels don't seem to become severely ill during a MERS-CoV infection. This contradictory outcome could be explained in multiple ways. CXCL10 increased more than six log-2 folds in MRC-5 poly: IC treated cells, while only 2.8 log-2 folds increased in Dubca poly: IC treated cells. The increased expression of CXCL10 in MRC-5 cells compared to Dubca cells could explain why humans are more susceptible to severe inflammation resulting from pro-inflammatory chemokines than camels. CCL5 is required for host survival during viral infections due to its role in clearing cellular corpses and preventing severe inflammation (223). Our high-throughput proteomics data showed CCL5 was the highest up-regulated protein in Dubca poly: IC treated cells, while it wasn't increased in MRC-5 Poly: IC treated cells.

On the other hand, it has been reported that camels infected with MERS-CoV get sick and display some disease symptoms like fever which is compatible with the increasing level of CXCL10 we observed in Dubca Poly: IC treated cells (224). However, the consequences of MERS-CoV infection in older camels can't be easily determined as camels are usually

slaughtered at younger ages for commercial purposes (225). Our high-throughput proteomics analysis of total cell lysate from MRC-5, Duba, and PaKiT cells treated with IFN and poly: IC could serve as a basis to predict the clinical outcome resulting from viral infections in humans and MERS-CoV and SARS-CoV-2 animal hosts in clinical samples.

Finally, different cell types have been used in this study. Using the same cell type in all three species (e.g., Lung cells) would be more reliable in analyzing the difference in changes of host proteome between human, bat, and camel cells in response to IFN and Poly: IC treatment.

Chapter 4. MERS-CoV ORF4A and ORF4B host protein interacting partners

4.1 Introduction

There is limited information regarding the role of MERS-CoV ORF4A & ORF4B in virus replication. One study has shown that MERS-CoV-ORF4A & ORF4B suppress the host immune response to facilitate virus replication (226). RIG-I and MDA-5 are cytoplasmic sensors that sense viral RNA and trigger IFN signaling pathway. PACT is a cellular dsRNA-binding protein that binds MDA5 and RIG-I to potentiate their functions in IFN production. It has been shown that ORF4A protein has a dsRNA-binding domain that binds to PACT in an RNA-dependent manner and prevents its interaction with RIG-I, thereby inhibiting host PACT-induced activation of RIG-I and disrupting IFN production (227).

NF-κB proteins promote the transcription of pro-inflammatory cytokines and regulate the expression of hundreds of genes essential for optimal immune responses. NF-κB retains in the cytoplasm in an inactive form. Once activated, it binds to karyopherin-α4 (importin-α3) to get translocated into the nucleus and initiates the transcription process. It has been shown that ORF4B inhibits robust NF-κB-dependent response during viral infection by binding to karyopherin-α4 (importin-α3), thereby preventing NF-κB nuclear translocation and production of NF-κB-dependent pro-inflammatory cytokines (228). However, further investigations are needed to explore other potential roles of MERS-CoV ORF4A & ORF4B proteins in virus replication and pathogenesis.

MERS-CoV ORF4A and MERS-CoV-ORF4B host protein-protein interactions were investigated by our lab using throughput quantitative proteomics. Two human cell lines (HEK293) have been generated, each expressing MERS-CoV ORF4A or MERS-CoV-ORF4B viral protein, tagged with the 'flag-tag' motif under the control of an inducible promoter, allowing them to be selectively induced when tetracycline is added to the media. The viral protein was induced for each cell line, and high throughput quantitative proteomics was conducted to identify possible human cellular proteins interacting with MERS-CoV-ORF4A or MERS-CoV-ORF4B. Data generated from the quantitative proteomics were analyzed (Unpublished data). Six cellular candidates with the highest confidence were selected to validate their interactions with the MERS-CoV ORF4A or MERS-CoV ORF4B (Table 26)

This chapter validates the interaction of MERS-CoV ORF4A & ORF4B proteins with the selected human cellular partners using Western Blot Analysis of Immunoprecipitation (IP-Western). Furthermore, the interaction of MERS-CoV ORF4A & ORF4B proteins with bat and

camel equivalent proteins was examined to investigate whether they interact with these viral proteins with higher or lower affinity than their human counterparts or whether these interactions are species-specific.

This analysis helps understand other potential roles of MERS-CoV ORF4A & ORFB proteins in virus replication and why MERS-CoV infection is lethal for humans but not for its animal hosts.

Table 26. The cellular proteins that were chosen to validate their interactions with MERS-CoV ORF4A and ORF4B proteins. Proteins' IDs , names and genes' symbols are obtained from UniProt: the universal protein knowledgebase in 2021.

UniProt ID	Protein name	Gene symbol	Fold change difference compared to mock cells
Q08211	Nuclear DNA helicase II or ATP-dependent RNA helicase A	NDH II or (DHX9)	≥1.5 log2 fold change
Q12905	Nuclear factor 45 or Interleukin enhancer-binding factor 2	NF45 or (ILF2)	≥1.5 log2 fold change
Q99729	Heterogeneous nuclear ribonucleoprotein A/B	HNRNPAB	≥1.5 log2 fold change
P07910	Heterogeneous nuclear ribonucleoproteins C1/C2	HNRNPC	≥1.5 log2 fold change
P22626	Heterogeneous nuclear ribonucleoproteins A2/B1	HNRNPA2B1	≥1.5 log2 fold change

O00629	Importin subunit alpha 3	KPNA4 (QIP1)	≥1.5 log2 fold change

Nuclear DNA helicase II (NDH II) or DExD/H-box 9 (DHX9) is a 1270 amino acid protein that is localized in the cell's nucleus but can shuttle to the cytoplasm to carry out critical cellular functions, e.g., DNA replication, transcriptional activation, and translational regulation (229). Moreover, NDHII plays a crucial role in the activation of NF-κB-mediated innate immune response against viral infections (230).

NF45 is a 390 amino acid DNA/RNA-binding protein that has a critical role in normal cell division. It forms a complex with its binding partners NF90 and NF110, and depletion of this complex retards cell growth by inhibiting DNA synthesis (231).

Heterogeneous nuclear ribonucleoproteins (hnRNPs) represent a large family of RNA-binding proteins (RBPs). More than 20 hnRNP proteins have been discovered (hnRNPs A1 to U) with molecular sizes ranging from 32-40 kDa in human cells. hnRNP proteins are involved in common cellular functions, including mRNA stabilization, alternative splicing, and transcriptional and translational regulations, but some hnRNP have unique functional properties. hnRNPAB is a 331 amino acid protein that binds RNA and is involved in multiple cellular functions, e.g., RNA splicing, transcription, and translation (232).

The HNRNPA2B1 is a 353 amino acid long RNA-binding protein involved in multiple cellular processes, such as RNA trafficking, translation, and stabilization (216). It acts as a nuclear DNA sensor to stimulate innate immune response following infection of DNA viruses. Once hnRNPA2B1 detects viral DNA in the cell's nucleus, it dimerizes and translocates to the cell's cytoplasm and interacts with STING. This interaction activates the TBK1-IRF3 signaling pathway leading to IFN-α/β production (233).

HNRNPC is a 306 amino acid long protein in the cell's nucleus. It is an RNA-binding protein that is required for optimal RNA expression, splicing, and shuttling proteins and RNA transcripts between the cell's nucleus and the cytoplasm. It has been shown that high levels of HNRNPC are associated with the progression of different cancers and poor overall survival rate in cancer patients (234) (235).

KPNA4 is one of the importin-α proteins belonging to nuclear transport receptors. It plays a role in importing nuclear proteins as an adaptor protein for nuclear receptors (236). It binds substrates with a simple or bipartite NLS (Nuclear localization signals) to form the importin-α/cargo complex, followed by the recruitment of importin-1 to create a trimeric complex. The trimeric complex transports the cargo protein into the nucleus via a nuclear pore. Growing

evidence showed that KPNA4 is the nuclear transporter protein for essential host proteins, such as p53 and NF-κB. A dramatic increase in KPNA4 levels is associated with tumor progression in cancer patients. KPNA4 mainly serves as an independent prognostic biomarker for lethal malignancies, including pancreatic ductal adenocarcinoma (PDAC) and hepatocellular carcinoma (HCC) (236–238).

4.2 Results

4.2.1 Cloning MERS-CoV ORF4A and ORF4B genes

MERS-CoV ORF4A and ORF4B flag-tagged genes were cloned in PCDNA5/FRT/TO-TOPO vector. 50 ng from each plasmid were transformed into chemically competent E. coli strain DH5-α. A single colony was picked and grown in a large volume of LB broth, and a midi-prep was performed to extract a high concentration of ORF4A and ORF4B plasmid DNA. Afterward, ORF4A and ORF4B inserts were confirmed using appropriate restriction enzymes (Figure 28).
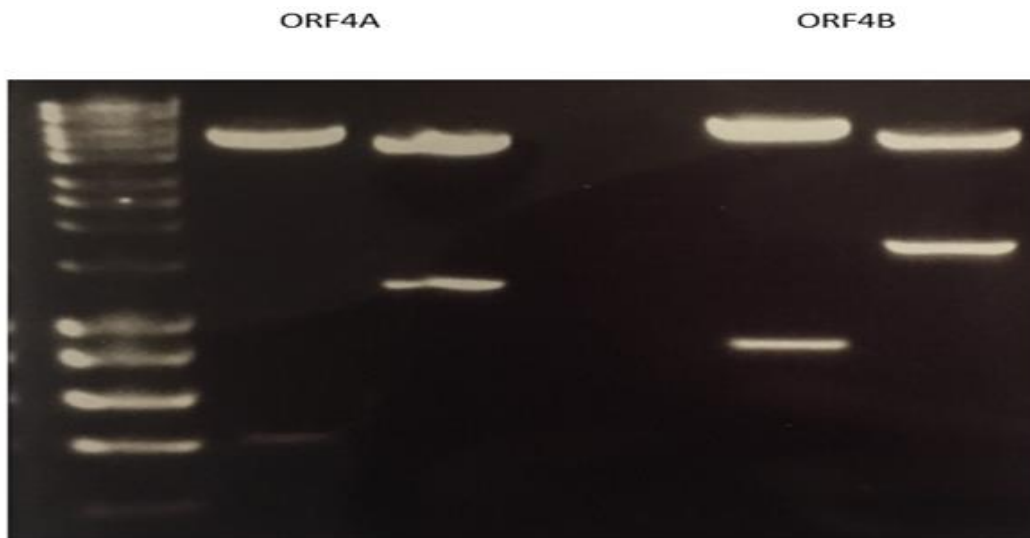
Figure 29. Cloning and analysis of ORF4A and ORF4B plasmids DNA by agarose gel electrophoresis.
50 ng from ORF4A or ORF4B flag-tagged plasmid DNA was transformed into competent E. coli DH5α. A single colony was selected and grew in 50ml of LB containing ampicillin with a final concentration of 100 μg/mL overnight as both plasmids contain ampicillin resistant gene. Then, ORF4A and ORF4B plasmids DNA were isolated using midi-prep. The identity of ORF4A and ORF4B DNA sequences were confirmed using XhoI, BamHI, and EcoRI restriction enzymes.

4.4 Validation of MERS-CoV ORF4A & ORF4B protein expression in MRC-5, PaKiT, Huh-7, HEK 293 and Dubca cells

MRC-5, PaKiT, Huh-7, HEK 293, and Dubca cells were transfected with ORF4A and ORF4B flag-tagged plasmid DNA to induce protein expression. The protein expression of MERS-CoV ORF4A and ORF4B were analyzed by Western Blotting (Figure 29). The molecular mass expected for the ORF4A and ORF4B proteins (tagged with the FLAG epitope) was 15 and 37 kDa, respectively. ORF4A and ORF4B protein expression were further validated using Indirect Immunofluorescence Assay (IFA) in A549 cells (Figure 30).
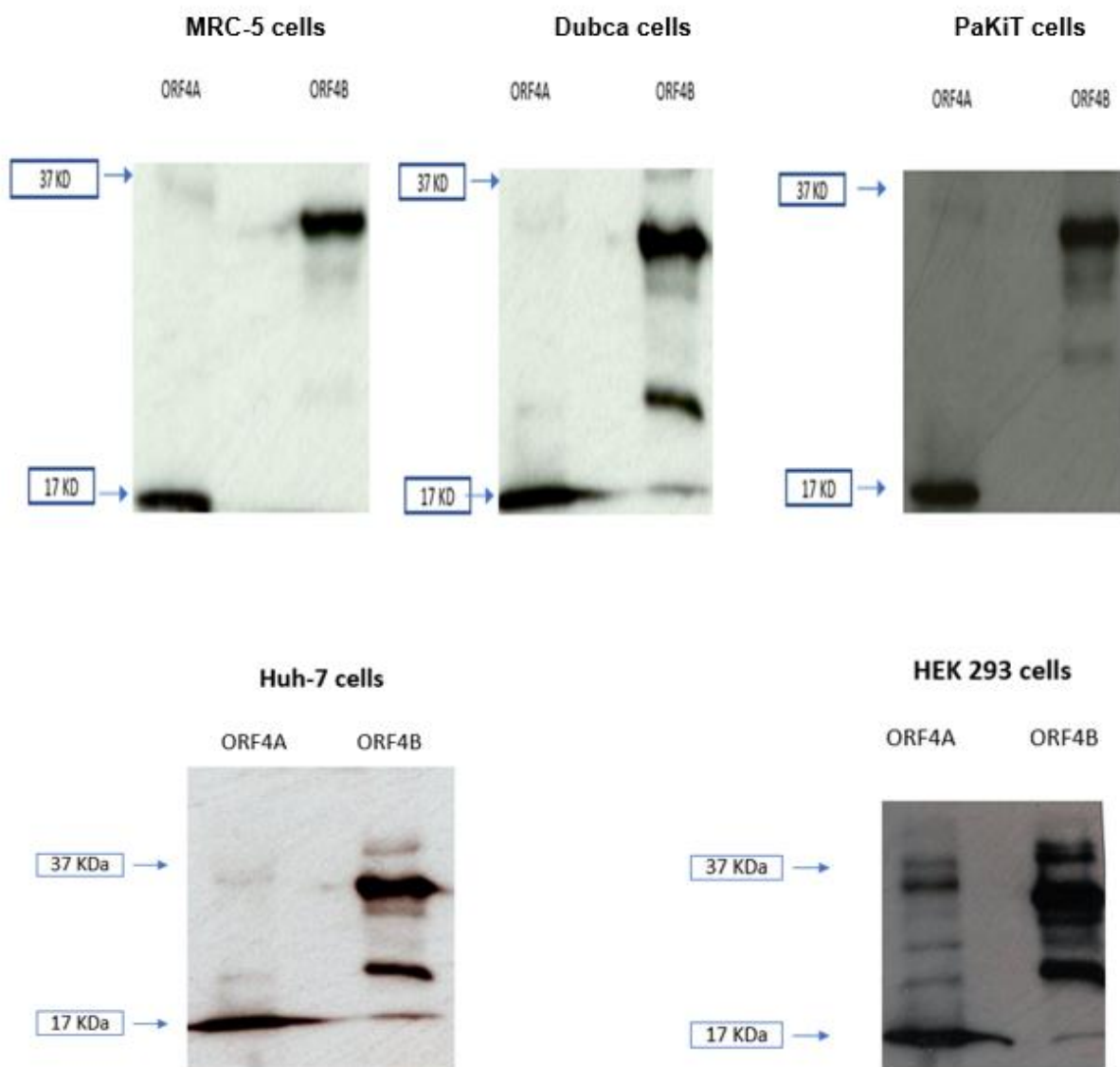
Figure 30. Analysis by western blot of ORF4A & ORF4B protein expression. MRC-5, Dubca, PaKiT, Huh-7, and HEK 293 cells were seeded in the six-wells plate before they were transfected with two μg of ORF4A or ORF4B flag-tagged plasmid DNA using PEI reagent. Transfected cells were incubated for 18 hrs before they were harvested and lysed with 2X sample buffer. Each sample was separated using a 10% SDS-PAGE gel and transferred to a PVDF membrane for immunoblotting with an anti-flag antibody.
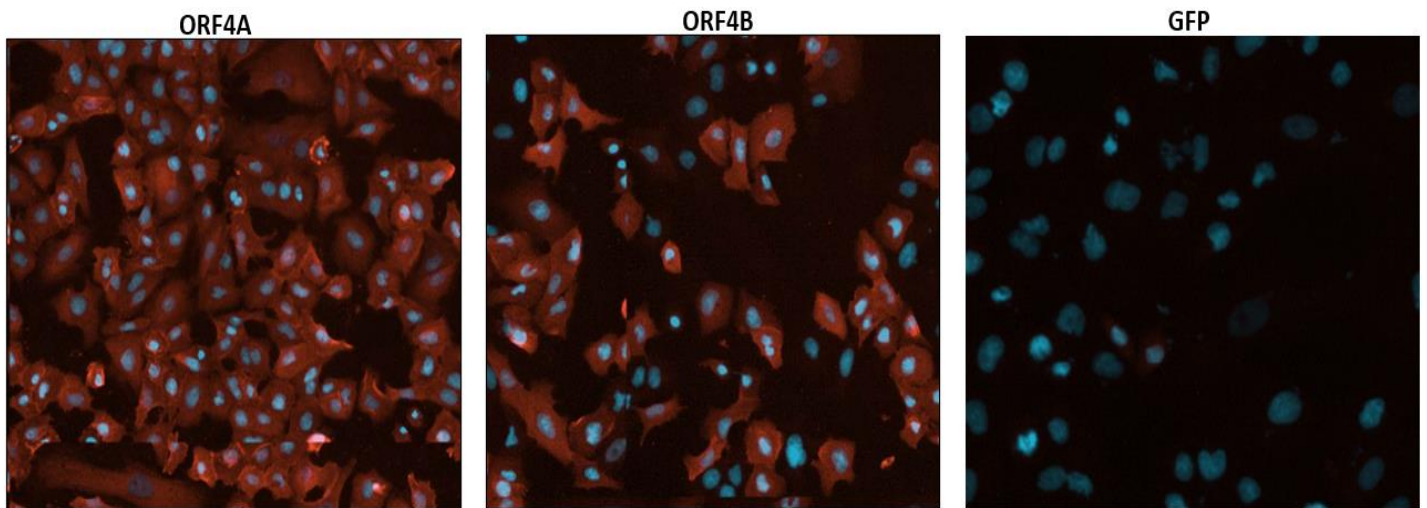
Figure 31. IFA analysis ORF4A & ORF4B protein expression. A549 cells transfected with 100 ng of either ORF4-flag tagged, ORF4B-flag tagged, or GFP expressing DNA plasmid (as a control) in 96 wells-plate. Cells were fixed with 4% paraformaldehyde, washed, and permeabilized with 1% (v/v) Triton-X 100 for 10 min. Then, cells were washed again and blocked for 30 min before staining with anti-flag primary antibody followed by an anti-mouse (Alexa Fluor 647 conjugated secondary antibody, red signal). DAPI was applied to stain the cells' nucleus.

4.5 Validating MERS-CoV ORF4 & ORF4B protein-protein interactions with their cellular partners.

Sample preparation for Western Blot Analysis of Immunoprecipitation (IP-Western):

Six host proteins that showed a significant enrichment with the MERS-CoV ORF4A or ORF4B proteins with the highest confidence were selected, as shown in (Table 26). Co-immunoprecipitation (co-IP) samples from A549, Dubca, and PaKiT cells expressing the MERS-CoV ORF4A or ORF4B proteins were prepared to validate their interactions with their cellular interacting partners (Figure 31). Briefly, A549, Dubca, and PaKiT cells were grown in a T-75 flask before they were transfected with ORF4A-flag tagged or ORF4B-flag tagged plasmid DNA and incubated for 18 hrs to allow the expression of the proteins. A negative control from each cell line was included. After that, cells were harvested, lysed, and sonicated. The immunocomplexes were then captured with anti-FLAG magnetic beads before samples were eluted. The input, non-bound, and pulldown samples were then used to validate the host protein interacting partners for MERS-CoV ORF4A and ORF4B proteins. The expression of ORF4A and ORF4B proteins in co-IP samples was confirmed by western blotting analysis (Figure 32) (Figure 33).
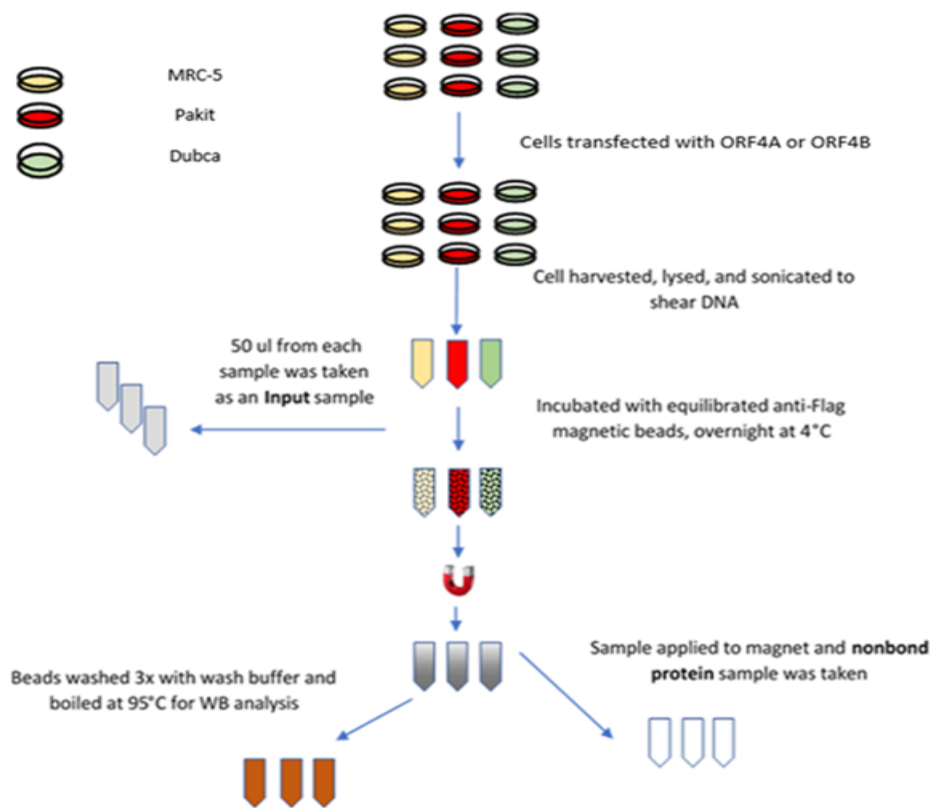
Figure 32. Preparation of co-IP samples from A549, Dubca, and PaKiT cells expressing ORF4A or ORF4B proteins. A549, Dubca, and PaKiT were transiently transfected with an appropriate concentration of ORF4A-flag tagged or ORF4B-flag tagged plasmid DNA using PEI. A negative control (no transfected plasmid) from each cell line was included. Three samples: Input, non-bound, and pulldown samples were prepared.

A549 cells

PaKiT cells

Dubca cells
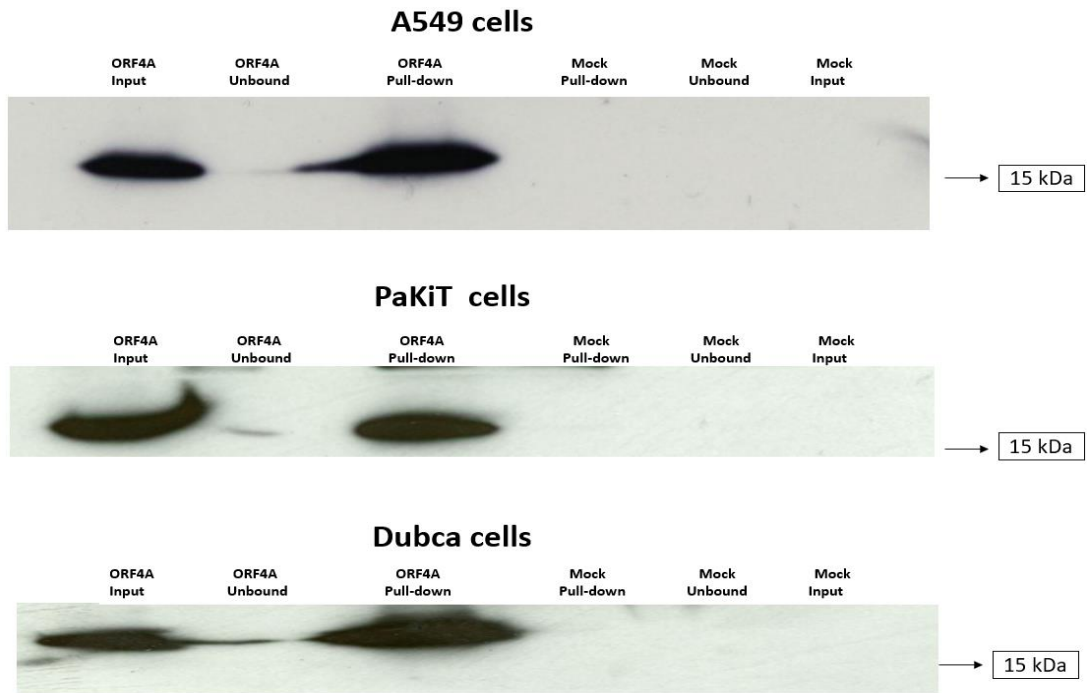
Figure 33. Confirmation of successful transfection of ORF4A plasmid DNA in co-IP samples by western blotting analysis. A549, Dubca, and PaKiT cells were transfected with ORF4A-flag tagged plasmid DNA. The input, non-bound, and pulldown samples were prepared and loaded into 10% SDS-PAGE gel. Proteins were separated and transferred to a PVDF membrane for immunoblotting with the anti-flag antibody. The molecular weight of ORF4A protein is 15 KDa.

PaKiT cells

A549 cells

Dubca cells
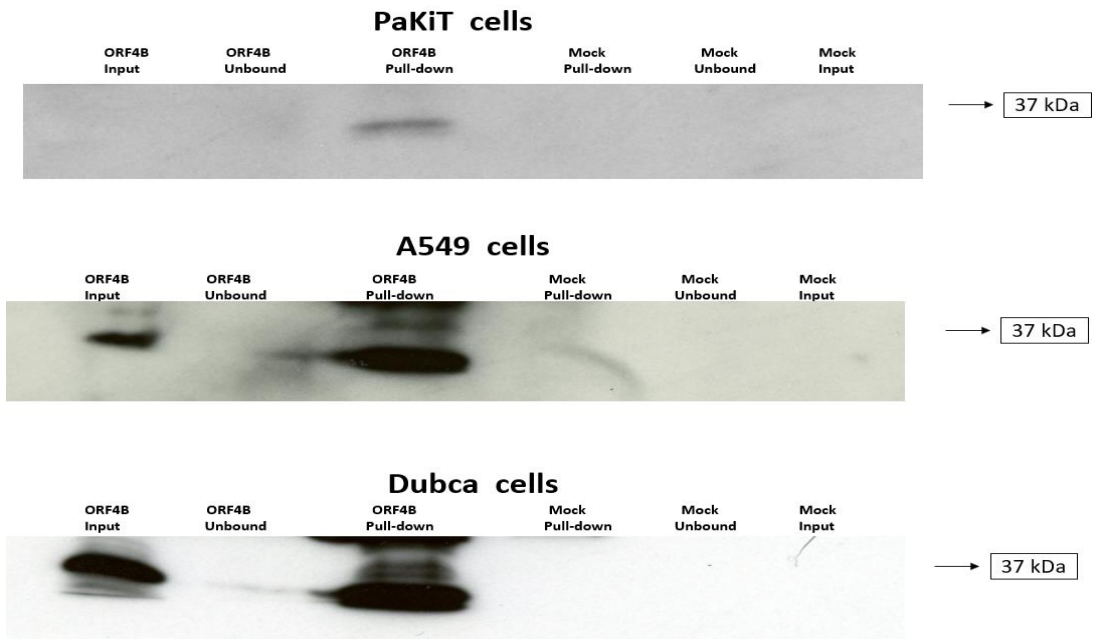
Figure 34.Confirmation of successful transfection of ORF4B plasmid DNA in co-IP samples by western blotting analysis. A549, Dubca, and PaKiT cells were transfected with ORF4B-flag tagged plasmid DNA. The input, non-bound, and pulldown samples were prepared and loaded into 10% SDS-PAGE gel. Proteins were separated and transferred to a PVDF membrane for immunoblotting with the anti-flag antibody. The molecular weight of ORF4B protein is 37 KDa.

130

After pulldown samples were prepared, as shown in (Figure 31), the potential interactions between MERS-CoV ORF4A with NDH II (DHX9) in A549 and its counterparts in Duba and PaKiT cells were examined. IP-Western analysis revealed that NDH II interacts with MERS-CoV ORF4A protein in A549 cells only. No NDH II protein was detected in ORF4A pulldown samples of PaKiT and Dubca cells indicating MERS-CoV ORF4A doesn't interact with bat and camel NDH II equivalent proteins. These results confirm the interaction of ORF4A with NDH II in A549, and this interaction is species-specific (Figure 34).

The high throughput proteomic dataset showed that NF45 (ILF2) is enriched in the MERS-CoV ORF4A pull-down sample. The IP-Western analysis confirmed the interaction between MERS-CoV ORF4A protein with NF45 in A549 cells and its equivalent proteins in PaKiT and Dubca cells. The amount of NF45 protein in MERS-CoV ORF4A pull-down samples was more than their controls in all three species (Figure 35).

IP-Western analysis revealed that hnRNPA2/B1 interacts with MERS-CoV ORF4A protein in A549 cells and its equivalent protein in Dubca cells, while it weakly interacts with bat counterpart of hnRNPA2/B1 as shown in ORF4A pull-down sample of PaKiT cells (Figure 36).

The IP-Western analysis confirmed the interaction of MERS-CoV ORF4A protein with hnRNPAB human protein and its camels and bat counterparts. The amount of hnRNPAB protein in MERS-CoV ORF4A pulldown samples of A549, Dubca, and PaKiT cells was more than in their control pull-down samples (Figure 37).

The IP-Western analysis validated the interaction of MERS-CoV ORF4A with hnRNPC1/C2 human protein and its camel counterpart, with a much stronger association between hnRNPC1/C2 and MERS-ORF4A in A549 cells. The IP-Western analysis didn't confirm the interaction of ORF4A protein with bat equivalent protein because the amount of hnRNPC1/C2 protein in the MERS-CoV ORF4A pull-down sample of PaKiT cells was similar to its control sample (Figure 38).

The IP-Western analysis confirmed the interaction of MERS-CoV ORF4B with the KPNA4 human protein and its camel counterpart, with a much stronger association between ORF4B and KPNA4 in A549 cells. The analysis showed weak interaction between MERS-CoV ORF4B and bat equivalent protein (Figure 39).
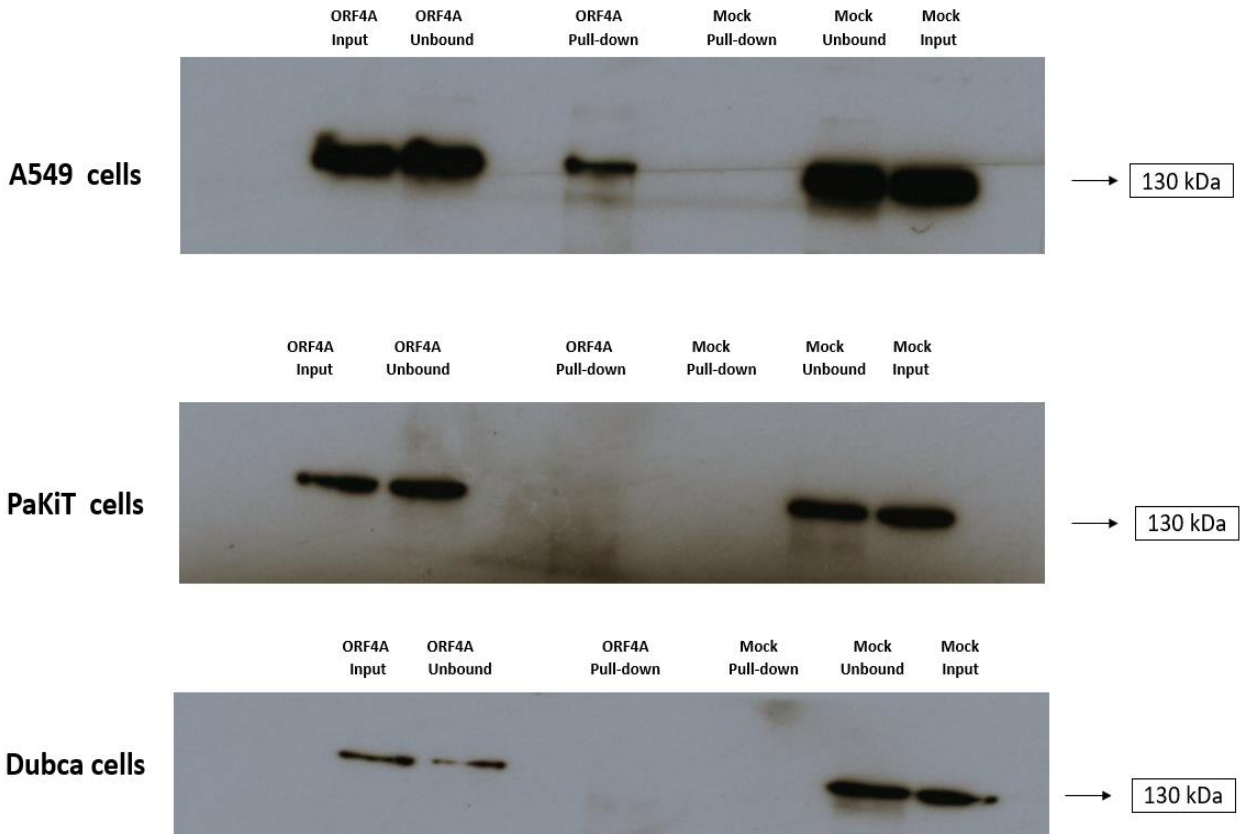
Figure 35.Validating the interaction of ORF4A with the cellular protein NDHII by IP-Western analysis.
A549, Dubca, and PaKiT cells were transfected with ORF4A plasmid DNA. Three samples: Input, non-bound, and pulldown samples were prepared and loaded into 10% SDS-PAGE gel. Proteins were separated and transferred to a PVDF membrane for immunoblotting with anti-NDH II antibody. The molecular weight of NDHII is 130 KDa.

Figure 36.Validating the interaction of ORF4A with the cellular protein NF45 by IP-Western analysis. A549, Dubca, and PaKiT cells were transfected with ORF4A plasmid DNA. Three samples: Input, non-bound, and pulldown samples were prepared by and loaded into 10% SDS-PAGE gel. Proteins were separated and transferred to a PVDF membrane for immunoblotting with anti NF45 antibody. The molecular weight of NF45 is 45 KDa.

Figure 37. Validating the interaction of ORF4A with the cellular protein hnRNPA2/B1 by IP-Western analysis. A549, Dubca, and PaKiT cells were transfected with ORF4A plasmid DNA. Three samples: Input, non-bound, and pulldown samples were prepared and loaded into 10% SDS-PAGE gel. Proteins were separated and transferred to a PVDF membrane for immunoblotting with anti hnRNPA2/B1 antibody. The molecular weight of hnRNPA2/B1 is 37 KDa.
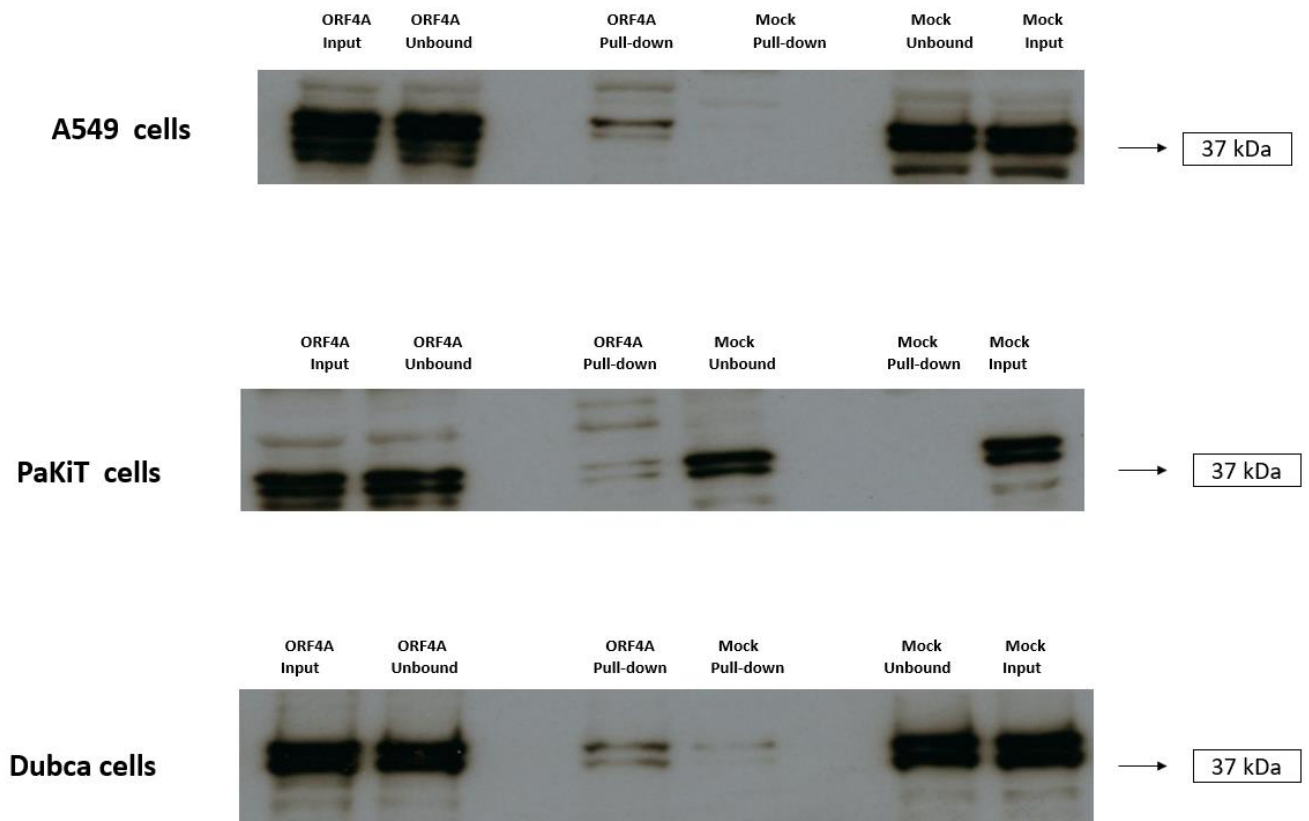
Figure 38. Validating the interaction of ORF4A with the cellular protein hnRNPAB by IP-Western analysis.
A549, Dubca, and PaKiT cells were transfected with ORF4A plasmid DNA. Three samples: Input, non-bound, and pulldown samples were prepared and loaded into 10% SDS-PAGE gel. Proteins were separated and transferred to a PVDF membrane for immunoblotting with anti hnRNPAB antibody. The molecular weight of hnRNPAB is 38 KDa.
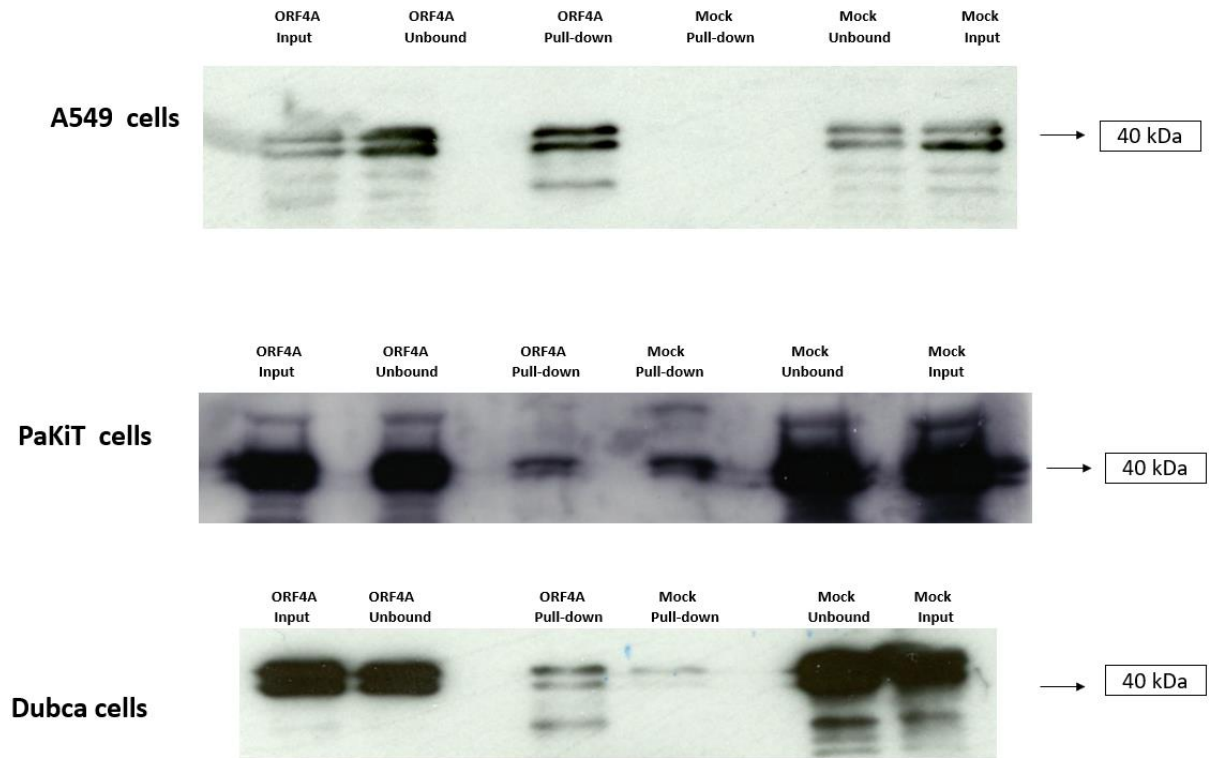
Figure 39. Validating the interaction of ORF4A with the cellular protein hnRNPC1/C2 by IP-Western analysis. A549, Dubca, and PaKiT were transfected with ORF4A plasmid DNA. Three samples: Input, non-bound, and pulldown samples were prepared and loaded into 10% SDS-PAGE gel. Proteins were separated and transferred to a PVDF membrane for immunoblotting with anti hnRNPC1/C2 antibody. The molecular weight of hnRNPC1/C2 is 40 KDa.
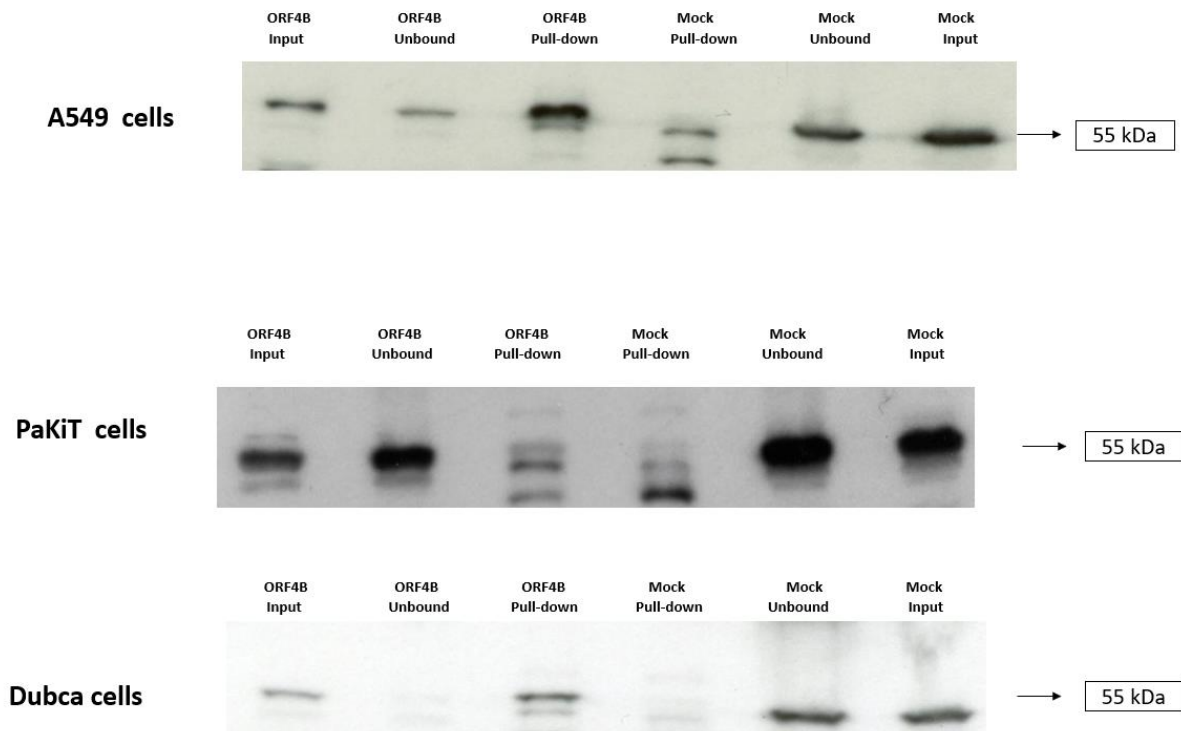
Figure 40.Validating the interaction of ORF4B with the cellular protein KPNA4 (QIP1) by IP-Western analysis. A549, Dubca, and PaKiT cells were transfected with ORF4B plasmid DNA. Three samples: Input, non-bound, and pulldown samples were prepared by Co-IP and loaded into 10% SDS-PAGE gel. Proteins were separated and transferred to a PVDF membrane for immunoblotting with anti KPNA4 (QIP1) antibody. The molecular weight of QIP1 is 55 KDa.

4.3 Discussion

MERS-CoV ORF4A and ORF 4B are accessory proteins that have roles in suppressing the host's immune response and enhancing virus replication. However, very few studies have been conducted to identify other potential functions of ORF4A and ORF4B proteins in the virus life cycle.

To investigate cellular proteins that ORF4A and ORF4B could exploit to facilitate virus replication, our lab conducted a TMT-MS-MS proteomics analysis of cells (HEK293) transfected with MERS-CoV ORF4A or ORF4B. Data generated from the quantitative proteomics was analyzed. Six cellular proteins enriched with the MERS-CoV ORF4A or MERS-CoV ORF4B (NDH II, NF45, hnRNPA2/B1, hnRNPAB, hnRNPC1/C2, KPNA4) with the highest confidence were selected to validate their interaction with these viral proteins and examine their roles in MERS-CoV replication.

4.3.1 Nuclear DNA helicase II

Nuclear DNA helicase II (NDH II) is a 1270 amino acid protein involved in many cellular processes, e.g., DNA replication, transcriptional activation, and translational regulation. It acts as an ATP-driven motor that can unwind double-stranded RNA and DNA in a nucleotide-dependent manner. NDH II comprises two double-stranded RNA binding domains (dsRBDs) at its N-terminus, a helicase core domain in the central part of the protein, and a glycine-rich single-stranded nucleic acid-binding domain at its C-terminus (240). NDH II is mainly found in the nuclei but can shuttle between the cell's nucleus and cytoplasm. Influenza A viruses are important pathogens that cause respiratory disease in humans and different animal species (241). It has been shown that depletion of NDHII protein decreased the viral yield substantially. In that study, a significant reduction of different viral RNAs species, such as vRNA and mRNA, was observed, indicating the vital role of NDHII in Influenza A replication and transcription (242).

Hepatitis C virus (HCV) is a single-stranded, positive-sense RNA virus. It is estimated that 180 million people are infected with HCV worldwide. HCV infection that continues over many years can cause severe illnesses, such as hepatocellular carcinoma (HCC) and lymphomas. The non-coding region of the HCV RNA genome (5'-UTR) is indispensable for viral replication. It interacts with viral and several cellular proteins to regulate viral RNA replication and translation (243). NDHII is one of the host cellular proteins that bind to the 5'-UTR regions of HCV. It has been shown that silencing the expression of NDHII reduced viral RNA synthesis

and viral proteins NS3 and NS5A, indicating the critical role of NDHII in HCV replication (244,245). Dengue virus (DENV) is a positive-sense, single-stranded RNA of 10.4 kb in length. The 5' and 3' ends of the DENV genome contain short noncoding regions that regulate viral RNA translation and replication (246). It has been reported that NDHII is engaged in a cellular protein complex that binds to 3' ends of the DENV genome and regulates the translation and replication of viral RNA. Depleting NDHII reduced the amounts of infectious particles of DENV in different cell lines. Moreover, it has been shown that NDHII knockdown significantly reduces replication levels of another flavivirus, the Japanese encephalitis virus (JEV) (247). Multiple reports showed that NDHII acts as a proviral factor in viral replication of a wide range of RNA viruses, such as HIV-1, Hepatitis E Virus (HEV), and Chikungunya Virus (CHIKV) (248). Different mechanisms have been proposed by which NDHII utilizes to facilitate the replication cycle of those viruses. However, the common feature of NDHII during viral replication is its association with certain regions of the viral genome (5'- and/or 3'-UTRs) that usually adopt complex secondary structures. As a result, NDHII may be used to regulate virus replication at various stages by remodeling the complex RNA structure with its helicase activity (248).

Our IP-Western analysis confirms the interaction of ORF4A with human NDH II protein but not with its bat and camel counterparts. As mentioned earlier, NDHII is a proviral factor of various RNA viruses. Therefore, it is tempting to speculate that the interaction of ORF4A with NDHII could be one factor that enhances MERS-CoV replication in human cells compared to the animal host cells. This finding suggests an answer to why MERS-CoV infection is so lethal for humans but not for animal hosts. However, further experiments are needed to examine the functional implications of ORF4A interaction with NDHII in human cells.

4.3.2 Nuclear factor 45 (NF45)

NF45 is a 390 amino acid RNA-binding protein encoded by the ILF2 gene and mainly located in the cell's nucleus. It is complexed with other RNA-Binding proteins such as 90 and NF110 to regulate the interleukin-2 (IL-2) promoter (249). NF45 has an N-terminal arginine-and-glycine-rich (RGG) domain at positions 3–22 and a domain associated with zinc fingers (DZF) at positions 104–338. NF45 is one of the host proteins involved directly or indirectly in viral replication. It has been shown that ectopic expression of NF45 enhances HIV infection and promotes virus production. The effect depends on RNA binding domains as deletion of the RNA-binding motif of NF45 diminishes the enhancement of viral infection and gene expression (255). On the other hand, A study showed that NF45 localizes with RNA-dependent RNA polymerase VP1, the capsid protein VP2, and the ribonucleoprotein VP3 of infectious bursal

disease virus (IBDV). In that study, depletion of NF45 enhances IBDV replication five-fold, indicating that NF45 is involved in cellular defense mechanisms against IBDV (234).

NF90 is an RNA/DNA-binding protein that dimerizes with NF45 through their common 'DZF' zinc fingers (DZF) domains at positions 104-338. NF45/NF90 complex is involved in several biological processes and plays a role in several viruses' replication. NF90 has been shown to be involved in host antiviral responses against multiple viruses. It disrupts vesicular stomatitis virus (VSV) replication by associating with viral RNA transcripts (250), suppresses influenza virus replication by binding to viral nucleoprotein (251), and disrupts the function of the Ebola virus polymerase by associating with VP35 (252). On the other hand, several viruses, including hepatitis B virus (HBV), hepatitis C virus (HCV), human papillomaviruses, dengue virus, and HIV, have been reported to hijack NF90 and utilize it to enhance their replication (253). Depleting the NF45 causes a dramatic decrease in the NF90 protein, which may positively or negatively affect viral replication (254).

Our IP- Western analysis confirmed the interaction of ORF4A with the human NF45 protein and its bat and camel counterparts. The interaction of ORF4A with the NF45 protein could have a direct or indirect role, by forming a complex with NF90, in promoting or decreasing viral replication. However, the functional implications of NF45 interaction with the ORF4A in MERS-CoV replication needed further examination in all three species.

4.3.3 heterogeneous nuclear ribonucleoprotein (hnRNPs)

Heterogeneous nuclear ribonucleoproteins (hnRNPs) are multifunctional proteins consisting of many RNA-binding proteins (RBPs). They contain an RNA recognition motif (RRM) and an arginine/glycine-rich domain (GRD). hnRNPs are involved in different stages of processing heterogeneous nuclear RNAs (hnRNAs) into mature mRNA. Also, they contribute to other aspects of RNA metabolism, such as mRNA stabilization, alternative splicing, and regulating gene expression. hnRNPs have similar characteristics, except for some differences in domain composition and functional properties (256). The alteration in expression levels of hnRNPs was associated with different cancer and neurodegenerative diseases, making hnRNPs more interested in disease research (257).

It has been revealed that the protein composition of hnRNP complexes in (HeLa) cells comprises 20 major hnRNP proteins and a smaller number of minor hnRNP proteins. hnRNPAB, hnRNPC1/C2, and hnRNPA2/B1 are examples of major hnRNP proteins (256).

4.3.3.1 (hnRNPA2/B1)

hnRNPA2/B1 is a highly expressed cellular protein encoded by the hnRNP A2/B1 gene. It is required for the proper localization of transcripts containing an A2 response element (A2RE), such as myelin basic protein (MBP) and neurogranin (NRGN) mRNA (258). hnRNPA2/B1 is also involved in various biological functions, including transcription, RNA processing, mRNA stability, and RNA trafficking and localization. Influenza virus NP is a structural protein that plays a crucial role in virus replication. Its primary function is to encapsulate the viral genome and interacts directly with the viral polymerase complex to enhance viral RNA replication (259). It has been shown that hnRNP A2/B1 binds directly to NP via its glycine-rich domain (GRD). Depleting hnRNPA2/B1 reduced viral RNA synthesis significantly, indicating that hnRNP A2/B1 is a proviral cellular factor for the influenza A virus infection (260). Japanese encephalitis virus (JEV) is a flavivirus spread by mosquitos and infects the central nervous system with a high fatality rate (261). The core protein of JEV plays a fundamental role in viral replication. hnRNPA2/B1 has been identified as a cellular binding partner of the JEV core protein, and depleting hnRNPA2/B1 protein resulted in a massive reduction in viral replication (262).

ORF4A interaction with human hnRNP A2/B1 and its bat and camel counterparts was validated by IP-Western analysis, although the association is weaker with the bat's counterpart. In contrast to humans and camels, bats don't show clinical symptoms of MERS-CoV infection. Therefore, it is tempting to hypothesize that the interaction of ORF4A with hnRNPA2/B1 enhances MERS-CoV replication in humans and camels more than in bats. However, further experiments are needed to confirm this hypothesis.

4.3.3.2 (hnRNPC1/C2)

hnRNPC1/C2 are abundant cellular proteins encoded by the HNRNPC gene. hnRNP C1/C2 are involved in various biological functions, such as transcriptional regulation, DNA repair, and RNA processing. They are mainly located in the cell's nucleus but can shuttle between the nucleus and the cytoplasm. hnRNP C mRNA is spliced into two isoforms, C1 and C2. Both isoforms possess a leucine zipper motif and RNA recognition motif. Heterotetramers of three molecules of C1 and one molecule of C2 are oligomerized to form a strong and specific RNA interaction. This oligomerization is mediated via a leucine zipper motif of C1 and C2 isomers. It has been shown that hnRNP C1/C2 interacts with the nonstructural protein of DENV NS1 and plays an essential role in viral replication at the stage of viral RNA synthesis. Depleting hnRNPC1/C2 in DENV-infected cells significantly reduced viral replication (247).

The ORF4A protein Interacts with hnRNPC1/C2 human protein and its camel counterpart, but not with bat equivalent protein. Recently, the role of hnRNPC1/C2 in MERS-CoV replication has been investigated. In that study, depletion of hnRNPC significantly reduced viral mRNA expression and viral replication in human lung adenocarcinoma (Calu-3) and human small airway epithelial (HSAEC) cells. Therefore, it is tempting to conclude that the absence of ORF4A-hnRNP C1/C2 interaction in PaKiT cells might be one factor that allows bats to control a limited replication of MERS-CoV compared to humans or even camels. However, further analysis is needed to confirm this conclusion.

4.3.3.3 (HNRPAB)

Hepatocellular carcinoma (HCC) is a highly lethal cancer resulting from chronic inflammation caused by the hepatitis B virus (HBV) or hepatitis C virus (HCV). Woodchuck hepatitis virus (WHV) causes a chronic infection in woodchucks, with hepatic injury, inflammation, cirrhosis, and HCC development. WHV is closely related to the human HBV in genome structure, morphology, replication, course of infection, and the development of HCC, making it an accepted animal model to study the HBV infection-induced HCC disease (263).

A study evaluated the transcriptional characteristics of viral infection-induced woodchuck hepatocellular carcinoma (HCC) and found that HNRPAB is highly up-regulated in that state, indicating a potential role of hnRNPAB in enhancing hepatitis B infection (264). We have shown that ORF4A interacts with hnRNPAB in all three species. Further experiments are needed to examine the effects of hnRNPAB depletion in MERS-CoV replication in Human and animal host cells.

4.3.4 KPNA4 (QIP1)

The α-karyopherins are divided into three sub-families including the importin-α1 subfamily, the importin-α2 subfamily, and the importin-α3 subfamily. KPNA4 belongs to the importin-α2 subfamily (250). The members of the importin-α2 subfamily are known for their specificity for NF-κB, which has a critical role in the expression of pro-inflammatory cytokines and the development of innate immunity. NF-κB is present in the cell's cytoplasm in association with the inhibitory protein IκB. During pathogens infection, IκB gets phosphorylated, ubiquitinated, and degraded, releasing NF-κB. KPNA4 binds to the released NF-κB and translocases it into the nucleus to promote the transcription of pro-inflammatory cytokines (251).

Our IP- Western analysis confirmed the interaction of ORF4B with KPNA4 human protein and its camel counterpart, with a much stronger association between ORF4B and human KPNA4. The role of ORF4B interaction with KPNA4 in MERS-CoV replication has been investigated recently. It was shown MERS-CoV ORF4B prevents NF-κB from translocating into the nucleus by outcompeting NF-κB for KPNA4 binding, thereby disrupting the NF-κB-mediated innate immune response and enhancing virus replication (252). Our IP-Western analysis showed the association of ORF4B with KPNA4 bat equivalent protein is much weaker than its human and camel counterparts, indicating that bats could maintain better NF-κB-mediated innate immune response than humans and camels. However, further experiments are needed to identify the functional implications of KPNA4 interaction with ORF4B in PaKiT and Dubca cells.

Chapter 5. Studying the functional role of ORF10 in SARS-CoV-2 replication

5.1 Introduction

The Coronavirus 2019 (COVID-19) pandemic has severely impacted public health, making targeting this newly emerging disease a key priority in medical research. Studying the functional roles of the SARS-2-CoV genes is crucial in understanding virus pathogenicity and identifying new therapeutic targets. Open reading frame 10 (ORF10) is one of the unique features of the SARS-CoV-2 genome, and its potential role in virus replication remains controversial. Multiple reports suggested that ORF10 protein may only be fleetingly present during infection and has no functional roles in virus replication and pathogenicity and, therefore, should not be treated as a protein-encoding gene (253)(254). On the other hand, ORF10 transcripts have been detected in patients infected with SARS-CoV-2, and the expression levels of ORF10 transcripts in patients with severe disease were much higher than in patients with moderate disease, suggesting the role of ORF10 in maximizing viral replication and pathogenesis (101). This chapter aims to shed light on the possible roles of the ORF10 protein in SARS-CoV-2 infection.

Reverse genetics is a powerful technique that can study the functional roles of viral genes as it allows the analysis of the phenotypic effects of genetically modified viruses (255). The nucleotide sequence of a particular gene can be changed by point mutations, directed deletions, or insertions. Furthermore, this technique can be used in vaccine development by designing recombinant viruses with reduced pathogenicity but capable of eliciting a robust immune response and mediating virus neutralization (256).

Recombination is one of the common features of RNA viruses. ''Targeted RNA recombination'' is a reverse genetic system that allows modifications to the viral RNA genome and was the first system used to study the function of coronaviruses genes (257). In that system, a synthetic donor RNA is transfected into cells infected with a recipient virus, allowing them to recombine naturally, exploiting the recombination feature of RNA viruses. Later on, reverse genetic approaches based on full-length cDNAs 'infectious clones' have been developed to bypass limitations presented in the targeted RNA recombination approach, such as the difficulty in studying lethal mutations of viruses. Several methods to design infectious clones containing full-length viral cDNA in a plasmid with an appropriate promoter have been developed, and *E. coli* has always been used as an intermediate host to clone viral cDNA genomes (258). However, because of their large genome size, the plasmid

system wasn't suitable for producing full-length cDNA clones of coronaviruses. Therefore, yeast artificial chromosome (YAC) and bacterial artificial chromosome (BAC) are now being in use to assemble, mutagenize and clone the entire genome of coronaviruses due to their ability to harbor massive DNA inserts (259).

Transformation-associated recombination (TAR) cloning is a unique method to assemble large overlapping DNA fragments in only one step, exploiting the high ability of homologous recombination in yeast. The joining process is driven by homologous recombination. Each cDNA fragment must share a short region of overlapping sequence (50-70 nt) with the next so that within the yeast cell they can be joined by homologous recombination (260). The viral cDNA overlapping fragments can be either generated by RT-PCR from the virus or synthesized de novo. Notably, a sequence encoding for a T7 RNA polymerase promoter at the 5′ end of the assembled construct should be incorporated to generate RNA run-off transcripts using T7 RNA polymerase (261). The two end fragments (containing 5′- and 3′-terminals) of the constructed viral cDNA genome must also share overlapping sequences with the linearized YAC plasmid vector to successfully generate YAC-based infectious cDNA clones (Figure 40).

TAR Recombination Principle:
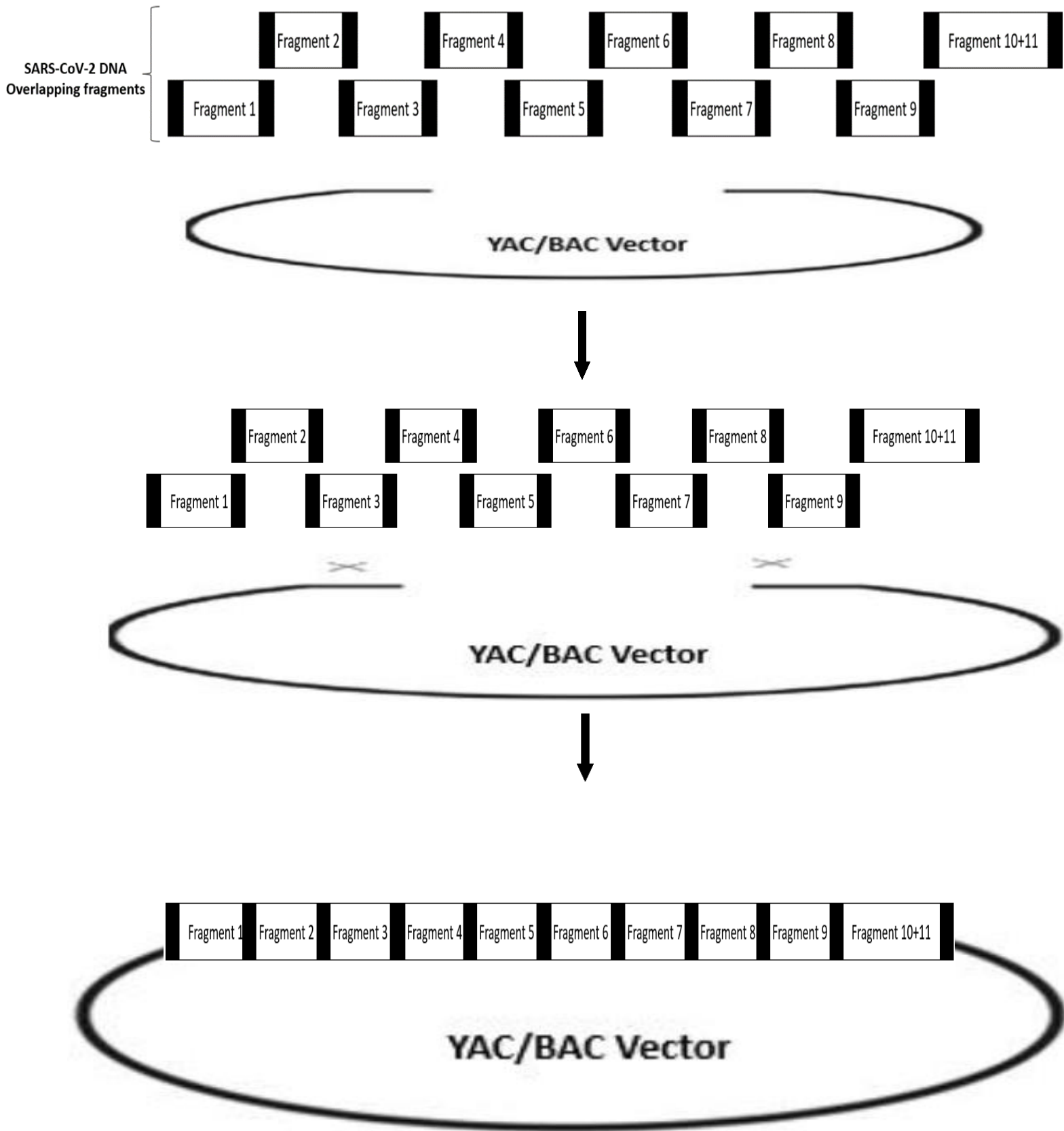
Figure 41. A schematic diagram for constructing a full-length SARS-CoV-2 cDNA infectious clone with the yeast shuttle vector pYES1L. Viral genome amplified in overlapping subgenomic fragments. A full-length viral infectious clone is assembled into a pYES1L vector by homologous recombination.

The main advantages of using a yeast-based reverse-genetics platform are simplicity, rapidity, and the ability to interchange cDNA fragments incorporating mutations of interest easily. (262). Infectious cDNA construct generated through a yeast-based reverse-genetics platform can later be cloned into bacterial artificial chromosomes (BAC). Compared to YAC, BAC is rarely chimeric, easily purified intact, enhances the stability of large DNA fragments, and produces more vectors per cell than YAC (261).

This chapter aims to shed light on the possible roles of the ORF10 in SARS-CoV-2 replication. SARS-CoV-2 ORF10 FLAG-tagged protein was successfully expressed in A549 cells. Immunoprecipitation of FLAG-tagged ORF10 proteins was performed, and high throughput quantitative proteomics was conducted to identify possible cellular interacting partners of ORF10 protein. Protein-protein interactions of ORF10 with its cellular partners were validated using IP-Western analysis. The reverse genetics technique was used to rescue the SARS-CoV-2 virus with either the ORF10 protein knocked out or replaced with fluorescent markers to elucidate the functional role of ORF10 protein in viral replication. Finally, the replicative fitness of the SARS-CoV-2 ORF10 mutant was characterized in different cell lines.

5.2 Results

5.2.1 Cloning SARS-CoV-2 ORF10 gene

ORF10 flag-tagged gene was cloned in pcDNA5/FRT/TO-TOPO vector. 50 ng from the plasmid was transformed into DH5-α, a single colony was picked and grown in a large volume of LB broth, and midi-prep was performed to extract a high concentration of DNA plasmid. After that, the DNA plasmid was confirmed using appropriate restriction enzymes (Figure 41).
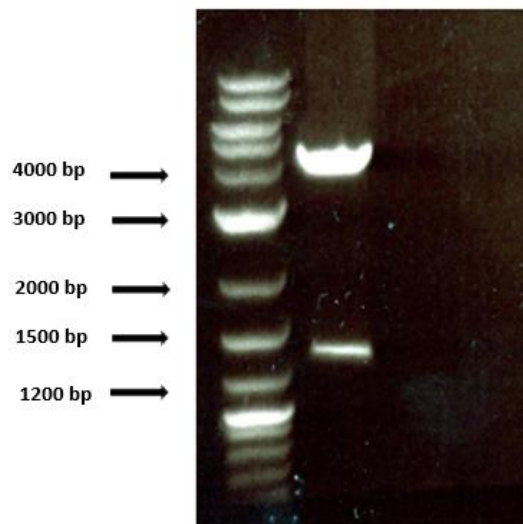
Figure 42.Cloning and analysis of ORF10 plasmid DNA by agarose gel electrophoresis. 50 ng from ORF10 plasmid DNA was transformed into competent E. coli DH5α, and a single colony was selected and grew in 50ml of LB containing ampicillin with a final concentration of 100 µg/mL overnight as the plasmid contains ampicillin resistant gene. Then, the ORF10 plasmid was isolated using midi-prep. The identity of ORF10 Plasmid DNA was confirmed using AVRII and BamHI restriction enzymes.

5.2.2 Validating ORF10 protein expression in A549 cells

A549 cells were transfected with ORF10 plasmid DNA to induce protein expression. Protein expression was analyzed by Western Blotting. The molecular mass expected for ORF10 (tagged with the FLAG epitope) was 10 kDa (Figure 42). ORF10 protein expression was further validated using Indirect Immunofluorescence Assay (IFA) (Figure 43).
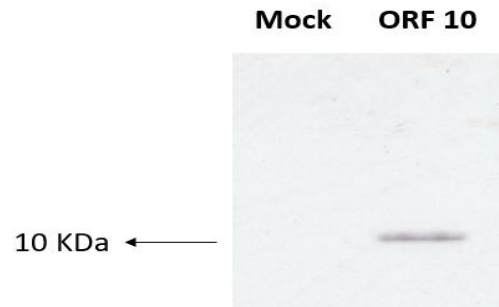
Figure 43. Examining ORF10 protein expression by Western Blotting analysis. A549 cells were seeded in the six-wells plate before they were transfected with two µg of ORF10 DNA plasmid using a PEI transfection reagent. Transfection mixture incubated for 18 hrs before cells were harvested and lysed with 2X sample buffer. The protein sample was separated using a 10% SDS-PAGE gel and transferred to a PVDF membrane for immunoblotting with an anti-flag antibody.
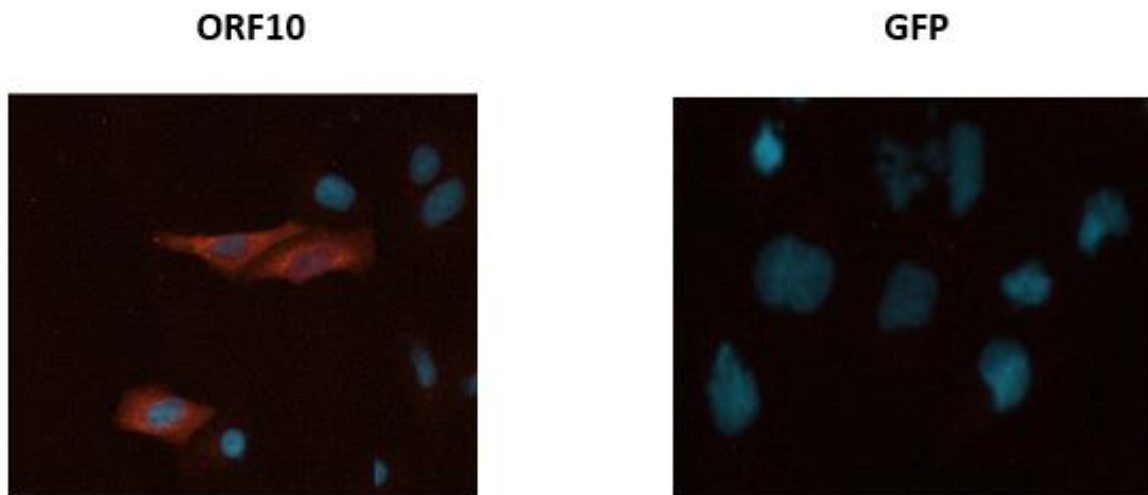
Figure 44. IFA analysis ORF10 protein expression. A549 cells were seeded in 96 wells-plate before they were transfected with 100 ng of either ORF10 plasmid or GFP plasmid (as a control). Cells were fixed with 4% paraformaldehyde, washed, and permeabilized with 1% (v/v) Triton-X 100 for 10 min. Then, cells were washed again and blocked for 30 min before staining with anti-flag primary antibody followed by an anti-mouse (Alexa Fluor 647 conjugated secondary antibody, red signal). DAPI was applied to stain the cell's nucleus.

5.2.3 Preparing co-IP samples from A549 cells expressing ORF10 protein for TMT-MS/MS analysis

A549 cells were grown in three T-75 flasks before they were transfected with ORF10 plasmid DNA for 18 hrs in triplicate. Three flasks of A549 cells that weren't transfected with the ORF10 plasmid DNA were included as mocks. After 18 hrs incubation, cells were harvested, lysed, and sonicated. The immunocomplexes were then captured with anti-FLAG magnetic beads before the samples were eluted (Figure 44). The expression of the ORF10 protein in pull-down samples was confirmed by Western Blotting analysis before they were sent for TMT-MS/MS analysis at the Faculty Proteomics facility to identify ORF10 protein potential host interacting partners (Figure 45).
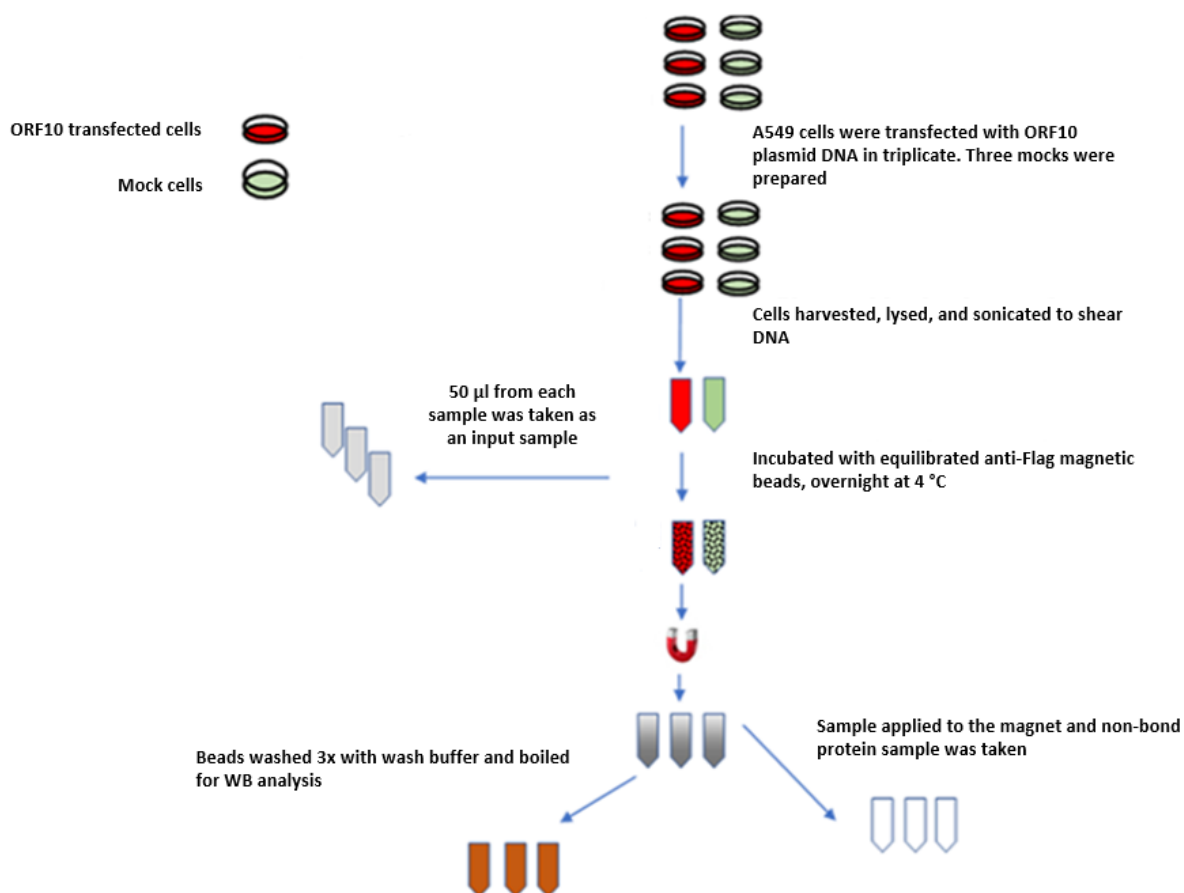
Figure 45. Preparation of co-IP samples from A549 cells expressing ORF10 protein for TMT-MS/MS analysis. Three T-75 flasks of A549 cells were transiently transfected with an appropriate concentration of ORF10 plasmid DNA. Three negative controls were included. Pull-down samples were prepared.
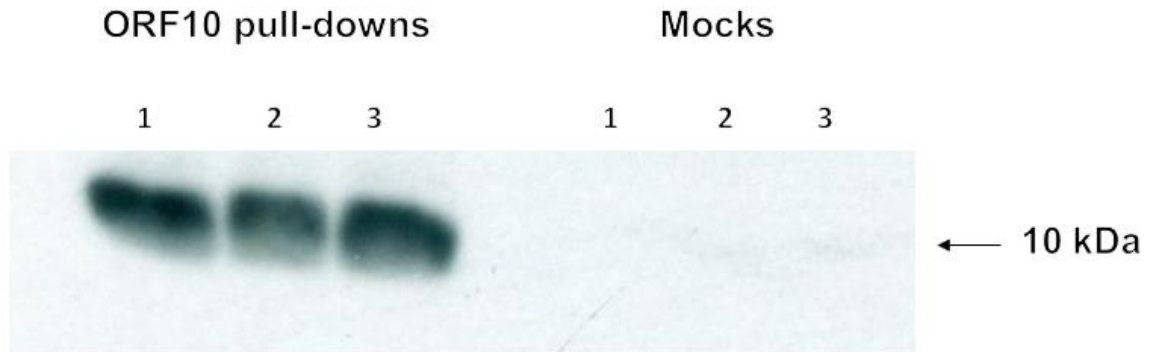
Figure 46. Confirmation of successful transfection of ORF10 plasmid DNA in co-IP samples by western blotting analysis before conducting TMT-MS/MS analysis. A549 cells were transfected with ORF10-flag tagged plasmid DNA. Pull-down samples were prepared and loaded into 10% SDS-PAGE gel. Proteins were separated and transferred to a PVDF membrane for immunoblotting with the anti-flag antibody. The molecular weight of ORF10 protein is 10 KDa.

5.2.4 TMT-MS/MS analysis of ORF10 co-IP samples

Data generated from TMT-MS/MS analysis of ORF10 co-IP samples were analyzed. Nineteen cellular proteins showed a significant enrichment with the ORF10 protein with the highest confidence, as shown in (Table 27). Proteins increased ≥ 1.7 log2 fold in the co-IP samples compared to mock proteins were analyzed by STRING analysis to reveal their specific host pathways. The analysis showed significant enrichment of proteins involved in the anti-viral immune response (Figure 46). IFIT1, OAS2, and MX1 cellular proteins were selected to validate their interactions with the ORF10 protein (Table 28).

Table 27. Cellular proteins increased ≥ 1.7 log2 fold in the ORF10 co-IP samples compared to mock cells. Proteins' IDs, names and genes' IDs are obtained from UniProt: the universal protein knowledgebase in 2021. The log2 fold change is an average of three replicates.

Uniport ID	Protein name & Gene ID	log2-fold change average: ORF10 / Mock
P20591	Interferon-induced GTP-binding protein Mx1. GN=MX1	12.632
P09914	Interferon-induced protein with tetratricopeptide repeats 1. GN=IFIT1	4.132
A0A087X0V5	2'-5' oligoadenylate synthase. GN=OAS2	4
P20592	Interferon-induced GTP-binding protein Mx2. GN=MX2	3.586
Q5T765	Interferon-induced protein with tetratricopeptide repeats 3, isoform CRA_a. GN=IFIT3	2.888
P05161	Ubiquitin-like protein ISG15. GN=ISG15	2.884
B3KN79	cDNA FLJ13894 fis, clone THYRO1001671, highly similar to 59 kDa 2'-5'-oligoadenylate synthetase-like protein.	2.825
Q16352	Alpha-internexin. GN=INA	2.215
Q7L0Y3	tRNA methyltransferase 10 homolog C. GN=TRMT10C	2.107
Q70UQ0	Inhibitor of nuclear factor kappa-B kinase-interacting protein. GN=IKBIP	2.063
Q6PJV4	THRAP3 protein (Fragment). GN=THRAP3	2.046
A0A5C2GK16	IG c1122_light_IGKV2-28_IGKJ2 (Fragment)	1.966
Q59EA2	Coronin (Fragment)	1.939
P19474	E3 ubiquitin-protein ligase TRIM21. GN=TRIM21	1.931
A0A0S2Z3X8	Rab GDP dissociation inhibitor (Fragment) OS=Homo sapiens OX=9606 GN=GDI1 PE=2 SV=1	1.93
P19525	Interferon-induced, double-stranded RNA-activated protein kinase. GN=EIF2AK2	1.859
Q13501	Sequestosome-1. GN=SQSTM1	1.785
A0A075B6S2	Immunoglobulin kappa variable 2D-29. GN=IGKV2D-29	1.782
E9PRY8	Elongation factor 1-delta. GN=EEF1D	1.731

Table 28. Cellular interaction partners that were chosen to validate their interaction with the ORF10 protein and their functions. Proteins' IDs, names and Genes' ID are obtained from UniProt: the universal protein knowledgebase in 2021.

UniProt ID	Gene ID	Protein name function	log2-fold change average: ORF10 / Mock
P09914	IFIT1	IFN-induced protein with tetratricopeptide repeats 1. It possesses antiviral activities such as sensing viral RNA and inhibiting the expression of viral mRNA (185).	≥ 4 log2 fold change
P29728	OAS2	2'-5'-oligoadenylate synthase 2. It senses viral dsRNA and is involved in initiating antiviral response by activating ribonuclease L (RNASEL), which eventually degrades viral RNA.	≥ 4 log2 fold change
P20591	MX1	Interferon-induced GTP-binding protein Mx1. It possesses antiviral activity against many RNA and some DNA viruses by targeting viral ribonucleocapsid (183) (184).	≥ 12 log2 fold change
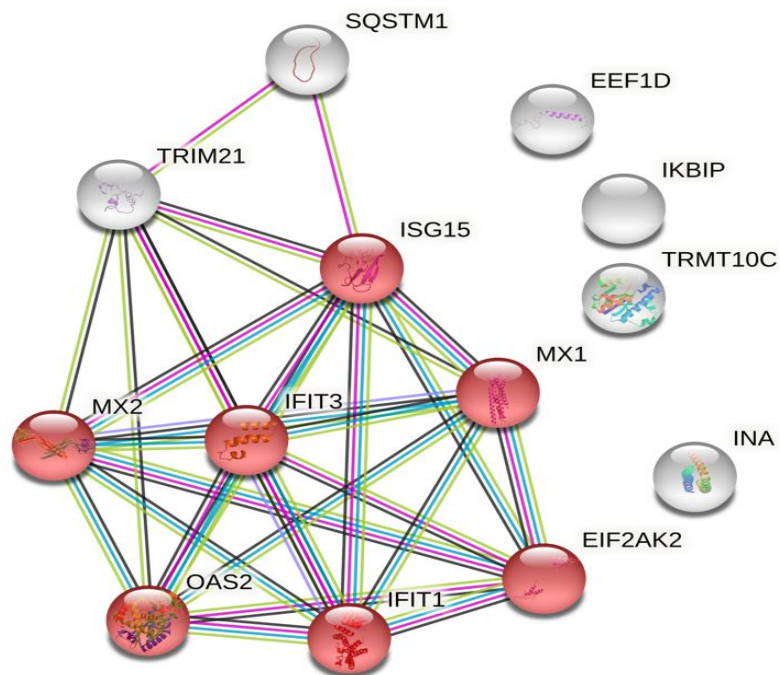
Figure 47. STRING analysis of proteins increased ≥ 1.7 log2 fold in ORF10 co-IP samples. The STRING database was searched to analyze host proteins that showed a ≥ 1.7 log2 fold increase in ORF10 co-IP compared to mock cells. Nodes representing proteins that most significantly enriched the GO term. Cellular proteins involved in the anti-viral immune response are shaded in red.

5.2.5 Validating the protein-protein interactions of the ORF10 protein with its cellular partners

The interactions of ORF10 protein with IFIT1, OAS2, and MX1 cellular proteins were validated using the IP-Western analysis. Briefly, A549 cells were grown in a T-75 flask before transfected with ORF10 plasmid DNA. ORF10 co-IP sample was then prepared as described in methods, section 2.3.3. Successful transfection of the ORF10 plasmid DNA was confirmed as shown in (Figure 47).
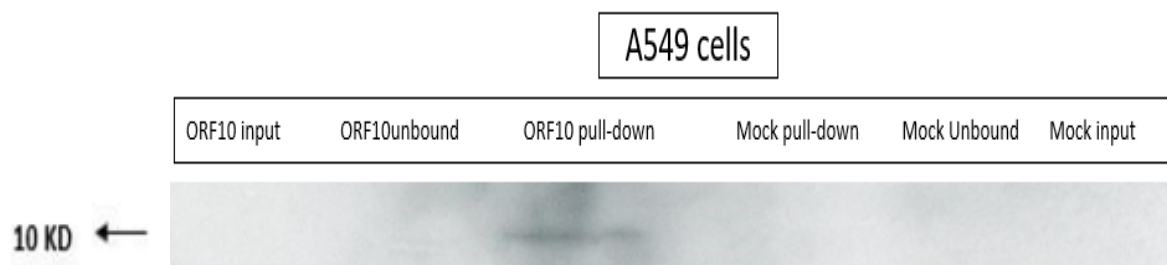
Figure 48. Confirmation of the successful transfection of ORF10 in co-IP sample. A549 cells were transfected with the ORF10 plasmid DNA. Input, non-bound, and pulldown samples were prepared by the co-IP protocol. Input, non-bound, and pull-down samples were loaded into each lane of 10% SDS-PAGE gel. Proteins were separated and transferred to a PVDF membrane for immunoblotting with an anti-flag antibody. The molecular weight of ORF10 was 10 KDa.

IP-Western analysis of input, non-bound, and pulldown samples confirms the interaction of ORF10 with the cellular protein OAS-2. The amount of OAS-2 protein in the ORF10 pulldown sample is more than the control pulldown sample (Figure 48). The interaction of cellular protein IFIT1 with ORF10 was also validated. The amount of IFIT1 protein in the ORF10 pulldown sample was more than its control pulldown (Figure 49). Finally, the proposed interaction between ORF10 protein with MX1 was confirmed by IP-Western analysis as the MX1 protein was detected in the ORF10 pulldown sample but not in control (Figure 50).

Figure 49. Validating the interaction of the ORF10 protein with the cellular protein OAS-2. A549 cells were transfected with SARS-CoV-2 ORF10 plasmid DNA. Input, non-bound, and pulldown samples were prepared following the co-IP protocol. Samples were loaded into a lane of 10% SDS-PAGE gel. Protein samples were separated and transferred to a PVDF membrane for immunoblotting with anti-OAS-2 antibody. The molecular weight of OAS-2 is 75 KDa.
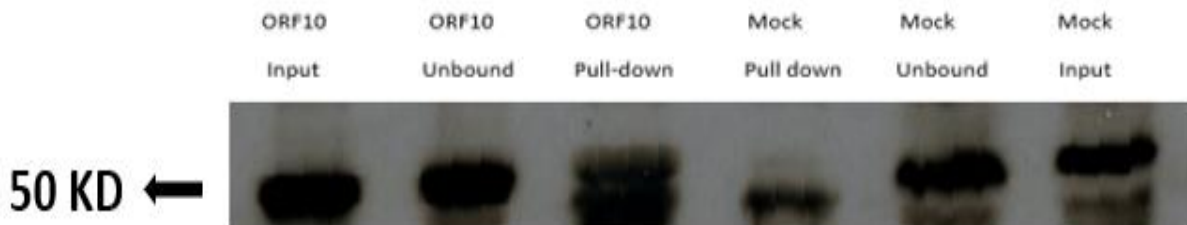
Figure 50. Validating the interaction of the ORF10 protein with the cellular protein IFIT1. A549 cells were transfected with SARS-CoV-2 ORF10 plasmid DNA. Input, non-bound, and pulldown samples were prepared following the co-IP protocol. Samples were loaded into a lane of 10% SDS-PAGE gel. Protein samples were separated and transferred to a PVDF membrane for immunoblotting with anti-IFIT1antibody. The molecular weight of IFIT1 is 50 KDa.

156
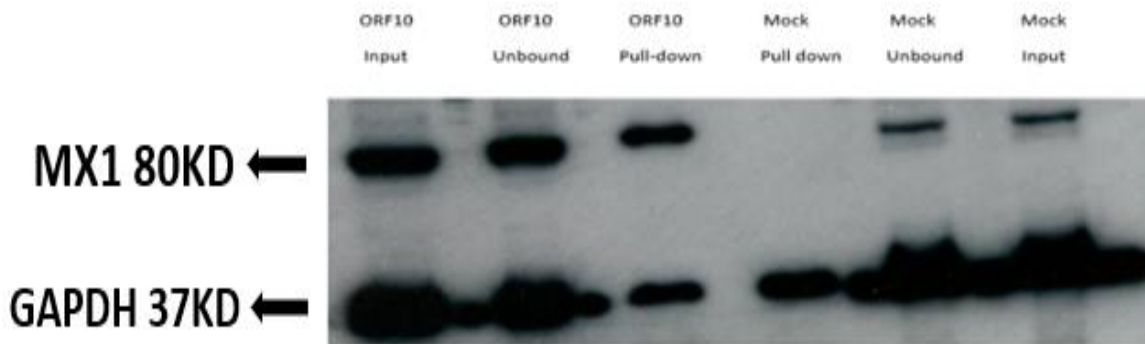
Figure 51. Validating the interaction of the ORF10 protein with the cellular protein MX1. A549 cells were transfected with SARS-CoV-2 ORF10 plasmid DNA. Input, non-bound, and pulldown samples were prepared following the co-IP protocol. Samples were loaded into a lane of 10% SDS-PAGE gel. Protein samples were separated and transferred to a PVDF membrane for immunoblotting with anti- MX1antibody. The molecular weight of MX1 and GAPDH are 80 KD and 37 KD, respectively.

5.2.6 Develop full-length cDNA constructs representing SARS-CoV-2 ORF10 mutants

IP-Western analysis validated the interaction of the ORF10 with the cellular proteins IFIT, MX1, and OAS-2, suggesting ORF10 might have a possible role in suppressing the host's innate immune response and enhancing the virus replication. To investigate this hypothesis, we developed full-length cDNA constructs representing SARS-CoV-2 ORF10 knockout, SARS-CoV-2ΔORF10mNeonGreen, and SARS-CoV-2ΔORF10mScarlet mutants using the reverse genetic approach (Figure 51). RNA transcripts from SARS-CoV-2 mutant constructs were *produced in vitro,* and permissive cells were transfected with RNA transcripts to recover infectious viruses. High-throughput proteomics analysis and the growth kinetics of SARS-CoV-2 mutant were conducted to assess the role of ORF10 protein in the virus replication.

Figure 52. Schematic outline of the workflow of construction of SARS-CoV-2 mutants using reverse genetics platform in this study.

Reverse Genetic work flow

Amplify DNA fragment to add the required homology (200ng each)

DNA fragments

linear cloning vector

MaV203 cells

PEG/LiAc solution

Incubate at 30C for 30 min

Add DMSO

Heat shock at 42 C for 20 min

Centrifugate at 200-400 X g for 5 min

Resuspend in 0.9% NaCl

Incubate transformation mix for 3 days

Pick 4–10 colonies
Resuspend in 15 µL of lysis buffer

5 µL of cell suspension

10 µL of cell suspension

Save 5 µL of cell suspension to transfer the final construct into *E. coli* when ready

Heat the cell suspension at 95°C for 5 minutes
Dilute lysate 1:5 in water

Yeast Colony PCR

4–5 glass beads
10 µL of lysis buffer
5 µL of saved cell suspension

PCR with 0.5 µL of lysate and 49.5 µL of PCR mix containing diagnostic primers

Vortex at room temperature for 5 minutes

Analyze PCR products using agarose gel electrophoresis and/or sequencing

Analysis of assembled construct

1 µL of cell lysate

Transfer of final assembled construct into *E. coli*

One Shot® TOP10 Electrocomp™ *E. coli*

Electroporate
Add 250 µL SOC
Recover for 1 hour at 37°C

Pick up a single colony and grow it up in 250ml of LB media

Plate on selective LB plates
Incubate overnight at 37°C

158

Amplification and Isolation BAC with NucleoBond Xtra BAC

DNA extraction and linearization

DNA extraction and precipitation

RNA production using In Vitro transcription

RNA electroporation into permissive cells to rescue mutant virus

SARS-CoV-2 ORF10 knockout, SARS-CoV-2ΔORF10mNeonGreen, and SARS-CoV-2ΔORF10mScarlet cDNA constructs were designed to incorporate a bacteriophage T7 promoter upstream at the 5' end to enable them to function as templates for *in vitro* transcription of RNA. a poly-A tail was incorporated into the 3' end of all three cDNA clones to assist RNA processing in the host cells. Transformation-associated recombination (TAR) cloning was used to assemble the cDNA genome corresponding to SARS-CoV-2 ORF10 KO, SARS-CoV-2ΔORF10mNeonGreen, and SARS-CoV-2ΔORF10mScarlet mutants (263).

There are two methionine (Met) residues in the ORF10 gene. The cDNA fragment containing the ORF10 KO gene was generated by mutating both Met codons using the site-directed mutagenesis technique (Figure 52, Figure 54). For SARS-CoV-2ΔORF10mNeonGreen and SARS-CoV-2ΔORF10mScarlet mutants, the ORF10 gene was replaced with either fluorescent markers mNeonGreen or mScarlet (Figure 52).
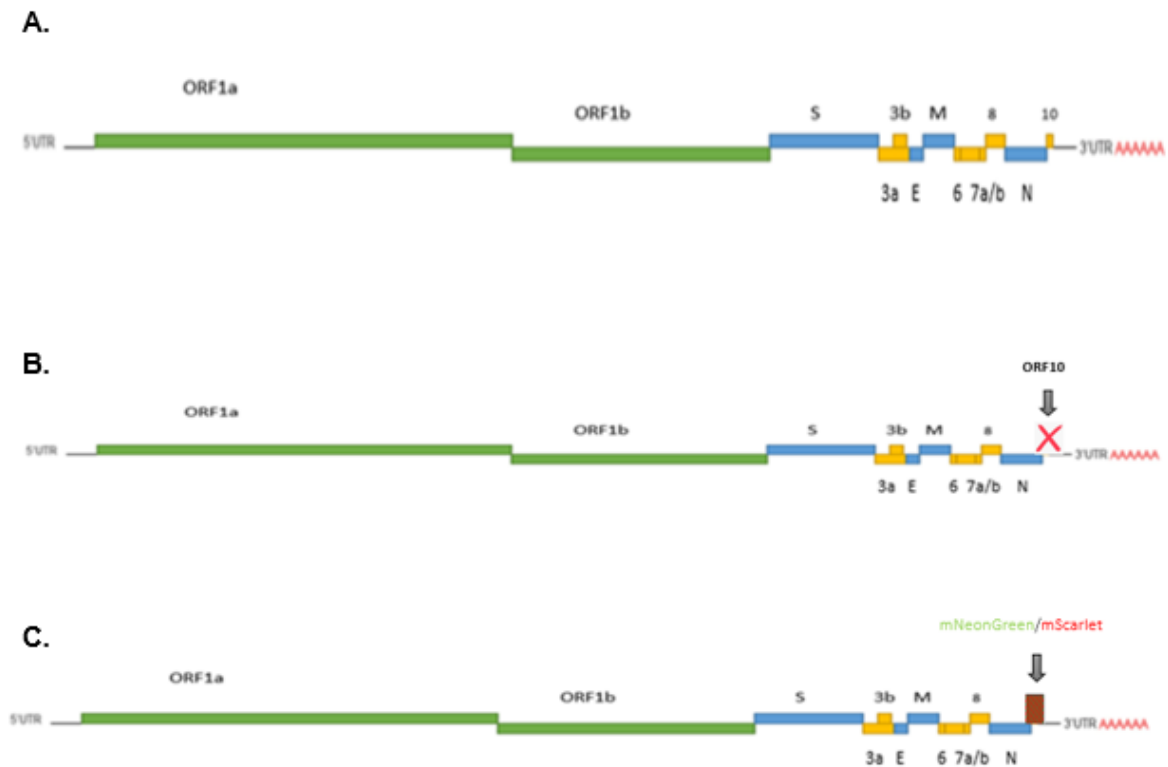
Figure 53. The SARS-CoV-2 genome structure illustrates the location of various ORFs (A). Schematic derivation of SARS-CoV-2 ORF10 KO genome **(B)**. Schematic derivation of SARS-CoV-2ΔORF10mNeonGreen & SARS-CoV-2ΔORF10mScarlet mutants' genomes **(C)**.

Ten cDNA fragments spanning the SARS-CoV-2 genome were kindly gifted by Prof. Davidson. The cDNA fragment sequences were commercially synthesized and cloned into pJet1.2 vectors (arrived as plasmids) (Table 29). All cDNA fragments were designed to overlap by 70 bp to facilitate homologous recombination in the Saccharomyces cerevisiae. Fragment 1 was designed to incorporate a bacteriophage T7 promoter upstream of the 5' UTR end. Fragment 10 +11 contains the ORF10 gene (Figure 53). Nine cDNA fragments were produced from (Fragment 1 pJet1.2 plasmid — Fragment 9 pJet1.2 plasmid) using high-fidelity DNA polymerase Platinum™ SuperFi II PCR Master Mix. All DNA fragments were then stored at -20 °C until the day of yeast assembly.

Table 29. The cDNA plasmids spanning the SARS-CoV-2 genome. Fragment 10 +11 pJet1.2 plasmid contains the ORF10 gene and is used to generate fragment 10 +11 ORF10 KO pJet1.2 plasmid, fragment 10+11ΔORF10mNeonGreen pJet1.2 plasmid, and fragment 10+11 ΔORF10mScarlet pJet1.2 plasmid.

Plasmid name	Fragment size
Fragment 1 pJet1.2 plasmid	2958 pb
Fragment 2 pJet1.2 plasmid	2940 pb
Fragment 3 pJet1.2 plasmid	2936 pb
Fragment 4 pJet1.2 plasmid	2940 pb
Fragment 5 pJet1.2 plasmid	2940 pb
Fragment 6 pJet1.2 plasmid	2940 pb
Fragment 7 pJet1.2 plasmid	2940 pb
Fragment 8 pJet1.2 plasmid	2940 pb
Fragment 9 pJet1.2 plasmid	2940 pb
Fragment 10 +11 pJet1.2 plasmid	4151 pb
Fragment 10 +11 ORF10 KO pJet1.2 plasmid.	4151 pb
Fragment 10 +11 ΔORF10mNeonGreen pJet1.2 plasmid	4745pb
Fragment 10 +11 ΔORF10mScarlet pJet1.2 plasmid	4733pb
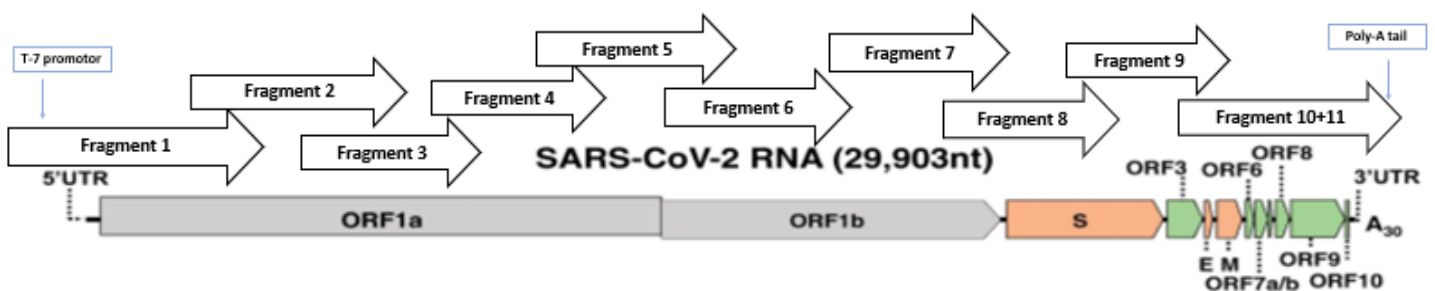
Figure 54. Schematic showing the SARS-CoV-2 genome organization and cDNA fragments that span the SARS-CoV-2 genome. Transformation-associated recombination (TAR) technique will be used to assemble cDNA fragments to generate YAC containing the full-length SARS-CoV-2 mutant genome.

5.2.6.1 Designing and obtaining ORF10 knockout gene

The ORF10 gene encodes two Met residues, including the start codon residue and another residue located in the middle of the gene. Both Met residues were mutated into stop codons (TAA) or (TAG) to confirm a complete disruption of ORF10 protein expression with a minimum conformational change in RNA structure (Figure 54, Figure 55).
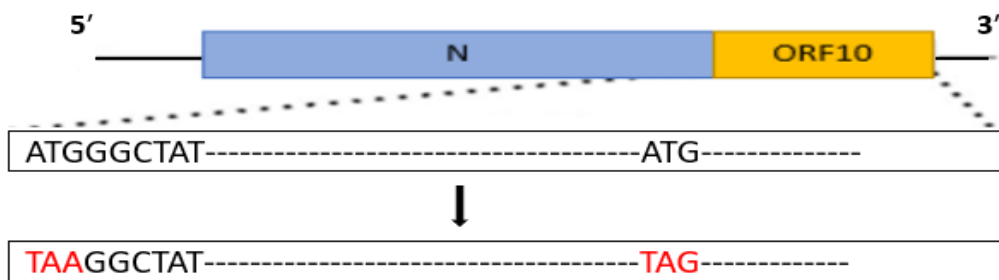
Figure 55. Schematic derivation of the ORF10 gene. The start codon and another downstream Met within the ORF10 gene were mutated into stop codons to disrupt ORF10 protein expression.

The cDNA fragment containing the ORF10 KO sequence was obtained through site-directed mutagenesis utilizing Fragment 10 +11 pJet1.2 plasmid as a template. The resulting cDNA containing the ORF10 KO was sequenced to confirm successful mutations before it ligated into the pJet1.2 Vector to generate (Fragment 10 +11 ORF10 KO) pJet1.2 plasmid (Figure 56).

Design of the ORF10 Knock out by Overlapping PCR extension
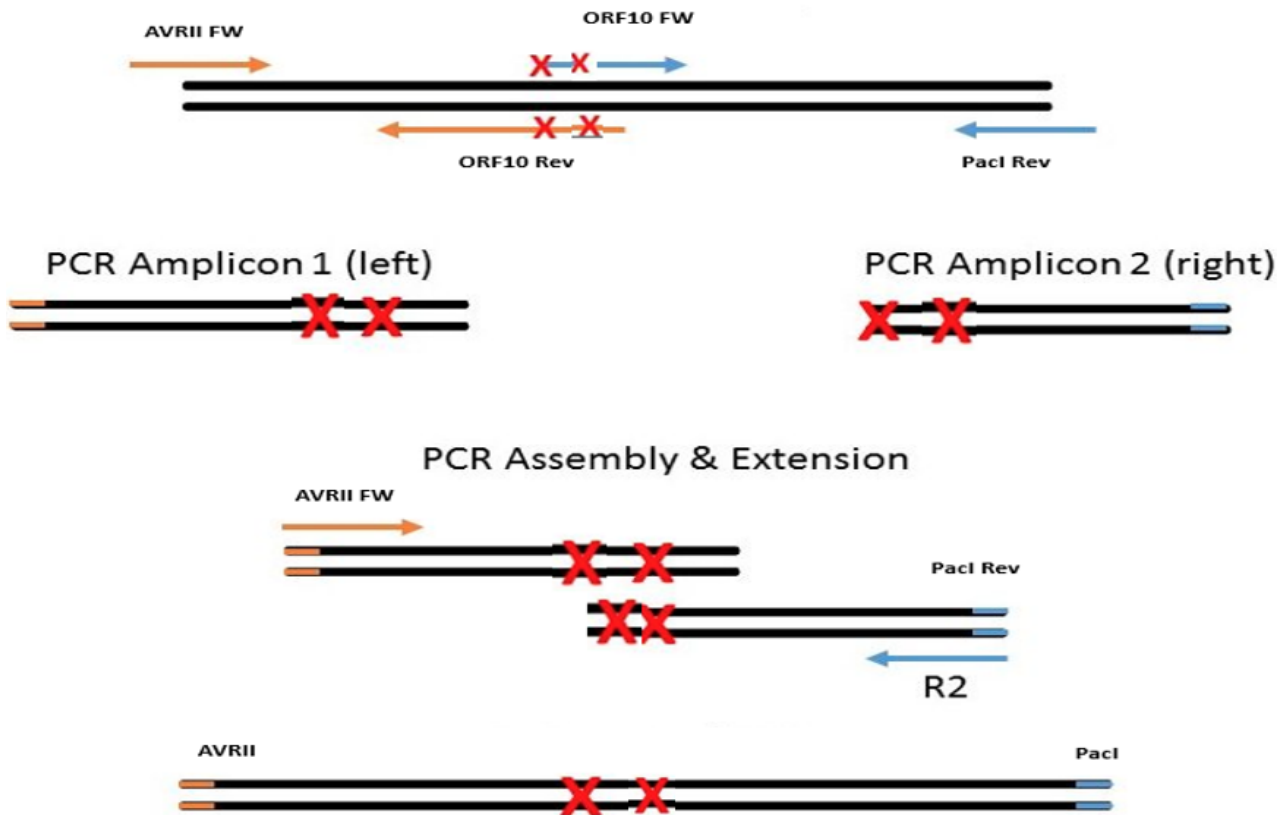
Figure 56. Schematic representation of site-directed mutagenesis strategy to knock out ORF10 gene.
Target DNA will be amplified in two separate PCR reactions using AVRII, ORF10Rev, ORF10 FW, and Pacl Rev.
The ORF10 Rev and ORF10 FW primers are mutagenic. The produced amplicons (left& right) will be mixed and
used as a template for the second round PCR using AVRIIFW and PaclRev primers.
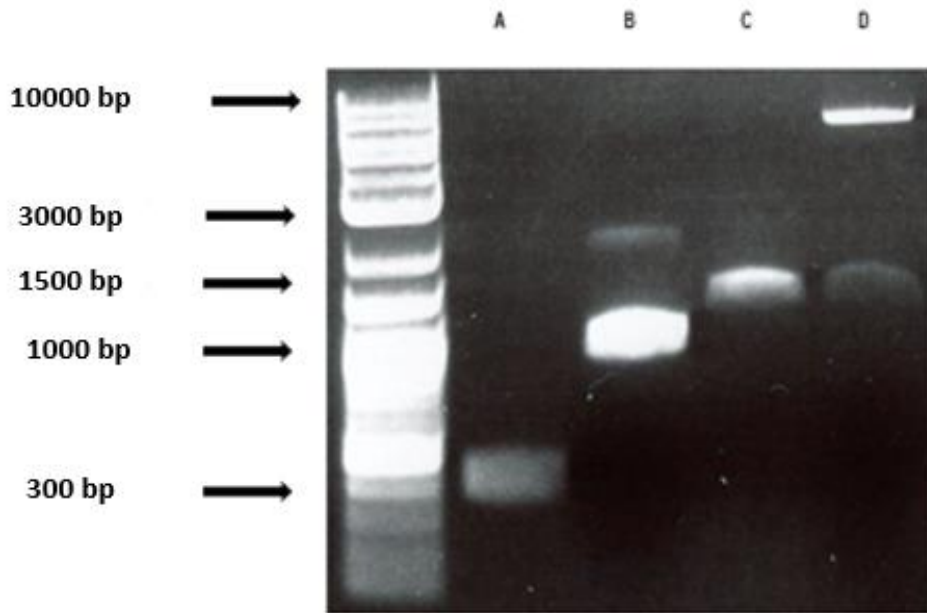
Figure 57. Obtaining and analyzing cDNA fragment containing the ORF10 KO sequence by agarose gel electrophoresis. The Met residues in the ORF10 gene were mutated into stop codons to disrupt the ORF10 protein expression using overlapping PCR as follows: a 375pb DNA fragment was amplified from the F10+11 fragment using ORF10FW and PacIRev primers (A). Then, a 1020bp DNA fragment was amplified by PCR using AVRIIFW and ORF10Rev primers (B). The produced PCR products were annealed using AVRIIFW and PacIRev primers (C). The final DNA product was then digested with AVRII and PacI restriction enzymes and ligated into F10+11 in pJet1.2 plasmid vector to generate (Fragment 10 +11 ORF10 KO) pJet1.2 plasmid (D). The desired mutations were confirmed by sanger sequencing. The PCR and digestion products were run on a 1% agarose gel, and DNA bands were visualized under a UV transilluminator.

5.2.6.2 Amplifying (Fragment 10 +11 ORF10 KO) pJet1.2 plasmid

DH5α competent E. coli was transformed with (Fragment 10 +11 ORF10 KO) pJet1.2 to amplify the plasmid for downstream applications. Following transformation, a few colonies were selected, and the bacteria were cultured overnight. Plasmid DNA was then extracted using the midiprep protocol. A restriction digest was carried out to check the size of the digestion products. DNA plasmid was sent for sanger sequencing to confirm the ORF10 knockout. cDNA fragment containing ORF10 KO gene was then amplified from Fragment 10 +11 ORF10 KO) pJet1.2 plasmid using high-fidelity DNA polymerase Platinum™ SuperFi II PCR Master Mix and saved until the day of the assembly (Figure 57).
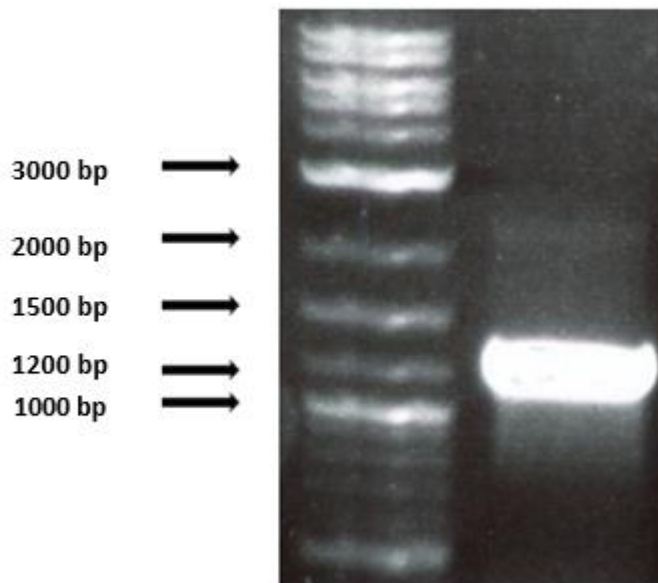
Figure 58. Amplifying ORF10 KO DNA sequence from (Fragment 10 +11 ORF10 KO) pJet1.2 and analyzing it by agarose gel electrophoresis. Fragment 10 +11 ORF10 KO pJet1.2 was used as a template to produce the overlapping cDNA fragment containing the ORF10 KO gene. The PCR product was then run on a 0.8% agarose gel at 100 V for 40 min and imaged under a UV transilluminator. The PCR product was then purified and saved at -20°C until the day of the assembly.

5.2.6.3 Designing and generating (Fragment 10 +11ΔORF10-mNeonGreen) & (Fragment 10 +11 ΔORF10mScarlet) pJet1.2 plasmids

To make SARS-CoV-2ΔORF10-mNeonGreen or SARS-CoV-2ΔORF10mScarlet cDNA genomes, the ORF10 gene in Fragment 10 +11 pJet1.2 plasmid was replaced with either mNeonGreen or mScarlet genes to generate (Fragment 10 +11ΔORF10-mNeonGreen) pJet1.2 plasmid and (Fragment 10 +11 ΔORF10mScarlet) pJet1.2 plasmids, respectively (Figure 58).
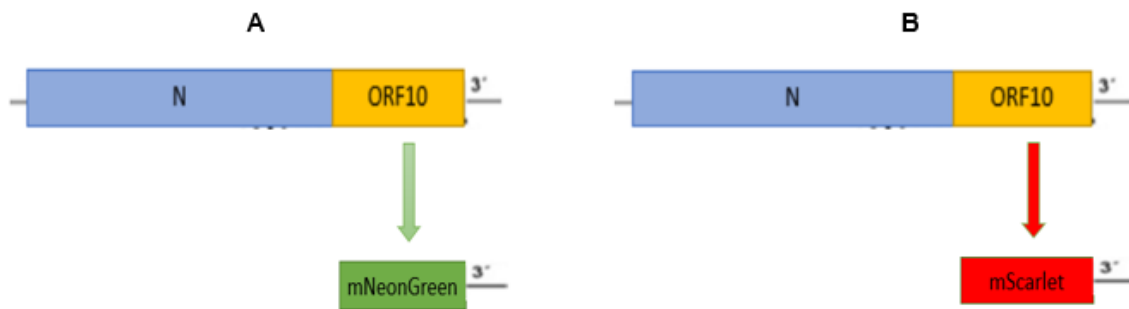
Figure 59.Schematic shows the construction of the (Fragment 10 +11ΔORF10-mNeonGreen) pJet1.2 and (Fragment 10 +11 ΔORF10mScarlet) pJet1.2 plasmids. The ORF10 gene was replaced with either fluorescent marker mNeonGreen **(A)** or mScarlet **(B)**.

mNeonGreen and mScarlet DNA sequences were liberated from their original plasmids through digestion with the appropriate restriction enzymes StuI and AscI. mNeonGreen and mScarlet DNA sequences were then separated from their vectors by agarose gel electrophoresis, excised from the gel, and extracted.

The ORF10 gene in (Fragment 10 +11 pJet1.2 plasmid) was digested with appropriate restriction enzymes StuI and AscI. The ORF10 DNA sequence was then separated from (Fragment 10 +11 pJet1.2 plasmid vector) by agarose gel electrophoresis, and Fragment 10 +11 pJet1.2 plasmid vector was then excised from the gel and extracted. mNeonGreen or mScarlet DNA sequences were then ligated into the digested Fragment 10 +11 pJet1.2 plasmid vector to generate either (Fragment 10 +11ΔORF10-mNeonGreen) pJet1.2 plasmid or (Fragment 10 +11 ΔORF10mScarlet) pJet1.2 plasmid (Figure 59). (Fragment 10 +11ΔORF10-mNeonGreen) pJet1.2 plasmid and (Fragment 10 +11 ΔORF10mScarlet) pJet1.2 plasmid were then sent for sanger sequencing.
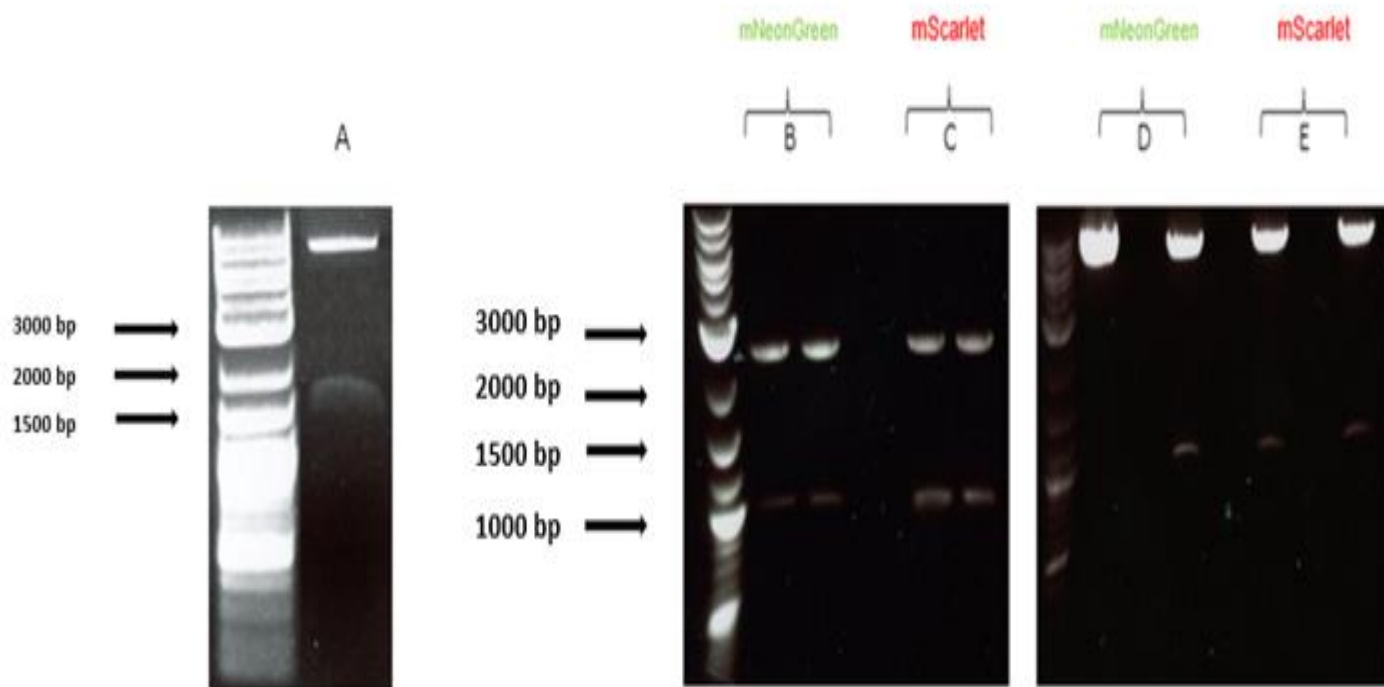
Figure 60. Generating (Fragment 10 +11ΔORF10-mNeonGreen) & (Fragment 10 +11 ΔORF10mScarlet) pJet1.2 plasmids and analyzing them by agarose gel electrophoresis. The ORF10 DNA sequence was liberated from Fragment 10 +11 pJet1.2 plasmid. Fragment 10 +11 pJet1.2 plasmid vector was then excised from the gel and extracted **(A)**. mNeonGreen DNA sequence was liberated from mNeonGreen pJet1.2 plasmid **(B)**. The DNA sequence (representing mNeonGreen) was then excised from the gel, extracted, and ligated into Fragment 10 +11 pJet1.2 plasmid vector generating (Fragment 10 +11ΔORF10-mNeonGreen) pJet1.2 plasmid **(D)**. mScarlet DNA sequence was liberated from mScarlet pJet1.2 plasmid **(C)**. The DNA sequence (representing mScarlet) was then excised from the gel, extracted, and ligated into Fragment 10 +11 pJet1.2 plasmid vector generating (Fragment 10 +11ΔORF10- mScarlet pJet1.2 plasmid) **(E)**.

cDNA fragments containing ΔORF10-mNeonGreen and ΔORF10mScarlet overlapping cDNA fragments were then amplified from (Fragment 10 +11ΔORF10-mNeonGreen) pJet1.2 plasmid and (Fragment 10 +11ΔORF10- mScarlet pJet1.2 plasmid), respectively, using high-fidelity DNA polymerase Platinum™ SuperFi II PCR Master Mix. cDNA fragments were then saved at -20°C until the day of the assembly (Figure 60).
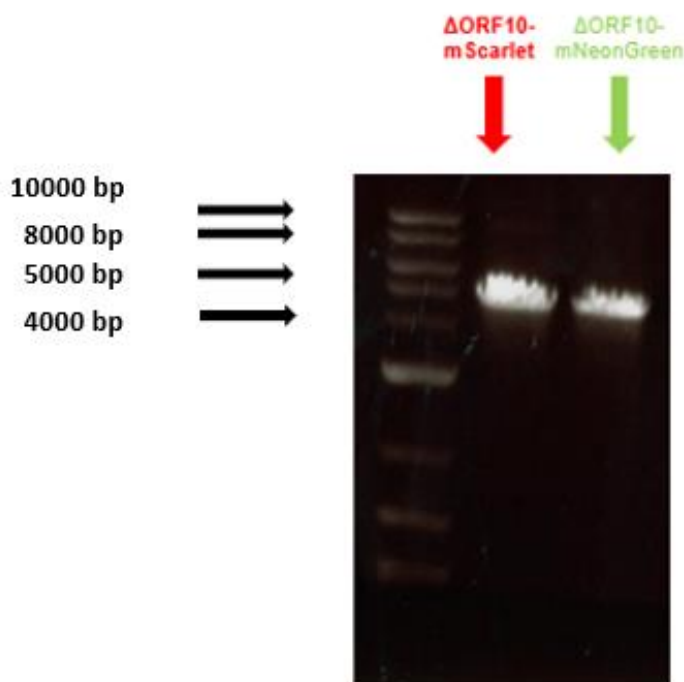
Figure 61. Amplifying ΔORF10-mNeonGreen and ΔORF10mScarlet overlapping cDNA sequences from (Fragment 10+11ΔORF10- mScarlet pJet1.2 plasmid) and (Fragment 10 +11ΔORF10-mNeonGreen pJet1.2 plasmid) and analyzing them by agarose gel electrophoresis. (Fragment 10+11ΔORF10- mScarlet pJet1.2 plasmid) and (Fragment 10 +11ΔORF10-mNeonGreen pJet1.2 plasmid) were used as a template to produce ΔORF10-mNeonGreen and ΔORF10mScarlet overlapping cDNA fragments. The PCR product was then run on a 0.8% agarose gel at 100 V for 40 min and imaged under a UV transilluminator. The product was purified using GeneJET PCR Purification Kit (Thermofisher) and stored at -20 °C until the day of the assembly.

5.2.6.4 Application of yeast-based TAR cloning to produce SARS-CoV-2 ORF10 KO, SARS-CoV-2ΔORF10mNeonGreen, and SARS-CoV-2ΔORF10mScarlet cDNA clones and verifying their correct assembly in pYES1L Vector

As mentioned earlier, nine cDNA fragments were produced from (Fragment 1 pJet1.2 plasmid — Fragment 9 pJet1.2 plasmid), and one cDNA fragment was produced from Fragment 10 +11 pJet1.2 ORF10 KO plasmid using high-fidelity DNA polymerase Platinum™ SuperFi II PCR Master Mix. All cDNA fragments were then mixed in appropriate concentrations and transformed into S. cerevisiae (pYES1L vector) (Figure 61). The resulting clones were then screened for the correct assembly of the yeast artificial chromosome (YAC) containing the cloned SARS-CoV-2 ORF10 KO genome by multiplex PCR covering the overlapping junctions between the recombined cDNA fragments.
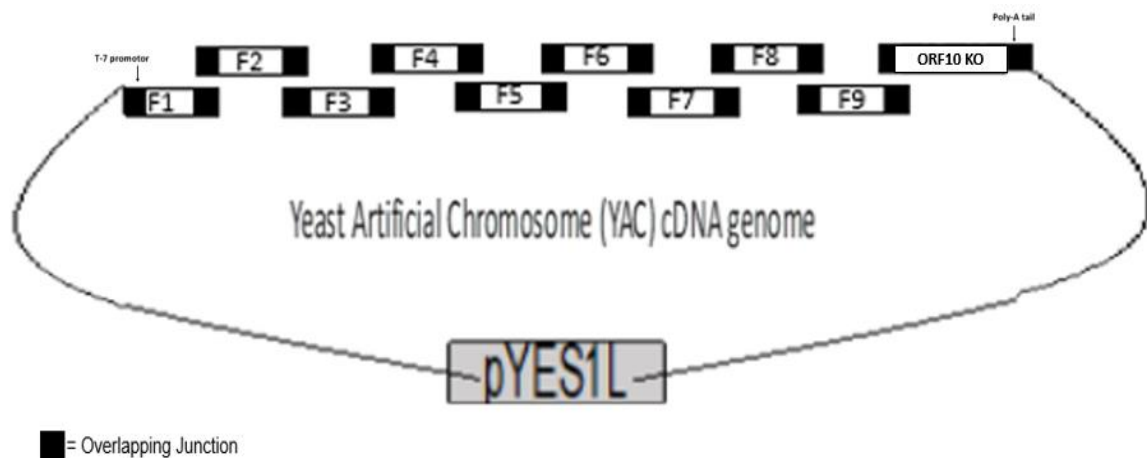
Figure 62. Schematic shows the generating SARS-CoV-2 ORF10 KO cDNA clone using yeast-based TAR cloning application. Nine cDNA fragments were generated from (Fragment 1 pJet1.2 plasmid— Fragment 9 pJet1.2 plasmid) and one cDNA fragment was generated from (Fragment 10 +11 pJet1.2 ORF10 KO plasmid). All cDNA fragments were then mixed and transformed into S. cerevisiae (pYES1L vector). The resulting clones were then screened for the correct assembly of the SARS-CoV-2 ORF10 KO clone by multiplex PCR, covering overlapping junctions between recombined cDNA fragments.

To make SARS-CoV-2ΔORF10mNeonGreen infectious cDNA clone, nine cDNA fragments were produced from (Fragment 1 pJet1.2 plasmid — Fragment 9 pJet1.2 plasmid), and a cDNA fragment containing ΔORF10-mNeonGreen was generated from (Fragment 10 +11ΔORF10-mNeonGreen) pJet1.2 plasmid using high-fidelity DNA polymerase Platinum™ SuperFi II PCR Master Mix. After that, all cDNA fragments were then mixed in appropriate concentrations and transformed into S. cerevisiae (pYES1L vector) (Figure 62). The resulting clones were screened for the correct assembly of the yeast artificial chromosome (YAC) containing the cloned SARS-CoV-2ΔORF10mNeonGreen genome by multiplex PCR covering the overlapping junctions between the recombined cDNA fragments.
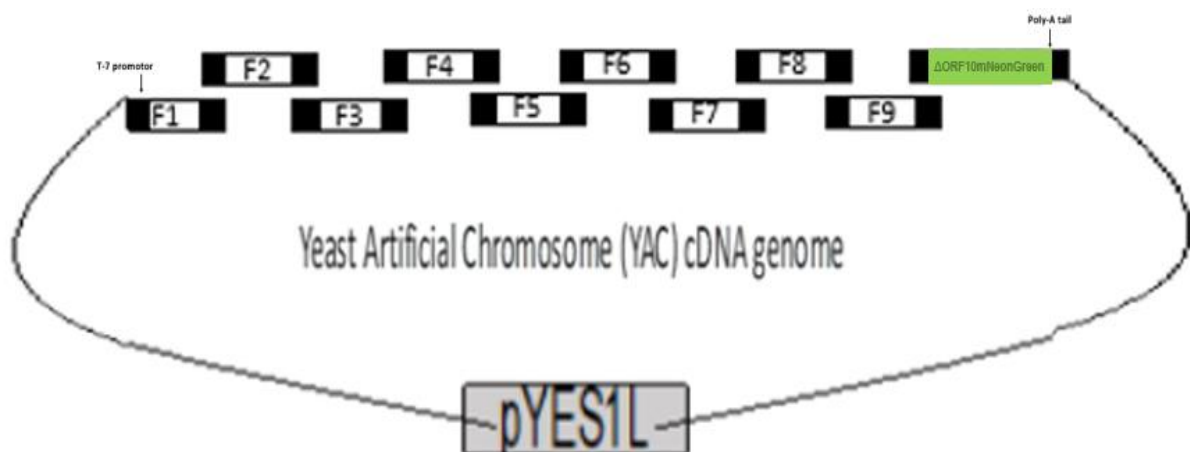
Figure 63. Schematic shows the generating SARS-CoV-2ΔORF10mNeonGreen cDNA clone using yeast-based TAR cloning application. Nine cDNA fragments were generated from (Fragment 1 pJet1.2 plasmid — Fragment 9 pJet1.2 plasmid). cDNA fragment containing ΔORF10-mNeonGreen was produced from (Fragment 10 +11ΔORF10-mNeonGreen) pJet1.2 plasmid. All cDNA fragments were then mixed and transformed into S. cerevisiae (pYES1L vector). The resulting clones were then screened for the correct assembly of the SARS-CoV-2ΔORF10-mNeonGreen by multiplex PCR, covering overlapping junctions between recombined cDNA fragments.

To make SARS-CoV-2ΔORF10mScarlet infectious cDNA clone, nine cDNA fragments were generated from (Fragment 1 pJet1.2 plasmid — Fragment 9 pJet1.2 plasmid), and one cDNA fragment containing ΔORF10-mScarlet was produced from (Fragment 10+11ΔORF10-mScarlet pJet1.2 plasmid) pJet1.2 plasmid using high-fidelity DNA polymerase Platinum™ SuperFi II PCR Master Mix. After that, all cDNA fragments were then mixed in appropriate concentrations and transformed into S. cerevisiae (pYES1L vector) (Figure 63). The resulting clones were then screened for the correct assembly of the yeast artificial chromosome (YAC) containing the cloned SARS-CoV-2ΔORF10-mScarlet genome by multiplex PCR covering the overlapping junctions between the recombined cDNA fragments.
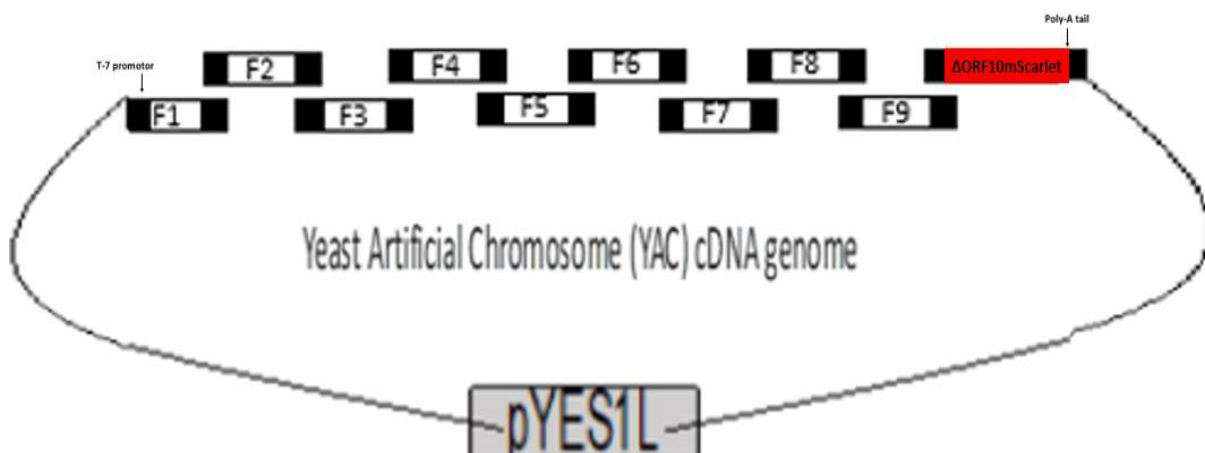
Figure 64. Schematic shows the generating SARS-CoV-2ΔORF10mScarlet cDNA clone using yeast-based TAR cloning application. Nine cDNA fragments were generated from (Fragment 1 pJet1.2 plasmid — Fragment 9 pJet1.2 plasmid). cDNA fragment containing ΔORF10-mScarlet was produced from (Fragment 10 +11ΔORF10-mScarlet) pJet1.2 plasmid. All cDNA fragments were then mixed and transformed into S. cerevisiae (pYES1L vector). The resulting clones were then screened for the correct assembly of the SARS-CoV-2ΔORF10mScarlet clone by multiplex PCR, covering overlapping junctions between recombined cDNA fragments.

In order to verify that the SARS-CoV-2 ORF10 KO cDNA construct had been correctly assembled, two sets of PCR primers were designed to generate 11 overlapping amplicons from the assembled full-length constructs (Table 30). Amplicons of the right size were achieved for the assembled SARS-CoV-2 ORF10 KO construct (Figure 64).

Table 30. The expected size of the PCR amplicons amplified from the SARS-CoV-2 ORF10 KO cDNA construct.

Primer set	Primer pair name	Replicon size
Set A	OL1	203bp
	OL2	387 bp
	OL3	446 bp
	OL4	523 bp
	OL5	618 bp
	OL9	307 bp
Set B	OL6	709 bp
	OL7	777 bp
	OL8	872 bp
	OL10	1006 bp
	OL11	1113 bp

Figure 65. Analysis of the PCR amplicons obtained from the assembled SARS-CoV-2 ORF10 KO cDNA construct in MaV203 Competent Yeast Cells by agarose gel electrophoresis. OL8 primers initially screened the right construct of the SARS-CoV-2 ORF10 KO genome in the set B primers. Three clones confirmed positive for the SARS-CoV-2 ORF10 KO cDNA construct **(A)**. The Positive clones were then screened by multiplex PCR for the remaining overlaps in set A primers **(B)**. After that, The positive clones were further screened by multiplex PCR for the remaining overlaps in set B primers **(C)**. OL6 was verified in standard PCR **(D)**.

Two sets of PCR primers were designed to generate 11 overlapping amplicons from the correct assembled SARS-CoV-2ΔORF10mNeonGreen construct (Table 31), and SARS-CoV-2ΔORF10mScarlet cDNA construct (Table 32). The Amplicons of the right size were achieved for the assembled SARS-CoV-2ΔORF10mScarlet construct (Figure 65) and SARS-CoV-2ΔORF10mNeonGreen construct (Figure 66).

Table 31. The expected size of the PCR amplicons amplified from the SARS-CoV-2ΔORF10mNeonGreen cDNA construct.

Primer set	Primer pair name	Replicon size
Set A	OL1	203bp
	OL2	387 bp
	OL3	446 bp
	OL4	523 bp
	OL5	618 bp
	OL9	307 bp
Set B	OL6	709 bp
	OL7	777 bp
	OL8	872 bp
	OL10	1006 bp
	OL11	1707 bp

Table 32. The expected size of the PCR amplicons amplified from the SARS-CoV-2ΔORF10mScarlet cDNA construct.

Primer set	Primer pair name	Replicon size
Set A	OL1	203bp
	OL2	387 bp
	OL3	446 bp
	OL4	523 bp
	OL5	618 bp
	OL9	307 bp
Set B	OL6	709 bp
	OL7	777 bp
	OL8	872 bp
	OL10	1006 bp
	OL11	1695 bp
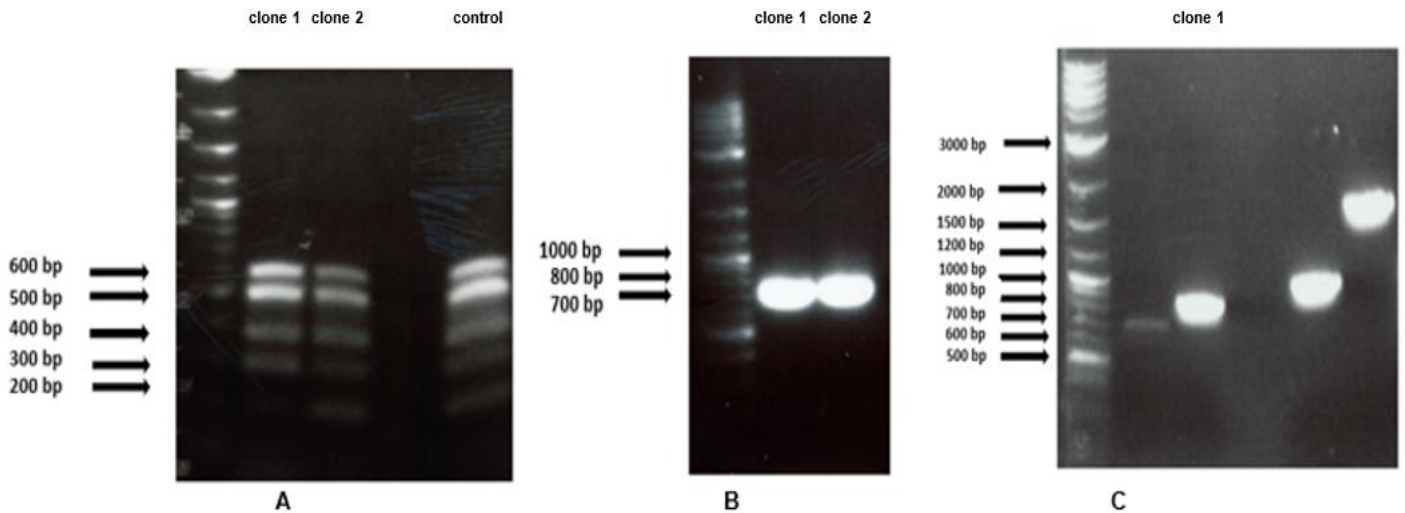
Figure 66. Analysis of the PCR amplicons obtained from the assembled SARS-CoV-2ΔORF10-mScarlet construct in MaV203 Competent Yeast Cells by agarose gel electrophoresis. Clone (1) and clone (2) were screened by multiplex PCR for the overlaps in set A primers, and both clones confirmed positive for the SARS-CoV-2ΔORF10mScarlet construct **(A)**. The Positive clones were then screened by multiplex PCR for the remaining overlaps in set B primers, but only OL-7 replicon was confirmed in both clones **(B)**. Then, OL-6, OL-8, OL-10, and OL10 replicons were verified individually using standard PCR in clone 1 only **(C)**.
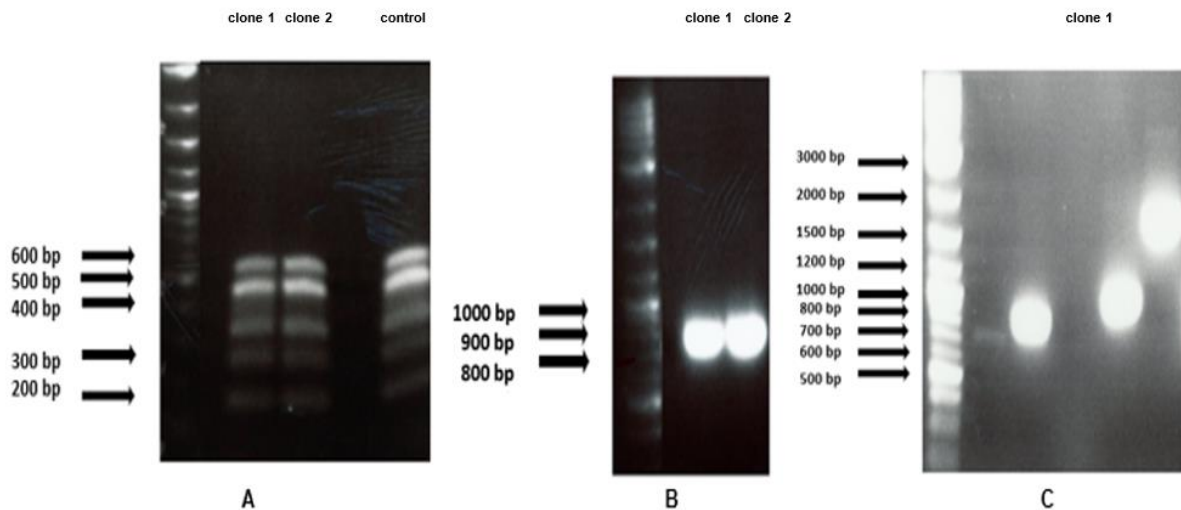
Figure 67. Analysis of the PCR amplicons obtained from the assembled SARS-CoV-2ΔORF10-mNeonGreen construct in MaV203 Competent Yeast Cells by agarose gel electrophoresis. Clone (1) and clone (2) were screened by multiplex PCR for the overlaps in set A primers, and both clones confirmed positive for the SARS-CoV-2ΔORF10mNeonGreen construct **(A)**. The Positive clones were then screened by multiplex PCR for the remaining overlaps in set B primers, but only OL 7 replicon was confirmed in both clones **(B)**. Then, OL-6, OL-8, OL-10, and OL10 replicons were verified individually using standard PCR in clone (1) only **(C)**.

175

5.2.6.5 Shuttling of SARS-CoV-2 ORF10 KO, SARS-CoV-2ΔORF10mNeonGreen, and SARS-CoV-2ΔORF10mScarlet YAC constructs into BAC

pYES1L Vector is a BAC/YAC shuttle vector and can be used to shuttle the assembled cDNA construct from yeast to E. coli. Therefore, positive yeast clones of SARS-CoV-2 ORF10 KO, SARS-CoV-2ΔORF10-mNeonGreen, and SARS-CoV-2ΔORF10-mScarlet cDNA were lysed and transformed into (E. coli) to produce BAC construct for each. Two colonies from each SARS-CoV-2 cDNA mutant were selected, and the bacteria were cultured overnight. The BAC construct of SARS-CoV-2 ORF10 KO, SARS-CoV-2ΔORF10mNeonGreen, and SARS-CoV-2ΔORF10mScarlet was then extracted and purified using the NucleoBond® Xtra BACprocedure. A restriction digest was carried out to check the size of the digestion products (Figure 67).
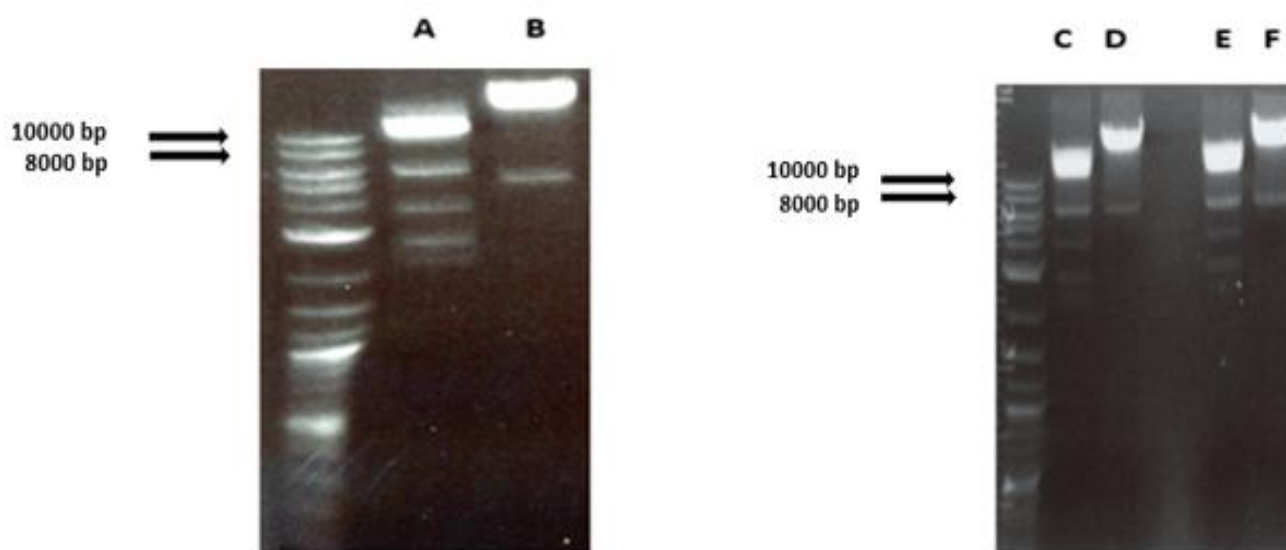
Figure 68. Analysis of SARS-CoV-2 ORF10 KO, SARS-CoV-2ΔORF10mNeonGreen, and SARS-CoV-2ΔORF10mScarlet BAC constructs by agarose gel electrophoresis. An individual yeast colony of SARS-CoV-2 ORF10 KO, SARS-CoV-2ΔORF10mNeonGreen, and SARS-CoV-2ΔORF10mScarlet assembled cDNA was picked and lysed using lysis buffer. Then, five microliters of each lysate were electroporated into One Shot™ TOP10 Electrocomp™ E. coli to shuttle the assembled cDNA construct from YAC to BAC. The BAC construct of the SARS-CoV-2 ORF10 KO cDNA was amplified in bacterial culture, extracted, and confirmed using EcoRI **(A)** or StuI **(B)** restriction enzymes. Similarly, the BAC construct of the SARS-CoV-2ΔORF10-mScarlet cDNA was amplified in bacterial culture, extracted, and verified using EcoRI **(C)** or StuI **(D)** restriction enzymes. Also, the BAC construct of the SARS-CoV-2ΔORF10-mNeonGreen cDNA was amplified in bacterial culture, extracted, and verified using EcoRI **(E)** or StuI **(F)** restriction enzymes. The digestion products were run on a 0.8% agarose gel at 100 V for 45 minutes. The DNA bands were visualized under a UV transilluminator.

5.2.6.6 Linerazing the SARS-CoV-2 ORF10 KO, SARS-CoV-2ΔORF10-mNeonGreen, and SARS-CoV-2ΔORF10m-Scarlet BAC constructs

The SARS-CoV-2 ORF10 KO, SARS-CoV-2ΔORF10-mNeonGreen, and SARS-CoV-2ΔORF10-mScarlet DNA plasmids were linearized using a unique restriction enzyme Asc1 (Figure 68). DNA of each plasmid was then extracted using the conventional phenol-chloroform extraction method, followed by sodium acetate/ethanol precipitation. The DNA pellets were resuspended in sterile, ultra-pure water and stored at -20⁰C until the day of *in vitro* transcription.
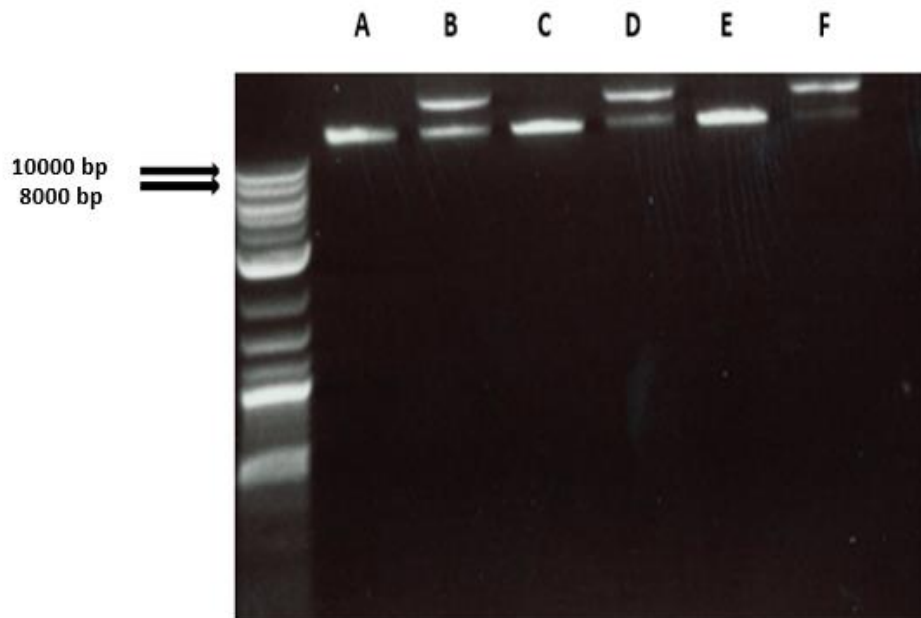
Figure 69. Analysis of linearized SARS-CoV-2 ORF10 KO, SARS-CoV-2ΔORF10-mNeonGreen, and SARS-CoV-2ΔORF10m-Scarlet BAC constructs by agarose gel electrophoresis. 15 µg of SARS-2 ORF10 KO DNA plasmid was linearized using Asc1 restriction enzyme. DNA was analyzed by 0.7% agarose gel post-digest **(A)** and pre-digest **(B)**. 15 µg of the SARS-2ΔORF10-mNeonGreen DNA plasmid was linearized using the Asc1 restriction enzyme. DNA was then analyzed by 0.7% agarose gel post-digest **(C)** and pre-digest **(D)**. 15 µg of the SARS-2ΔORF10-mScarlet DNA plasmid was linearized using Asc1 restriction enzyme. DNA was then analyzed by 0.7% agarose gel post-digest **(E)** and pre-digest **(F)**. After that, all three linearized DNA were harvested by Phenol-Chloroform and extraction, followed by sodium acetate/ethanol precipitation. DNA pellets were then resuspended in sterile water.

5.2.6.7 Transcribing full-length RNA constructs

In vitro transcription (IVT) was performed utilizing linearized DNA templates of SARS-2 ORF10 KO, SARS-2ΔORF10-mNeonGreen, and SARS-2ΔORF10-mScarlet to produce infectious RNA, using run-off T7 RNA polymerase-based transcription (Figure 69). Analysis of the RNA transcripts by spectrophotometer and agarose gel electrophoresis showed an excellent yield of SARS-2 ORF10 KO, SARS-2ΔORF10-mNeonGreen, and SARS-2ΔORF10-mScarlet RNA had been produced (Figure 70).
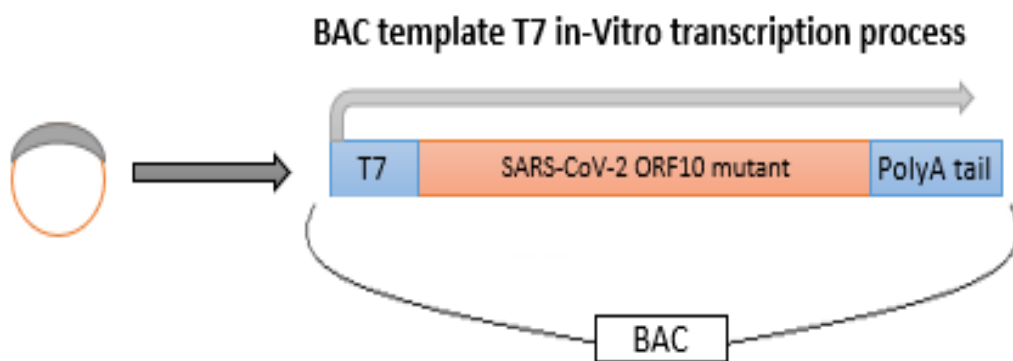
Figure 70. A schematic diagram shows *in vitro* transcription of a linearized DNA template of SARS-2 ORF10 KO, SARS-2ΔORF10-mNeonGreen, and SARS-2ΔORF10-mScarlet using T7 RNA polymerase-based transcription.
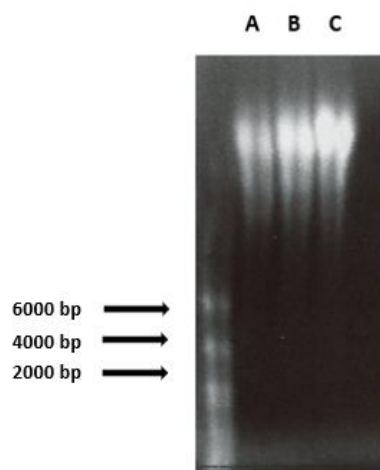
Figure 71. Analysis of the SARS-2 ORF10 KO, SARS-2ΔORF10-mNeonGreen, and SARS-2ΔORF10-mScarlet RNA transcripts by denaturing agarose gel electrophoresis. RNA obtained by in vitro transcription (IVT) from SARS-2ΔORF10-mScarlet linearized DNA template **(A)**, SARS-2ΔORF10-mNeonGreen linearized DNA template **(B)**, and SARS-2 ORF10 KO linearized DNA template **(C)**. Briefly, 1.5 µg of linearised template of each construct was used as a template to perform the IVT reaction for 3 hrs at 30 °C. Afterward, each reaction mixture was treated with RQ1 RNase-Free DNase to degrade the DNA template. RNA was then analyzed by running 1µL of IVT product on agarose gel at 50V for 2 hrs under denaturing conditions.

5.2.6.8 Transfecting mammalian cells with full-length RNA constructs to produce infectious viruses

SARS-2 ORF10 KO, SARS-2ΔORF10-mNeonGreen, and SARS-2ΔORF10-mScarlet RNA RNA transcripts were electroporated into permissive BAN (BHK-hACE2-SCoV2N) cells. After 72 hrs, viral RNA was extracted from an aliquot of cell culture supernatant (P0), and the rest of the supernatant was passaged on VTN (VeroE6 TMPRSS2) cells for virus propagation (P1). Viral RNA was also extracted from an aliquot of cell culture supernatant in P1. Viral RNA from P0 and P1 were reverse transcribed and PCR amplified to generate a 1 kb amplicon from the SARS-CoV-2 ORF10 KO, or 1.6 kb amplicons from the SARS-2ΔORF10-mNeonGreen and the SARS-2ΔORF10-mScarlet. The RT-PCR products were then analyzed by agarose gel electrophoresis, and the expected band was only seen in P0 and P1 of SARS-2 ORF10 KO, indicating that the SARS-2 ORF10 KO mutant was successfully rescued. SARS-2ΔORF10-mNeonGreen and SARS-2ΔORF10-mScarlet mutants could not be rescued even after three attempts (Figure 71). VTN cells harvesting and virus titration was kindly conducted by Dr. Milligan in the biosafety level (BSL3). The ORF10 knockout in SARS-2 ORF10 KO mutant was confirmed by nanopore direct RNA sequencing and Sanger sequencing (Figure 72).
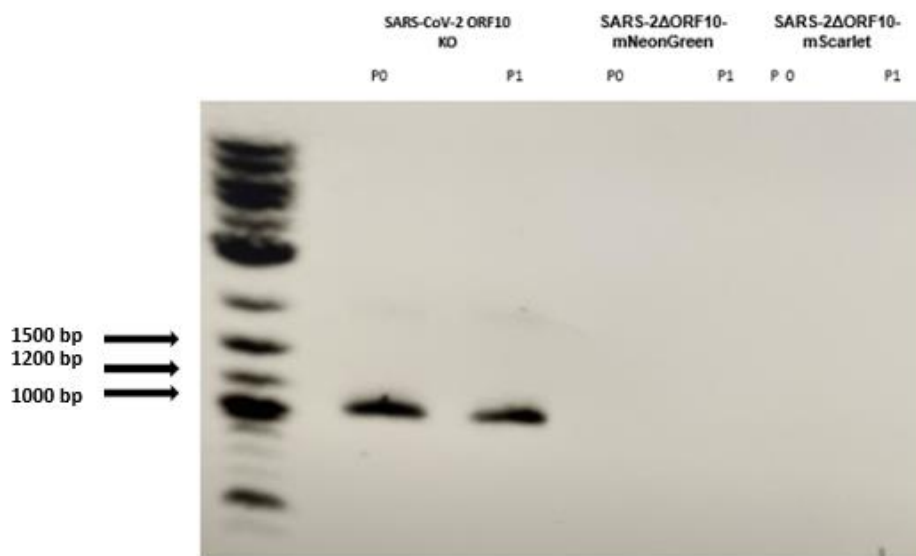
Figure 72. Analysis of the RT-PCR amplicons obtained from P0 and P1 of each viral RNA extractions by agarose gel electrophoresis. BAN cells electroporated with RNA product that was generated from IVT reaction of SARS-2 ORF10 KO, SARS-2ΔORF10-mNeonGreen, and SARS-2ΔORF10-mScarlet **(P0)**. The supernatant was passaged on to VTN cells **(P1)**. An aliquot of cell culture supernatant was taken from each passage **(P0 and P1)**, and the RNA was extracted. An RT-PCR was carried out on the extracted RNA using primers that would yield a 1 kb amplicon for SARS-CoV-2 ORF10 KO, or 1.6kb from SARS-2ΔORF10-mNeonGreen and SARS-2ΔORF10-mScarlet mutants. PCR products were run on a 0.7% agarose gel at 100 V for 40 minutes and imaged under a UV transilluminator. Only SARS-CoV-2 ORF10 KO mutant was successfully rescued.
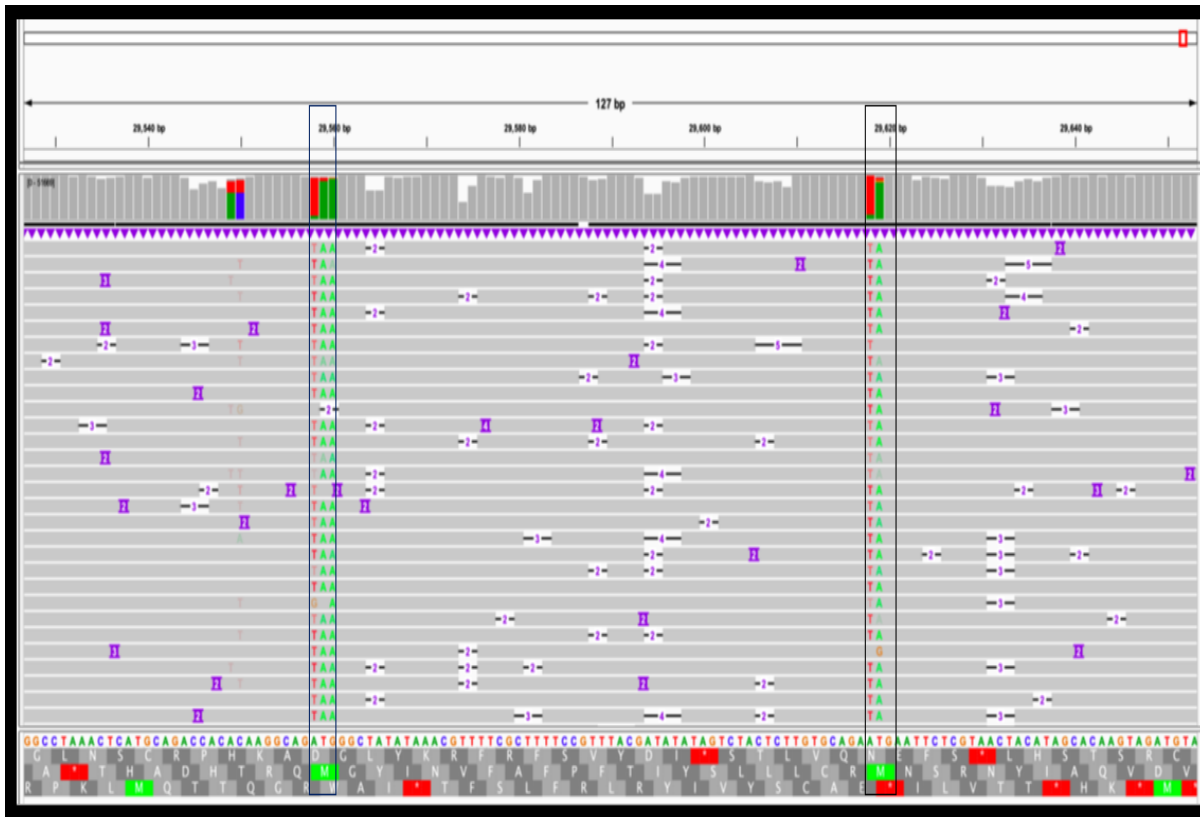
Figure 73. Confirming ORF10 knockout in SARS-2 ORF10 KO mutant by nanopore direct RNA sequencing. BAN cells were electroporated with the RNA product that was generated from the IVT reaction of the SARS-2 ORF10 KO plasmid DNA. After 72hrs, the supernatant was passaged on VTN cells. Total RNA was extracted from VTN-infected cells and sequenced using nanopore direct RNA sequencing. The sequencing data was mapped to the SARS-CoV-2 genome by Prof. Matthews and manually checked to ensure the virus was mutated as intended.

5.2.7 TMT-MS/MS analysis of SARS-CoV-2 ORF10 KO and SARS-CoV-2 W.T infected cells

The cellular proteome of SARS-CoV-2 ORF10 KO infected cells was investigated using high-throughput proteomics analysis to uncover more information on how ORF10 protein may be modulating the host's innate immune proteins or other aspects. A549-ACE-2 cells were used in the experiment as they are stably transfected with the human ACE2, which increases their permissively to SARS-CoV-2 infection. Briefly, A549 ACE-2 cells were infected with either SARS-CoV-2 wild type (W.T) or SARS-CoV-2 ORF10 KO, and total protein samples were collected at 18 hours post-infection. Western blotting analysis successfully confirmed the viral infections before conducting TMT-MS/MS analysis (Figure 73). Experiments were done in triplicate by Dr. Milligan at BSL 3. Bioinformatic analysis on the resultant datasets was then performed to identify similarities and differences in dysregulation levels of the host's proteins between the viruses.
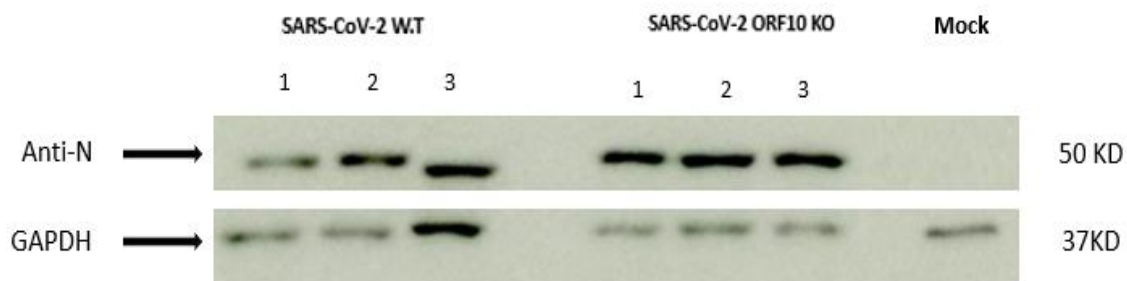
Figure 74. Confirmation of successful infection of A549 ACE-2 cells with SARS-CoV-2 W.T or SARS-CoV-2 ORF10 KO mutant before conducting TMT-MS/MS analysis. A549 ACE-2 cells were infected with either SARS-CoV-2 W.T or SARS-CoV-2 ORF10 KO mutant. Samples were harvested 18 hrs post-infection. The infections were confirmed by western blotting analysis using SARS-CoV-2 anti-N antibody before conducting quantitative proteomics analysis. The molecular weight of N protein is 49 KDa. The Experiments were performed in triplicate.

5.2.8 Bioinformatic analysis of high-throughput proteomics datasets produced from SARS-CoV-2 W.T and SARS-CoV-2 ORF10 KO infected cells

Overall, proteomics datasets showed no significant changes in the host's protein abundance between the SARS-CoV-2 W.T and SARS-CoV-2 ORF10 KO infected cells (Figure 74). The majority of the host's proteins increased ≥ 1.5 log2 fold in both viruses-infected cells overlapped (Figure 75). Most of the host's proteins decreased ≥ 1.5 log2 fold in SARS-CoV-2 W.T infected cells overlapped with the host's proteins decreased ≥ log2 fold in SARS-CoV-2 ORF10 KO infected cells (Figure 76). More importantly, there was no significant difference in the expression of the host's innate immune proteins between both viruses, including some proteins that have been shown to interact with ORF10 (Table 33).
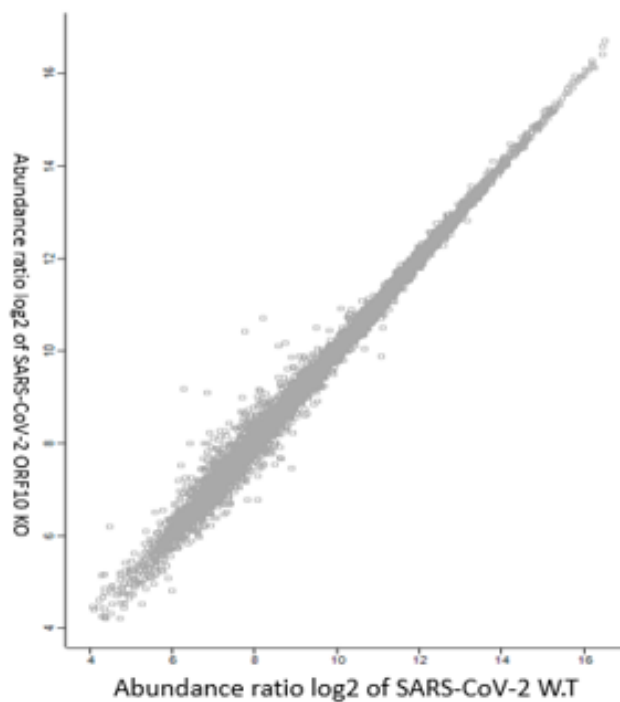
Figure 75. Quantification of host proteins in SARS-CoV-2 W.T infected cells relative to host proteins in SARS-CoV-2 ORF10 KO infected cells. The scatter plot of log2-transformed TMT ratios from both samples is obtained by Perseus software. The grey dots represent all proteins detected.
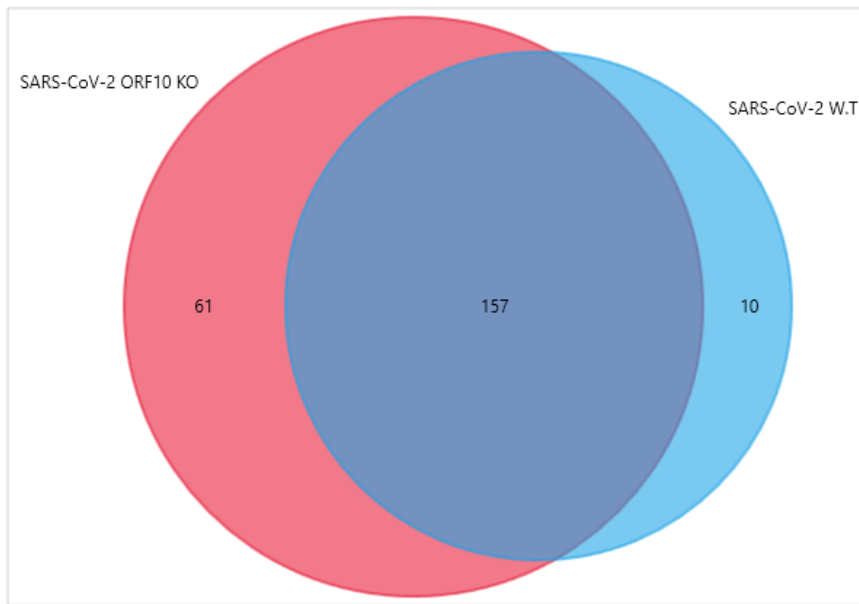
Figure 76. The Venn diagram shows the number of unique and overlapping host proteins that increased ≥ 1.5 log2 fold in SARS-CoV-2 W.T cells and SARS-CoV-2 ORF10 KO infected cells compared to mock-infected cells.
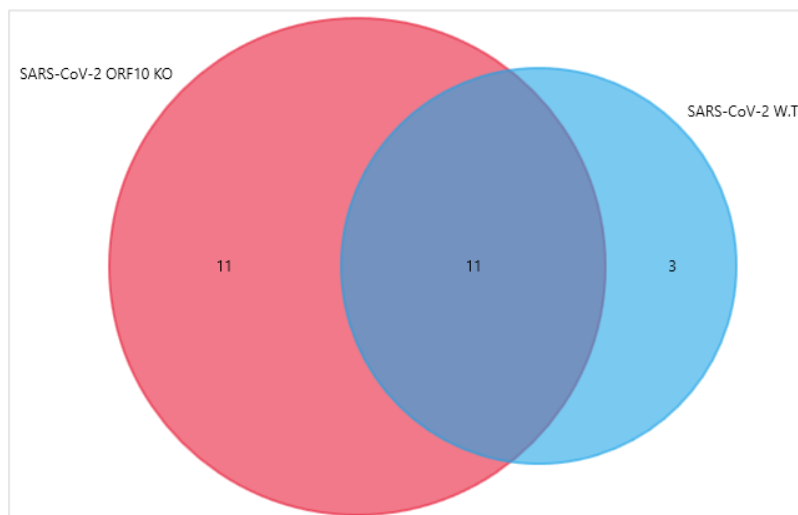
Figure 77. The Venn diagram shows the number of unique and overlapping host proteins that decreased ≥ 1.5 log2 fold in SARS-CoV-2 W.T infected cells and SARS-CoV-2 ORF10 KO infected cells compared to mock-infected cells.

Table 33. High-throughput quantitative proteomics analysis showed the expression levels of proteins involved in innate immune response or proteins that have been shown to interact with ORF10 in SARS-CoV-2 W.T or SARS-CoV-2 ORF10 KO infected cells. Proteins' names are obtained from UniProt: the universal protein knowledgebase in 2021.

Host innate immune proteins	SARS-CoV-2 W.T/Mock log2 fold difference	SARS-CoV-2 ORF10 KO /Mock log2 fold difference	SARS-CoV-2 W.T/ SARS-CoV-2 ORF10 KO log2 fold difference
IFIT1	0.15	-0.03	0.18
OAS1	-0.22	-0.36	0.14
IFIT3	0.10	0.02	0.08
ISG15	-0.17	-0.21	0.04
IKBIP	0.03	-0.05	0.07

5.2.8.1 Host proteins increased in SARS-CoV-2 ORF10 KO infected cells compared to mock-infected cells

Two hundred nineteen host proteins were ≥ 1.5 log2 fold up-regulated in SARS-CoV-2 ORF10 KO infected cells compared with mock-infected cells (Table 34). The STRING database was searched to analyze the interactions between host proteins that showed a ≥ 1.5 log2 fold increase in SARS-CoV-2 ORF10 KO cells compared with mock-infected cells (Figure 77).

Table 34. Cellular proteins increased ≥ 1.5 log2-fold in SARS-CoV-2 ORF10 KO infected cells. Proteins' IDs and names are obtained from UniProt: the universal protein knowledgebase in 2021. Uniprot IDs shown in RED are for proteins significantly changed in amount (p-value < 0.05).

Uniprot ID	Protein name	Log2-fold-change difference
Q8NEB7	Acrosin-binding protein (Acrosin-binding protein, 60 kDa form) (Cancer/testis antigen 23) (CT23) (Cancer/testis antigen OY-TES-1) (Proacrosin-binding protein sp32) [Cleaved into: Acrosin-binding protein, mature form (Acrosin-binding protein, 32 kDa form, mature form)]	7.80
E9PJF7	Translationally-controlled tumor protein (Fragment)	7.33
Q7L8C5	Synaptotagmin-13 (Synaptotagmin XIII) (SytXIII)	7.05

Q9NV92	NEDD4 family-interacting protein 2 (NEDD4 WW domain-binding protein 5A) (Putative MAPK-activating protein PM04/PM05/PM06/PM07) (Putative NF-kappa-B-activating protein 413)	6.66
Q0VFZ6	Protein CFAP210 (Cilia- and flagella- associated protein 210) (Coiled-coil domain-containing protein 173)	6.31
Q9BXA5	Succinate receptor 1 (G-protein coupled receptor 91) (P2Y purinoceptor 1-like)	5.81
Q7L8A9	Tubulinyl-Tyr carboxypeptidase 1 (EC 3.4.17.17) (Tubulin carboxypeptidase 1) (Tyrosine carboxypeptidase 1) (TTCP 1) (Vasohibin-1)	5.38
A6NGH7	Coiled-coil domain-containing protein 160	5.27
Q13201	Multimerin-1 (EMILIN-4) (Elastin microfibril interface located protein 4) (Elastin microfibril interfacer 4) (Endothelial cell multimerin) [Cleaved into: Platelet glycoprotein Ia*; 155 kDa platelet multimerin (p-155) (p155)]	5.01
A0A0B4J2F0	Protein PIGBOS1 (PIGB opposite strand protein 1)	4.69
P51589	Cytochrome P450 2J2 (EC 1.14.14.-) (Albendazole monooxygenase (hydroxylating)) (EC 1.14.14.74) (Albendazole monooxygenase (sulfoxide-forming)) (EC 1.14.14.73) (Arachidonic acid epoxygenase) (CYPIIJ2) (Hydroperoxy icosatetraenoate isomerase) (EC 5.4.4.7)	4.64
P06239	Tyrosine-protein kinase Lck (EC 2.7.10.2) (Leukocyte C-terminal Src kinase) (LSK) (Lymphocyte cell-specific protein-tyrosine kinase) (Protein YT16) (Proto-oncogene Lck) (T cell-specific protein-tyrosine kinase) (p56-LCK)	4.63
A0A2R8YE65	Connector enhancer of kinase suppressor of ras 2 (Fragment)	4.56
A0A087WWI0	Leucine-rich melanocyte differentiation-associated protein	4.51
Q9P0S9	Transmembrane protein 14C	4.27
Q8TAQ2	SWI/SNF complex subunit SMARCC2 (BRG1-associated factor 170) (BAF170) (SWI/SNF complex 170 kDa subunit) (SWI/SNF-related matrix-associated actin-dependent regulator of chromatin subfamily C member 2)	4.25
P04732	Metallothionein-1E (MT-1E) (Metallothionein-IE) (MT-IE)	4.19
A6NJB7	Proline-rich protein 19	4.17
U3KQS2	Glucose-6-phosphate exchanger SLC37A4	4.15
H7C2K6	Band 4.1-like protein 1 (Fragment)	4.11
P08195	4F2 cell-surface antigen heavy chain (4F2hc) (4F2 heavy chain antigen) (Lymphocyte activation antigen 4F2 large subunit) (Solute carrier family 3 member 2) (CD antigen CD98)	3.99
O14793	Growth/differentiation factor 8 (GDF-8) (Myostatin)	3.75
Q07352	mRNA decay activator protein ZFP36L1 (Butyrate response factor 1) (EGF-response factor 1) (ERF-1) (TPA-induced sequence 11b) (Zinc finger protein 36, C3H1 type-like 1) (ZFP36-like 1)	3.75
Q56UN5	Mitogen-activated protein kinase kinase kinase 19 (EC 2.7.11.1) (Regulated in COPD, protein kinase) (SPS1/STE20-related protein kinase YSK4)	3.68
Q5TA12	Protein dopey-1	3.65
Q4G163	F-box only protein 43 (Endogenous meiotic inhibitor 2)	3.64
P41252	Isoleucine--tRNA ligase, cytoplasmic	3.63
Q12857	Nuclear factor 1 A-type (NF1-A) (Nuclear factor 1/A) (CCAAT-box-binding transcription factor) (CTF) (Nuclear factor I/A) (NF-I/A) (NFI-A) (TGGCA-binding protein)	3.59
P00395	Cytochrome c oxidase subunit 1 (EC 7.1.1.9) (Cytochrome c oxidase polypeptide I)	3.54
Q9H3M0	Potassium voltage-gated channel subfamily F member 1 (Voltage-gated potassium channel subunit Kv5.1) (kH1)	3.52
Q8NG08	DNA helicase B (hDHB) (EC 3.6.4.12)	3.50
Q8NEB5	Phospholipid phosphatase 5 (EC 3.1.3.4) (EC 3.1.3.81) (Phosphatidic acid phosphatase type 2 domain-containing protein 1B)	3.47

Q8TD57	Dynein axonemal heavy chain 3 (Axonemal beta dynein heavy chain 3) (HsADHC3) (Ciliary dynein heavy chain 3) (Dnahc3-b)	3.45
G3V5X1	tRNA (guanine(37)-N1)-methyltransferase (Fragment)	3.31
P05060	Secretogranin-1 (Chromogranin-B) (CgB) (Secretogranin I) (SgI) [Cleaved into: PE-11; GAWK peptide; CCB peptide]	3.24
P60602	Reactive oxygen species modulator 1 (ROS modulator 1) (Epididymis tissue protein Li 175) (Glyrichin) (Mitochondrial targeting GxxxG motif protein) (MTGM) (Protein MGR2 homolog)	3.17
A0A0C4DFM5	Myotilin (Myotilin, isoform CRA_b)	3.15
Q8TAB3	Protocadherin-19	3.15
Q86VQ0	Lebercilin (Leber congenital amaurosis 5 protein)	3.15
O60840	Voltage-dependent L-type calcium channel subunit alpha-1F (Voltage-gated calcium channel subunit alpha Cav1.4)	3.14
Q5TCS8	Adenylate kinase 9 (AK 9) (EC 2.7.4.4) (EC 2.7.4.6) (Adenylate kinase domain-containing protein 1) (Adenylate kinase domain-containing protein 2)	3.14
P55345	Protein arginine N-methyltransferase 2 (EC 2.1.1.319) (Histone-arginine N-methyltransferase PRMT2)	3.13
Q6ZNF0	Acid phosphatase type 7 (EC 3.1.3.2) (Purple acid phosphatase long form)	3.09
P0CF75	Endogenous Bornavirus-like nucleoprotein 1 (Endogenous Borna-like N element-1) (EBLN-1)	3.04
Q9H6S3	Epidermal growth factor receptor kinase substrate 8-like protein 2 (EPS8-like protein 2) (Epidermal growth factor receptor pathway substrate 8-related protein 2) (EPS8-related protein 2)	3.02
H0YL33	Annexin	3.02
Q6ZP82	Coiled-coil domain-containing protein 141 (Coiled-coil protein associated with myosin II and DISC1)	2.96
A0A087WU35	Zinc finger protein 714	2.94
P49716	CCAAT/enhancer-binding protein delta (C/EBP delta) (Nuclear factor NF-IL6-beta) (NF-IL6-beta)	2.90
Q00839	Heterogeneous nuclear ribonucleoprotein U (hnRNP U) (GRIP120) (Nuclear p120 ribonucleoprotein) (Scaffold-attachment factor A) (SAF-A) (p120) (pp120)	2.85
P85299	Proline-rich protein 5 (Protein observed with Rictor-1) (Protor-1)	2.83
B8ZZS0	BET1-like protein	2.79
Q96RD9	Fc receptor-like protein 5 (FcR-like protein 5) (FcRL5) (BXMAS1) (Fc receptor homolog 5) (FcRH5) (Immune receptor translocation-associated protein 2) (CD antigen CD307e)	2.78
Q96MM3	Zinc finger protein 42 homolog (Zfp-42) (Reduced expression protein 1) (REX-1) (hREX-1) (Zinc finger protein 754)	2.77
Q6ZT07	TBC1 domain family member 9 (TBC1 domain family member 9A)	2.76
Q8NB66	Protein unc-13 homolog C (Munc13-3)	2.75
P0DI81	Trafficking protein particle complex subunit 2 (Sedlin)	2.74
Q8WXI7	Mucin-16 (MUC-16) (Ovarian cancer-related tumor marker CA125) (CA-125) (Ovarian carcinoma antigen CA125)	2.73
Q6NUP7	Serine/threonine-protein phosphatase 4 regulatory subunit 4	2.73
P48436	Transcription factor SOX-9	2.73
H7C3M7	FERM, ARHGEF and pleckstrin domain-containing protein 2 (Fragment)	2.72
G3V342	Unconventional myosin-Ia	2.68
A0A0A0MTJ0	Thyrotropin receptor	2.64
Q96N46	Tetratricopeptide repeat protein 14 (TPR repeat protein 14)	2.58

Q9BSJ5	Uncharacterized protein C17orf80 (Cell migration-inducing gene 3 protein) (Human lung cancer oncogene 8 protein) (HLC-8)	2.58
Q5VYM1	Uncharacterized protein C9orf131	2.58
Q96KE9	BTB/POZ domain-containing protein 6 (Lens BTB domain protein)	2.58
Q8N1H7	Protein SIX6OS1 (Six6 opposite strand transcript 1)	2.54
Q6IMN6	Caprin-2 (C1q domain-containing protein 1) (Cytoplasmic activation/proliferation-associated protein 2) (Gastric cancer multidrug resistance-associated protein) (Protein EEG-1) (RNA granule protein 140)	2.50
G3V3T2	BTB/POZ domain-containing protein 7	2.48
O95096	Homeobox protein Nkx-2.2 (Homeobox protein NK-2 homolog B)	2.47
Q6ZRI0	Otogelin	2.44
Q2VWA4	SKI family transcriptional corepressor 2 (Functional Smad-suppressing element on chromosome 18) (Fussel-18) (LBX1 corepressor 1-like protein) (Ladybird homeobox corepressor 1-like protein)	2.43
Q9P2Q2	FERM domain-containing protein 4A	2.41
Q8N8R3	Mitochondrial basic amino acids transporter (Carnitine/acylcarnitine translocase-like) (CACT-like) (Mitochondrial carnitine/acylcarnitine carrier protein CACL) (Mitochondrial ornithine transporter 3) (Solute carrier family 25 member 29)	2.41
Q8TEQ0	Sorting nexin-29 (RUN domain-containing protein 2A)	2.38
Q5T8A7	Protein phosphatase 1 regulatory subunit 26	2.38
Q9Y4F9	Rho family-interacting cell polarization regulator 2	2.36
A0A087WXX8	Succinate dehydrogenase [ubiquinone] iron-sulfur subunit, mitochondrial (EC 1.3.5.1) (Iron-sulfur subunit of complex II) (Fragment)	2.36
H7BXM4	Collagen alpha-3(IV) chain (Fragment)	2.35
Q96F46	Interleukin-17 receptor A (IL-17 receptor A) (IL-17RA) (CDw217) (CD antigen CD217)	2.34
V9GYH0	Homeobox domain-containing protein (Fragment)	2.34
P55085	Proteinase-activated receptor 2 (PAR-2) (Coagulation factor II receptor-like 1) (G-protein coupled receptor 11) (Thrombin receptor-like 1) [Cleaved into: Proteinase-activated receptor 2, alternate cleaved 1; Proteinase-activated receptor 2, alternate cleaved 2]	2.33
P48431	Transcription factor SOX-2	2.31
Q9BVV6	Protein TALPID3	2.30
Q02641	Voltage-dependent L-type calcium channel subunit beta-1 (CAB1) (Calcium channel voltage-dependent subunit beta 1)	2.29
Q96JJ6	Junctophilin-4	2.27
Q8N8U9	BMP-binding endothelial regulator protein (Bone morphogenetic protein-binding endothelial cell precursor-derived regulator) (Protein crossveinless-2) (hCV2)	2.27
Q14469	Transcription factor HES-1 (Class B basic helix-loop-helix protein 39) (bHLHb39) (Hairy and enhancer of split 1) (Hairy homolog) (Hairy-like protein) (hHL)	2.26
Q7Z553	MAM domain-containing glycosylphosphatidylinositol anchor protein 2 (MAM domain-containing protein 1)	2.24
K7EM54	HAUS augmin-like complex subunit 1	2.21
P54315	Inactive pancreatic lipase-related protein 1 (PL-RP1)	2.21
Q9NXT0	Zinc finger protein 586	2.18
G1UD79	PABIR family member 2 (Synoviocyte proliferation associated in collagen-induced arthritis 2)	2.16
O95841	Angiopoietin-related protein 1 (Angiopoietin-3) (ANG-3) (Angiopoietin-like protein 1)	2.16
Q2KHR2	DNA-binding protein RFX7 (Regulatory factor X 7) (Regulatory factor X domain-containing protein 2)	2.15

Q8NDX6	Zinc finger protein 740 (OriLyt TD-element-binding protein 7)	2.14
Q5THK1	Protein PRR14L (Proline rich 14-like protein)	2.13
P30411	B2 bradykinin receptor (B2R) (BK-2 receptor)	2.13
Q9UBC5	Unconventional myosin-Ia (Brush border myosin I) (BBM-I) (BBMI) (Myosin I heavy chain) (MIHC)	2.13
P82251	b(0,+)-type amino acid transporter 1 (b(0,+)AT1) (Glycoprotein-associated amino acid transporter b0,+AT1) (Solute carrier family 7 member 9)	2.12
Q5JTY5	COBW domain-containing protein 3 (Cobalamin synthase W domain-containing protein 3)	2.10
P16989	Y-box-binding protein 3 (Cold shock domain-containing protein A) (DNA-binding protein A) (Single-strand DNA-binding protein NF-GMB)	2.10
B5MEC4	Polycomb group RING finger protein 3	2.10
Q9NS15	Latent-transforming growth factor beta-binding protein 3	2.09
Q5JQC9	A-kinase anchor protein 4 (AKAP-4) (A-kinase anchor protein 82 kDa) (AKAP 82) (hAKAP82) (Major sperm fibrous sheath protein) (HI) (Protein kinase A-anchoring protein 4) (PRKA4)	2.09
P19256	Lymphocyte function-associated antigen 3 (Ag3) (Surface glycoprotein LFA-3) (CD antigen CD58)	2.06
Q01954	Zinc finger protein basonuclin-1	2.06
Q5MNZ9	WD repeat domain phosphoinositide-interacting protein 1 (WIPI-1) (Atg18 protein homolog) (WD40 repeat protein interacting with phosphoinositides of 49 kDa) (WIPI 49 kDa)	2.05
Q96GE4	Centrosomal protein of 95 kDa (Cep95) (Coiled-coil domain-containing protein 45)	2.05
Q9H5I5	Piezo-type mechanosensitive ion channel component 2 (Protein FAM38B)	2.04
Q9NR56	Muscleblind-like protein 1 (Triplet-expansion RNA-binding protein)	2.03
Q6PJT7	Zinc finger CCCH domain-containing protein 14 (Mammalian suppressor of tau pathology-2) (MSUT-2) (Renal carcinoma antigen NY-REN-37)	2.03
Q13275	Semaphorin-3F (Sema III/F) (Semaphorin IV) (Sema IV)	2.02
Q5T124	UBX domain-containing protein 11 (Colorectal tumor-associated antigen COA-1) (Socius) (UBX domain-containing protein 5)	2.01
Q9HBE1	POZ-, AT hook-, and zinc finger-containing protein 1 (BTB/POZ domain zinc finger transcription factor) (Protein kinase A RI subunit alpha-associated protein) (Zinc finger and BTB domain-containing protein 19) (Zinc finger protein 278) (Zinc finger sarcoma gene protein)	2.00
Q9NRD9	Dual oxidase 1 (EC 1.11.1.-) (EC 1.6.3.1) (Large NOX 1) (Long NOX 1) (NADPH thyroid oxidase 1) (Thyroid oxidase 1)	1.99
H7C1D1	Uncharacterized protein (Fragment)	1.97
A0A1B0GTZ2	Putative coiled-coil domain-containing protein 196 (Long intergenic non-protein coding RNA 238)	1.96
J3KR56	Receptor activity-modifying protein 3	1.95
Q9UN66	Protocadherin beta-8 (PCDH-beta-8) (Protocadherin-3l)	1.95
Q9NRN5	Olfactomedin-like protein 3 (HNOEL-iso) (hOLF44)	1.94
Q8TD10	Mirror-image polydactyly gene 1 protein	1.92
G3V2E4	Glycine hydroxymethyltransferase (EC 2.1.2.1)	1.92
O75628	GTP-binding protein REM 1 (GTPase-regulating endothelial cell sprouting) (Rad and Gem-like GTP-binding protein 1)	1.92
A6NFE2	Single-pass membrane and coiled-coil domain-containing protein 2	1.91
P00439	Phenylalanine-4-hydroxylase (PAH) (EC 1.14.16.1) (Phe-4-monooxygenase)	1.91
M0QX68	Pregnancy-specific beta-1-glycoprotein 3	1.91
P11277	Spectrin beta chain, erythrocytic (Beta-I spectrin)	1.91

P0C870	Bifunctional peptidase and (3S)-lysyl hydroxylase JMJD7	1.90
P48165	Gap junction alpha-8 protein (Connexin-50) (Cx50) (Lens fiber protein MP70)	1.89
Q8WYL5	Protein phosphatase Slingshot homolog 1 (EC 3.1.3.16) (EC 3.1.3.48) (SSH-like protein 1) (SSH-1L) (hSSH-1L)	1.89
Q86Z23	Complement C1q-like protein 4 (C1q and tumor necrosis factor-related protein 11) (C1q/TNF-related protein 11)	1.88
E5RJT0	Eukaryotic translation initiation factor 3 subunit H (Fragment)	1.88
P01588	Erythropoietin (Epoetin)	1.88
Q9BT67	NEDD4 family-interacting protein 1 (Breast cancer-associated protein SGA-1M) (NEDD4 WW domain-binding protein 5) (Putative MAPK-activating protein PM13) (Putative NF-kappa-B-activating protein 164) (Putative NFKB and MAPK-activating protein)	1.86
Q9Y3V2	RWD domain-containing protein 3 (RWD domain-containing sumoylation enhancer) (RSUME)	1.86
Q9BX59	Tapasin-related protein (TAPASIN-R) (TAP-binding protein-like) (TAP-binding protein-related protein) (TAPBP-R) (Tapasin-like)	1.85
Q96S95	Calcium/calmodulin-dependent protein kinase II inhibitor 2 (CaM-KII inhibitory protein) (CaM-KIIN)	1.85
A0A0C4DG89	RNA helicase (EC 3.6.4.13)	1.85
Q8TED9	Actin filament-associated protein 1-like 1 (AFAP1-like protein 1)	1.84
Q7Z3D6	D-glutamate cyclase, mitochondrial (EC 4.2.1.48)	1.83
I3L3R5	Coiled-coil domain-containing glutamate-rich protein 2	1.83
Q9HAY2	Melanoma-associated antigen F1 (MAGE-F1) (MAGE-F1 antigen)	1.83
Q9UQN3	Charged multivesicular body protein 2b (CHMP2.5) (Chromatin-modifying protein 2b) (CHMP2b) (Vacuolar protein sorting-associated protein 2-2) (Vps2-2) (hVps2-2)	1.82
O95149	Snurportin-1 (RNA U transporter 1)	1.82
Q7L099	Protein RUFY3 (RUN and FYVE domain-containing protein 3) (Rap2-interacting protein x) (RIPx) (Single axon-regulated protein) (Singar)	1.81
A0A2R8YEZ0	Protein ABHD18	1.80
S4R2Z7	39S ribosomal protein L42, mitochondrial	1.79
Q6PFW1	Inositol hexakisphosphate and diphosphoinositol-pentakisphosphate kinase 1 (EC 2.7.4.24) (Diphosphoinositol pentakisphosphate kinase 1) (Histidine acid phosphatase domain-containing protein 2A) (IP6 kinase) (Inositol pyrophosphate synthase 1) (InsP6 and PP-IP5 kinase 1) (VIP1 homolog) (hsVIP1)	1.79
Q5JTC6	APC membrane recruitment protein 1 (Amer1) (Protein FAM123B) (Wilms tumor gene on the X chromosome protein)	1.78
A0A7I2RN43	DnaJ homolog subfamily B member 5	1.78
Q1HG43	Dual oxidase maturation factor 1 (Dual oxidase activator 1) (Numb-interacting protein)	1.77
Q15038	DAZ-associated protein 2 (Deleted in azoospermia-associated protein 2)	1.77
P38570	Integrin alpha-E (HML-1 antigen) (Integrin alpha-IEL) (Mucosal lymphocyte 1 antigen) (CD antigen CD103) [Cleaved into: Integrin alpha-E light chain; Integrin alpha-E heavy chain]	1.77
Q96KS0	Prolyl hydroxylase EGLN2 (EC 1.14.11.-) (Egl nine homolog 2) (EC 1.14.11.29) (Estrogen-induced tag 6) (EIT-6) (HPH-3) (Hypoxia-inducible factor prolyl hydroxylase 1) (HIF-PH1) (HIF-prolyl hydroxylase 1) (HPH-1) (Prolyl hydroxylase domain-containing protein 1) (PHD1)	1.77
O00534	von Willebrand factor A domain-containing protein 5A (Breast cancer suppressor candidate 1) (BCSC-1) (Loss of heterozygosity 11 chromosomal region 2 gene A protein)	1.76

Q13237	cGMP-dependent protein kinase 2 (cGK 2) (cGK2) (EC 2.7.11.12) (cGMP-dependent protein kinase II) (cGKII)	1.76
Q7L2Z9	Centromere protein Q (CENP-Q)	1.76
Q9BUB4	tRNA-specific adenosine deaminase 1 (hADAT1) (EC 3.5.4.34) (tRNA-specific adenosine-37 deaminase)	1.76
P62341	Thioredoxin reductase-like selenoprotein T (SelT) (EC 1.8.1.9)	1.75
Q9ULS5	Transmembrane and coiled-coil domain protein 3	1.74
O95807	Transmembrane protein 50A (Small membrane protein 1)	1.74
Q96K19	E3 ubiquitin-protein ligase RNF170 (EC 2.3.2.27) (Putative LAG1-interacting protein) (RING finger protein 170) (RING-type E3 ubiquitin transferase RNF170)	1.74
Q9HB58	Sp110 nuclear body protein (Interferon-induced protein 41/75) (Speckled 110 kDa) (Transcriptional coactivator Sp110)	1.73
P06748	Nucleophosmin (NPM) (Nucleolar phosphoprotein B23) (Nucleolar protein NO38) (Numatrin)	1.71
Q86VD7	Mitochondrial coenzyme A transporter SLC25A42 (Solute carrier family 25 member 42)	1.71
Q6IQ55	Tau-tubulin kinase 2 (EC 2.7.11.1)	1.71
Q9C0I3	Serine-rich coiled-coil domain-containing protein 1 (Coiled-coil serine-rich protein 1)	1.71
P60059	Protein transport protein Sec61 subunit gamma	1.69
P31146	Coronin-1A (Coronin-like protein A) (Clipin-A) (Coronin-like protein p57) (Tryptophan aspartate-containing coat protein) (TACO)	1.69
B7WNH4	Small integral membrane protein 7	1.69
Q6P0Q8	Microtubule-associated serine/threonine-protein kinase 2 (EC 2.7.11.1)	1.68
A0A3B3IT33	Putative tripartite motif-containing protein 51G (Tripartite motif-containing 51G pseudogene)	1.67
Q92562	Polyphosphoinositide phosphatase (EC 3.1.3.-) (EC 3.1.3.36) (EC 3.1.3.86) (Phosphatidylinositol 3,5-bisphosphate 5-phosphatase) (SAC domain-containing protein 3) (Serine-protein phosphatase FIG4) (EC 3.1.3.16)	1.67
O95727	Cytotoxic and regulatory T-cell molecule (Class-I MHC-restricted T-cell-associated molecule) (CD antigen CD355)	1.67
P00740	Coagulation factor IX (EC 3.4.21.22) (Christmas factor) (Plasma thromboplastin component) (PTC) [Cleaved into: Coagulation factor IXa light chain; Coagulation factor IXa heavy chain]	1.66
Q9BTF0	THUMP domain-containing protein 2	1.65
Q8NBM8	Prenylcysteine oxidase-like (EC 1.8.3.-)	1.63
Q5T1H1	Protein eyes shut homolog (Epidermal growth factor-like protein 10) (EGF-like protein 10) (Epidermal growth factor-like protein 11) (EGF-like protein 11) (Protein spacemaker homolog)	1.63
O15105	Mothers against decapentaplegic homolog 7 (MAD homolog 7) (Mothers against DPP homolog 7) (Mothers against decapentaplegic homolog 8) (MAD homolog 8) (Mothers against DPP homolog 8) (SMAD family member 7) (SMAD 7) (Smad7) (hSMAD7)	1.63
Q9P2G4	Microtubule-associated protein 10 (Microtubule regulator of 120 KDa)	1.63
Q8WU58	Protein FAM222B	1.63
Q15149	Plectin (PCN) (PLTN) (Hemidesmosomal protein 1) (HD1) (Plectin-1)	1.62
Q9HBL7	Plasminogen receptor (KT) (Plg-R(KT))	1.62
Q9Y6H5	Synphilin-1 (Sph1) (Alpha-synuclein-interacting protein)	1.62
Q8NEM8	Cytosolic carboxypeptidase 3 (EC 3.4.17.-) (ATP/GTP-binding protein-like 3) (Protein deglutamylase CCP3)	1.62
A6NHL2	Tubulin alpha chain-like 3	1.62

A0A8C8KX99	Centromere protein I	1.61
H3BUF0	E3 ubiquitin-protein ligase ZNRF1 (Fragment)	1.61
Q9NSK7	Protein C19orf12	1.61
Q6WRI0	Immunoglobulin superfamily member 10 (IgSF10) (Calvaria mechanical force protein 608) (CMF608)	1.61
Q8IV76	Circadian clock protein PASD1 (Cancer/testis antigen 63) (CT63) (OX-TES-1) (PAS domain-containing protein 1)	1.61
Q9UHW5	GPN-loop GTPase 3 (ATP-binding domain 1 family member C)	1.60
Q7LFL8	CXXC-type zinc finger protein 5 (CF5) (Putative MAPK-activating protein PM08) (Putative NF-kappa-B-activating protein 102) (Retinoid-inducible nuclear factor) (RINF)	1.60
Q9NVV5	Androgen-induced gene 1 protein (AIG-1) (Fatty acid esters of hydroxy fatty acids hydrolase AIG1) (FAHFA hydrolase AIG1) (EC 3.1.-.-)	1.60
A0A0A0MTQ8	Coiled-coil domain-containing protein 175	1.60
H0YCR7	Ribonuclease inhibitor (Fragment)	1.59
Q4L180	Filamin A-interacting protein 1-like (130 kDa GPBP-interacting protein) (90 kDa GPBP-interacting protein) (Protein down-regulated in ovarian cancer 1) (DOC-1)	1.58
Q9NSA3	Beta-catenin-interacting protein 1 (Inhibitor of beta-catenin and Tcf-4)	1.58
P22455	Fibroblast growth factor receptor 4 (FGFR-4) (EC 2.7.10.1) (CD antigen CD334)	1.58
Q9UGU5	HMG domain-containing protein 4 (HMG box-containing protein 4) (High mobility group protein 2-like 1) (Protein HMGBCG)	1.57
Q9Y250	Leucine zipper putative tumor suppressor 1 (F37/esophageal cancer-related gene-coding leucine-zipper motif) (Fez1)	1.57
A0A590UJL7	FERM and PDZ domain-containing protein 4	1.56
A6NE52	WD repeat-containing protein 97	1.56
Q92828	Coronin-2A (IR10) (WD repeat-containing protein 2)	1.56
O43147	Small G protein signaling modulator 2 (RUN and TBC1 domain-containing protein 1)	1.56
Q96LX7	Coiled-coil domain-containing protein 17	1.55
Q9NXR8	Inhibitor of growth protein 3 (p47ING3)	1.55
Q9Y586	Protein mab-21-like 2	1.55
Q9Y5G5	Protocadherin gamma-A8 (PCDH-gamma-A8)	1.55
M0R091	Zinc finger protein 671	1.53
Q6ZU69	Protein FAM205A	1.52
Q9Y600	Cysteine sulfinic acid decarboxylase (EC 4.1.1.29) (Aspartate 1-decarboxylase) (EC 4.1.1.11) (Cysteine-sulfinate decarboxylase) (Sulfinoalanine decarboxylase)	1.52
O60331	Phosphatidylinositol 4-phosphate 5-kinase type-1 gamma (PIP5K1gamma) (PtdIns(4)P-5-kinase 1 gamma) (EC 2.7.1.68) (Type I phosphatidylinositol 4-phosphate 5-kinase gamma)	1.52
Q9UI40	Sodium/potassium/calcium exchanger 2 (Na(+)/K(+)/Ca(2+)-exchange protein 2) (Retinal cone Na-Ca+K exchanger) (Solute carrier family 24 member 2)	1.51
Q9Y5E1	Protocadherin beta-9 (PCDH-beta-9) (Protocadherin-3H)	1.51
Q13501	Sequestosome-1	1.50
Q16881	Thioredoxin reductase 1, cytoplasmic (TR) (EC 1.8.1.9) (Gene associated with retinoic and interferon-induced mortality 12 protein) (GRIM-12) (Gene associated with retinoic and IFN-induced mortality 12 protein) (KM-102-derived reductase-like factor) (Peroxidase TXNRD1) (EC 1.11.1.2) (Thioredoxin reductase TR1)	1.50

Figure 78. STRING analysis of proteins increased ≥ 1.5 log2 fold in SARS-CoV-2 ORF10 KO infected cells. The STRING database was searched to analyze the interactions between host proteins that showed a ≥ 1.5- log2 fold increase in SARS-CoV-2 ORF10 KO infected cells compared to mock-infected cells. Nodes representing proteins that most significantly enriched the GO term.

5.2.8.2 Host proteins decreased in SARS-CoV-2 ORF10 KO infected cells compared to mock-infected cells

Twenty-two host proteins were ≥ 1.5 log2 fold down-regulated in SARS-CoV-2 ORF10 KO infected cells compared with mock-infected cells (Table 35). The STRING database was searched to analyze the interactions between host proteins that showed a ≥ 1.5 log2 fold decrease in SARS-CoV-2 ORF10 KO infected cells (Figure 78).

Table 35. Cellular proteins decreased ≥1.5 log2-fold in SARS-CoV-2 ORF10 KO infected cells. Proteins' IDs and names are obtained from UniProt: the universal protein knowledgebase in 2021. Uniprot IDs shown in Blue are for proteins significantly changed in amount (p-value < 0.05).

UniProt ID	Protein name	Log2-fold-change difference
O43278	Kunitz-type protease inhibitor 1 (Fragment)	-4.67
P02795	Metallothionein-2 (MT-2) (Metallothionein-2A) (Metallothionein-II) (MT-II)	-2.89
Q12955	Ankyrin-3 (ANK-3) (Ankyrin-G)	-2.72
P25705	ATP synthase subunit alpha, mitochondrial (ATP synthase F1 subunit alpha)	-2.35
Q2M3V2	Ankyrin repeat domain-containing protein SOWAHA (Ankyrin repeat domain-containing protein 43) (Protein sosondowah homolog A)	-2.25
O14604	Thymosin beta-4, Y-chromosomal	-2.17
P55061	Bax inhibitor 1 (BI-1) (Testis-enhanced gene transcript protein) (Transmembrane BAX inhibitor motif-containing protein 6)	-2.09
Q8NA57	Chromosome 12 Open Reading Frame 50 (C12orf50)	-2.00
Q13822	Ectonucleotide pyrophosphatase/phosphodiesterase family member 2 (E-NPP 2) (EC 3.1.4.39) (Autotaxin) (Extracellular lysophospholipase D) (LysoPLD)	-1.98
Q92576	PHD finger protein 3 (Fragment)	-1.83
Q99538	Legumain (EC 3.4.22.34) (Asparaginyl endopeptidase) (Protease, cysteine 1)	-1.80
Q9NX78	Transmembrane protein 260	-1.75
Q9UPQ3	Arf-GAP with GTPase, ANK repeat and PH domain-containing protein 1 (AGAP-1) (Centaurin-gamma-2) (Cnt-g2) (GTP-binding and GTPase-activating protein 1) (GGAP1)	-1.70
O14521	Succinate dehydrogenase [ubiquinone] cytochrome b small subunit, mitochondrial (CybS) (CII-4) (QPs3) (Succinate dehydrogenase complex subunit D) (Succinate-ubiquinone oxidoreductase cytochrome b small subunit) (Succinate-ubiquinone reductase membrane anchor subunit)	-1.68
Q9Y6K8	Adenylate kinase isoenzyme 5 (AK 5) (EC 2.7.4.3) (EC 2.7.4.6) (ATP-AMP transphosphorylase 5)	-1.66
P61024	Cyclin-dependent kinases regulatory subunit 1 (CKS-1)	-1.66
Q5VUG0	Scm-like with four MBT domains protein 2 (Scm-like with 4 MBT domains protein 2)	-1.65
P02679	Fibrinogen gamma chain	-1.61
P26358	DNA (cytosine-5)-methyltransferase 1	-1.59
O95864	Acyl-CoA 6-desaturase (EC 1.14.19.3) (Delta(6) fatty acid desaturase) (D6D) (Delta(6) desaturase) (Delta-6 desaturase) (Fatty acid desaturase 2)	-1.57
Q53EL6	Programmed cell death protein 4 (Neoplastic transformation inhibitor protein) (Nuclear antigen H731-like) (Protein 197/15a)	-1.53

| Q96NU7 | Probable imidazolonepropionase (EC 3.5.2.7) (Amidohydrolase domain-containing protein 1) | -1.50 |
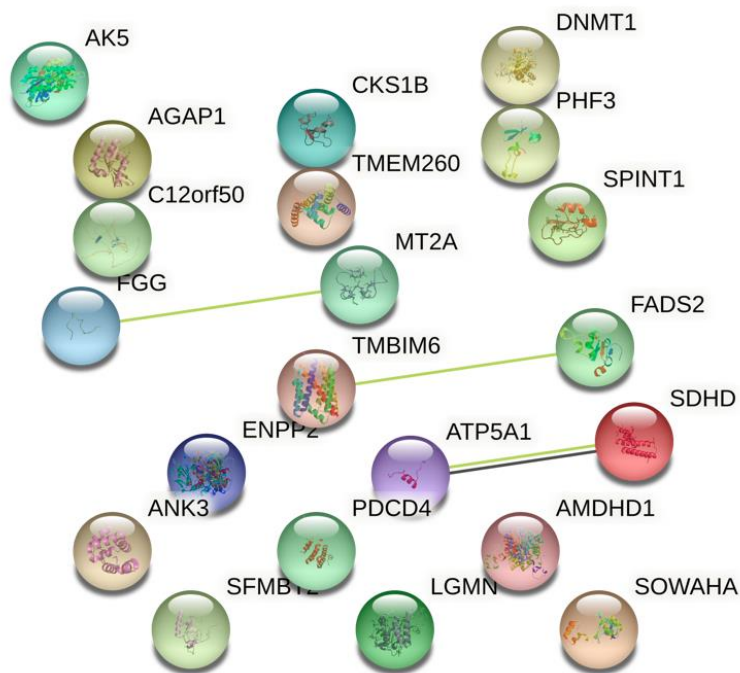
Figure 79. STRING analysis of proteins that decreased ≥ 1.5 log2 fold in SARS-CoV-2 ORF10 KO infected cells. The STRING database was searched to analyze the interactions between host proteins that showed a ≥ 1.5 log2 fold decrease in SARS-CoV-2 ORF10 KO infected A549-ACE-2 cells compared to mock-infected cells. Nodes representing proteins that most significantly enriched the GO term.

5.2.8.3 Host proteins increased in SARS-CoV-2 W.T infected cells compared to mock-infected cells

One hundred sixty-eight proteins were ≥ 1.5 log2-fold up-regulated in SARS-CoV-2 W.T infected cells compared with mock-infected cells (Table 36). The STRING database was searched to analyze the interactions between the host's proteins that showed a ≥ 1.5 log2 fold increase in SARS-CoV-2 W.T infected cells compared to mock-infected cells (Figure 79).

Table 36. The cellular proteins increased ≥1.5 log2-fold in SARS-CoV-2 W.T infected cells. Proteins' IDs and names are obtained from UniProt: the universal protein knowledgebase in 2021. Uniprot IDs shown in Red are for proteins significantly changed in amount (p-value < 0.05).

UniProt ID	Protein name	Log2-fold-change difference
Q8NEB7	Acrosin-binding protein (Acrosin-binding protein, 60 kDa form) (Cancer/testis antigen 23) (CT23) (Cancer/testis antigen OY-TES-1) (Proacrosin-binding protein sp32) [Cleaved into: Acrosin-binding protein, mature form (Acrosin-binding protein, 32 kDa form, mature form)]	7.36
Q7L8C5	Synaptotagmin-13 (Synaptotagmin XIII) (SytXIII)	7.09
P13693	Translationally-controlled tumor protein (Fragment)	7.06
Q9NV92	NEDD4 family-interacting protein 2 (NEDD4 WW domain-binding protein 5A) (Putative MAPK-activating protein PM04/PM05/PM06/PM07) (Putative NF-kappa-B-activating protein 413)	6.53
Q0VFZ6	Protein CFAP210 (Cilia- and flagella- associated protein 210) (Coiled-coil domain-containing protein 173)	6.13
A6NGH7	Coiled-coil domain-containing protein 160	5.89
Q9BXA5	Succinate receptor 1 (G-protein coupled receptor 91) (P2Y purinoceptor 1-like)	5.79
Q7L8A9	Tubulinyl-Tyr carboxypeptidase 1 (EC 3.4.17.17) (Tubulin carboxypeptidase 1) (Tyrosine carboxypeptidase 1) (TTCP 1) (Vasohibin-1)	5.73
Q13201	Multimerin-1 (EMILIN-4) (Elastin microfibril interface located protein 4) (Elastin microfibril interfacer 4) (Endothelial cell multimerin) [Cleaved into: Platelet glycoprotein Ia*; 155 kDa platelet multimerin (p-155) (p155)]	5.38
P51589	Cytochrome P450 2J2 (EC 1.14.14.-) (Albendazole monooxygenase (hydroxylating)) (EC 1.14.14.74) (Albendazole monooxygenase (sulfoxide-forming)) (EC 1.14.14.73) (Arachidonic acid epoxygenase) (CYPIIJ2) (Hydroperoxy icosatetraenoate isomerase) (EC 5.4.4.7)	4.59
A0A0B4J2F0	Protein PIGBOS1 (PIGB opposite strand protein 1)	4.22
Q9H2I8	Leucine-rich melanocyte differentiation-associated protein	4.15
Q8TAQ2	SWI/SNF complex subunit SMARCC2 (BRG1-associated factor 170) (BAF170) (SWI/SNF complex 170 kDa subunit) (SWI/SNF-related matrix-associated actin-dependent regulator of chromatin subfamily C member 2)	4.08

Q56UN5	Mitogen-activated protein kinase kinase kinase 19 (EC 2.7.11.1) (Regulated in COPD, protein kinase) (SPS1/STE20-related protein kinase YSK4)	4.05
Q8WXI2	Connector enhancer of kinase suppressor of ras 2 (Fragment)	4.04
Q8TD57	Dynein axonemal heavy chain 3 (Axonemal beta dynein heavy chain 3) (HsADHC3) (Ciliary dynein heavy chain 3) (Dnahc3-b)	3.99
P06239	Tyrosine-protein kinase Lck (EC 2.7.10.2) (Leukocyte C-terminal Src kinase) (LSK) (Lymphocyte cell-specific protein-tyrosine kinase) (Protein YT16) (Proto-oncogene Lck) (T cell-specific protein-tyrosine kinase) (p56-LCK)	3.99
Q9H4G0	Band 4.1-like protein 1 (Fragment)	3.91
A6NJB7	Proline-rich protein 19	3.89
Q5JWR5	Protein dopey-1	3.86
Q4G163	F-box only protein 43 (Endogenous meiotic inhibitor 2)	3.85
O43826	Glucose-6-phosphate exchanger SLC37A4	3.75
P04732	Metallothionein-1E (MT-1E) (Metallothionein-IE) (MT-IE)	3.63
P00395	Cytochrome c oxidase subunit 1 (EC 7.1.1.9) (Cytochrome c oxidase polypeptide I)	3.55
Q6ZNF0	Acid phosphatase type 7 (EC 3.1.3.2) (Purple acid phosphatase long form)	3.43
Q9UBF9	Myotilin (Myotilin, isoform CRA_b)	3.41
P41252	Isoleucine--tRNA ligase, cytoplasmicIARS1	3.39
Q9P0S9	Transmembrane protein 14C	3.36
P05060	Secretogranin-1 (Chromogranin-B) (CgB) (Secretogranin I) (SgI) [Cleaved into: PE-11; GAWK peptide; CCB peptide]	3.32
O14793	Growth/differentiation factor 8 (GDF-8) (Myostatin)	3.31
P08195	4F2 cell-surface antigen heavy chain (4F2hc) (4F2 heavy chain antigen) (Lymphocyte activation antigen 4F2 large subunit) (Solute carrier family 3 member 2) (CD antigen CD98)	3.26
Q8NG08	DNA helicase B (hDHB) (EC 3.6.4.12)	3.25
Q9H3M0	Potassium voltage-gated channel subfamily F member 1 (Voltage-gated potassium channel subunit Kv5.1) (kH1)	3.19
Q12857	Nuclear factor 1 A-type (NF1-A) (Nuclear factor 1/A) (CCAAT-box-binding transcription factor) (CTF) (Nuclear factor I/A) (NF-I/A) (NFI-A) (TGGCA-binding protein)	3.17
Q9UN66	Protocadherin beta-8 (PCDH-beta-8) (Protocadherin-3I)	3.11
Q5TCS8	Adenylate kinase 9 (AK 9) (EC 2.7.4.4) (EC 2.7.4.6) (Adenylate kinase domain-containing protein 1) (Adenylate kinase domain-containing protein 2)	3.11
Q07352	mRNA decay activator protein ZFP36L1 (Butyrate response factor 1) (EGF-response factor 1) (ERF-1) (TPA-induced sequence 11b) (Zinc finger protein 36, C3H1 type-like 1) (ZFP36-like 1)	3.04
Q32P41	tRNA (guanine(37)-N1)-methyltransferase (Fragment)	3.01
O60840	Voltage-dependent L-type calcium channel subunit alpha-1F (Voltage-gated calcium channel subunit alpha Cav1.4)	2.99
P60602	Reactive oxygen species modulator 1 (ROS modulator 1) (Epididymis tissue protein Li 175) (Glyrichin) (Mitochondrial targeting GxxxG motif protein) (MTGM) (Protein MGR2 homolog)	2.99
Q8NEB5	Phospholipid phosphatase 5 (EC 3.1.3.4) (EC 3.1.3.81) (Phosphatidic acid phosphatase type 2 domain-containing protein 1B)	2.97
P16473	Thyrotropin receptor	2.95
P0CF75	Endogenous Bornavirus-like nucleoprotein 1 (Endogenous Borna-like N element-1) (EBLN-1)	2.94
Q6ZP82	Coiled-coil domain-containing protein 141 (Coiled-coil protein associated with myosin II and DISC1)	2.85

Q96KE9	BTB (POZ) domain containing 6, isoform CRA_b (BTB/POZ domain-containing protein 6)	2.80
P49716	CCAAT/enhancer-binding protein delta (C/EBP delta) (Nuclear factor NF-IL6-beta) (NF-IL6-beta)	2.73
Q9H6S3	Epidermal growth factor receptor kinase substrate 8-like protein 2 (EPS8-like protein 2) (Epidermal growth factor receptor pathway substrate 8-related protein 2) (EPS8-related protein 2)	2.72
P85299	Proline-rich protein 5 (Protein observed with Rictor-1) (Protor-1)	2.71
Q86VQ0	Lebercilin (Leber congenital amaurosis 5 protein)	2.66
Q96N38	Zinc finger protein 714	2.65
Q8WXI7	Mucin-16 (MUC-16) (Ovarian cancer-related tumor marker CA125) (CA-125) (Ovarian carcinoma antigen CA125)	2.64
O95096	Homeobox protein Nkx-2.2 (Homeobox protein NK-2 homolog B)	2.63
O94887	FERM, ARHGEF and pleckstrin domain-containing protein 2 (Fragment)	2.62
Q9NYM9	BET1-like protein	2.60
P55345	Protein arginine N-methyltransferase 2 (EC 2.1.1.319) (Histone-arginine N-methyltransferase PRMT2)	2.60
Q96MM3	Zinc finger protein 42 homolog (Zfp-42) (Reduced expression protein 1) (REX-1) (hREX-1) (Zinc finger protein 754)	2.59
Q8TAB3	Protocadherin-19	2.53
P48431	Transcription factor SOX-2	2.53
Q8N1H7	Protein SIX6OS1 (Six6 opposite strand transcript 1)	2.47
Q00839	Heterogeneous nuclear ribonucleoprotein U (hnRNP U) (GRIP120) (Nuclear p120 ribonucleoprotein) (Scaffold-attachment factor A) (SAF-A) (p120) (pp120)	2.47
Q6NUP7	Serine/threonine-protein phosphatase 4 regulatory subunit 4	2.46
Q5T8A7	Protein phosphatase 1 regulatory subunit 26	2.46
Q96N46	Tetratricopeptide repeat protein 14 (TPR repeat protein 14)	2.43
P48436	Transcription factor SOX-9	2.40
Q02641	Voltage-dependent L-type calcium channel subunit beta-1 (CAB1) (Calcium channel voltage-dependent subunit beta 1)	2.38
Q8N8R3	Mitochondrial basic amino acids transporter (Carnitine/acylcarnitine translocase-like) (CACT-like) (Mitochondrial carnitine/acylcarnitine carrier protein CACL) (Mitochondrial ornithine transporter 3) (Solute carrier family 25 member 29)	2.38
Q5T124	UBX domain-containing protein 11 (Colorectal tumor-associated antigen COA-1) (Socius) (UBX domain-containing protein 5)	2.38
Q8NB66	Protein unc-13 homolog C (Munc13-3)	2.37
Q9NXT0	Zinc finger protein 586	2.36
P07355	Annexin	2.35
Q01955	Collagen alpha-3(IV) chain (Fragment)	2.30
Q9BSJ5	Uncharacterized protein C17orf80 (Cell migration-inducing gene 3 protein) (Human lung cancer oncogene 8 protein) (HLC-8)	2.21
Q5MNZ9	WD repeat domain phosphoinositide-interacting protein 1 (WIPI-1) (Atg18 protein homolog) (WD40 repeat protein interacting with phosphoinositides of 49 kDa) (WIPI 49 kDa)	2.20
Q6ZRI0	Otogelin	2.18
Q6IMN6	Caprin-2 (C1q domain-containing protein 1) (Cytoplasmic activation/proliferation-associated protein 2) (Gastric cancer multidrug resistance-associated protein) (Protein EEG-1) (RNA granule protein 140)	2.17
Q9P2Q2	FERM domain-containing protein 4A	2.17
Q96CS2	HAUS augmin-like complex subunit 1	2.16

P48165	Gap junction alpha-8 protein (Connexin-50) (Cx50) (Lens fiber protein MP70)	2.14
Q9BVV6	Protein TALPID3	2.13
Q2VWA4	SKI family transcriptional corepressor 2 (Functional Smad-suppressing element on chromosome 18) (Fussel-18) (LBX1 corepressor 1-like protein) (Ladybird homeobox corepressor 1-like protein)	2.12
P0DI81	Trafficking protein particle complex subunit 2 (Sedlin)	2.10
Q9UBC5	Unconventional myosin-Ia	2.10
Q9NRD9	Dual oxidase 1 (EC 1.11.1.-) (EC 1.6.3.1) (Large NOX 1) (Long NOX 1) (NADPH thyroid oxidase 1) (Thyroid oxidase 1)	2.09
Q7Z553	MAM domain-containing glycosylphosphatidylinositol anchor protein 2 (MAM domain-containing protein 1)	2.09
Q9UBC5	Unconventional myosin-Ia (Brush border myosin I) (BBM-I) (BBMI) (Myosin I heavy chain) (MIHC)	2.08
P55085	Proteinase-activated receptor 2 (PAR-2) (Coagulation factor II receptor-like 1) (G-protein coupled receptor 11) (Thrombin receptor-like 1) [Cleaved into: Proteinase-activated receptor 2, alternate cleaved 1; Proteinase-activated receptor 2, alternate cleaved 2]	2.08
Q96F46	Interleukin-17 receptor A (IL-17 receptor A) (IL-17RA) (CDw217) (CD antigen CD217)	2.07
Q8TEQ0	Sorting nexin-29 (RUN domain-containing protein 2A)	2.05
Q01954	Zinc finger protein basonuclin-1	2.03
Q9NZ20	Group 3 secretory phospholipase A2PLA2G3	2.02
Q13275	Semaphorin-3F (Sema III/F) (Semaphorin IV) (Sema IV)	2.02
O95841	Angiopoietin-related protein 1 (Angiopoietin-3) (ANG-3) (Angiopoietin-like protein 1)	1.99
P11277	Spectrin beta chain, erythrocytic (Beta-I spectrin)	1.99
Q9NS15	Latent-transforming growth factor beta-binding protein 3	1.99
Q15038	DAZ-associated protein 2 (Deleted in azoospermia-associated protein 2)	1.98
Q9BX59	Tapasin-related protein (TAPASIN-R) (TAP-binding protein-like) (TAP-binding protein-related protein) (TAPBP-R) (Tapasin-like)	1.98
Q0P651	Protein ABHD18	1.96
Q9NRN5	Olfactomedin-like protein 3 (HNOEL-iso) (hOLF44)	1.93
Q9BT67	NEDD4 family-interacting protein 1 (Breast cancer-associated protein SGA-1M) (NEDD4 WW domain-binding protein 5) (Putative MAPK-activating protein PM13) (Putative NF-kappa-B-activating protein 164) (Putative NFKB and MAPK-activating protein)	1.92
G5EDS1	Homeobox domain-containing protein (Fragment)	1.92
Q5JQC9	A-kinase anchor protein 4 (AKAP-4) (A-kinase anchor protein 82 kDa) (AKAP 82) (hAKAP82) (Major sperm fibrous sheath protein) (HI) (Protein kinase A-anchoring protein 4) (PRKA4)	1.92
P00439	Phenylalanine-4-hydroxylase (PAH) (EC 1.14.16.1) (Phe-4-monooxygenase)	1.91
P01588	Erythropoietin (Epoetin)	1.90
P38570	Integrin alpha-E (HML-1 antigen) (Integrin alpha-IEL) (Mucosal lymphocyte 1 antigen) (CD antigen CD103) [Cleaved into: Integrin alpha-E light chain; Integrin alpha-E heavy chain]	1.90
Q9H5I5	Piezo-type mechanosensitive ion channel component 2 (Protein FAM38B)	1.89
Q9NR56	Muscleblind-like protein 1 (Triplet-expansion RNA-binding protein)	1.89
Q8TC76	Protein FAM110B	1.87
Q96GE4	Centrosomal protein of 95 kDa (Cep95) (Coiled-coil domain-containing protein 45)	1.85
A6NFE2	Single-pass membrane and coiled-coil domain-containing protein 2	1.84

Q96S95	Calcium/calmodulin-dependent protein kinase II inhibitor 2 (CaM-KII inhibitory protein) (CaM-KIIN)	1.83
Q6ZT07	TBC1 domain family member 9 (TBC1 domain family member 9A)	1.83
Q86Z23	Complement C1q-like protein 4 (C1q and tumor necrosis factor-related protein 11) (C1q/TNF-related protein 11)	1.83
Q9HAY2	Melanoma-associated antigen F1 (MAGE-F1) (MAGE-F1 antigen)	1.78
P82251	b(0,+)-type amino acid transporter 1 (b(0,+)AT1) (Glycoprotein-associated amino acid transporter b0,+AT1) (Solute carrier family 7 member 9)	1.78
O75628	GTP-binding protein REM 1 (GTPase-regulating endothelial cell sprouting) (Rad and Gem-like GTP-binding protein 1)	1.77
P06748	Nucleophosmin (NPM) (Nucleolar phosphoprotein B23) (Nucleolar protein NO38) (Numatrin)	1.75
Q9Y3V2	RWD domain-containing protein 3 (RWD domain-containing sumoylation enhancer) (RSUME)	1.75
O00534	von Willebrand factor A domain-containing protein 5A (Breast cancer suppressor candidate 1) (BCSC-1) (Loss of heterozygosity 11 chromosomal region 2 gene A protein)	1.74
Q8N8U9	BMP-binding endothelial regulator protein (Bone morphogenetic protein-binding endothelial cell precursor-derived regulator) (Protein crossveinless-2) (hCV2)	1.73
Q2KHR2	DNA-binding protein RFX7	1.73
Q16557	Pregnancy-specific beta-1-glycoprotein 3	1.73
Q9Y5G5	Protocadherin gamma-A8 (PCDH-gamma-A8)	1.73
P16989	Y-box-binding protein 3 (Cold shock domain-containing protein A) (DNA-binding protein A) (Single-strand DNA-binding protein NF-GMB)	1.72
A0A7I2RN43	DnaJ homolog subfamily B member 5	1.71
Q5JTC6	APC membrane recruitment protein 1 (Amer1) (Protein FAM123B) (Wilms tumor gene on the X chromosome protein)	1.71
P19256	Lymphocyte function-associated antigen 3 (Ag3) (Surface glycoprotein LFA-3) (CD antigen CD58)	1.71
Q6WRI0	Immunoglobulin superfamily member 10 (IgSF10) (Calvaria mechanical force protein 608) (CMF608)	1.71
Q8TED9	Actin filament-associated protein 1-like 1 (AFAP1-like protein 1)	1.71
A0A1B0GTZ2	Putative coiled-coil domain-containing protein 196 (Long intergenic non-protein coding RNA 238)	1.69
Q9C0I3	Serine-rich coiled-coil domain-containing protein 1 (Coiled-coil serine-rich protein 1)	1.69
Q6PJT7	Zinc finger CCCH domain-containing protein 14 (Mammalian suppressor of tau pathology-2) (MSUT-2) (Renal carcinoma antigen NY-REN-37)	1.69
Q3KNV8	Polycomb group RING finger protein 3	1.69
P54315	Inactive pancreatic lipase-related protein 1 (PL-RP1)	1.68
Q8NEM8	Cytosolic carboxypeptidase 3 (EC 3.4.17.-) (ATP/GTP-binding protein-like 3) (Protein deglutamylase CCP3)	1.68
Q7Z309	PABIR family member 2 (Synoviocyte proliferation associated in collagen-induced arthritis 2)	1.68
Q9P203	BTB/POZ domain-containing protein 7	1.67
Q8TD10	Mirror-image polydactyly gene 1 protein	1.66
P21912	Succinate dehydrogenase [ubiquinone] iron-sulfur subunit, mitochondrial (EC 1.3.5.1) (Iron-sulfur subunit of complex II) (Fragment)	1.66
O95807	Transmembrane protein 50A (Small membrane protein 1)	1.66
Q8NDX6	Zinc finger protein 740 (OriLyt TD-element-binding protein 7)	1.65
Q8WU58	Protein FAM222B	1.65

Q9Y586	Protein mab-21-like 2	1.63
Q7LFL8	CXXC-type zinc finger protein 5 (CF5) (Putative MAPK-activating protein PM08) (Putative NF-kappa-B-activating protein 102) (Retinoid-inducible nuclear factor) (RINF)	1.62
A6NE52	WD repeat-containing protein 97	1.62
Q9UQN3	Charged multivesicular body protein 2b (CHMP2.5) (Chromatin-modifying protein 2b) (CHMP2b) (Vacuolar protein sorting-associated protein 2-2) (Vps2-2) (hVps2-2)	1.61
Q14469	Transcription factor HES-1 (Class B basic helix-loop-helix protein 39) (bHLHb39) (Hairy and enhancer of split 1) (Hairy homolog) (Hairy-like protein) (hHL)	1.61
Q13237	cGMP-dependent protein kinase 2 (cGK 2) (cGK2) (EC 2.7.11.12) (cGMP-dependent protein kinase II) (cGKII)	1.60
P30411	B2 bradykinin receptor (B2R) (BK-2 receptor)	1.60
Q92674	Centromere protein I	1.59
Q5H9M0	PWWP domain-containing DNA repair factor 3B (PWWP3B) (Mutated melanoma-associated antigen 1-like protein 1) (MUM1-like protein 1) (PWWP domain-containing protein MUM1L1)	1.59
Q9NYS7	WD repeat and SOCS box-containing protein 2 (WSB-2) (CS box-containing WD protein)	1.59
Q5JTY5	COBW domain-containing protein 3 (Cobalamin synthase W domain-containing protein 3)	1.59
Q14CM0	FERM and PDZ domain-containing protein 4	1.58
Q6ZU69	Protein FAM205A	1.57
Q9BUB4	tRNA-specific adenosine deaminase 1 (hADAT1) (EC 3.5.4.34) (tRNA-specific adenosine-37 deaminase)	1.57
Q7L099	Protein RUFY3 (RUN and FYVE domain-containing protein 3) (Rap2-interacting protein x) (RIPx) (Single axon-regulated protein) (Singar)	1.57
Q5THK1	Protein PRR14L (Proline rich 14-like protein)	1.56
Q8WYL5	Protein phosphatase Slingshot homolog 1 (EC 3.1.3.16) (EC 3.1.3.48) (SSH-like protein 1) (SSH-1L) (hSSH-1L)	1.56
Q96KS0	Prolyl hydroxylase EGLN2 (EC 1.14.11.-) (Egl nine homolog 2) (EC 1.14.11.29) (Estrogen-induced tag 6) (EIT-6) (HPH-3) (Hypoxia-inducible factor prolyl hydroxylase 1) (HIF-PH1) (HIF-prolyl hydroxylase 1) (HPH-1) (Prolyl hydroxylase domain-containing protein 1) (PHD1)	1.55
P52926	High mobility group protein HMGI-C (High mobility group AT-hook protein 2)	1.54
O15372	Eukaryotic translation initiation factor 3 subunit H (Fragment)	1.54
Q5TIA1	Meiosis inhibitor protein 1 (Meiosis defective protein 1)	1.53
Q9BTF0	THUMP domain-containing protein 2	1.53
Q9Y6G3	39S ribosomal protein L42, mitochondrial	1.52
Q1HG43	Dual oxidase maturation factor 1 (Dual oxidase activator 1) (Numb-interacting protein)	1.52
Q96RD9	Fc receptor-like protein 5 (FcR-like protein 5) (FcRL5) (BXMAS1) (Fc receptor homolog 5) (FcRH5) (Immune receptor translocation-associated protein 2) (CD antigen CD307e)	1.52
Q9HBE1	POZ-, AT hook-, and zinc finger-containing protein 1 (BTB/POZ domain zinc finger transcription factor) (Protein kinase A RI subunit alpha-associated protein) (Zinc finger and BTB domain-containing protein 19) (Zinc finger protein 278) (Zinc finger sarcoma gene protein)	1.50
Q4L180	Filamin A-interacting protein 1-like (130 kDa GPBP-interacting protein) (90 kDa GPBP-interacting protein) (Protein down-regulated in ovarian cancer 1) (DOC-1)	1.50
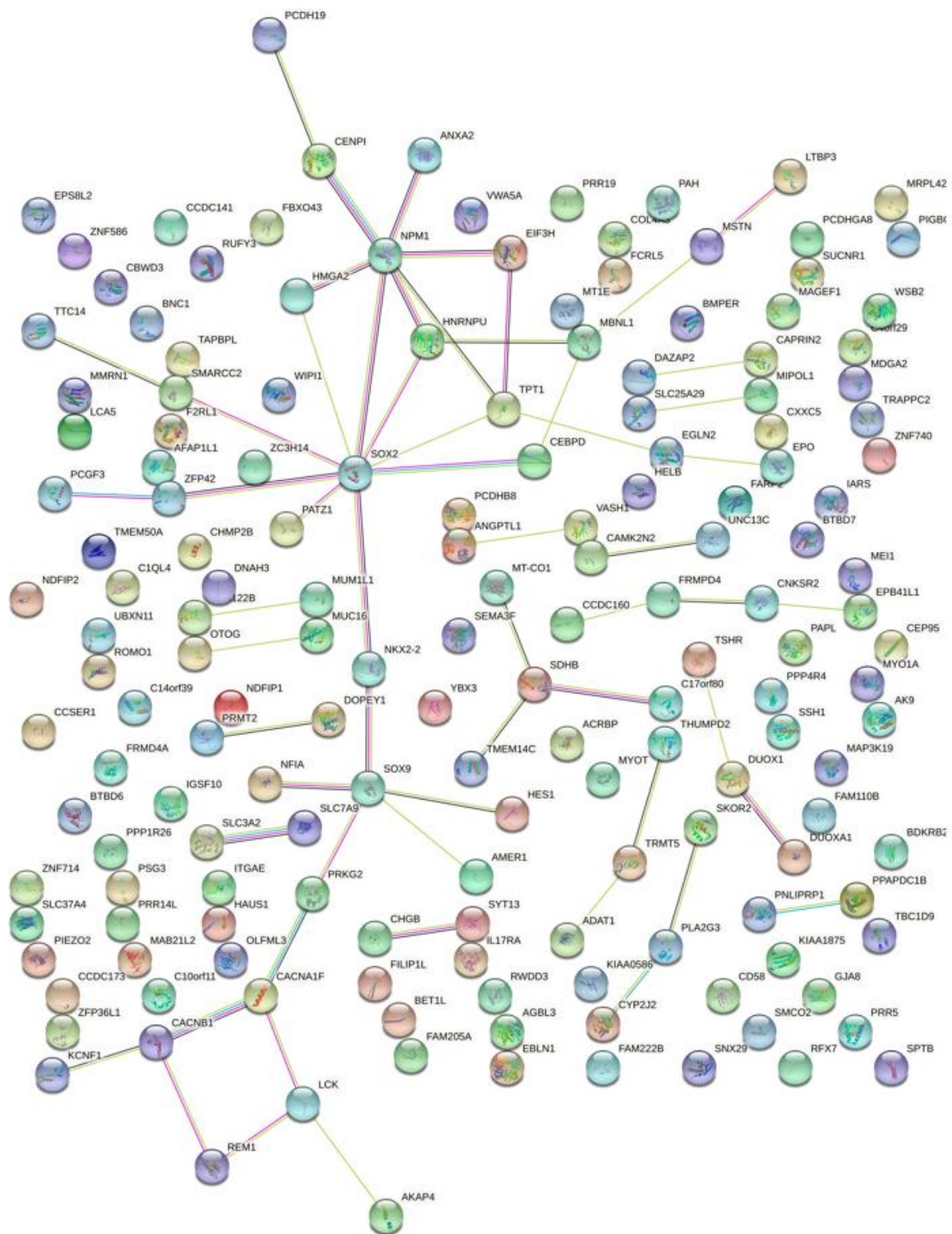
Figure 80. STRING analysis of proteins that increased ≥ 1.5 log2 fold in SARS-CoV-2 W.T infected cells.
The STRING database was searched to analyze the interactions between the host's proteins that showed a ≥ 1.5 log2 fold increase in SARS-CoV-2 W.T infected A549-ACE-2 cells compared to mock-infected cells. Nodes representing proteins that most significantly enriched the GO term.

5.2.8.4 Host proteins decreased in SARS-CoV-2 W.T infected cells compared to mock-infected cells

Fourteen host proteins were ≥ 1.5 log2-fold down-regulated in SARS-CoV-2 W.T infected cells compared with mock-infected cells (Table 37). The STRING database was searched to analyze the interactions between host proteins that showed a ≥ 1.5 log2-fold decrease in SARS-CoV-2 W.T infected cells compared to mock-infected cells (Figure 80).

Table 37. The cellular proteins decreased ≥1.5 log2 fold in SARS-CoV-2 W.T infected cells. Proteins' IDs and names are obtained from UniProt: the universal protein knowledgebase in 2021.

| UniProt ID	Protein name	Log2-fold-change difference
O43278	Kunitz-type protease inhibitor 1 (Fragment)	-4.49
Q12955	Ankyrin-3 (ANK-3) (Ankyrin-G)	-2.77
P25705	ATP synthase subunit alpha, mitochondrial (ATP synthase F1 subunit alpha)	-2.37
P02795	Metallothionein-2 (MT-2) (Metallothionein-2A) (Metallothionein-II) (MT-II)	-2.12
Q2M3V2	Ankyrin repeat domain-containing protein SOWAHA (Ankyrin repeat domain-containing protein 43) (Protein sosondowah homolog A)	-2.03
O14604	Thymosin beta-4, Y-chromosomal	-1.96
Q14995	Nuclear receptor subfamily 1 group D member 2 (Orphan nuclear hormone receptor BD73) (Rev-erb alpha-related receptor) (RVR) (Rev-erb-beta) (V-erbA-related protein 1-related) (EAR-1R)	-1.86
Q8IXS2	Dynein regulatory complex subunit 2 (Coiled-coil domain-containing protein 65) (Testis development protein NYD-SP28)	-1.72
Q99538	Legumain (EC 3.4.22.34) (Asparaginyl endopeptidase) (Protease, cysteine 1)	-1.72
Q9Y6K8	Adenylate kinase isoenzyme 5 (AK 5) (EC 2.7.4.3) (EC 2.7.4.6) (ATP-AMP transphosphorylase 5)	-1.70
Q9UPQ3	Arf-GAP with GTPase, ANK repeat and PH domain-containing protein 1 (AGAP-1) (Centaurin-gamma-2) (Cnt-g2) (GTP-binding and GTPase-activating protein 1) (GGAP1)	-1.68
P55061	Bax inhibitor 1 (BI-1) (Testis-enhanced gene transcript protein) (Transmembrane BAX inhibitor motif-containing protein 6)	-1.54
Q13822	Ectonucleotide pyrophosphatase/phosphodiesterase family member 2 (E-NPP 2) (EC 3.1.4.39) (Autotaxin) (Extracellular lysophospholipase D) (LysoPLD)	-1.51
P36888	Receptor-type tyrosine-protein kinase FLT3 (EC 2.7.10.1) (FL cytokine receptor) (Fetal liver kinase-2) (FLK-2) (Fms-like tyrosine kinase 3) (FLT-3) (Stem cell tyrosine kinase 1) (STK-1) (CD antigen CD135)	-1.50
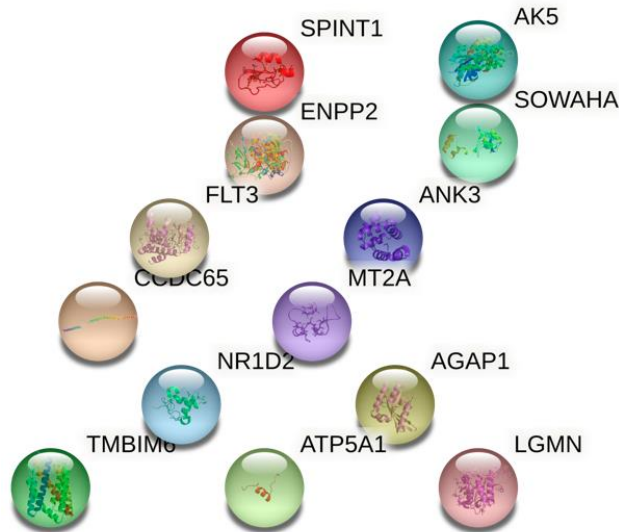
Figure 81. STRING analysis of proteins that decreased ≥ 1.5 log2 fold in SARS-CoV-2 W.T infected cells. The STRING database was searched to analyze the interactions between host proteins that showed a ≥ 1.5 log2 fold decrease in SARS-CoV-2 W.T infected cells compared to mock-infected cells. Nodes representing proteins that most significantly enriched the GO term.

5.2.8.5 Host proteins increased in SARS-CoV-2 ORF10 KO infected cells compared to SARS-CoV-2 WT infected cells

Sixty-one host proteins were ≥ 1.5 log2-fold upregulated in SARS-CoV-2 ORF10 KO infected cells compared to mock-infected cells. These proteins were also elevated in SARS-CoV-2 WT infected cells but below the level of 1.5 log2 fold-change (Table 38).

Table 38. Cellular protein increased ≥ 1.5 log2-fold in SARS-CoV-2 ORF10 KO infected cells but below the level of 1.5 log2-fold change in SARS-CoV-2 WT infected cells. Proteins' IDs, names and genes' symbols are obtained from UniProt: the universal protein knowledgebase in 2021.

UniProt ID	Protein name	Gene symbol
E9PJF7	Translationally-controlled tumor protein	TPT1
A0A2R8YE65	Connector enhancer of kinase suppressor of ras 2	CNKSR2
A0A087WWI0	Leucine-rich melanocyte differentiation-associated protein	LRMDA
U3KQS2	Glucose-6-phosphate exchanger SLC37A4	SLC37A4
H7C2K6	Band 4.1-like protein 1	EPB41L1
Q5TA12	Protein dopey-1	DOP1A
P41252	Isoleucine--tRNA ligase, cytoplasmic, EC 6.1.1.5 (Isoleucyl-tRNA synthetase, IRS, IleRS)	IARS1

G3V5X1	tRNA (guanine(37)-N1)-methyltransferase	TRMT5
A0A0C4DFM5	Myotilin (Myotilin, isoform CRA_b)	MYOT
H0YL33	Annexin	ANXA2
A0A087WU35	Zinc finger protein 714	ZNF714
B8ZZS0	BET1-like protein	BET1L
H7C3M7	FERM, ARHGEF and pleckstrin domain-containing protein 2	FARP2
G3V342	Unconventional myosin-Ia	MYO1A
A0A0A0MTJ0	Thyrotropin receptor	TSHR
Q5VYM1	Uncharacterized protein C9orf131	C9orf131
Q96KE9	BTB/POZ domain-containing protein 6 (Lens BTB domain protein)	BTBD6 BDPL
G3V3T2	BTB/POZ domain-containing protein 7	BTBD7
Q9Y4F9	Rho family-interacting cell polarization regulator 2	RIPOR2
A0A087WXX8	Succinate dehydrogenase [ubiquinone] iron-sulfur subunit, mitochondrial, EC 1.3.5.1 (Iron-sulfur subunit of complex II)	SDHB
H7BXM4	Collagen alpha-3(IV) chain	COL4A3
V9GYH0	Homeobox domain-containing protein	
Q96JJ6	Junctophilin-4, JP-4 (Junctophilin-like 1 protein)	JPH4
K7EM54	HAUS augmin-like complex subunit 1	HAUS1
G1UD79	PABIR family member 2 (Synoviocyte proliferation associated in collagen-induced arthritis 2)	PABIR2
Q2KHR2	DNA-binding protein RFX7 (Regulatory factor X 7) (Regulatory factor X domain-containing protein 2)	RFX7
B5MEC4	Polycomb group RING finger protein 3	PCGF3
Q9NS15	Latent-transforming growth factor beta-binding protein 3, LTBP-3	LTBP3
J3KR56	Receptor activity-modifying protein 3	
G3V2E4	Glycine hydroxymethyltransferase, EC 2.1.2.1	RAMP3
M0QX68	Pregnancy-specific beta-1-glycoprotein 3	SHMT2
P0C870	Bifunctional peptidase and (3S)-lysyl hydroxylase JMJD7, EC 1.14.11.63, EC 3.4.-.- (JmjC domain-containing protein 7) (Jumonji domain-containing protein 7) (L-lysine (3S)-hydroxylase JMJD7)	PSG3
E5RJT0	Eukaryotic translation initiation factor 3 subunit H	JMJD7
A0A0C4DG89	RNA helicase, EC 3.6.4.13	EIF3H
Q7Z3D6	D-glutamate cyclase, mitochondrial, EC 4.2.1.48	DDX46
I3L3R5	Coiled-coil domain-containing glutamate-rich protein 2	DGLUCY C14orf159
O95149	Snurportin-1 (RNA U transporter 1)	CCER2
A0A2R8YEZ0	Protein ABHD18	SNUPN RNUT1 SPN1
S4R2Z7	39S ribosomal protein L42, mitochondrial	ABHD18
Q6PFW1	Inositol hexakisphosphate and diphosphoinositol-pentakisphosphate kinase 1, EC 2.7.4.24 (Diphosphoinositol pentakisphosphate kinase 1) (Histidine acid phosphatase domain-containing protein 2A) (IP6 kinase) (Inositol pyrophosphate	MRPL42

	synthase 1) (InsP6 and PP-IP5 kinase 1) (VIP1 homolog, hsVIP1)	
Q7L2Z9	Centromere protein Q, CENP-Q	PPIP5K1
P62341	Thioredoxin reductase-like selenoprotein T, SelT, EC 1.8.1.9	CENPQ C6orf139
Q9ULS5	Transmembrane and coiled-coil domain protein 3	SELENOT SELT UNQ150/PRO176
Q96K19	E3 ubiquitin-protein ligase RNF170, EC 2.3.2.27 (Putative LAG1-interacting protein) (RING finger protein 170) (RING-type E3 ubiquitin transferase RNF170)	TMCC3 KIAA1145
Q9HB58	Sp110 nuclear body protein (Interferon-induced protein 41/75) (Speckled 110 kDa) (Transcriptional coactivator Sp110)	RNF170
Q86VD7	Mitochondrial coenzyme A transporter SLC25A42 (Solute carrier family 25 member 42)	SP110
Q6IQ55	Tau-tubulin kinase 2, EC 2.7.11.1	SLC25A42
P60059	Protein transport protein Sec61 subunit gamma	TTBK2 KIAA0847
P31146	Coronin-1A (Coronin-like protein A, Clipin-A) (Coronin-like protein p57) (Tryptophan aspartate-containing coat protein, TACO)	SEC61G
B7WNH4	Small integral membrane protein 7	CORO1A CORO1
Q6P0Q8	Microtubule-associated serine/threonine-protein kinase 2, EC 2.7.11.1	SMIM7
A0A3B3IT33	Putative tripartite motif-containing protein 51G (Tripartite motif-containing 51G pseudogene)	MAST2 KIAA0807 MAST205
Q92562	Polyphosphoinositide phosphatase, EC 3.1.3.-, EC 3.1.3.36, EC 3.1.3.86 (Phosphatidylinositol 3,5-bisphosphate 5-phosphatase) (SAC domain-containing protein 3) (Serine-protein phosphatase FIG4, EC 3.1.3.16)	TRIM51G TRIM51GP
O95727	Cytotoxic and regulatory T-cell molecule (Class-I MHC-restricted T-cell-associated molecule) (CD antigen CD355)	FIG4 KIAA0274 SAC3
P00740	Coagulation factor IX, EC 3.4.21.22 (Christmas factor) (Plasma thromboplastin component, PTC) [Cleaved into: Coagulation factor IXa light chain; Coagulation factor IXa heavy chain]	CRTAM
Q8NBM8	Prenylcysteine oxidase-like, EC 1.8.3.-	F9
Q5T1H1	Protein eyes shut homolog (Epidermal growth factor-like protein 10, EGF-like protein 10) (Epidermal growth factor-like protein 11, EGF-like protein 11) (Protein spacemaker homolog)	PCYOX1L PSEC0105
O15105	Mothers against decapentaplegic homolog 7, MAD homolog 7, Mothers against DPP homolog 7 (Mothers against decapentaplegic homolog 8, MAD homolog 8, Mothers against DPP homolog 8) (SMAD family member 7, SMAD 7, Smad7, hSMAD7)	EYS C6orf178

Q9P2G4	Microtubule-associated protein 10 (Microtubule regulator of 120 KDa)	SMAD7 MADH7 MADH8
Q15149	Plectin, PCN, PLTN (Hemidesmosomal protein 1, HD1) (Plectin-1)	MAP10 KIAA1383 MTR120
Q9HBL7	Plasminogen receptor (KT), Plg-R(KT)	PLEC PLEC1
Q9Y6H5	Synphilin-1, Sph1 (Alpha-synuclein-interacting protein)	PLGRKT C9orf46
A6NHL2	Tubulin alpha chain-like 3	SNCAIP

5.2.8.6 Host proteins increased in SARS-CoV-2 W.T infected cells compared to SARS-CoV-2 ORF10 KO infected cells

Ten host proteins were ≥ 1.5 log2 fold up-regulated in SARS-CoV-2 W.T infected cells compared to mock-infected cells. These proteins were also elevated in SARS-CoV-2 ORF10 KO infected cells but below the level of 1.5 log2 fold-change (Table 39).

Table 39. Cellular protein increased ≥ 1.5 log2 fold in SARS-CoV-2 W.T infected cells but below 1.5 log2-fold in SARS-CoV-2 ORF10 KO infected cells. Proteins' IDs, names and genes' symbols are obtained from UniProt: the universal protein knowledgebase in 2021.

UniProt ID	Protein name	Gene symbol
P13693	Translationally-controlled tumor protein, TCTP (Fortilin) (Histamine-releasing factor, HRF) (p23)	TPT1
Q9H2I8	Leucine-rich melanocyte differentiation-associated protein	LRMDA
Q8WXI2	Connector enhancer of kinase suppressor of ras 2, Connector enhancer of KSR 2 (CNK homolog protein 2, CNK2)	CNKSR2 CNK2
Q9H4G0	Band 4.1-like protein 1 (Erythrocyte membrane protein band 4.1-like 1) (Neuronal protein 4.1, 4.1N)	EPB41L1
Q5JWR5	Protein dopey-1	DOP1A DOPEY
O43826	Glucose-6-phosphate exchanger SLC37A4 (Glucose-5-phosphate transporter) (Glucose-6-phosphate translocase) (Solute carrier family 37 member 4) (Transformation-related gene 19 protein, TRG-19)	SLC37A4 G6PT
Q9UBF9	Myotilin (57 kDa cytoskeletal protein) (Myofibrillar titin-like Ig domains protein) (Titin immunoglobulin domain protein)	MYOT TTID
P41252	Isoleucine--tRNA ligase, cytoplasmic, EC 6.1.1.5 (Isoleucyl-tRNA synthetase, IRS, IleRS)	IARS1 IARS
Q32P41	tRNA (guanine(37)-N1)-methyltransferase, EC 2.1.1.228 (M1G-methyltransferase) (tRNA [GM37] methyltransferase) (tRNA methyltransferase 5 homolog)	TRMT5
P16473	Thyrotropin receptor (Thyroid-stimulating hormone receptor, TSH-R)	TSHR LGR3

5.2.9 Growth kinetics of SARS-CoV-2 ORF10 KO and SARS-CoV-2 W.T.

The replicative fitness of SARS-CoV-2 ORF10 KO was examined in VTN and A549-ACE2 cells. VTN cells lack the ability to express type I IFNs, so the growth kinetics was also performed in A549-ACE2 cells to elucidate the role of ORF10 in suppressing host's innate immune response. VTN and A549-ACE2 were infected with SARS-CoV-2 ORF10 KO and SARS-CoV-2 W.T at an MOI of 0.01 for 1 hr before removing the viral inoculum. Culture supernatant samples were collected at 5.5, 19, 27, and 48 hpi, and viral RNA was extracted and quantified by real-time polymerase chain reaction (RT-qPCR) (Figure 81). An input sample was also taken during infection (Time point 0). There was no relevant difference in replication between SARS-CoV-2 ORF10 KO and SARS-CoV-2 W.T in VTN cells. In A549-ACE2, the viral growth of SARS-CoV-2 ORF10 KO was slightly higher than SARS-CoV-2 W.T at time points 19 hrs and 27 hpi, indicating ORF10 KO was advantageous for virus replication. However, as the infection progressed, the viral growth of SARS-CoV-2 ORF10 KO and SARS-CoV-2 W.T were similar at 48hpi. The experiment was kindly conducted by Dr. Milligan in the BSL3.
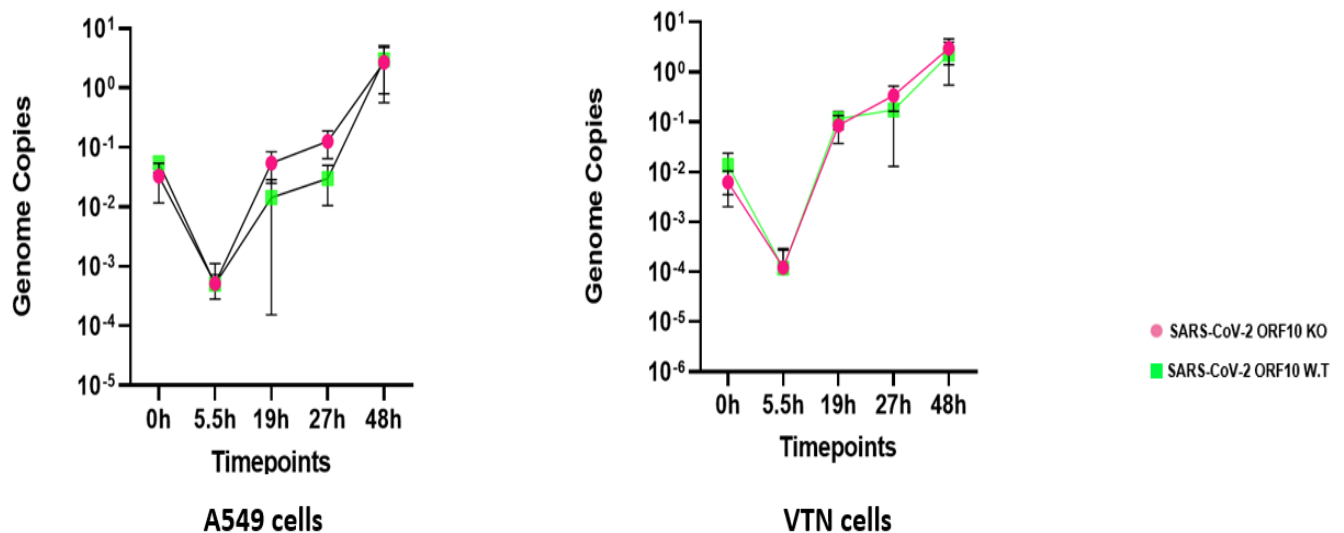
Figure 82. SARS-CoV-2 ORF10 KO and SARS-CoV-2 W.T growth kinetics in VTN and A549-ACE2 cells. VTN and A549-ACE2 cells were infected with SARS-CoV-2 ORF10 KO and SARS-CoV-2 W.T at an MOI of 0.01. The culture supernatants were collected at the indicated time points, and viral RNA copies were quantified by RT-qPCR.

5.3 Discussion

The TMT/MS-MS analysis of ORF10 co-IP samples showed enrichment of host proteins implicated in the anti-viral immune response with the SARS-CoV-2 ORF10 protein. The IP-Western analysis validated the interaction of ORF10 with some of these proteins, including IFIT1, OAS2, and MX1. As mentioned earlier, IFN-induced proteins with tetratricopeptide repeat 1 (IFIT1) is an essential antiviral protein strongly induced by type I IFN. It acts as a viral RNA sensor by recognizing the triphosphate group on its 5' terminus (PPP-RNA). It possesses antiviral activity by inhibiting the expression of viral mRNA (264). The human 2′, 5′-oligoadenylate synthetase (OAS2) is an IFN-induced gene activated by viral double-stranded RNA. It exerts antiviral activity via the IFN-activated Jak/STAT signaling pathway (265). MX1 is an Interferon-induced gene with antiviral activity. MX1 inhibits viral replication by recognizing and inactivating viral ribonucleoprotein complexes and blocking the transcription of viral RNA (266).

Based on these results, we hypothesized that ORF10 protein might play a role in enhancing viral replication by suppressing the anti-viral immune response. I used a reverse genetics platform to rescue the SARS-CoV-2 virus with either the ORF10 protein knocked out or replaced with fluorescent markers. SARS-CoV-2 ORF10 KO was successfully rescued, while fluorescent protein substitution viruses could not be rescued despite several attempts. To elucidate the functional role of ORF10 protein in modulating the host's immune proteins or cellular proteome, a high-throughput proteomics analysis of SARS-CoV-2 W.T and SARS-CoV-2 ORF10 KO infected cells we conducted. Moreover, the replicative fitness of SARS-CoV-2 ORF10 KO was examined in cells lacking type I IFN (VTN) and in cells expressing IFN (A549-ACE2).

While conducting our study, recent work suggested that ORF10 abrogates IFN-I signaling and suppresses the innate immune response to facilitate virus replication. In that study, mRNA levels of IFN-stimulated genes, such as ISG15 and OAS-1, and their proteins expression decreased upon overexpression of ORF10 before Poly (I: C) treatment or infection with SARS-CoV-2 (100). In contrast to that study, our high-throughput quantitative proteomic results showed no significant changes in the host's proteins abundance between SARS-CoV-2 W.T and SARS-CoV-2 ORF10 KO infected cells. More importantly, the data showed no significant difference in the expression of innate immune proteins between SARS-CoV-2 W.T and SARS-CoV-2 ORF10 KO infected cells.

The growth kinetics of the SARS-CoV-2 W.T and SARS-CoV-2 ORF10 KO showed no difference in the replication dynamics between the two viruses in VTN and A549-ACE2 cells,

indicating ORF10 KO didn't affect the virus fitness and didn't suppress host' immune response. However, we can't exclude any other roles that ORF10 might play in virus replication. RNA itself is recognized as a critical modulator in regulating RNA viruses' transcription, translation, and replication. The RNA structure of the ORF10 sequence could have a regulatory role that is more important than its coding function in the virus life cycle since we couldn't rescue ORF10-fluorescent protein substitution viruses.

The 5′-UTR is located upstream of the first open reading frame, never gets translated, and possesses a wide variety of high-order RNA structures. These high-order structural elements are indispensable in regulating fundamental processes of a virus's life cycle, such as enhancing the stability and translational efficiency of viral mRNA and controlling gene expression (267). The 5' UTRs of coronaviruses have an array of conserved RNA stem-loops, such as SL1, SL2, SL3, SL4, and SL5, which play critical regulatory roles for RNA synthesis and viral replication (268). SL1 helical stem-loop is indispensable for coronaviruses replication. Disruption of the SL1 RNA structure prevents the synthesis of minus-sense subgenomic RNA (269). The non-structural protein 1 (Nsp1) is one of the SARS-CoV-2 virulence factors that causes a complete halt in host translation. It has been shown that the SL1 region of the SARS-CoV-2 is critical in bypassing Nsp1-mediated translational suppression. Targeting the SL1 RNA structure causes viral translation to be susceptible to Nsp1 shutdown, indicating the crucial role of SL1 in SARS-CoV-2 replication (270). SL2 is the most conserved RNA segment in the 5′UTR region of coronaviruses and has a vital role in virus replication. It has been shown that the SL2 segment is critical for subgenomic RNA synthesis, although nucleotide sequences are not necessary (271). SL3 contains a transcription-regulating sequence (TRS) and is involved in the production of discontinuous transcription of subgenomic mRNAs. SL4 has a short upstream uORF which is not critical for viral replication. However, SL3 and SL4 have roles in directing subgenomic RNA synthesis, and deletion of either one of them is lethal for virus replication (272) (273) (274). SL5 contains the start codon for the ORF1ab, which encodes the viral replicase/transcriptase polyprotein and is involved in viral RNA packaging (275).

The 3′ UTR of the RNA viruses are highly structured and involved in modulating various aspects of the virus life cycle. In addition to regulating the cyclization, replication, and translation of viral genomic RNA, the 3′ UTR element structures are also involved in modulating the host cell response by directly or indirectly interacting with viral or cellular nucleotides and proteins(276).

The SARS-CoV-2 RNA tertiary structure has been deciphered recently, uncovering many long-range duplexes, stem-loop structures, and higher-order junctions. Based on the SARS-

CoV-2 RNA tertiary structure (277), It was found that ORF10 is a part of a structure within the 3 UTR region and, therefore, could have a role in regulating viral RNA synthesis and translation (Figure 82). Hyper-variable region (HVR) is one of the RNA elements at 3′ UTR of coronaviruses, and its relevance in viral replication is poorly understood. However, it has been shown that deletion of the HVR in coronaviruses doesn't affect viral RNA synthesis in cell culture but reduces virus pathogenicity in mice, indicating a possible role of HVR in suppressing the immune response rather than modulating viral RNA synthesis (277,278) (279). HVR contains subregions that are highly conserved among coronaviruses. Stem-loop II-like motif (S2M) is one of the subregions in HVR that is conserved in coronaviruses, including SARS-CoV-2. Although S2M structure has been shown to be substantial for some RNA viruses, such as astrovirus VA1 (VA1) and classic human astrovirus 1 (HAstV1), it is dispensable for SARS-CoV-2 replication, which raises the question of why a highly conserved RNA element has different functional activities in the viral replication (280).
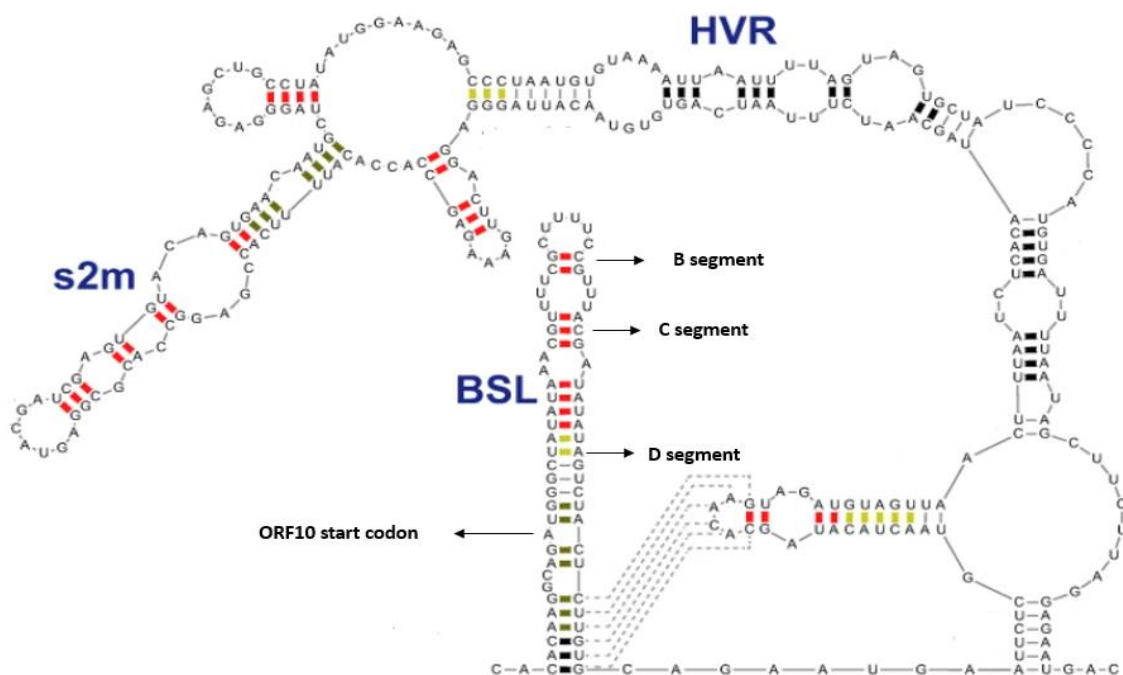
Figure 83. The landscape of the SARS-CoV-2 3′ UTR. The SARS-CoV-2 3′ UTR's secondary structure includes the HVR region containing the S2M sub-region and the bulged stem-loop (BSL). Stem segments B, C, and D are shown.

One of the conserved structural elements of 3′ UTR is the bulged stem-loop (BSL), which consists of three stem segments (D, C, and B). Segment B represents the terminal segment adjacent to the loop of the BSL structure, whereas C and D represent the middle and bottom

segments, respectively. The SARS-CoV-2 RNA tertiary structure showed that the ORF10 start codon is located within the BSL region in segment D (281). Although disruption of the loop of BLS structure or the adjacent stem segment B had no effect on Mouse hepatitis virus (MHV) replication, the structural conservation of C and D segments, rather than their nucleotides sequence conservation, were found to be essential for virus replication (282) (283). Therefore, the RNA structure of ORF10 could be more relevant for SARS-CoV-2 replication than its coding function, which also might explain why we couldn't rescue SARS-CoV-2ΔORF10mNeonGreen and SARS-CoV-2ΔORF10mScarlet mutants despite several attempts.

Chapter 6. General discussion and future directions.

Different studies have been conducted in this thesis. Chapter three focused on providing potential answers to why bat-borne viruses, *e.g.,* MERS-CoV and SARS-CoV-2, are so lethal when they adapt to cause human disease but not in their animal hosts. It is proposed that the innate immune system of animal hosts responds to MERS-CoV and SARS-CoV-2 infections differently than humans, allowing them to be persistently infected without clinical symptoms (192,193). In chapter three, I conducted a high-throughput proteomic analysis to investigate the alteration of host innate immune proteins' expression in bat, human, and camel cells in response to innate immune system stimuli IFN and Poly: IC. Poly: IC has been used in this study because it has a similar innate immune stimulatory effect to viral dsRNA such as MERS-CoV and SARS-CoV-2(284).

In the IFN treatment condition, the induced alterations in the expression of innate immune proteins were highly similar in all three species. This alteration includes significant increasing in abundance of anti-viral proteins, *e.g.,* IFIT1, IFIT2, IFIT3, DDX58, and ISG15, in the three cell lines.

However, a marked difference in the expression of pro-inflammatory cytokines between the three species was observed in the Poly: IC treatment condition. As mentioned, excessive production of pro-inflammatory cytokines resulting from viral infections, including MERS-CoV or Covid-19, are associated with the disease's severity (213). CXCL10 is one of the pro-inflammatory cytokines, and its increased levels are associated with acute lung injury (ALI) or acute respiratory distress syndrome (ARDS) in respiratory virus infections (200) (285). In the Poly: IC treatment condition, the CXCL10 protein abundance was highly increased (5.86 log-2) in MRC-5 cells, while it was less increased (2.88 log-2) in Dubca cells but didn't increase in Pakit cells. Although CXCL10 was elevated in Dubca Poly:IC treated cells, the abundance of CCL2, which is a chemokine that has a crucial role in host survival during viral infection by protecting macrophages from virus-induced apoptosis, was much higher than CXCL10 level (5.2 log2) (219)(220).

The findings from chapter three confirm the previous reports concluding that while the IFN-stimulated genes expression is constitutively highly activated in bats, this animal host evolved unique methods to decrease severe virus-induced pro-inflammatory cytokines such as CXCL10(286,287). Our results in chapter three provide a potential answer to why bats can host many deadly viruses without clinical symptoms.

Dubca cells lack the DPP4 receptor, the main receptor for MERS-CoV (33). Therefore, This cell line can't be infected with MERS-CoV. It would be very interesting to establish new Dubca cell lines stably expressing the DPPR4 receptors to conduct a comparative

quantitative proteomic analysis on proteins contained in total cell lysates from MESR-CoV and SARS-CoV-2 infected cells in the three species. This will provide more informative and precise answers to why MERS-CoV and SARS-CoV-2 are lethal to humans but not in their animal hosts.

Identifying viral-host protein-protein interactions is important for the understanding of virology and pathogenicity. There is limited information regarding the role of MERS-CoV ORF4A & ORF4B in virus infection. Chapter four focused on identifying the cellular interacting partners for MERS-CoV ORF4A & ORF4B proteins utilizing throughput quantitative proteomics information provided previously by our lab in human cells. Furthermore, the interaction of MERS-CoV ORF4A & ORF4B proteins with bat and camel equivalent proteins was examined to investigate whether they interact with these viral proteins with higher or lower affinity than their human counterparts or whether these interactions are species-specific.

In this chapter, I validated the interaction of MERS-CoV ORF4A with NDH II in human cells and showed that this interaction is species-specific, as the IP-Western analysis confirmed that MERS-CoV ORF4A doesn't interact with bat and camel equivalents. NDH II is known to be engaged in a cellular protein complex that binds to 3' and 5' ends of the viral genome, that usually adopt complex secondary structures, and facilitates genome replication by remodeling the complex RNA structure using its helicase activity(230) (288). Therefore, it is tempting to hypothesize that the association between ORF4A and NDHII may be of the factors that enhances MERS-CoV replication in human cells more than its animal hosts. This interesting finding is worth following up by studying the effects of depleting NDH II on MERS-CoV-2 replication in human cells.

Interestingly, The IP-Western analysis showed a strong interaction between MERS-CoV ORF4B and KPNA4 human protein, but weaker interactions between ORF4B and bat and camel counterparts. Recently, a study has shown that MERS-CoV ORF4B prevents NF-κB from translocating into the nucleus by outcompeting NF-κB for KPNA4 binding, thereby disrupting the NF-κB-mediated innate immune response and enhancing virus replication (252). Similar studies should be conducted to examine the effect of the interactions between MERS-CoV ORF4B and bat and camel KPNA4 equivalent proteins on virus replication.

NF45 is an RNA-binding protein that has a direct or indirect role in viruses' replication (233) (234). hnRNPA2/B1 & hnRNPAB, are two of the major hnRNPs involved in various biological functions, such as RNA processing and mRNA stability, and play major roles in the replication of RNA viruses such as Influenza and JEV (246) . In chapter four, I validated the interaction of MERS-CoV ORF4A with NF45, hnRNPA2/B1, and hnRNPAB in human cells and with bat and camel counterparts. The importance of these interactions during MERS-

CoV infection in human and animal hosts should be tested by depleting NF45, hnRNPA2/B1, and hnRNPAB proteins and observing the effect of protein depletion on viral replication. hnRNPC1/C2 are abundant cellular proteins involved in various biological functions, such as transcriptional regulation and RNA processing, and have been shown to play important roles in viral replication at the stage of viral RNA synthesis(247). Using IP-Western analysis, the interaction between MERS-CoV ORF4B and hnRNPC1/C2 was confirmed in human and camel equivalent proteins but not with the bat counterpart. A study examined the importance of this interaction was examined in human cells (Calu-3 & HSAEC) and found that depleting hnRNPC reduced MERS-CoV mRNA expression and replication (289). It would be interesting to test the role of this interaction in virus replication using camel cells to investigate whether this interaction has a similar effect on MERS-CoV replication in this animal host.

Studying the functional roles of the SARS-2-CoV genes is crucial in understanding virus pathogenicity and identifying new therapeutic targets. Open reading frame 10 (ORF10) is one of the unique features of the SARS-CoV-2 genome, and its potential role in virus replication remains controversial. In chapter five, the focus was on identifying the possible roles of the ORF10 protein in SARS-CoV-2 replication utilizing reverse genetics techniques and high-throughput proteomics analysis.

In chapter five, ORF10 protein expression was confirmed using western blotting analysis. Then, high-throughput quantitative proteomics analysis of ORF10 co-IP samples was conducted to identify cellular interacting partners. The analysis showed that the ORF10 binds to several antiviral proteins, including MX1, OAS-2, and IFIT1. I validated the interaction of ORF10 protein with these cellular anti-viral proteins by IP-Western analysis. Based on these results, I hypothesized that ORF10 protein might play a role in enhancing viral replication by suppressing the expression host's anti-viral proteins. To test this hypothesis, I used a reverse genetics platform to rescue the SARS-CoV-2 virus with either the ORF10 protein knocked out or replaced with fluorescent markers. ORF10 protein knocked out was mediated by mutating the start codon and another methionine residue in the middle of the ORF10 gene. SARS-CoV-2 ORF10 KO was successfully rescued, while fluorescent protein substitution viruses could not be rescued despite several attempts. The growth kinetics of SARS-CoV-2 ORF10 KO was characterized in Vero cells to examine whether the introduced mutations affected the virus' RNA structure. The results showed no difference in the replication dynamics between SARS-CoV-2 ORF10 and SARS-CoV-2 W.T in VTN cells.

To investigate the role of ORF10 in suppressing the expression of host's anti-viral proteins, a high-throughput quantitative proteomics analysis of SARS-CoV-2 ORF10 and SARS-CoV-2

W.T infected A549-ACE-2 cells was conducted. In general, the analysis showed no significant changes in the host's proteins abundance between SARS-CoV-2 W.T and SARS-CoV-2 ORF10 KO infected cells. Unexpectedly, the data showed no significant difference in the expression of innate immune proteins between SARS-CoV-2 W.T and SARS-CoV-2 ORF10 KO infected cells, indicating ORF10 doesn't suppress the expression of the anti-viral proteins. To further test the role of ORF10 in suppressing the host's innate immune response, the growth kinetics of SARS-CoV-2 W.T and SARS-CoV-2 ORF10 KO in immune-competent cells A549-ACE-2 was conducted. The results showed no relevant difference in replication kinetics between SARS-CoV-2 ORF10 KO and SARS-CoV-2 W.T, indicating ORF10 doesn't inhibit anti-viral immune response.

Although our data showed that ORF10 protein is not required in the suppression host's innate immune response, we can't exclude any other roles that ORF10 might play in virus replication. ORF10 is a part of a structure within the 3 UTR region of the virus's genome, which contains critical secondary and tertiary structures and other sequence elements in modulating various aspects of the virus life cycle, such as RNA synthesis and replication(281). This could explain why we couldn't rescue SARS-CoV-2ΔORF10mNeonGreen and SARS-CoV-2ΔORF10mScarlet mutants despite several attempts. In conclusion, we have tentative evidence that while ORF10 protein may of utility, it's not essential in virus replication, but there maybe essential RNA structures needed for viral replication within its coding region since we couldn't rescue ORF10-fluorescent protein substitution mutants.

Appendix A

- **10 X SDS Running buffer (1L)**

Tris-Base 30.3g.

Glycine 144.1g.

SDS 10g.

dH2O up to 1L.

- **Transfer Buffer (1L)**

Tris base: 3.03g

Glycine: 14.4g

200ml methanol

dH2O up to 1L H2O

- **6X Sample buffer**

7ml (0.5M) Tris-HCl Ph 6.8.

3ml Glycerol.

1.2g SDS.

- **2X sample buffer**

  2 ml of 6X sample buffer diluted in 4 ml of dH2O

- **1.5 M Tris-HCl pH 8.8**

  36.30 g of Tris base dissolved in 100ml of dH2O

  pH adjusted with HCl and made up to 200 ml with dH2O

- **0.5 M Tris-HCl pH 6.8**

  6 g of Tris base dissolved in 60 ml of dH2O

  pH adjusted with HCl and made up to 100 ml with dH2O

- **Resolving Gel recipes**

	15%	
	1x	2x
H2O	1.7 ml	3.4 ml
40% Acrylamide Mix	1.9 ml	3.8 ml
1.5M Tris pH 8.8	1.3 ml	2.6 ml
10% SDS	50 μl	100 μl
10% APS*	50 μl	100 μl
TEMED*	3 μl	6 μl
Total volume:	5 ml	10 l

- **Stacking Gel recipe**

	5%	
	1x	2x
H2O	2.4 ml	4.8 ml
40% Acrylamide Mix	0.5 ml	1 ml
0.5M Tris pH 6.8	1. ml	2 ml
10% SDS	40 μl	80 μl
10% APS*	40 μl	80 μl
TEMED*	4 μl	8 μl
Total volume:	4 ml	8 ml

- **Blocking solution**

2.5 g of skim milk in 50 ml TPBS

- **Western blotting washing buffer (PBST)**

500 μl of TWEEN diluted in 500ml PBS.

- **Cell lysis – RIPA Buffer recipe**

Stock Solution	RIPA Buffer Recipe	Volumes for 1 Ml RIPA (μl)
1.5 M TRIS-HCL PH 7.6	25mM TRIS-HCL pH 7.6	16.7
5 M NaCl	150 mM NaCl	30
-	1% (v/v) NP-40	10
10% SDS solution	0.1% (v/v) SDS	10
10% SDOC solution	0.1% (v/v) sodium deoxycholate (SDOC)	100
-	Make up with final volume with dH2O	823.3
100X Halt protease inhibitor cocktail	1X protease inhibitor	10

- **Immunoprecipitation Stock Buffers**

  10X Stock T.B.S. for preparation of other buffers

  25 ml of 1M Tris/Cl.

  15 ml of 5M NaCL.

  10 ml molecular biology grade water.

- **10% Triton X-100**

  1 ml Dilute Triton X-100.

  9 ml molecular grade water.

- **Immunoprecipitation Protease inhibitor**

  One Tablet cOmplete, Mini, EDTA-free Protease Inhibitor Cocktail

  1.5 ml sterile water.

- **Equilibration buffer**

  1 ml 10X Stock T.B.S. buffer.
  9 ml H2O.

- **Wash buffer**

  1ml 10X Stock T.B.S. buffer.
  9ml H2O.

- **Immunoprecipitation Lysis Buffer 5 mls**

  0.5 ml 10X Stock TBS buffer

  10 ul of 500 mM EDTA

  0.5 ml 10% Triton X-100

  3.75 ml H2O.

  0.7 ml of 7X Protease Inhibitor

- **RNA running buffer X10**

  41.85g MOPS

  4.10g NaAC

  1.461g EDTA

  H2o up to 500ml

- **LB-agar plate**

  10 g tryptone, 10 g NaCl, 5 g yeast extract dissolved in 1 L with

dH2O

PH adjusted to 7 with concentrated NaOH

Autoclave for 20 min at 121°C

Cool to ~55°C, add ampicillin or kanamycin if needed, and pour into 10 cm plates

Let harden at Room temperature, invert and store at 4°C

- **Protease inhibitor**

  (cOmplete, Mini, EDTA-free Protease Inhibitor Cocktail – Roche)
  1 tablet added directly to 10 ml of RIPA buffer

- **10X MOPS pH 7**

  20.95 g 3-(N-morpholino) propanesulfonic acid (MOPS), 4.1 g NaOAc, 1.86 g EDTA
  Dissolved in 400 ml DEPC (Diethylpyrocarbonate)-treated dH2O
  pH Adjusted with NaOH and make up to 500 ml with dH2O
  Autoclave for 20 min at 121°C
  Store in dark

- **Yeast-agar plate**

  6.8g of Yeast Nitrogen Base w/o AA dissolved in 800ml of dH2O
  20g of agar added and pH adjusted to 5.8 using NaOH/HCl,
  autoclave for 20 min at 121°C
  cool down to ~75°C and add 100ml X10 20% w/v Glucose and mix
  add 100ml X10 Yeast drop out supplement and pour into 10 cm plates
  Let harden at Room temperature, invert and store at 4°C

- **X10 Yeast Drop Out Supplement without Tryptophan**

  3.84g YSDO dissolved in 200ml of dH2O

Sterilize using a 0.22um syringe filter.

- **X10 20% D-Glucose**

    40g D-Glucose dissolved in 200ml of dH2O
    Sterilize using a 0.22um syringe filter.
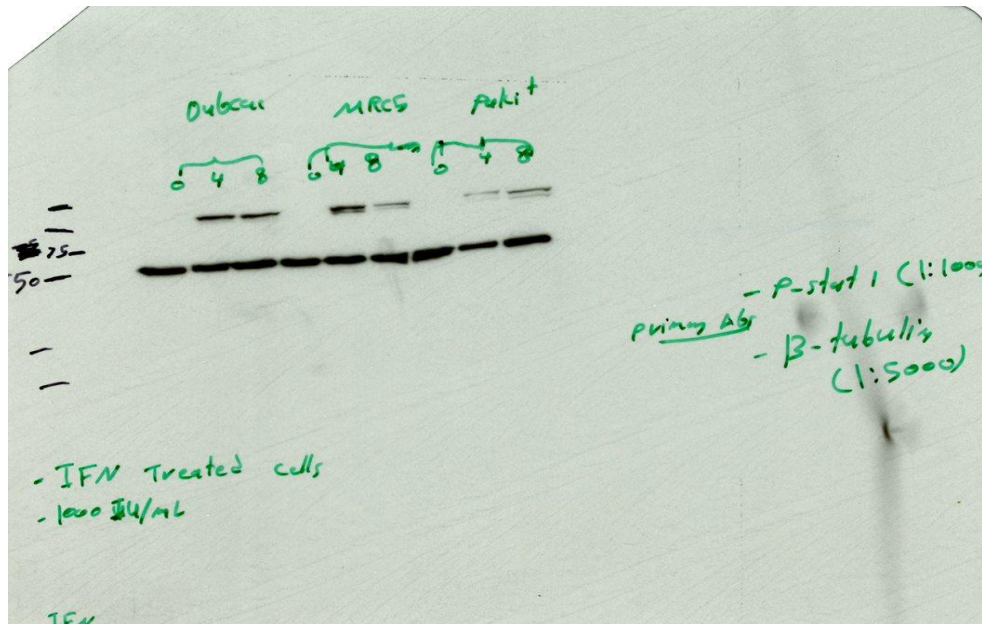
- **Figure 84. Innate immune response induction via JAK/STAT signaling pathway**. Dubca, MRC-5, and PaKiT cells were treated with IFN (1000 IU/mL) for 4 hrs or 8hrs. The induction of innate immune response was confirmed by western blotting analysis using anti phospho-STAT1 antibody. The molecular weight of P-STAT1 protein is 85 KDa.
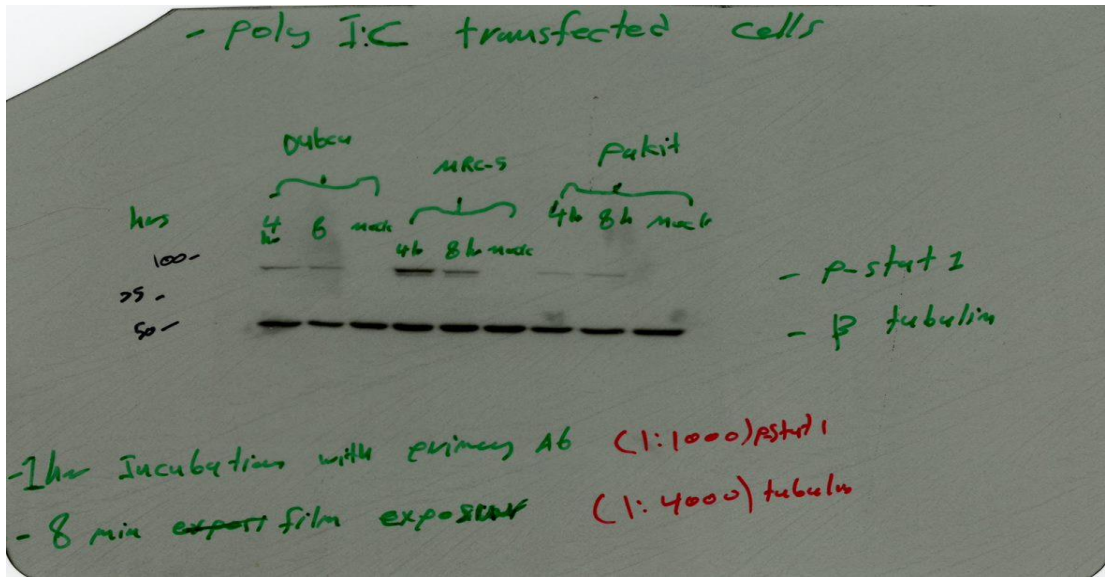
- **Figure 85. Stimulation of the innate immune response via cytoplasmic dsRNA sensors.** Dubca, MRC-5, and PaKiT cells were transfected with 750ng/ml of Poly: IC (a synthetic analog of double-stranded RNA that stimulates the innate immune response signaling pathway via different cytoplasmic dsRNA sensors) for 4hrs or 8 hrs. The induction of innate immune response was confirmed by western blotting analysis using anti phospho- STAT1 antibody. The molecular weight of P-STAT1 protein is 85 KDa.
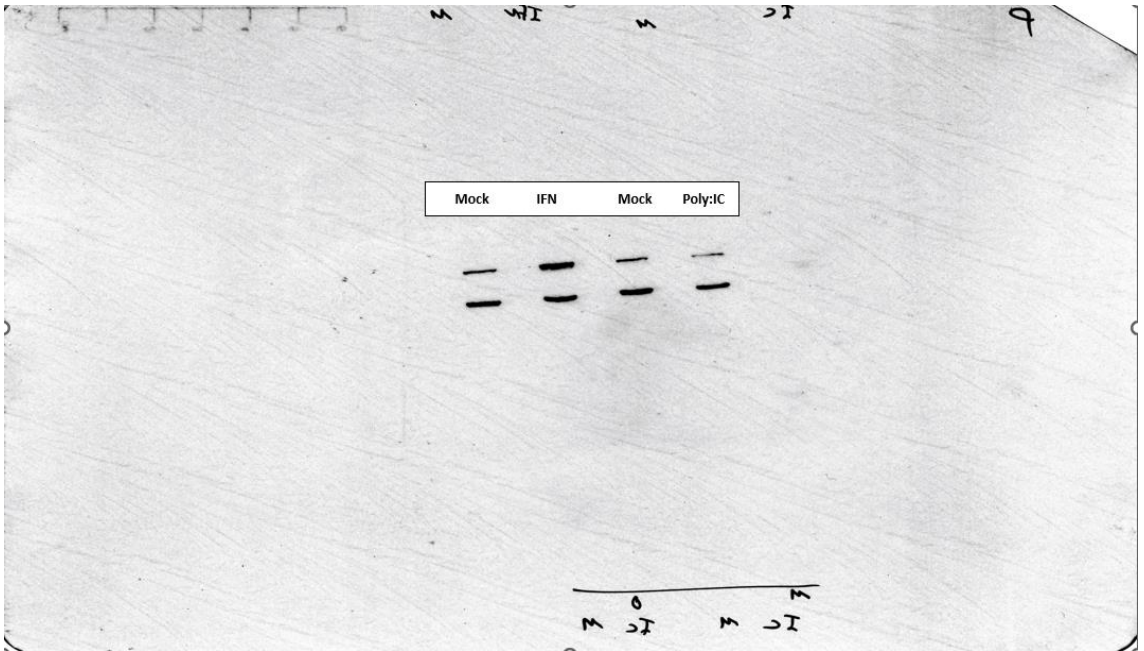
- **Figure 86. Examining the level of STAT1 expression upon stimulating the innate immune response of PaKit cells.** PaKit cells were treated with IFN or transfected with Poly:IC for 4 hrs. Cells were harvested and the STAT1 expression was examined by western blotting analysis using anti-STAT1 antibody. The molecular weight of STAT1 protein is 85 KDa.

Dubca cells   MRC-5 cells

Poly: IC Mock   Poly:IC Mock
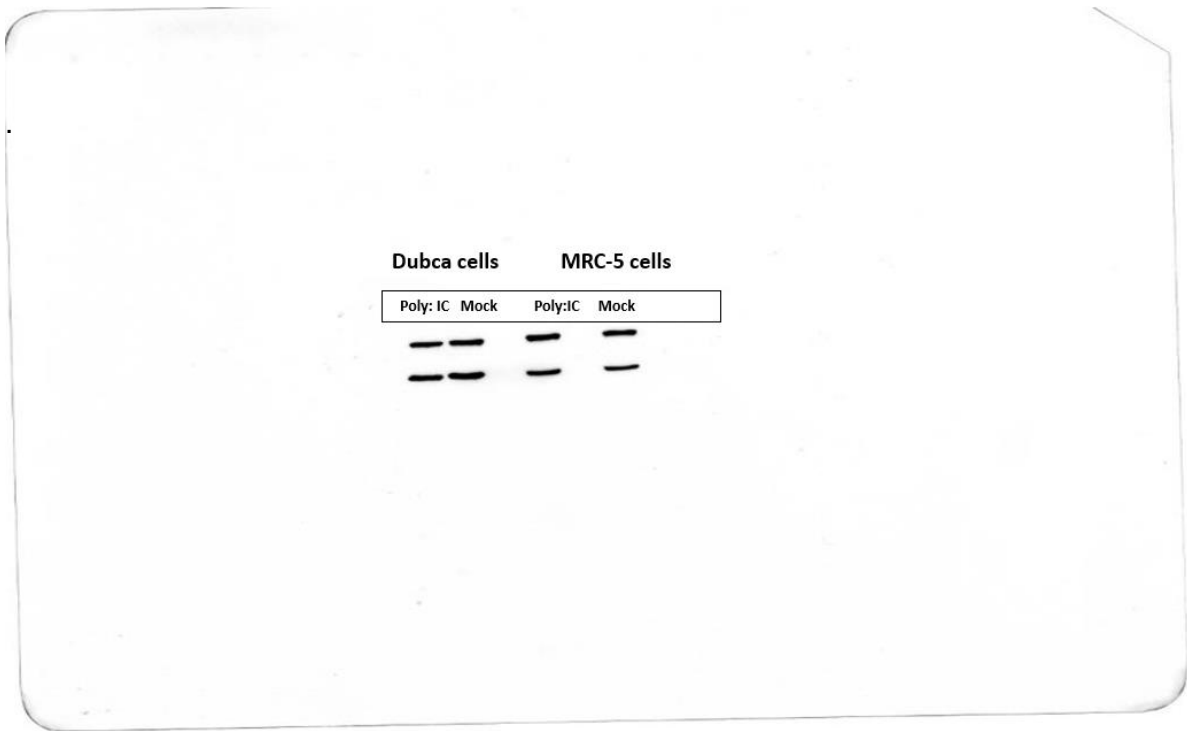
- **Figure 87. Examining the level of STAT1 expression upon stimulating the innate immune response of Dubca and MRC-5 cells.** Dubca and MRC-5 cells were transfected with Poly:IC for 4 hrs. Cells were harvested and the STAT1 expression was examined by western blotting analysis using anti-STAT1 antibody. The molecular weight of STAT1 protein is 85 KDa.

Dubca cells

IFN   Mock   IFN   Mock
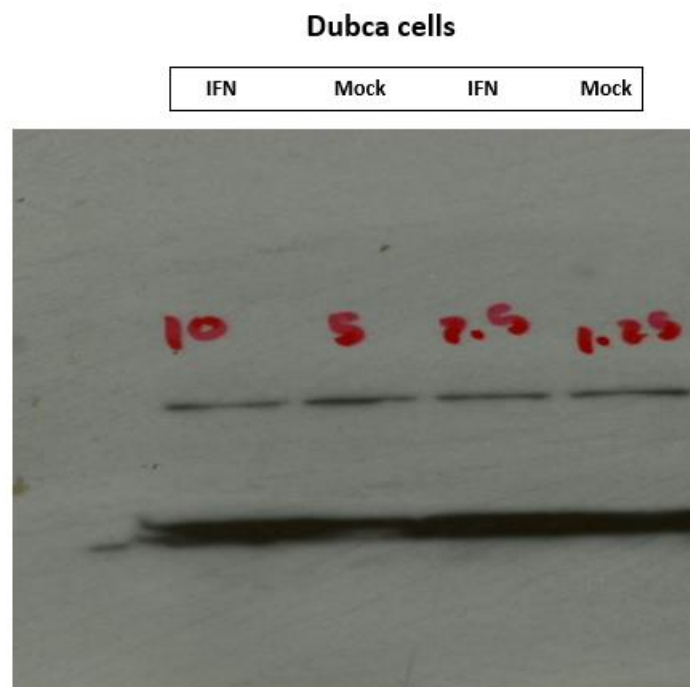
- **Figure 88. Examining the level of STAT1 expression upon stimulating the innate immune response of Dubca cells.** Dubca cells were treated with IFN for 4 hrs. Cells were harvested and the STAT1 expression was examined by western blotting analysis using anti-STAT1 antibody. The molecular weight of STAT1 protein is 85 KDa.

223

- **Figure 89. Examining the level of STAT1 expression upon stimulating the innate immune response of MRC-5 cells.** MRC-5 cells were treated with IFN for 4 hrs. Cells were harvested and the STAT1 expression was examined by western blotting analysis using anti-STAT1 antibody. The molecular weight of STAT1 protein is 85 KDa.

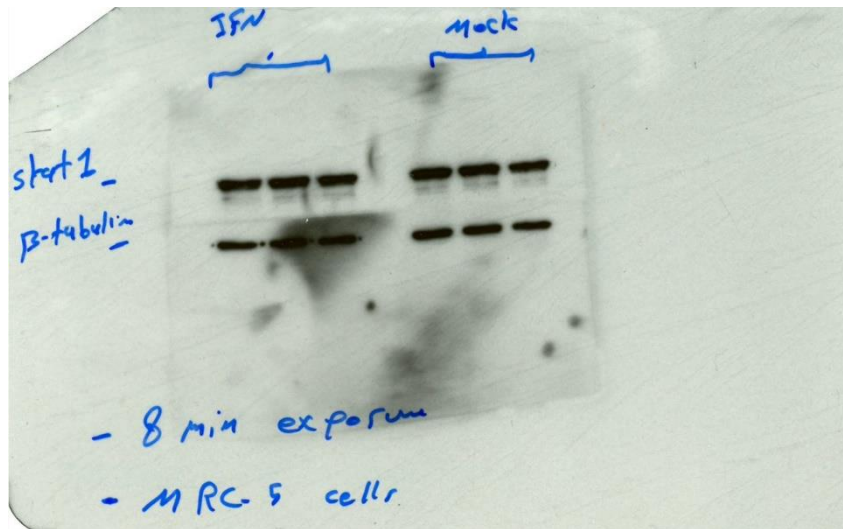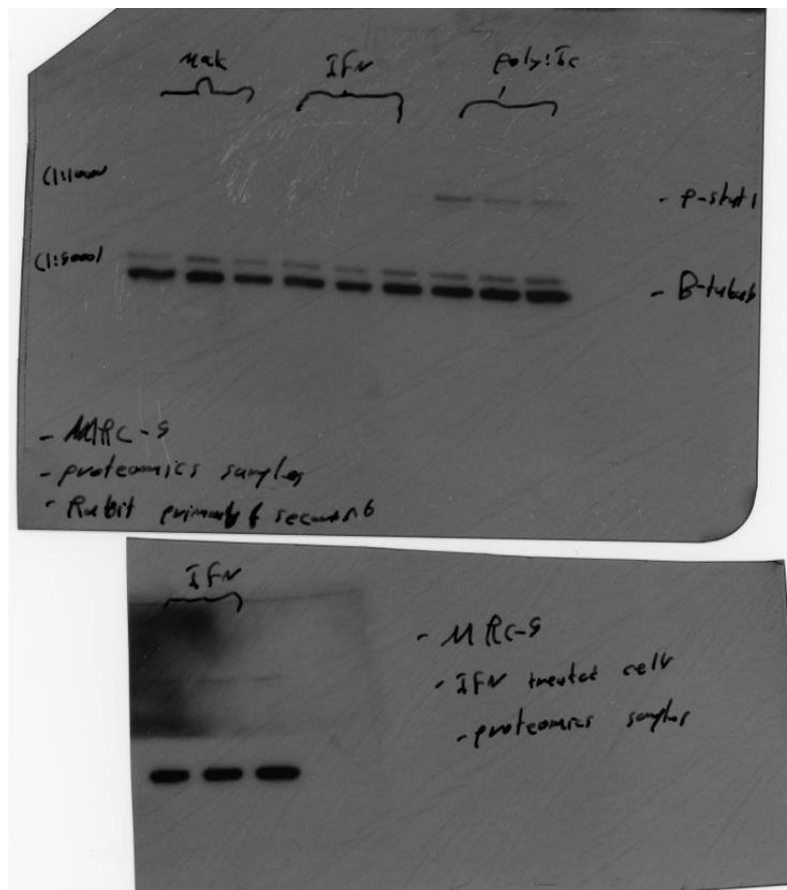- **Figure 90. Confirming the induction of innate immune response in cells before sending samples for TMT-MS/MS analysis.** MRC-5 cells were grown in T-25 flasks and were either treated with 1000IU/mL of IFN or transfected with 750ng/mL of Poly: IC for 4 hrs. Cells were harvested and lysed using RIPA buffer. The induction of innate immune response was confirmed using anti-phospho STAT1 antibody before conducting TMT-MS/MS Analysis. The molecular weight of P-STAT1 protein is 85 KDa.

224
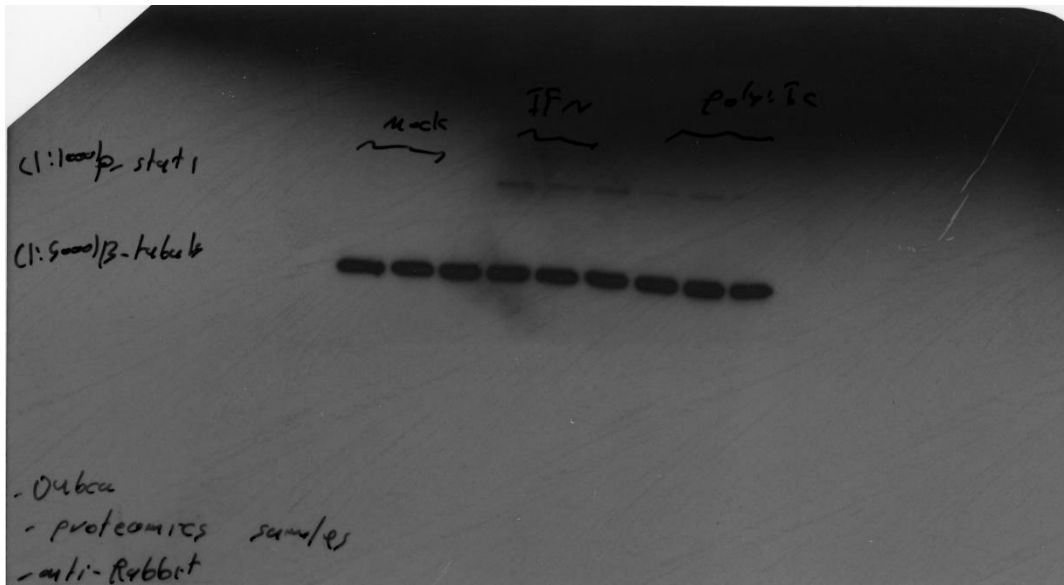
- **Figure 91. Confirming the induction of innate immune response in cells before sending samples for TMT-MS/MS analysis.** Dubca cells were grown in T-25 flasks and were either treated with 1000IU/mL of IFN or transfected with 750ng/mL of Poly: IC for 4 hrs. Cells were harvested and lysed using RIPA buffer. The induction of innate immune response was confirmed using anti-phospho STAT1 antibody before conducting TMT-MS/MS Analysis. The molecular weight of P-STAT1 protein is 85 KDa
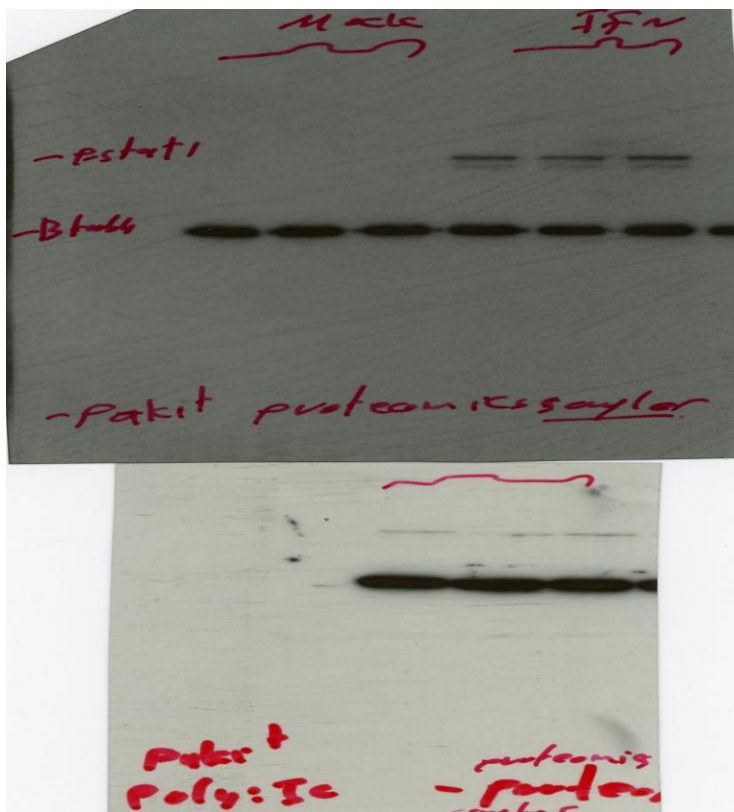
- **Figure 92. Confirming the induction of innate immune response in cells before sending samples for TMT-MS/MS analysis.** PaKit cells were grown in T-25 flasks and were either treated with 1000IU/mL of IFN or transfected with 750ng/mL of Poly: IC for 4 hrs. Cells were harvested and lysed using RIPA buffer. The induction of innate immune response was confirmed using anti-phospho STAT1 antibody before conducting TMT-MS/MS Analysis. The molecular weight of P-STAT1 protein is 85 KDa
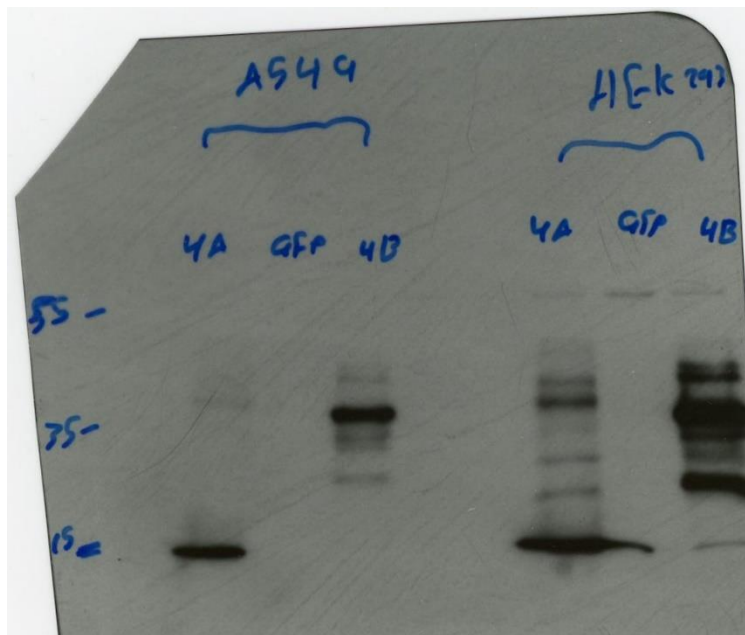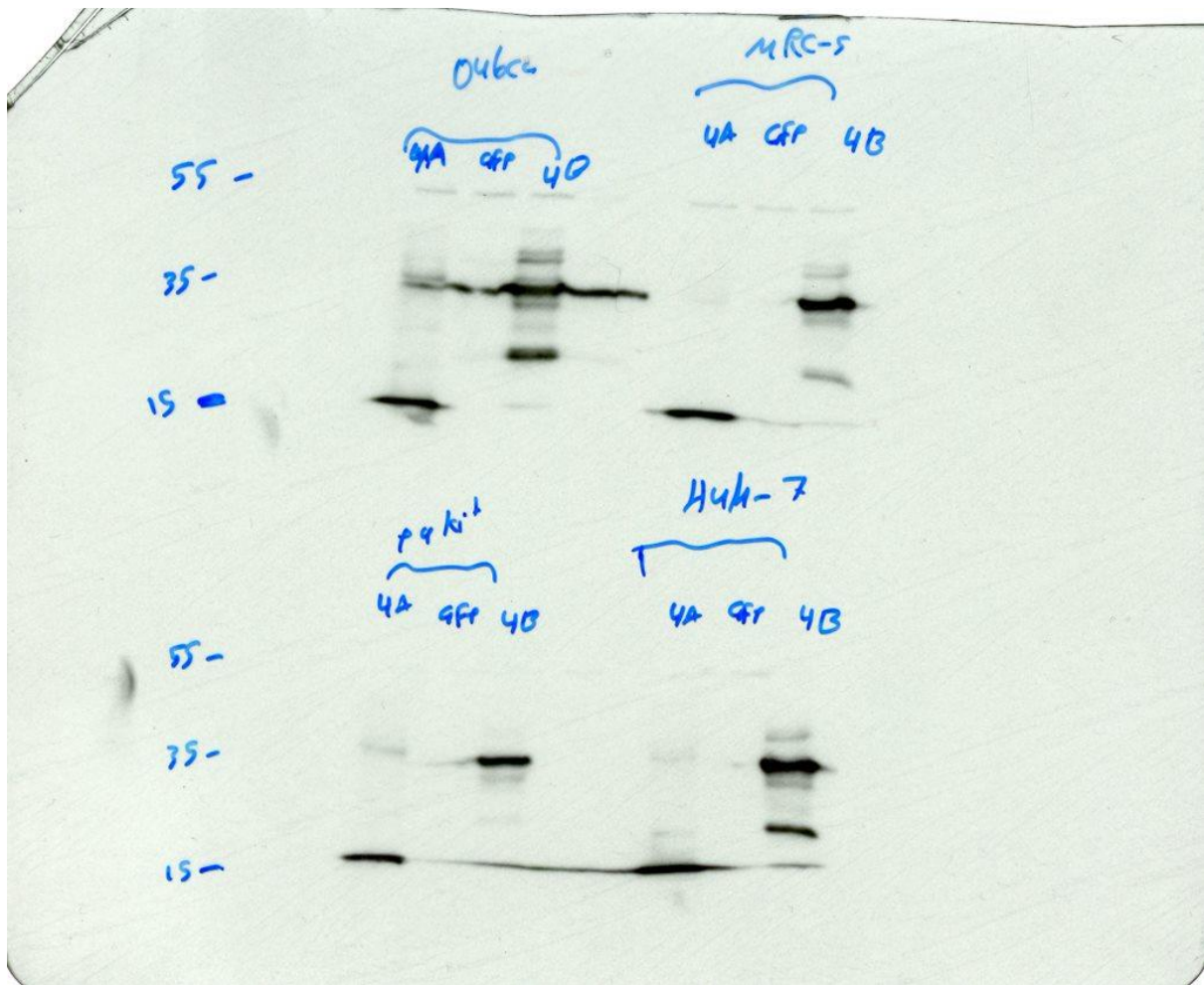
- **Figure 93. Analysis by western blot of ORF4A & ORF4B protein expression**. MRC-5, Dubca, PaKiT, Huh-7, A549 and HEK 293 cells were seeded in the six-wells plate before they were transfected with two µg of ORF4A or ORF4B flag-tagged plasmid DNA using PEI reagent. Transfected cells were incubated for 18 hrs before they were harvested and lysed with 2X sample buffer. Each sample was separated using a 10% SDS-PAGE gel and transferred to a PVDF membrane for immunoblotting with an anti-flag antibody.

Dubca cells   PaKit cells

A2/B1   A3/B2   peki

A549 cells

A549 and QIP1 good result

50 –

25 –

15 KDa ⟶
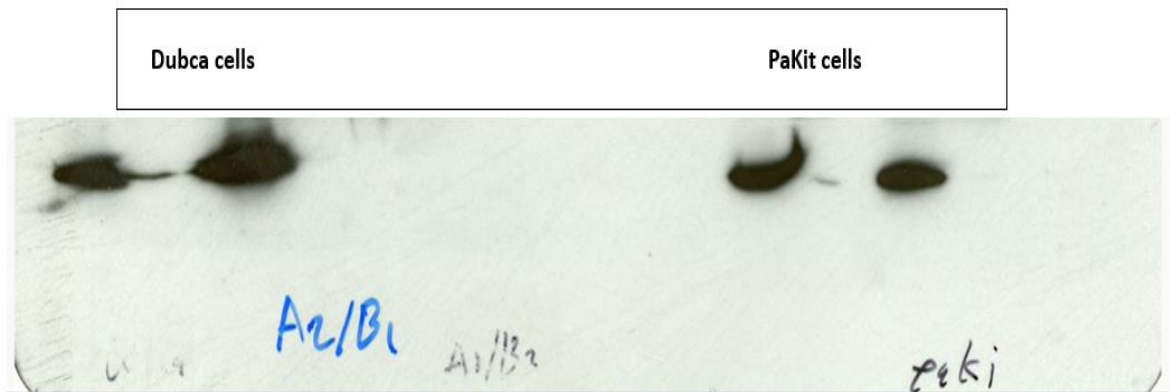
A549 and QIP1 better Results

- **Confirmation of successful transfection of ORF4A plasmid DNA in co-IP samples by western blotting analysis.** A549, Dubca, and PaKiT cells were transfected with ORF4A-flag tagged plasmid DNA. The input, non-bound, and pulldown samples were prepared and loaded into 10% SDS-PAGE gel. Proteins were separated and transferred to a PVDF membrane for immunoblotting with the anti-flag antibody. The molecular weight of ORF4A protein is 15 KDa.

- **Figure 94.Confirmation of successful transfection of ORF4B plasmid DNA in co-IP samples by western blotting analysis**. A549, Dubca, and PaKiT cells were transfected with ORF4B-flag tagged plasmid DNA. The input, non-bound, and pulldown samples were prepared and loaded into 10% SDS-PAGE gel. Proteins were separated and transferred to a PVDF membrane for immunoblotting with the anti-flag antibody. The molecular weight of ORF4B protein is 37 KDa.
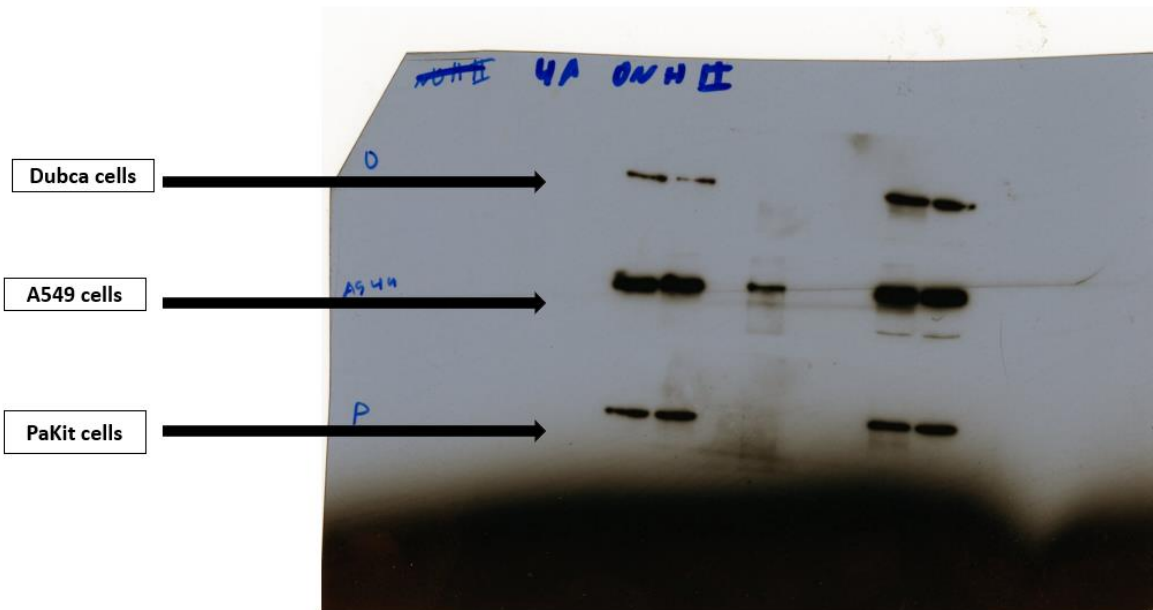
- **Figure 95. Western blot. Validating the interaction of ORF4A with the cellular protein NDHII by IP-Western analysis.** A549, Dubca, and PaKiT cells were transfected with ORF4A plasmid DNA. Three samples: Input, non-bound, and pulldown samples were prepared and loaded into 10% SDS-PAGE gel. Proteins were separated and transferred to a PVDF membrane for immunoblotting with anti-NDH II antibody. The molecular weight of NDHII is 130 KDa

- **Figure 36. Validating the interaction of ORF4A with the cellular protein NF45 by IP-Western analysis.** A549, Dubca, and PaKiT cells were transfected with ORF4A plasmid DNA. Three samples: Input, non-bound, and pulldown samples were prepared by and loaded into 10% SDS-PAGE gel. Proteins were separated and transferred to a PVDF membrane for immunoblotting with anti NF45 antibody. The molecular weight of NF45 is 45 KDa.

229

- **Figure 96. Validating the interaction of ORF4A with the cellular protein hnRNPA2/B1 by IP-Western analysis.** A549, Dubca, and PaKiT cells were transfected with ORF4A plasmid DNA. Three samples: Input, non-bound, and pulldown samples were prepared and loaded into 10% SDS-PAGE gel. Proteins were separated and transferred to a PVDF membrane for immunoblotting with anti hnRNPA2/B1 antibody. The molecular weight of hnRNPA2/B1 is 37 KDa

- **Figure 97. Validating the interaction of ORF4A with the cellular protein hnRNPAB by IP-Western analysis.** A549, Dubca, and PaKiT cells were transfected with ORF4A plasmid DNA. Three samples: Input, non-bound, and pulldown samples were prepared and loaded into 10% SDS-PAGE gel. Proteins were separated and transferred to a PVDF membrane for immunoblotting with anti hnRNPAB antibody. The molecular weight of hnRNPAB is 38 KDa

PaKit cells

A549 cells

Dubca cells

- **Figure 98.Validating the interaction of ORF4A with the cellular protein hnRNPC1/C2 by IP-Western analysis.** A549, Dubca, and PaKiT were transfected with ORF4A plasmid DNA. Three samples: Input, non-bound, and pulldown samples were prepared and loaded into 10% SDS-PAGE gel. Proteins were separated and transferred to a PVDF membrane for immunoblotting with anti hnRNPC1/C2 antibody. The molecular weight of hnRNPC1/C2 is 40 KDa
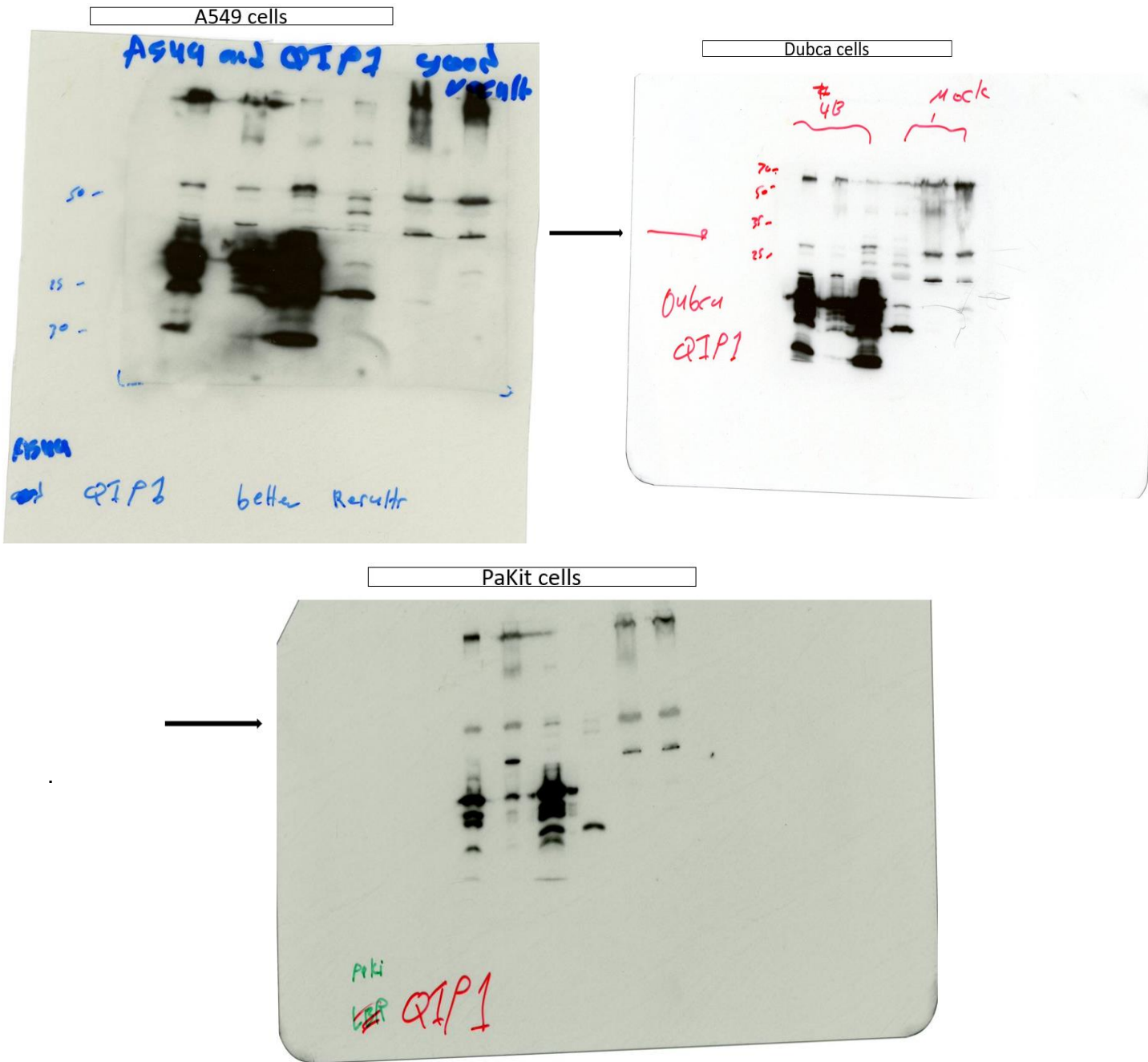
- **Figure 99. Validating the interaction of ORF4B with the cellular protein KPNA4 (QIP1) by IP-Western analysis.** A549, Dubca, and PaKiT cells were transfected with ORF4B plasmid DNA. Three samples: Input, non-bound, and pulldown samples were prepared by Co-IP and loaded into 10% SDS-PAGE gel. Proteins were separated and transferred to a PVDF membrane for immunoblotting with anti KPNA4 (QIP1) antibody. The molecular weight of QIP1 is 55 KDa
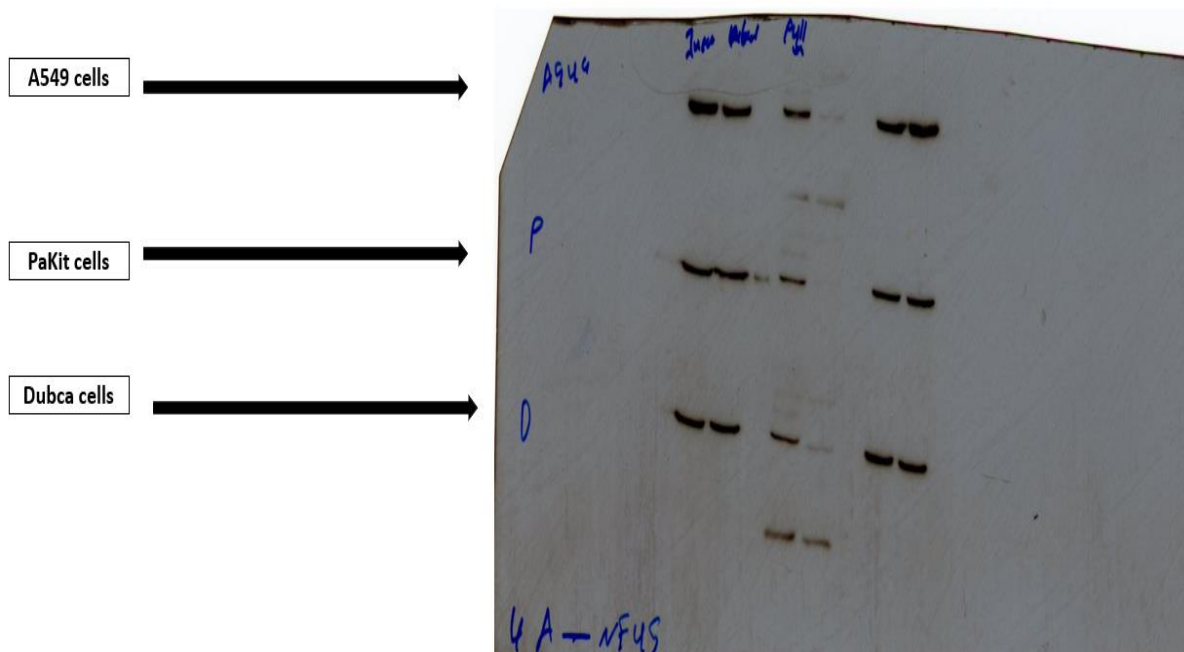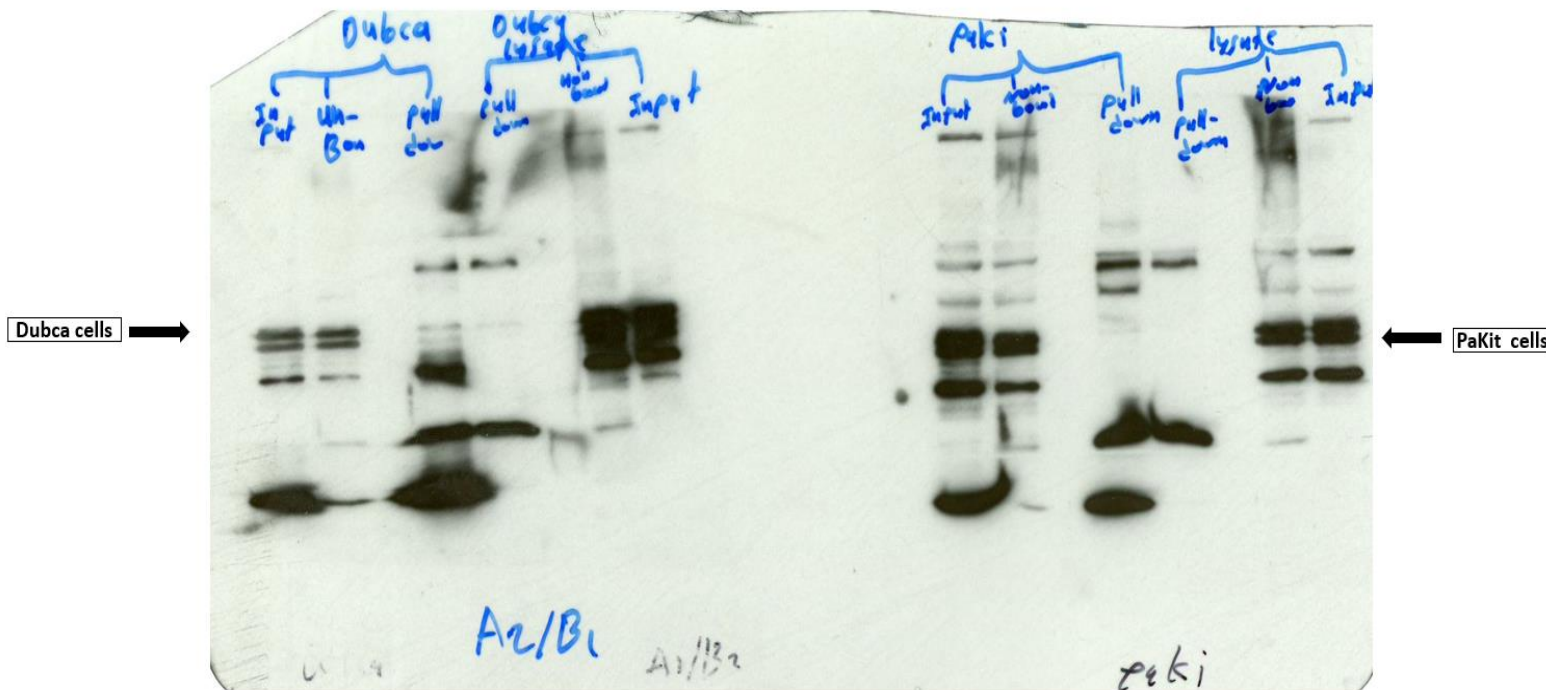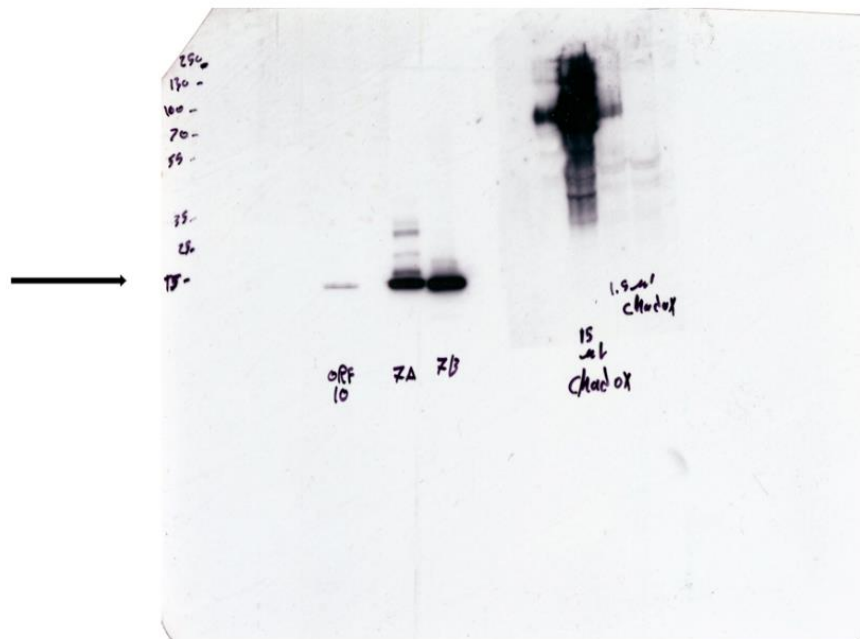
- **Figure 100. Examining ORF10 protein expression by Western Blotting analysis**. A549 cells were seeded in the six-wells plate before they were transfected with two μg of ORF10 DNA plasmid using a PEI transfection reagent. Transfection mixture incubated for 18 hrs before cells were harvested and lysed with 2X sample buffer. The protein sample was separated using a 10% SDS-PAGE gel and transferred to a PVDF membrane for immunoblotting with an anti-flag antibody.
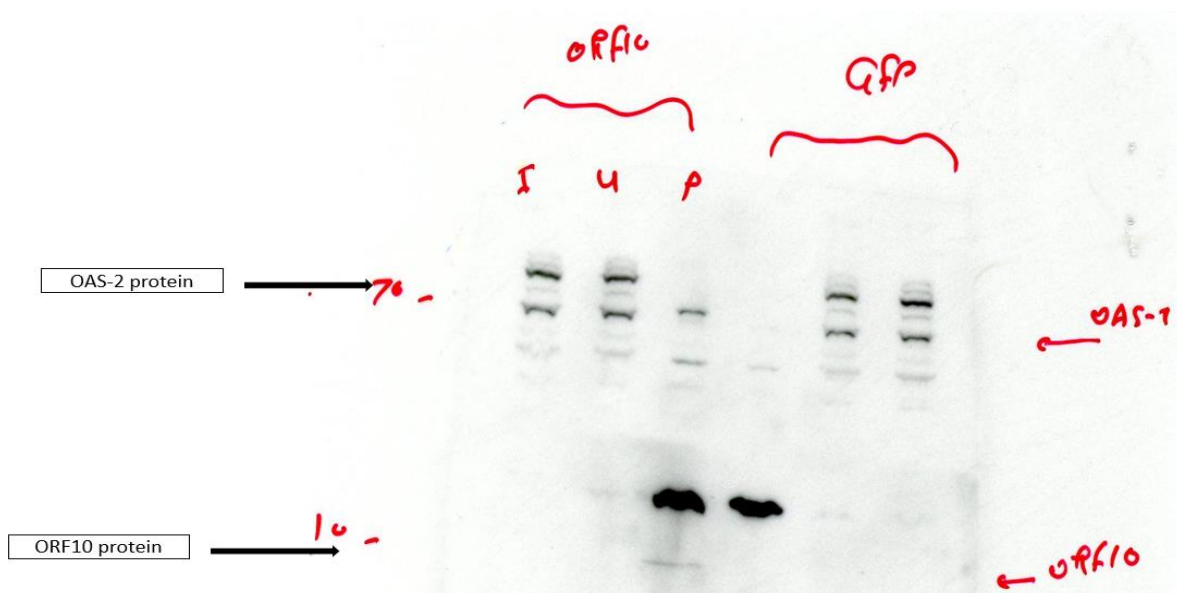
- **Figure 101. Validating the interaction of the ORF10 protein with the cellular protein OAS-2.** A549 cells were transfected with SARS-CoV-2 ORF10 plasmid DNA. Input, non-bound, and pulldown samples were prepared following the co-IP protocol. Samples were loaded into a lane of 10% SDS-PAGE gel. Protein samples were separated and transferred to a PVDF membrane for immunoblotting with anti-OAS-2 antibody. The molecular weight of OAS-2 is 75 KDa.
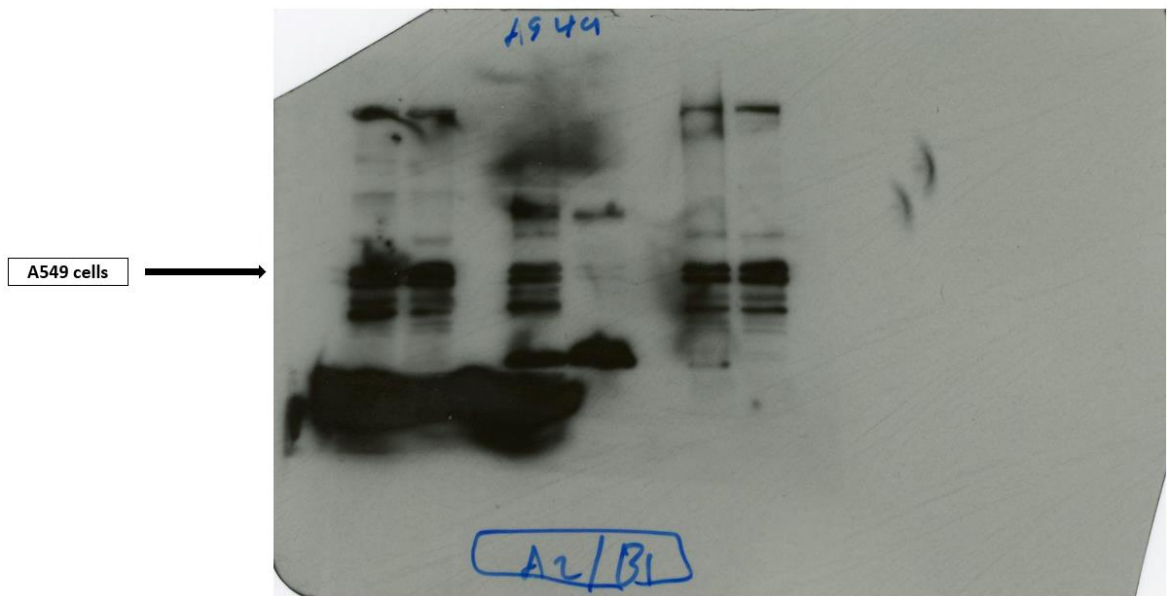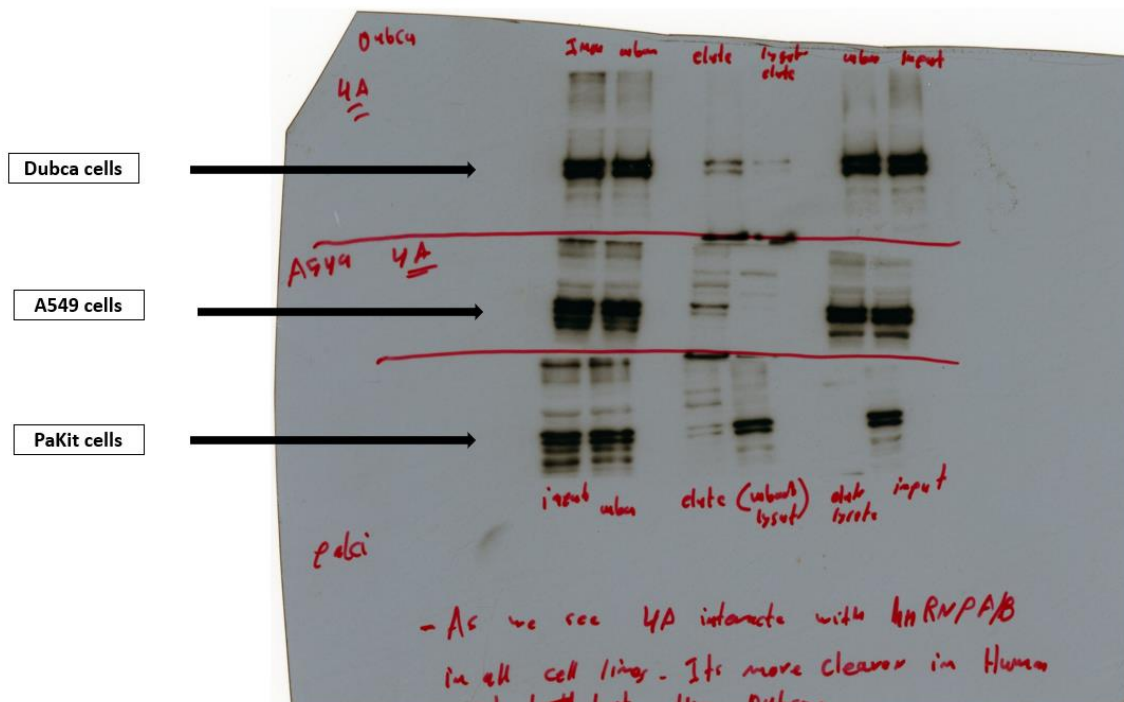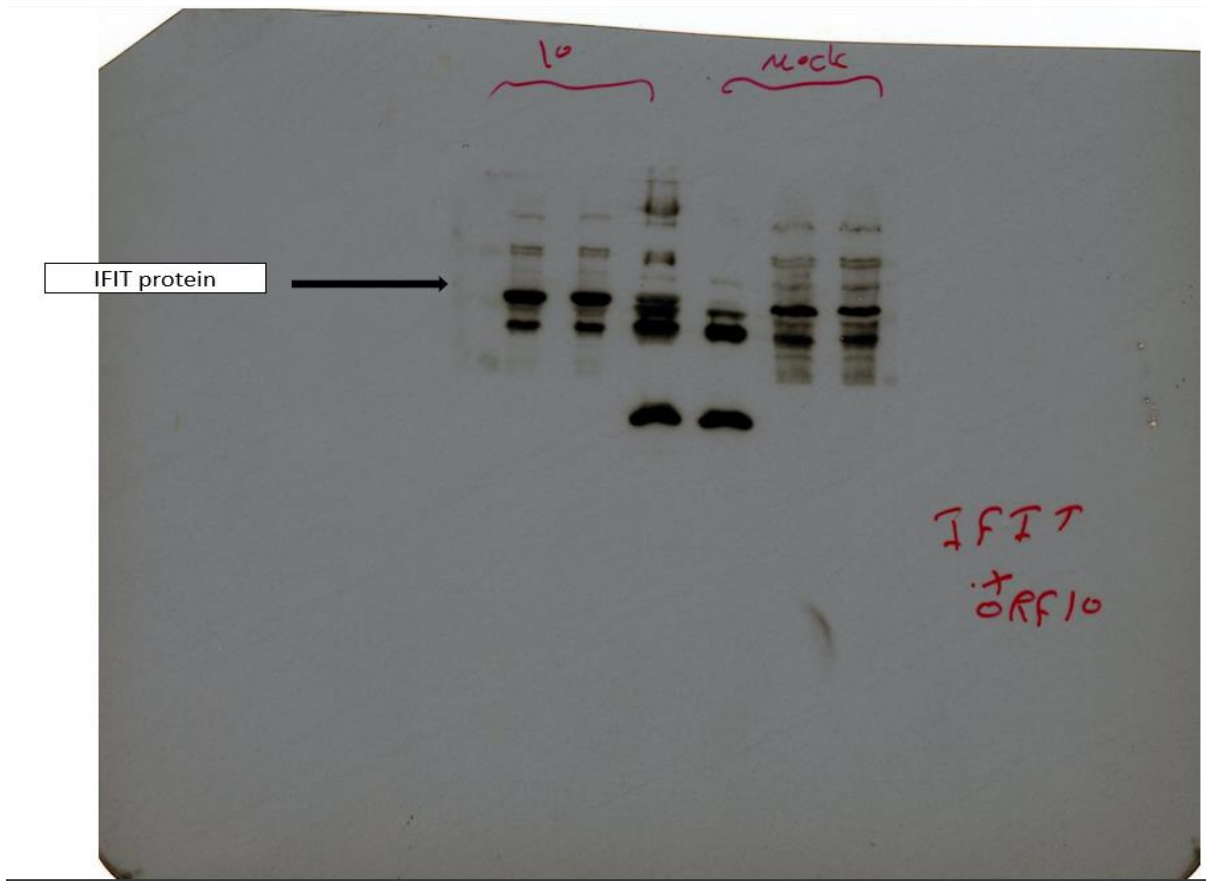
- **Figure 102. Validating the interaction of the ORF10 protein with the cellular protein IFIT1.** A549 cells were transfected with SARS-CoV-2 ORF10 plasmid DNA. Input, non-bound, and pulldown samples were prepared following the co-IP protocol. Samples were loaded into a lane of 10% SDS-PAGE gel. Protein samples were separated and transferred to a PVDF membrane for immunoblotting with anti-IFIT1antibody. The molecular weight of IFIT1 is 50 KDa.
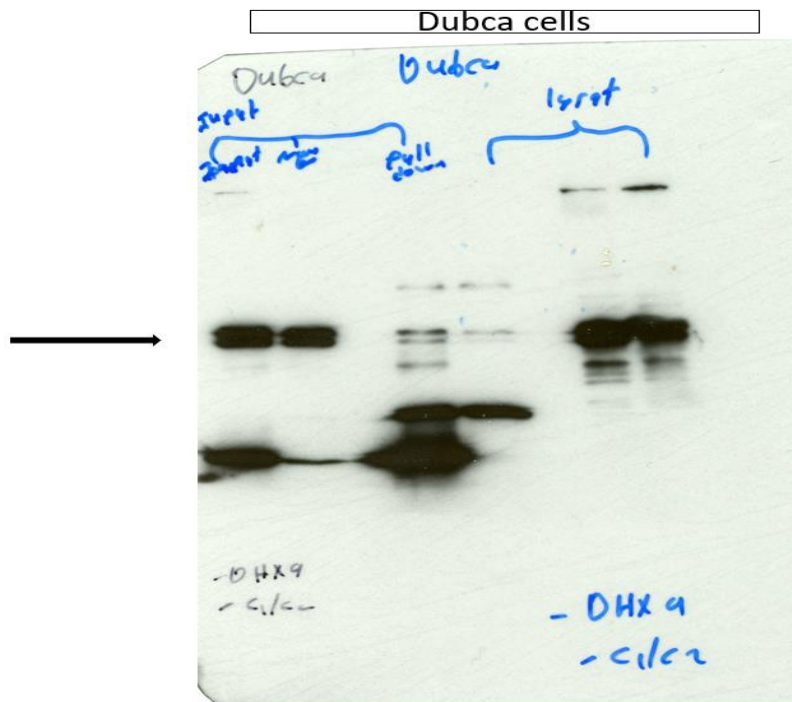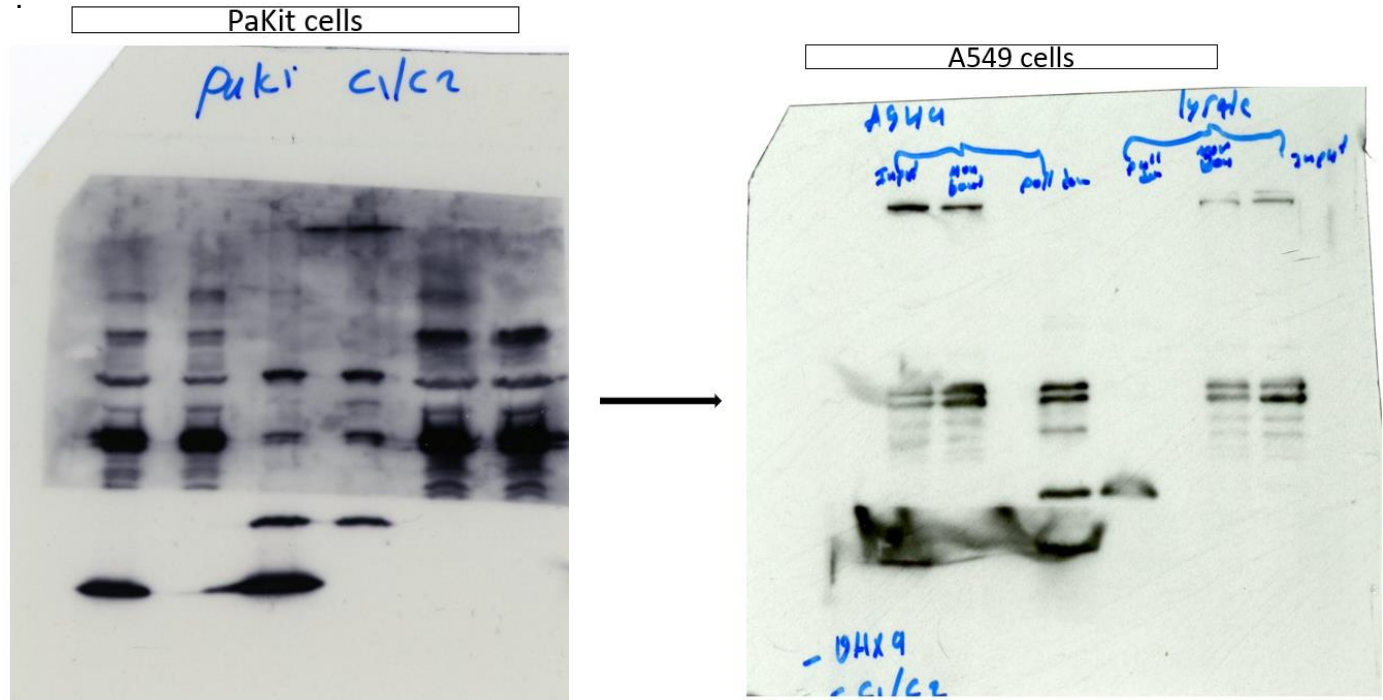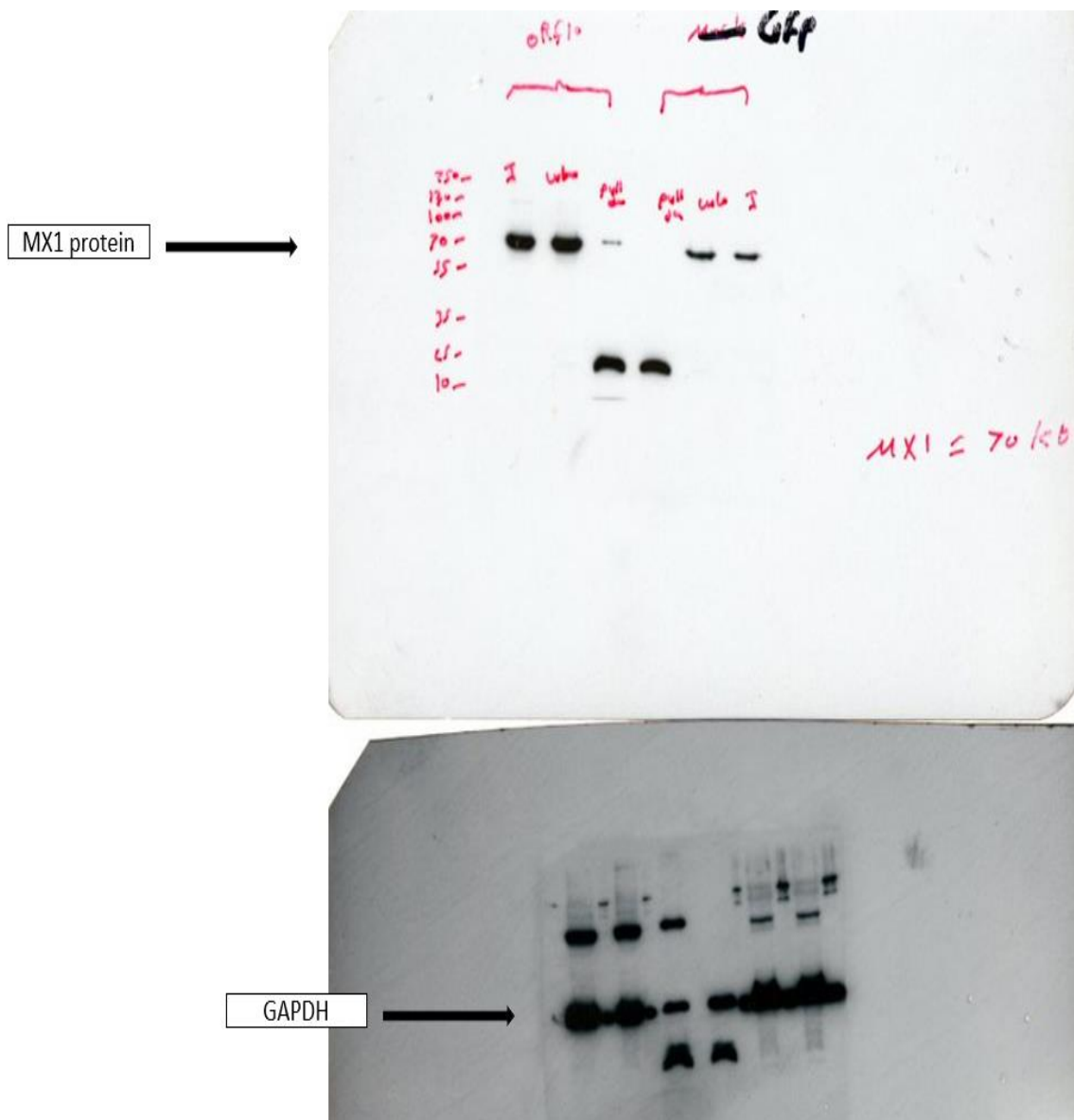
- **Figure 103. Validating the interaction of the ORF10 protein with the cellular protein MX1.** A549 cells were transfected with SARS-CoV-2 ORF10 plasmid DNA. Input, non-bound, and pulldown samples were prepared following the co-IP protocol. Samples were loaded into a lane of 10% SDS-PAGE gel. Protein samples were separated and transferred to a PVDF membrane for immunoblotting with anti-MX1antibody. The molecular weight of MX1 and GAPDH are 80 KD and 37 KD, respectively.
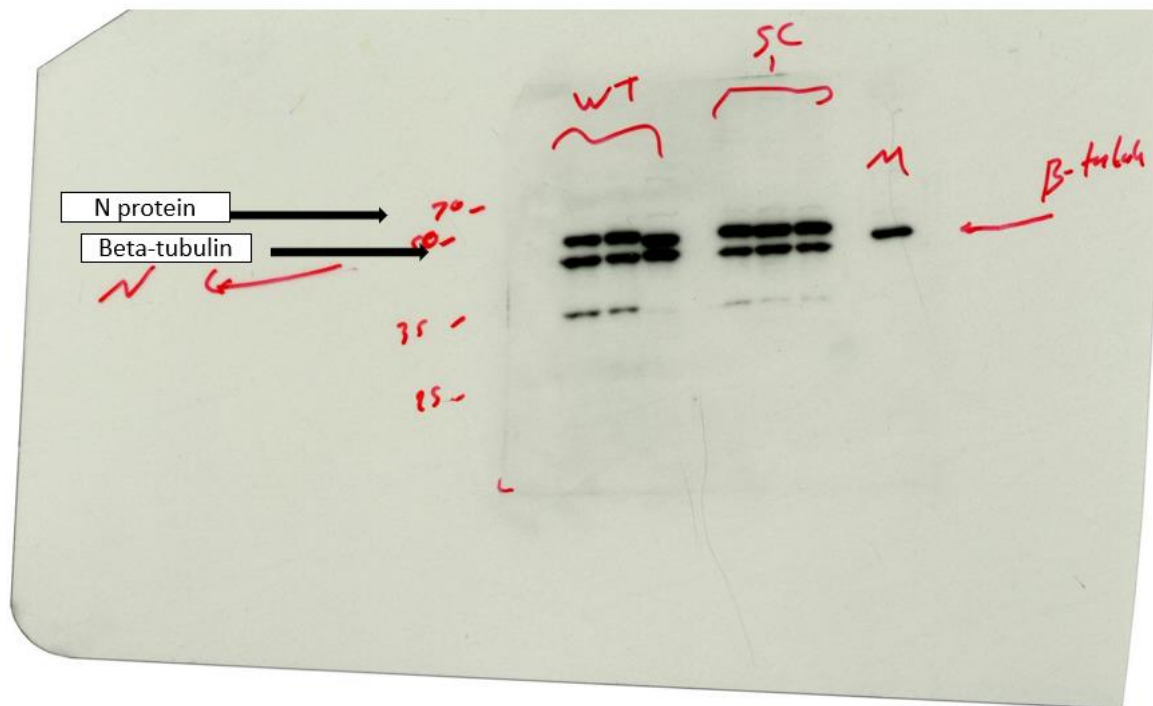
- **Figure 104. Confirmation of successful infection of A549 ACE-2 cells with SARS-CoV-2 W.T or SARS-CoV-2 ORF10 KO mutant before conducting TMT-MS/MS analysis.** A549 ACE-2 cells were infected with either SARS-CoV-2 W.T or SARS-CoV-2 ORF10 KO mutant. Samples were harvested 18 hrs post-infection. The infections were confirmed by western blotting analysis using SARS-CoV-2 anti-N antibody before conducting quantitative proteomics analysis. The molecular weight of N protein is 49 KDa. The Experiments were performed in triplicate.

Appendix B

Publications

- **Abdulaziz Almuqrin**, Andrew D. Davidson, Maia Kavanagh Williamson, Philip A. Lewis, Kate J. Heesom, Susan Morris, Sarah C. Gilbert & David A. Matthews. SARS-CoV-2 vaccine ChAdOx1 nCoV-19 infection of human cell lines reveals low levels of viral backbone gene transcription alongside very high levels of SARS-CoV-2 S glycoprotein gene transcription. Genome Med. (2021). 15;13(1):43.

- Camilla Ugolini, Logan Mulroney, Adrien Leger, Matteo Castelli, Elena Criscuolo, Maia Kavanagh Williamson, Andrew D Davidson, **Abdulaziz Almuqrin**, Roberto Giambruno, Miten Jain, Gianmaria Frigè, Hugh Olsen, George Tzertzinis, Ira Schildkraut, Madalee G Wulf, Ivan R Corrêa, Jr, Laurence Ettwiller, Nicola Clementi, Massimo Clementi, Nicasio Mancini, Ewan Birney, Mark Akeson, Francesco Nicassio, David A Matthews, and Tommaso Leonardi. Nanopore ReCappable sequencing maps SARS-CoV-2 5′ capping sites and provides new insights into the structure of sgRNAs. Nucleic Acids Res. 2022 Apr 8; 50(6): 3475–3489.

- Kapil Gupta, Christine Toelzer , Maia Kavanagh Williamson , Deborah K Shoemark , A Sofia F Oliveira, David A Matthews , **Abdulaziz Almuqrin** , Oskar Staufer, Sathish K N Yadav, Ufuk Borucu, Frederic Garzoni, Daniel Fitzgerald , Joachim Spatz, Adrian J Mulholland, Andrew D Davidson, Christiane Schaffitzel, Imre Berger. Structural insights in cell-type specific evolution of intra-host diversity by SARS-CoV-2. Nat Commun.2022 Jan 11;13(1):222.

References

1. van Boheemen S, de Graaf M, Lauber C, Bestebroer TM, Raj VS, Zaki AM, et al. Genomic characterization of a newly discovered coronavirus associated with acute respiratory distress syndrome in humans. mBio [Internet]. 2012 [cited 2022 Jan 17];3(6). Available from: https://pubmed.ncbi.nlm.nih.gov/23170002/

2. V'kovski P, Kratzel A, Steiner S, Stalder H, Thiel V. Coronavirus biology and replication: implications for SARS-CoV-2. Nature Reviews Microbiology 2020 19:3 [Internet]. 2020 Oct 28 [cited 2022 Feb 4];19(3):155–70. Available from: https://www.nature.com/articles/s41579-020-00468-6

3. Liu DX, Liang JQ, Fung TS. Human Coronavirus-229E, -OC43, -NL63, and -HKU1 (Coronaviridae). Encyclopedia of Virology [Internet]. 2021 [cited 2022 Jan 21];428. Available from: /pmc/articles/PMC7204879/

4. Sharma A, Ahmad Farouk I, Lal SK. COVID-19: A Review on the Novel Coronavirus Disease Evolution, Transmission, Detection, Control and Prevention. Viruses [Internet]. 2021 Feb 1 [cited 2022 Feb 4];13(2). Available from: /pmc/articles/PMC7911532/

5. Memish ZA, Zumla AI, Al-Hakeem RF, Al-Rabeeah AA, Stephens GM. Family Cluster of Middle East Respiratory Syndrome Coronavirus Infections. New England Journal of Medicine [Internet]. 2013 Jun 27 [cited 2022 Jan 18];368(26):2487–94. Available from: https://www.nejm.org/doi/10.1056/NEJMoa1303729

6. Home - ProMED - ProMED-mail [Internet]. [cited 2022 Jan 18]. Available from: https://promedmail.org/

7. Wang N, Shang J, Jiang S, Du L. Subunit Vaccines Against Emerging Pathogenic Human Coronaviruses. Front Microbiol. 2020 Feb 28;11:298.

8. Lam WK, Zhong NS, Tan WC. Overview on SARS in Asia and the world. Respirology [Internet]. 2003 Nov [cited 2022 Jan 17];8 Suppl(Suppl 1). Available from: https://pubmed.ncbi.nlm.nih.gov/15018125/

9. Zaki AM, van Boheemen S, Bestebroer TM, Osterhaus ADME, Fouchier RAM. Isolation of a novel coronavirus from a man with pneumonia in Saudi Arabia. N Engl J Med [Internet]. 2012 Nov 8 [cited 2022 Jan 17];367(19):1814–20. Available from: https://pubmed.ncbi.nlm.nih.gov/23075143/

10. WHO EMRO | MERS outbreaks | MERS-CoV | Health topics [Internet]. [cited 2022 Jan 17]. Available from: http://www.emro.who.int/health-topics/mers-cov/mers-outbreaks.html

11. Oh MD, Park WB, Park SW, Choe PG, Bang JH, Song KH, et al. Middle East respiratory syndrome: what we learned from the 2015 outbreak in the Republic of Korea. Korean J Intern Med [Internet]. 2018 Mar 1 [cited 2022 Jan 17];33(2):233–46. Available from: https://pubmed.ncbi.nlm.nih.gov/29506344/

12. Middle East respiratory syndrome coronavirus (MERS-CoV) [Internet]. [cited 2022 Jan 17]. Available from: https://www.who.int/health-topics/middle-east-respiratory-syndrome-coronavirus-mers#tab=tab_1

13. Chafekar A, Fielding BC. MERS-CoV: Understanding the Latest Human Coronavirus Threat. Viruses [Internet]. 2018 Feb 24 [cited 2022 Jan 17];10(2). Available from: https://pubmed.ncbi.nlm.nih.gov/29495250/

14. Shehata MM, Gomaa MR, Ali MA, Kayali G. Middle East respiratory syndrome coronavirus: a comprehensive review. Front Med [Internet]. 2016 Jun 1 [cited 2022 Jan 17];10(2):120–36. Available from: https://pubmed.ncbi.nlm.nih.gov/26791756/

15. Miguel E, Chevalier V, Ayelet G, ben Bencheikh MN, Boussini H, Chu DK, et al. Risk factors for MERS coronavirus infection in dromedary camels in Burkina Faso, Ethiopia, and Morocco, 2015. Euro Surveill [Internet]. 2017 Mar 30 [cited 2022 Jan 17];22(13). Available from: https://pubmed.ncbi.nlm.nih.gov/28382915/

16. Wernery U, Lau SKP, Woo PCY. Genomics and zoonotic infections: Middle East respiratory syndrome. Rev Sci Tech [Internet]. 2016 Apr 1 [cited 2022 Jan 17];35(1):191–202. Available from: https://pubmed.ncbi.nlm.nih.gov/27217178/

17. Mackay IM, Arden KE. An Opportunistic Pathogen Afforded Ample Opportunities: Middle East Respiratory Syndrome Coronavirus. Viruses [Internet]. 2017 Dec 1 [cited 2022 Jan 17];9(12). Available from: https://pubmed.ncbi.nlm.nih.gov/29207494/

18. Yang Y, Zhang L, Geng H, Deng Y, Huang B, Guo Y, et al. Protein Cell & Protein Cell The structural and accessory proteins M, ORF 4a, ORF 4b, and ORF 5 of Middle East respiratory syndrome coronavirus (MERS-CoV) are potent interferon antagonists. Protein Cell. 2013;4(12):951–61.

19. Bialek SR, Allen D, Alvarado-Ramy F, Arthur R, Balajee A, Bell D, et al. First Confirmed Cases of Middle East Respiratory Syndrome Coronavirus (MERS-CoV) Infection in the United States, Updated Information on the Epidemiology of MERS-CoV Infection, and Guidance for the Public, Clinicians, and Public Health Authorities — May 2014. MMWR Morb Mortal Wkly Rep [Internet]. 2014 [cited 2022 Jan 17];63(19):431. Available from: /pmc/articles/PMC5779407/

20. Zhang N, Tang J, Lu L, Jiang S, Du L. Receptor-binding domain-based subunit vaccines against MERS-CoV. Virus Res [Internet]. 2015 Apr 16 [cited 2022 Jan 17];202:151–9. Available from: https://pubmed.ncbi.nlm.nih.gov/25445336/

21. Liu DX, Fung TS, Chong KKL, Shukla A, Hilgenfeld R. Accessory proteins of SARS-CoV and other coronaviruses. Antiviral Res [Internet]. 2014 [cited 2022 Jan 18];109(1):97. Available from: /pmc/articles/PMC7113789/

22. Du L, He Y, Zhou Y, Liu S, Zheng BJ, Jiang S. The spike protein of SARS-CoV--a target for vaccine and therapeutic development. Nat Rev Microbiol [Internet]. 2009 [cited 2022 Jan 18];7(3):226–36. Available from: https://pubmed.ncbi.nlm.nih.gov/19198616/

23. Chang CY, Liu HM, Chang MF, Chang SC. Middle East Respiratory Syndrome Coronavirus Nucleocapsid Protein Suppresses Type I and Type III Interferon Induction by Targeting RIG-I Signaling. J Virol [Internet]. 2020 Jun 16 [cited 2022 Jan 18];94(13). Available from: /pmc/articles/PMC7307178/

24. Verheije MH, Hagemeijer MC, Ulasli M, Reggiori F, Rottier PJM, Masters PS, et al. The Coronavirus Nucleocapsid Protein Is Dynamically Associated with the Replication-Transcription Complexes. J Virol [Internet]. 2010 Nov [cited 2022 Jan 18];84(21):11575–9. Available from: https://journals.asm.org/doi/abs/10.1128/JVI.00569-10

25.   Schoeman D, Fielding BC. Coronavirus envelope protein: current knowledge. Virology Journal 2019 16:1 [Internet]. 2019 May 27 [cited 2022 Jan 18];16(1):1–22. Available from: https://virologyj.biomedcentral.com/articles/10.1186/s12985-019-1182-0

26.   Surya W, Li Y, Verdià-Bàguena C, Aguilella VM, Torres J. MERS coronavirus envelope protein has a single transmembrane domain that forms pentameric ion channels. Virus Res [Internet]. 2015 Apr 2 [cited 2022 Feb 2];201:61–6. Available from: https://pubmed.ncbi.nlm.nih.gov/25733052/

27.   Nieto-Torres JL, DeDiego ML, Álvarez E, Jiménez-Guardeño JM, Regla-Nava JA, Llorente M, et al. Subcellular location and topology of severe acute respiratory syndrome coronavirus envelope protein. Virology [Internet]. 2011 [cited 2022 Jan 18];415(2):69–82. Available from: https://pubmed.ncbi.nlm.nih.gov/21524776/

28.   Gorbalenya AE, Enjuanes L, Ziebuhr J, Snijder EJ. Nidovirales: Evolving the largest RNA virus genome. Virus Res [Internet]. 2006 [cited 2022 Jan 17];117(1):17. Available from: /pmc/articles/PMC7114179/

29.   García-Sastre A, Biron CA. Type 1 interferons and the virus-host relationship: a lesson in détente. Science [Internet]. 2006 May 12 [cited 2022 Jan 19];312(5775):879–82. Available from: https://pubmed.ncbi.nlm.nih.gov/16690858/

30.   Fehr AR, Perlman S. Coronaviruses: An Overview of Their Replication and Pathogenesis. Coronaviruses [Internet]. 2015 Feb 26 [cited 2022 Jan 17];1282:1. Available from: /pmc/articles/PMC4369385/

31.   Song Z, Xu Y, Bao L, Zhang L, Yu P, Qu Y, et al. From SARS to MERS, Thrusting Coronaviruses into the Spotlight. Viruses [Internet]. 2019 Jan 1 [cited 2022 Jan 17];11(1). Available from: https://pubmed.ncbi.nlm.nih.gov/30646565/

32.   Shokri S, Mahmoudvand S, Taherkhani R, Farshadpour F. Modulation of the immune response by Middle East respiratory syndrome coronavirus. J Cell Physiol [Internet]. 2019 Mar 1 [cited 2022 Jan 17];234(3):2143–51. Available from: https://pubmed.ncbi.nlm.nih.gov/30146782/

33.   Lu L, Liu Q, Du L, Jiang S. Middle East respiratory syndrome coronavirus (MERS-CoV): challenges in identifying its source and controlling its spread. Microbes Infect [Internet]. 2013 [cited 2022 Feb 7];15(8–9):625–9. Available from: https://pubmed.ncbi.nlm.nih.gov/23791956/

34.   Lu L, Liu Q, Du L, Jiang S. Middle East respiratory syndrome coronavirus (MERS-CoV): challenges in identifying its source and controlling its spread. Microbes Infect [Internet]. 2013 [cited 2022 Jan 17];15(8–9):625–9. Available from: https://pubmed.ncbi.nlm.nih.gov/23791956/

35.   Mielech AM, Chen Y, Mesecar AD, Baker SC. Nidovirus papain-like proteases: multifunctional enzymes with protease, deubiquitinating and deISGylating activities. Virus Res [Internet]. 2014 Dec 19 [cited 2022 Jan 17];194:184–90. Available from: https://pubmed.ncbi.nlm.nih.gov/24512893/

36.   Lin SC, Ho CT, Chuo WH, Li S, Wang TT, Lin CC. Effective inhibition of MERS-CoV infection by resveratrol. BMC Infect Dis [Internet]. 2017 Feb 13 [cited 2022 Jan 17];17(1). Available from: https://pubmed.ncbi.nlm.nih.gov/28193191/

37. Nakamura M, Saito H, Ikeda M, Hokari R, Kato N, Hibi T, et al. An antioxidant resveratrol significantly enhanced replication of hepatitis C virus. World J Gastroenterol [Internet]. 2010 Jan 14 [cited 2022 Jan 17];16(2):184–92. Available from: https://pubmed.ncbi.nlm.nih.gov/20066737/

38. Berardi V, Ricci F, Castelli M, Galati G, Risuleo G. Resveratrol exhibits a strong cytotoxic activity in cultured cells and has an antiviral action against polyomavirus: potential clinical use. J Exp Clin Cancer Res [Internet]. 2009 [cited 2022 Jan 17];28(1). Available from: https://pubmed.ncbi.nlm.nih.gov/19570215/

39. Huang C, Wang Y, Li X, Ren L, Zhao J, Hu Y, et al. Clinical features of patients infected with 2019 novel coronavirus in Wuhan, China. Lancet [Internet]. 2020 Feb 15 [cited 2022 Jul 1];395(10223):497. Available from: /pmc/articles/PMC7159299/

40. Lu R, Zhao X, Li J, Niu P, Yang B, Wu H, et al. Genomic characterisation and epidemiology of 2019 novel coronavirus: implications for virus origins and receptor binding. Lancet [Internet]. 2020 Feb 22 [cited 2022 Jan 20];395(10224):565–74. Available from: https://pubmed.ncbi.nlm.nih.gov/32007145/

41. Zhu N, Zhang D, Wang W, Li X, Yang B, Song J, et al. A Novel Coronavirus from Patients with Pneumonia in China, 2019. N Engl J Med [Internet]. 2020 Feb 20 [cited 2022 Jan 20];382(8):727–33. Available from: https://pubmed.ncbi.nlm.nih.gov/31978945/

42. Chowdhury SD, Oommen AM. Epidemiology of COVID-19. Journal of Digestive Endoscopy [Internet]. 2020 Mar [cited 2022 Jan 20];11(1):3. Available from: /pmc/articles/PMC7364648/

43. Responding to COVID-19 [Internet]. [cited 2022 Jan 20]. Available from: https://www.gavi.org/covid19?gclid=Cj0KCQiAraSPBhDuARIsAM3Js4phz7zJATq2UEGwL__slEf oTHxm6-u1SIIGgOufnJjB1KPkB-nU_Q4aAvQ0EALw_wcB

44. Clinical Spectrum | COVID-19 Treatment Guidelines [Internet]. [cited 2022 Jan 20]. Available from: https://www.covid19treatmentguidelines.nih.gov/overview/clinical-spectrum/

45. Yesudhas D, Srivastava A, Gromiha MM. COVID-19 outbreak: history, mechanism, transmission, structural studies and therapeutics. Infection [Internet]. 2021 Apr 1 [cited 2022 Jan 19];49(2):1. Available from: /pmc/articles/PMC7472674/

46. Guan W jie, Ni Z yi, Hu Y, Liang W hua, Ou C quan, He J xing, et al. Clinical Characteristics of Coronavirus Disease 2019 in China. N Engl J Med [Internet]. 2020 Apr 30 [cited 2022 Jan 23];382(18):1708–20. Available from: https://pubmed.ncbi.nlm.nih.gov/32109013/

47. People with Certain Medical Conditions | CDC [Internet]. [cited 2022 Jan 23]. Available from: https://www.cdc.gov/coronavirus/2019-ncov/need-extra-precautions/people-with-medical-conditions.html

48. WHO Coronavirus (COVID-19) Dashboard | WHO Coronavirus (COVID-19) Dashboard With Vaccination Data [Internet]. [cited 2022 Jan 23]. Available from: https://covid19.who.int/

49. Doremalen N van, Bushmaker T, Morris DH, Holbrook MG, Gamble A, Williamson BN, et al. Aerosol and Surface Stability of SARS-CoV-2 as Compared with SARS-CoV-1. N Engl J Med [Internet]. 2020 Apr 16 [cited 2022 Jan 21];382(16):1564–7. Available from: /pmc/articles/PMC7121658/

50.   Riddell S, Goldie S, Hill A, Eagles D, Drew TW. The effect of temperature on persistence of SARS-CoV-2 on common surfaces. Virol J [Internet]. 2020 Oct 7 [cited 2022 Jan 21];17(1). Available from: https://pubmed.ncbi.nlm.nih.gov/33028356/

51.   Zhou P, Yang X lou, Wang XG, Hu B, Zhang L, Zhang W, et al. A pneumonia outbreak associated with a new coronavirus of probable bat origin. Nature [Internet]. 2020 Mar 12 [cited 2022 Jan 23];579(7798):270. Available from: /pmc/articles/PMC7095418/

52.   Naqvi AAT, Fatima K, Mohammad T, Fatima U, Singh IK, Singh A, et al. Insights into SARS-CoV-2 genome, structure, evolution, pathogenesis and therapies: Structural genomics approach. Biochim Biophys Acta Mol Basis Dis [Internet]. 2020 Oct 1 [cited 2022 Jan 23];1866(10):165878. Available from: /pmc/articles/PMC7293463/

53.   Yuan M, Wu NC, Zhu X, Lee CCD, So RTY, Lv H, et al. A highly conserved cryptic epitope in the receptor binding domains of SARS-CoV-2 and SARS-CoV. Science [Internet]. 2020 May 8 [cited 2022 Jan 28];368(6491):630–3. Available from: https://pubmed.ncbi.nlm.nih.gov/32245784/

54.   Yao H, Song Y, Chen Y, Wu N, Xu J, Sun C, et al. Molecular Architecture of the SARS-CoV-2 Virus. Cell [Internet]. 2020 Oct 29 [cited 2022 Jan 28];183(3):730. Available from: /pmc/articles/PMC7474903/

55.   Ke Z, Oton J, Qu K, Cortese M, Zila V, McKeane L, et al. Structures and distributions of SARS-CoV-2 spike proteins on intact virions. Nature [Internet]. 2020 Dec 17 [cited 2022 Jan 28];588(7838):498. Available from: /pmc/articles/PMC7116492/

56.   Kadam SB, Sukhramani GS, Bishnoi P, Pable AA, Barvkar VT. SARS-CoV-2, the pandemic coronavirus: Molecular and structural insights. J Basic Microbiol [Internet]. 2021 Mar 1 [cited 2022 Jan 24];61(3):180. Available from: /pmc/articles/PMC8013332/

57.   Peacock TP, Goldhill DH, Zhou J, Baillon L, Frise R, Swann OC, et al. The furin cleavage site in the SARS-CoV-2 spike protein is required for transmission in ferrets. Nature Microbiology 2021 6:7 [Internet]. 2021 Apr 27 [cited 2022 Jan 28];6(7):899–909. Available from: https://www.nature.com/articles/s41564-021-00908-w

58.   Cao Y, Yang R, Lee I, Zhang W, Sun J, Wang W, et al. Characterization of the SARS-CoV-2 E Protein: Sequence, Structure, Viroporin, and Inhibitors. Protein Sci [Internet]. 2021 Jun 1 [cited 2022 Jan 24];30(6):1114. Available from: /pmc/articles/PMC8138525/

59.   Nieva JL, Madan V, Carrasco L. Viroporins: structure and biological functions. Nat Rev Microbiol [Internet]. 2012 Aug [cited 2022 Jan 24];10(8):563. Available from: /pmc/articles/PMC7097105/

60.   Zheng Y, Zhuang MW, Han L, Zhang J, Nan ML, Zhan P, et al. Severe acute respiratory syndrome coronavirus 2 (SARS-CoV-2) membrane (M) protein inhibits type I and III interferon production by targeting RIG-I/MDA-5 signaling. Signal Transduction and Targeted Therapy 2021 5:1 [Internet]. 2020 Dec 28 [cited 2022 Jan 24];5(1):1–13. Available from: https://www.nature.com/articles/s41392-020-00438-7

61.   Kang S, Yang M, Hong Z, Zhang L, Huang Z, Chen X, et al. Crystal structure of SARS-CoV-2 nucleocapsid protein RNA binding domain reveals potential unique drug targeting sites. Acta Pharm Sin B [Internet]. 2020 Jul 1 [cited 2022 Jan 25];10(7):1228. Available from: /pmc/articles/PMC7194921/

62.   Cong Y, Ulasli M, Schepers H, Mauthe M, V'kovski P, Kriegenburg F, et al. Nucleocapsid Protein Recruitment to Replication-Transcription Complexes Plays a Crucial Role in Coronaviral Life Cycle. J Virol [Internet]. 2020 Jan 31 [cited 2022 Jan 25];94(4). Available from: /pmc/articles/PMC6997762/

63.   Semerdzhiev SA, Fakhree MAA, Segers-Nolten I, Blum C, Claessens MMAE. Interactions between SARS-CoV-2 N-Protein and α-Synuclein Accelerate Amyloid Formation. ACS Chem Neurosci [Internet]. 2022 Jan 5 [cited 2022 Jan 25];13(1):143–50. Available from: https://pubs.acs.org/doi/full/10.1021/acschemneuro.1c00666

64.   V'kovski P, Kratzel A, Steiner S, Stalder H, Thiel V. Coronavirus biology and replication: implications for SARS-CoV-2. Nature Reviews Microbiology 2020 19:3 [Internet]. 2020 Oct 28 [cited 2022 Jul 3];19(3):155–70. Available from: https://www.nature.com/articles/s41579-020-00468-6

65.   Almeida MS, Johnson MA, Herrmann T, Geralt M, Wüthrich K. Novel β-Barrel Fold in the Nuclear Magnetic Resonance Structure of the Replicase Nonstructural Protein 1 from the Severe Acute Respiratory Syndrome Coronavirus. J Virol [Internet]. 2007 Apr [cited 2022 Jan 25];81(7):3151. Available from: /pmc/articles/PMC1866046/

66.   Harcourt BH, Jukneliene D, Kanjanahaluethai A, Bechill J, Severson KM, Smith CM, et al. Identification of Severe Acute Respiratory Syndrome Coronavirus Replicase Products and Characterization of Papain-Like Protease Activity. J Virol [Internet]. 2004 Dec 15 [cited 2022 Jan 25];78(24):13600. Available from: /pmc/articles/PMC533933/

67.   Lei J, Kusov Y, Hilgenfeld R. Nsp3 of coronaviruses: Structures and functions of a large multi-domain protein. Antiviral Res [Internet]. 2018 Jan 1 [cited 2022 Jan 25];149:58. Available from: /pmc/articles/PMC7113668/

68.   Kadam SB, Sukhramani GS, Bishnoi P, Pable AA, Barvkar VT. SARS-CoV-2, the pandemic coronavirus: Molecular and structural insights. J Basic Microbiol [Internet]. 2021 Mar 1 [cited 2022 Feb 9];61(3):180–202. Available from: https://pubmed.ncbi.nlm.nih.gov/33460172/

69.   Manolaridis I, Wojdyla JA, Panjikar S, Snijder EJ, Gorbalenya AE, Berglind H, et al. Structure of the C-terminal domain of nsp4 from feline coronavirus. Acta Crystallogr D Biol Crystallogr [Internet]. 2009 [cited 2022 Jan 25];65(8):839. Available from: /pmc/articles/PMC2714721/

70.   Anand K, Palm GJ, Mesters JR, Siddell SG, Ziebuhr J, Hilgenfeld R. Structure of coronavirus main proteinase reveals combination of a chymotrypsin fold with an extra α-helical domain. EMBO J [Internet]. 2002 Jul 1 [cited 2022 Jan 25];21(13):3213. Available from: /pmc/articles/PMC126080/

71.   Cottam EM, Whelband MC, Wileman T. Coronavirus NSP6 restricts autophagosome expansion. Autophagy [Internet]. 2014 [cited 2022 Jan 25];10(8):1426. Available from: /pmc/articles/PMC4203519/

72.   te Velthuis AJW, van den Worm SHE, Snijder EJ. The SARS-coronavirus nsp7+nsp8 complex is a unique multimeric RNA polymerase capable of both de novo initiation and primer extension. Nucleic Acids Res [Internet]. 2012 Feb [cited 2022 Jan 25];40(4):1737. Available from: /pmc/articles/PMC3287201/

73.   Egloff MP, Ferron F, Campanacci V, Longhi S, Rancurel C, Dutartre H, et al. The severe acute respiratory syndrome-coronavirus replicative protein nsp9 is a single-stranded RNA-binding

subunit unique in the RNA virus world. Proc Natl Acad Sci U S A [Internet]. 2004 Mar 16 [cited 2022 Jan 25];101(11):3792. Available from: /pmc/articles/PMC374323/

74.   Subissi L, Posthuma CC, Collet A, Zevenhoven-Dobbe JC, Gorbalenya AE, Decroly E, et al. One severe acute respiratory syndrome coronavirus protein complex integrates processive RNA polymerase and exonuclease activities. Proc Natl Acad Sci U S A [Internet]. 2014 Sep 16 [cited 2022 Jan 25];111(37):E3900–9. Available from: /pmc/articles/PMC4169972/

75.   Jang KJ, Jeong S, Kang DY, Sp N, Yang YM, Kim DE. A high ATP concentration enhances the cooperative translocation of the SARS coronavirus helicase nsP13 in the unwinding of duplex RNA. Sci Rep [Internet]. 2020 Dec 1 [cited 2022 Jan 25];10(1). Available from: /pmc/articles/PMC7066239/

76.   Tahir M. Coronavirus genomic nsp14-ExoN, structure, role, mechanism, and potential application as a drug target. J Med Virol [Internet]. 2021 Jul 1 [cited 2022 Jul 3];93(7):4258. Available from: /pmc/articles/PMC8250946/

77.   Gribble J, Stevens LJ, Agostini ML, Anderson-Daniels J, Chappell JD, Lu X, et al. The coronavirus proofreading exoribonuclease mediates extensive viral recombination. PLoS Pathog [Internet]. 2021 Jan 19 [cited 2022 Jan 25];17(1). Available from: /pmc/articles/PMC7846108/

78.   Frazier MN, Dillard LB, Krahn JM, Perera L, Williams JG, Wilson IM, et al. Characterization of SARS2 Nsp15 nuclease activity reveals it's mad about U. Nucleic Acids Res [Internet]. 2021 Sep 27 [cited 2022 Jan 25];49(17):10136–49. Available from: https://academic.oup.com/nar/article/49/17/10136/6353805

79.   Vithani N, Ward MD, Zimmerman MI, Novak B, Borowsky JH, Singh S, et al. SARS-CoV-2 Nsp16 activation mechanism and a cryptic pocket with pan-coronavirus antiviral potential. Biophys J. 2021 Jul 20;120(14):2880–9.

80.   Silvas JA, Vasquez DM, Park JG, Chiem K, Allué-Guardia A, Garcia-Vilanova A, et al. Contribution of SARS-CoV-2 Accessory Proteins to Viral Pathogenicity in K18 Human ACE2 Transgenic Mice. J Virol [Internet]. 2021 Aug 10 [cited 2022 Jan 26];95(17):402–23. Available from: /pmc/articles/PMC8354228/

81.   Liu DX, Fung TS, Chong KKL, Shukla A, Hilgenfeld R. Accessory proteins of SARS-CoV and other coronaviruses. Antiviral Res. 2014 Sep 1;109(1):97–109.

82.   Zhang Y, Sun H, Pei R, Mao B, Zhao Z, Li H, et al. The SARS-CoV-2 protein ORF3a inhibits fusion of autophagosomes with lysosomes. Cell Discovery 2021 7:1 [Internet]. 2021 May 4 [cited 2022 Jul 3];7(1):1–12. Available from: https://www.nature.com/articles/s41421-021-00268-z

83.   Dhruv Yadav P, Hajjo R, Robert Shorthouse D, Kant Narayan R, Roy BC, Zhao RY, et al. Understanding the Role of SARS-CoV-2 ORF3a in Viral Pathogenesis and COVID-19. Frontiers in Microbiology | www.frontiersin.org [Internet]. 2022 [cited 2022 Aug 29];1:854567. Available from: www.frontiersin.org

84.   Zhang X, Liu Y, Liu J, Bailey AL, Plante KS, Plante JA, et al. A trans-complementation system for SARS-CoV-2 recapitulates authentic viral replication without virulence. Cell [Internet]. 2021 Apr 15 [cited 2022 Jul 3];184(8):2229-2238.e13. Available from: https://pubmed.ncbi.nlm.nih.gov/33691138/

85.   Zhang J, Ejikemeuwa A, Gerzanich V, Nasr M, Tang Q, Simard JM, et al. Understanding the Role of SARS-CoV-2 ORF3a in Viral Pathogenesis and COVID-19. Front Microbiol. 2022 Mar 9;13:583.

86.   Lee JG, Huang W, Lee H, van de Leemput J, Kane MA, Han Z. Characterization of SARS-CoV-2 proteins reveals Orf6 pathogenicity, subcellular localization, host interactions and attenuation by Selinexor. Cell Biosci [Internet]. 2021 Dec 1 [cited 2022 Jan 26];11(1). Available from: https://pubmed.ncbi.nlm.nih.gov/33766124/

87.   Frieman M, Yount B, Heise M, Kopecky-Bromberg SA, Palese P, Baric RS. Severe acute respiratory syndrome coronavirus ORF6 antagonizes STAT1 function by sequestering nuclear import factors on the rough endoplasmic reticulum/Golgi membrane. J Virol [Internet]. 2007 Sep 15 [cited 2022 Jan 26];81(18):9812–24. Available from: https://pubmed.ncbi.nlm.nih.gov/17596301/

88.   Lee JG, Huang W, Lee H, van de Leemput J, Kane MA, Han Z. Characterization of SARS-CoV-2 proteins reveals Orf6 pathogenicity, subcellular localization, host interactions and attenuation by Selinexor. Cell Biosci [Internet]. 2021 Dec 1 [cited 2022 Jul 3];11(1):1–12. Available from: https://cellandbioscience.biomedcentral.com/articles/10.1186/s13578-021-00568-7

89.   Miyamoto Y, Itoh Y, Suzuki T, Tanaka T, Sakai Y, Koido M, et al. SARS-CoV-2 ORF6 disrupts nucleocytoplasmic trafficking to advance viral replication. Communications Biology 2022 5:1 [Internet]. 2022 May 19 [cited 2022 Jul 3];5(1):1–15. Available from: https://www.nature.com/articles/s42003-022-03427-4

90.   Schaecher SR, Mackenzie JM, Pekosz A. The ORF7b protein of severe acute respiratory syndrome coronavirus (SARS-CoV) is expressed in virus-infected cells and incorporated into SARS-CoV particles. J Virol [Internet]. 2007 Jan 15 [cited 2022 Jan 26];81(2):718–31. Available from: https://pubmed.ncbi.nlm.nih.gov/17079322/

91.   Yoshimoto FK. The Proteins of Severe Acute Respiratory Syndrome Coronavirus-2 (SARS CoV-2 or n-COV19), the Cause of COVID-19. Protein J [Internet]. 2020 Jun 1 [cited 2022 Jan 26];39(3):198–216. Available from: https://pubmed.ncbi.nlm.nih.gov/32447571/

92.   Redondo N, Zaldívar-López S, Garrido JJ, Montoya M. SARS-CoV-2 Accessory Proteins in Viral Pathogenesis: Knowns and Unknowns. Front Immunol. 2021 Jul 7;12:2698.

93.   Li JY, Liao CH, Wang Q, Tan YJ, Luo R, Qiu Y, et al. The ORF6, ORF8 and nucleocapsid proteins of SARS-CoV-2 inhibit type I interferon signaling pathway. Virus Res [Internet]. 2020 Sep 1 [cited 2022 Jan 26];286. Available from: https://pubmed.ncbi.nlm.nih.gov/32589897/

94.   Yadav R, Chaudhary JK, Jain N, Chaudhary PK, Khanra S, Dhamija P, et al. Role of Structural and Non-Structural Proteins and Therapeutic Targets of SARS-CoV-2 for COVID-19. Cells [Internet]. 2021 Apr 1 [cited 2022 Jan 26];10(4):821. Available from: /pmc/articles/PMC8067447/

95.   Zhang Y, Chen Y, Li Y, Huang F, Luo B, Yuan Y, et al. The ORF8 protein of SARS-CoV-2 mediates immune evasion through down-regulating MHC-I. Proc Natl Acad Sci U S A [Internet]. 2021 Jun 8 [cited 2022 Jan 26];118(23). Available from: https://www.pnas.org/content/118/23/e2024202118

96.   Zinzula L. Lost in deletion: The enigmatic ORF8 protein of SARS-CoV-2. Biochem Biophys Res Commun [Internet]. 2021 Jan 1 [cited 2022 Jul 3];538:116. Available from: /pmc/articles/PMC7577707/

97.   Finkel Y, Mizrahi O, Nachshon A, Weingarten-Gabbay S, Morgenstern D, Yahalom-Ronen Y, et al. The coding capacity of SARS-CoV-2. Nature 2020 589:7840 [Internet]. 2020 Sep 9 [cited 2022 Jan 27];589(7840):125–30. Available from: https://www.nature.com/articles/s41586-020-2739-1

98.   Mishra DrS. ORF10: Molecular Insights into the Contagious Nature of Pandemic Novel Coronavirus 2019-nCoV. ChemRxiv [Internet]. 2020 May 12 [cited 2022 Feb 7]; Available from: https://chemrxiv.org/engage/chemrxiv/article-details/60c74b7d702a9b8dac18b443

99.   Schuster NA. Characterization and structural prediction of the putative ORF10 protein in SARS-CoV-2. bioRxiv [Internet]. 2021 Jan 4 [cited 2022 Jan 27];2020.10.26.355784. Available from: https://www.biorxiv.org/content/10.1101/2020.10.26.355784v2

100.   Li X, Hou P, Ma W, Wang X, Wang H, Yu Z, et al. SARS-CoV-2 ORF10 suppresses the antiviral innate immune response by degrading MAVS through mitophagy. Cellular & Molecular Immunology 2021 19:1 [Internet]. 2021 Nov 29 [cited 2022 Jan 27];19(1):67–78. Available from: https://www.nature.com/articles/s41423-021-00807-4

101.   Liu T, Jia P, Fang B, Zhao Z. Differential Expression of Viral Transcripts From Single-Cell RNA Sequencing of Moderate and Severe COVID-19 Patients and Its Implications for Case Severity. Front Microbiol. 2020 Oct 16;11:2568.

102.   Mena EL, Donahue CJ, Vaites LP, Li J, Rona G, O'Leary C, et al. ORF10-Cullin-2-ZYG11B complex is not required for SARS-CoV-2 infection. Proc Natl Acad Sci U S A [Internet]. 2021 Apr 1 [cited 2022 Feb 9];118(17). Available from: /pmc/articles/PMC8092598/

103.   Mena EL, Donahue CJ, Vaites LP, Li J, Rona G, O'Leary C, et al. ORF10-Cullin-2-ZYG11B complex is not required for SARS-CoV-2 infection. Proc Natl Acad Sci U S A [Internet]. 2021 Apr 1 [cited 2022 Jan 27];118(17). Available from: https://www.pnas.org/content/118/17/e2023157118

104.   Ugolini C, Mulroney L, Leger A, Castelli M, Criscuolo E, Williamson MK, et al. Nanopore ReCappable sequencing maps SARS-CoV-2 5' capping sites and provides new insights into the structure of sgRNAs. Nucleic Acids Res [Internet]. 2022 Apr 8 [cited 2022 Jul 4];50(6):3475–89. Available from: https://pubmed.ncbi.nlm.nih.gov/35244721/

105.   Hoffmann M, Kleine-Weber H, Schroeder S, Krüger N, Herrler T, Erichsen S, et al. SARS-CoV-2 Cell Entry Depends on ACE2 and TMPRSS2 and Is Blocked by a Clinically Proven Protease Inhibitor. Cell [Internet]. 2020 Apr 16 [cited 2022 Jan 28];181(2):271. Available from: /pmc/articles/PMC7102627/

106.   Koch J, Uckeley ZM, Doldan P, Stanifer M, Boulant S, Lozach PY. TMPRSS2 expression dictates the entry route used by SARS-CoV-2 to infect host cells. EMBO J [Internet]. 2021 Aug 16 [cited 2022 Jan 28];40(16):e107821. Available from: https://onlinelibrary.wiley.com/doi/full/10.15252/embj.2021107821

107.   Shang J, Wan Y, Luo C, Ye G, Geng Q, Auerbach A, et al. Cell entry mechanisms of SARS-CoV-2. Proc Natl Acad Sci U S A [Internet]. 2020 May 26 [cited 2022 Jan 28];117(21):11727–34. Available from: https://www.pnas.org/content/117/21/11727

108. Hoffmann M, Pöhlmann S. How SARS-CoV-2 makes the cut. Nature Microbiology 2021 6:7 [Internet]. 2021 Jun 30 [cited 2022 Jan 28];6(7):828–9. Available from: https://www.nature.com/articles/s41564-021-00931-x

109. Cantuti-Castelvetri L, Ojha R, Pedro LD, Djannatian M, Franz J, Kuivanen S, et al. Neuropilin-1 facilitates SARS-CoV-2 cell entry and infectivity. Science (1979). 2020 Nov 13;370(6518).

110. Daly JL, Simonetti B, Klein K, Chen KE, Williamson MK, Antón-Plágaro C, et al. Neuropilin-1 is a host factor for SARS-CoV-2 infection. Science (1979) [Internet]. 2020 Nov 13 [cited 2022 Jan 28];370(6518):861–5. Available from: https://www.science.org/doi/abs/10.1126/science.abd3072

111. Malone B, Urakova N, Snijder EJ, Campbell EA. Structures and functions of coronavirus replication–transcription complexes and their relevance for SARS-CoV-2 drug design. Nature Reviews Molecular Cell Biology 2021 23:1 [Internet]. 2021 Nov 25 [cited 2022 Jan 28];23(1):21–39. Available from: https://www.nature.com/articles/s41580-021-00432-z

112. Ziebuhr J, Snijder EJ, Gorbalenya AE. Virus-encoded proteinases and proteolytic processing in the Nidovirales. J Gen Virol [Internet]. 2000 [cited 2022 Jan 28];81(Pt 4):853–79. Available from: https://pubmed.ncbi.nlm.nih.gov/10725411/

113. Kim D, Lee JY, Yang JS, Kim JW, Kim VN, Chang H. The Architecture of SARS-CoV-2 Transcriptome. Cell [Internet]. 2020 May 14 [cited 2022 Jan 28];181(4):914-921.e10. Available from: https://pubmed.ncbi.nlm.nih.gov/32330414/

114. Wang D, Jiang A, Feng J, Li G, Guo D, Sajid M, et al. The SARS-CoV-2 subgenome landscape and its novel regulatory features. Mol Cell [Internet]. 2021 May 20 [cited 2022 Jan 28];81(10):2135-2147.e5. Available from: https://pubmed.ncbi.nlm.nih.gov/33713597/

115. Sola I, Almazán F, Zúñiga S, Enjuanes L. Continuous and Discontinuous RNA Synthesis in Coronaviruses. Annu Rev Virol [Internet]. 2015 Nov 9 [cited 2022 Dec 8];2(1):265–88. Available from: https://pubmed.ncbi.nlm.nih.gov/26958916/

116. Brian DA, Baric RS. Coronavirus genome structure and replication. Curr Top Microbiol Immunol [Internet]. 2005 [cited 2022 Dec 2];287:1–30. Available from: https://link.springer.com/chapter/10.1007/3-540-26765-4_1

117. Duffy S. Why are RNA virus mutation rates so damn high? PLoS Biol [Internet]. 2018 Aug 13 [cited 2022 Jan 31];16(8). Available from: /pmc/articles/PMC6107253/

118. WHO announces simple, easy-to-say labels for SARS-CoV-2 Variants of Interest and Concern [Internet]. [cited 2022 Jul 5]. Available from: https://www.who.int/news/item/31-05-2021-who-announces-simple-easy-to-say-labels-for-sars-cov-2-variants-of-interest-and-concern

119. Plante JA, Liu Y, Liu J, Xia H, Johnson BA, Lokugamage KG, et al. Spike mutation D614G alters SARS-CoV-2 fitness. Nature 2020 592:7852 [Internet]. 2020 Oct 26 [cited 2022 Jan 31];592(7852):116–21. Available from: https://www.nature.com/articles/s41586-020-2895-3

120. Cascella M, Rajnik M, Cuomo A, Dulebohn SC, di Napoli R. Features, Evaluation, and Treatment of Coronavirus (COVID-19). StatPearls [Internet]. 2022 Jan 5 [cited 2022 Jan 31]; Available from: https://www.ncbi.nlm.nih.gov/books/NBK554776/

121.   Davies NG, Abbott S, Barnard RC, Jarvis CI, Kucharski AJ, Munday JD, et al. Estimated transmissibility and impact of SARS-CoV-2 lineage B.1.1.7 in England. Science [Internet]. 2021 Apr 9 [cited 2022 Jan 31];372(6538). Available from: /pmc/articles/PMC8128288/

122.   Davies NG, Jarvis CI, van Zandvoort K, Clifford S, Sun FY, Funk S, et al. Increased mortality in community-tested cases of SARS-CoV-2 lineage B.1.1.7. Nature [Internet]. 2021 May 13 [cited 2022 Jan 31];593(7858):270–4. Available from: https://pubmed.ncbi.nlm.nih.gov/33723411/

123.   Tegally H, Wilkinson E, Giovanetti M, Iranzadeh A, Fonseca V, Giandhari J, et al. Detection of a SARS-CoV-2 variant of concern in South Africa. Nature [Internet]. 2021 Apr 15 [cited 2022 Jan 31];592(7854):438–43. Available from: https://pubmed.ncbi.nlm.nih.gov/33690265/

124.   Wibmer CK, Ayres F, Hermanus T, Madzivhandila M, Kgagudi P, Oosthuysen B, et al. SARS-CoV-2 501Y.V2 escapes neutralization by South African COVID-19 donor plasma. bioRxiv [Internet]. 2021 Mar 1 [cited 2022 Jan 31]; Available from: /pmc/articles/PMC7836116/

125.   Wang P, Casner RG, Nair MS, Wang M, Yu J, Cerutti G, et al. Increased Resistance of SARS-CoV-2 Variant P.1 to Antibody Neutralization. bioRxiv [Internet]. 2021 Apr 9 [cited 2022 Jan 31]; Available from: https://pubmed.ncbi.nlm.nih.gov/33688656/

126.   Mlcochova P, Kemp S, Dhar MS, Papa G, Meng B, Ferreira IATM, et al. SARS-CoV-2 B.1.617.2 Delta variant replication and immune evasion. Nature 2021 599:7883 [Internet]. 2021 Sep 6 [cited 2022 Jan 31];599(7883):114–9. Available from: https://www.nature.com/articles/s41586-021-03944-y

127.   Chen J, Wang R, Gilby NB, Wei GW. Omicron (B.1.1.529): Infectivity, vaccine breakthrough, and antibody resistance. 2021 Dec 1 [cited 2022 Jan 31]; Available from: http://arxiv.org/abs/2112.01318

128.   Collie S, Champion J, Moultrie H, Bekker LG, Gray G. Effectiveness of BNT162b2 Vaccine against Omicron Variant in South Africa. https://doi.org/101056/NEJMc2119270 [Internet]. 2021 Dec 29 [cited 2022 Jan 31]; Available from: https://www.nejm.org/doi/full/10.1056/NEJMc2119270

129.   Kokic G, Hillen HS, Tegunov D, Dienemann C, Seitz F, Schmitzova J, et al. Mechanism of SARS-CoV-2 polymerase stalling by remdesivir. Nat Commun [Internet]. 2021 Dec 1 [cited 2022 Feb 1];12(1). Available from: /pmc/articles/PMC7804290/

130.   Awadasseid A, Wu Y, Tanaka Y, Zhang W. Effective drugs used to combat SARS-CoV-2 infection and the current status of vaccines. Biomedicine & Pharmacotherapy [Internet]. 2021 May 1 [cited 2022 Feb 1];137:111330. Available from: /pmc/articles/PMC7843108/

131.   Manabe T, Kambayashi D, Akatsu H, Kudo K. Favipiravir for the treatment of patients with COVID-19: a systematic review and meta-analysis. BMC Infect Dis [Internet]. 2021 Dec 1 [cited 2022 Feb 2];21(1):1–13. Available from: https://bmcinfectdis.biomedcentral.com/articles/10.1186/s12879-021-06164-x

132.   Gupta A, Gonzalez-Rojas Y, Juarez E, Crespo Casal M, Moya J, Falci DR, et al. Early Treatment for Covid-19 with SARS-CoV-2 Neutralizing Antibody Sotrovimab. New England Journal of Medicine [Internet]. 2021 Nov 18 [cited 2022 Jul 5];385(21):1941–50. Available from: https://www.nejm.org/doi/10.1056/NEJMoa2107934

133. Dong Y, Dai T, Wei Y, Zhang L, Zheng M, Zhou F. A systematic review of SARS-CoV-2 vaccine candidates. Signal Transduction and Targeted Therapy 2020 5:1 [Internet]. 2020 Oct 13 [cited 2022 Feb 1];5(1):1–14. Available from: https://www.nature.com/articles/s41392-020-00352-y

134. Martínez-Flores D, Zepeda-Cervantes J, Cruz-Reséndiz A, Aguirre-Sampieri S, Sampieri A, Vaca L. SARS-CoV-2 Vaccines Based on the Spike Glycoprotein and Implications of New Viral Variants. Front Immunol. 2021 Jul 12;12:2774.

135. Nance KD, Meier JL. Modifications in an Emergency: The Role of N1-Methylpseudouridine in COVID-19 Vaccines. ACS Cent Sci [Internet]. 2021 May 26 [cited 2022 Jul 5];7(5):748–56. Available from: https://pubs.acs.org/doi/full/10.1021/acscentsci.1c00197

136. Kyriakidis NC, López-Cortés A, González EV, Grimaldos AB, Prado EO. SARS-CoV-2 vaccines strategies: a comprehensive review of phase 3 candidates. npj Vaccines 2021 6:1 [Internet]. 2021 Feb 22 [cited 2022 Feb 1];6(1):1–17. Available from: https://www.nature.com/articles/s41541-021-00292-w

137. Tatsis N, Ertl HCJ. Adenoviruses as vaccine vectors. Mol Ther [Internet]. 2004 Oct [cited 2022 Feb 1];10(4):616–29. Available from: https://pubmed.ncbi.nlm.nih.gov/15451446/

138. Berkner KL. Development of adenovirus vectors for the expression of heterologous genes. Biotechniques [Internet]. 1988 [cited 2022 Feb 1];6(7):616–29. Available from: https://pubmed.ncbi.nlm.nih.gov/3078719/

139. Leppard KN. Adenoviruses: Molecular Biology. Encyclopedia of Virology. 2008 Jan 1;17–23.

140. Bangari DS, Mittal SK. Development of nonhuman adenoviruses as vaccine vectors. Vaccine [Internet]. 2006 Feb 13 [cited 2022 Feb 1];24(7):849–62. Available from: https://pubmed.ncbi.nlm.nih.gov/16297508/

141. Kremer EJ, Boutin S, Chillon M, Danos O. Canine Adenovirus Vectors: an Alternative for Adenovirus-Mediated Gene Transfer. J Virol [Internet]. 2000 Jan [cited 2022 Feb 1];74(1):505. Available from: /pmc/articles/PMC111562/

142. Mendonça SA, Lorincz R, Boucher P, Curiel DT. Adenoviral vector vaccine platforms in the SARS-CoV-2 pandemic. npj Vaccines 2021 6:1 [Internet]. 2021 Aug 5 [cited 2022 Feb 1];6(1):1–14. Available from: https://www.nature.com/articles/s41541-021-00356-x

143. Almuqrin A, Davidson AD, Williamson MK, Lewis PA, Heesom KJ, Morris S, et al. SARS-CoV-2 vaccine ChAdOx1 nCoV-19 infection of human cell lines reveals low levels of viral backbone gene transcription alongside very high levels of SARS-CoV-2 S glycoprotein gene transcription. Genome Med [Internet]. 2021 Dec 1 [cited 2022 Feb 1];13(1):1–17. Available from: https://genomemedicine.biomedcentral.com/articles/10.1186/s13073-021-00859-1

144. Yuan S, Jiang SC, Li ZL. Analysis of Possible Intermediate Hosts of the New Coronavirus SARS-CoV-2. Front Vet Sci [Internet]. 2020 Jun 9 [cited 2022 Mar 18];7:379. Available from: /pmc/articles/PMC7297130/

145. Mohd HA, Al-Tawfiq JA, Memish ZA. Middle East Respiratory Syndrome Coronavirus (MERS-CoV) origin and animal reservoir. 2016;

146. Han HJ, Yu H, Yu XJ. Evidence for zoonotic origins of Middle East respiratory syndrome coronavirus. J Gen Virol [Internet]. 2016 Feb 1 [cited 2022 Mar 18];97(Pt 2):274. Available from: /pmc/articles/PMC7087374/

147. Akira S, Uematsu S, Takeuchi O. Pathogen Recognition and Innate Immunity. Cell. 2006 Feb 24;124(4):783–801.

148. Cui J, Chen Y, Wang HY, Wang RF. Mechanisms and pathways of innate immune activation and regulation in health and cancer. Hum Vaccin Immunother [Internet]. 2014 Nov 1 [cited 2022 Mar 18];10(11):3270. Available from: /pmc/articles/PMC4514086/

149. Goubau D, Deddouche S, Reis e Sousa C. Cytosolic Sensing of Viruses. Immunity [Internet]. 2013 May 23 [cited 2022 Mar 18];38(5):855. Available from: /pmc/articles/PMC7111113/

150. Nelemans T, Kikkert M. Viral Innate Immune Evasion and the Pathogenesis of Emerging RNA Virus Infections. Viruses 2019, Vol 11, Page 961 [Internet]. 2019 Oct 18 [cited 2022 Mar 18];11(10):961. Available from: https://www.mdpi.com/1999-4915/11/10/961/htm

151. Liu T, Zhang L, Joo D, Sun SC. NF-κB signaling in inflammation. Signal Transduct Target Ther [Internet]. 2017 [cited 2022 Mar 21];2. Available from: https://pubmed.ncbi.nlm.nih.gov/29158945/

152. Levy DE, Marié IJ, Durbin JE. Induction and function of type I and III interferon in response to viral infection. Curr Opin Virol [Internet]. 2011 [cited 2022 Mar 18];1(6):476–86. Available from: https://pubmed.ncbi.nlm.nih.gov/22323926/

153. Jensen S, Thomsen AR. Sensing of RNA viruses: a review of innate immune receptors involved in recognizing RNA virus invasion. J Virol [Internet]. 2012 Mar 15 [cited 2022 Mar 18];86(6):2900–10. Available from: https://pubmed.ncbi.nlm.nih.gov/22258243/

154. Chow KT, Gale M, Loo YM. RIG-I and Other RNA Sensors in Antiviral Immunity. Annu Rev Immunol [Internet]. 2018 Apr 26 [cited 2022 Mar 21];36:667–94. Available from: https://pubmed.ncbi.nlm.nih.gov/29677479/

155. Common SM, Shadbolt T, Walsh K, Sainsbury AW. The risk from SARS-CoV-2 to bat species in england and mitigation options for conservation field workers. Transbound Emerg Dis [Internet]. 2021 [cited 2022 Mar 18]; Available from: /pmc/articles/PMC8014681/

156. Levy DE, Marié IJ, Durbin JE. Induction and Function of Type I and III Interferon in Response to Viral Infection. Curr Opin Virol [Internet]. 2011 [cited 2022 Mar 21];1(6):476. Available from: /pmc/articles/PMC3272644/

157. Pérez-Girón J v., Belicha-Villanueva A, Hassan E, Gómez-Medina S, Cruz JLG, Lüdtke A, et al. Mucosal poly IC improves protection elicited by replicating influenza vaccines via enhanced dendritic cell function and T cell immunity. J Immunol [Internet]. 2014 Aug 1 [cited 2022 Mar 22];193(3):1324. Available from: /pmc/articles/PMC4111144/

158. Medzhitov R. Recognition of microorganisms and activation of the immune response. Nature [Internet]. 2007 Oct 18 [cited 2022 Mar 22];449(7164):819–26. Available from: https://pubmed.ncbi.nlm.nih.gov/17943118/

159. Ishibashi M, Wakita T, Esumi M. 2',5'-Oligoadenylate synthetase-like gene highly induced by hepatitis C virus infection in human liver is inhibitory to viral replication in vitro. Biochem

Biophys Res Commun [Internet]. 2010 Feb 12 [cited 2022 Mar 29];392(3):397–402. Available from: https://pubmed.ncbi.nlm.nih.gov/20074559/

160. Leisching G, Wiid I, Baker B. The Association of OASL and Type I Interferons in the Pathogenesis and Survival of Intracellular Replicating Bacterial Species. Front Cell Infect Microbiol. 2017 May 19;7(MAY):196.

161. Stawowczyk M, van Scoy S, Kumar KP, Reich NC. The interferon stimulated gene 54 promotes apoptosis. J Biol Chem [Internet]. 2011 Mar 4 [cited 2022 Apr 11];286(9):7257–66. Available from: https://pubmed.ncbi.nlm.nih.gov/21190939/

162. Netherton CL, Simpson J, Haller O, Wileman TE, Takamatsu HH, Monaghan P, et al. Inhibition of a Large Double-Stranded DNA Virus by MxA Protein. J Virol [Internet]. 2009 Mar [cited 2022 Mar 29];83(5):2310–20. Available from: https://journals.asm.org/journal/jvi

163. Andersson I, Bladh L, Mousavi-Jazi M, Magnusson KE, Lundkvist Å, Haller O, et al. Human MxA protein inhibits the replication of Crimean-Congo hemorrhagic fever virus. J Virol [Internet]. 2004 Apr 15 [cited 2022 Mar 29];78(8):4323–9. Available from: https://pubmed.ncbi.nlm.nih.gov/15047845/

164. Raychoudhuri A, Shrivastava S, Steele R, Kim H, Ray R, Ray RB. ISG56 and IFITM1 proteins inhibit hepatitis C virus replication. J Virol [Internet]. 2011 Dec 15 [cited 2022 Mar 29];85(24):12881–9. Available from: https://pubmed.ncbi.nlm.nih.gov/21976647/

165. Zhou Z, Wang N, Woodson SE, Dong Q, Wang J, Liang Y, et al. Antiviral activities of ISG20 in positive-strand RNA virus infections. Virology [Internet]. 2011 Jan 20 [cited 2022 Mar 29];409(2):175. Available from: /pmc/articles/PMC3018280/

166. Liu GQ, Lee JH, Parker ZM, Acharya D, Chiang JJ, van Gent M, et al. ISG15-dependent activation of the sensor MDA5 is antagonized by the SARS-CoV-2 papain-like protease to evade host innate immunity. Nat Microbiol [Internet]. 2021 Apr 1 [cited 2022 Apr 11];6(4):467–78. Available from: https://pubmed.ncbi.nlm.nih.gov/33727702/

167. Loo YM, Gale M. Immune signaling by RIG-I-like receptors. Immunity [Internet]. 2011 May 27 [cited 2022 Apr 11];34(5):680–92. Available from: https://pubmed.ncbi.nlm.nih.gov/21616437/

168. Perng YC, Lenschow DJ. ISG15 in antiviral immunity and beyond. Nature Reviews Microbiology 2018 16:7 [Internet]. 2018 May 16 [cited 2022 Mar 29];16(7):423–39. Available from: https://www.nature.com/articles/s41579-018-0020-5

169. Liu GQ, Lee JH, Parker ZM, Acharya D, Chiang JJ, van Gent M, et al. ISG15-dependent activation of the sensor MDA5 is antagonized by the SARS-CoV-2 papain-like protease to evade host innate immunity. Nat Microbiol [Internet]. 2021 Apr 1 [cited 2022 Apr 20];6(4):467–78. Available from: https://pubmed.ncbi.nlm.nih.gov/33727702/

170. Narayana SK, Helbig KJ, McCartney EM, Eyre NS, Bull RA, Eltahla A, et al. The Interferon-induced Transmembrane Proteins, IFITM1, IFITM2, and IFITM3 Inhibit Hepatitis C Virus Entry. J Biol Chem [Internet]. 2015 Oct 23 [cited 2022 Mar 29];290(43):25946–59. Available from: https://pubmed.ncbi.nlm.nih.gov/26354436/

171.   Buchrieser J, Dufloo J, Hubert M, Monel B, Planas D, Rajah MM, et al. Syncytia formation by SARS-CoV-2-infected cells. EMBO J [Internet]. 2020 Dec [cited 2022 Apr 11];39(23). Available from: https://pubmed.ncbi.nlm.nih.gov/33051876/

172.   Romagnani P, Annunziato F, Lazzeri E, Cosmi L, Beltrame C, Lasagni L, et al. Interferon-inducible protein 10, monokine induced by interferon gamma, and interferon-inducible T-cell alpha chemoattractant are produced by thymic epithelial cells and attract T-cell receptor (TCR) αβ+CD8+ single-positive T cells, TCRγδ+ T cells, and natural killer-type cells in human thymus. Blood. 2001 Feb 1;97(3):601–7.

173.   Malekshahi Z, Schiela B, Bernklau S, Banki Z, Würzner R, Stoiber H. Interference of the Zika Virus E-Protein With the Membrane Attack Complex of the Complement System. Front Immunol [Internet]. 2020 Oct 28 [cited 2022 Apr 11];11. Available from: https://pubmed.ncbi.nlm.nih.gov/33193347/

174.   Anderson SL, Carton JM, Lou J, Xing L, Rubin BY. Interferon-induced guanylate binding protein-1 (GBP-1) mediates an antiviral effect against vesicular stomatitis virus and encephalomyocarditis virus. Virology [Internet]. 1999 Mar 30 [cited 2022 Jul 7];256(1):8–14. Available from: https://pubmed.ncbi.nlm.nih.gov/10087221/

175.   Youssef L, Miranda J, Blasco M, Paules C, Crovetto F, Palomo M, et al. Complement and coagulation cascades activation is the main pathophysiological pathway in early-onset severe preeclampsia revealed by maternal proteomics. Scientific Reports 2021 11:1 [Internet]. 2021 Feb 4 [cited 2022 Apr 5];11(1):1–13. Available from: https://www.nature.com/articles/s41598-021-82733-z

176.   Li W, Garringer HJ, Goodwin CB, Richine B, Acton A, VanDuyn N, et al. Systemic and Cerebral Iron Homeostasis in Ferritin Knock-Out Mice. PLoS One [Internet]. 2015 Jan 28 [cited 2022 Apr 12];10(1). Available from: /pmc/articles/PMC4309591/

177.   Miles AL, Burr SP, Grice GL, Nathan JA. The vacuolar-ATPase complex and assembly factors, TMEM199 and CCDC115, control HIF1α prolyl hydroxylation by regulating cellular iron levels. Elife [Internet]. 2017 Mar 15 [cited 2022 Apr 12];6. Available from: https://pubmed.ncbi.nlm.nih.gov/28296633/

178.   Busse DC, Habgood-Coote D, Clare S, Brandt C, Bassano I, Kaforou M, et al. Interferon-Induced Protein 44 and Interferon-Induced Protein 44-Like Restrict Replication of Respiratory Syncytial Virus. J Virol [Internet]. 2020 Aug 31 [cited 2022 Apr 13];94(18). Available from: https://journals.asm.org/doi/full/10.1128/JVI.00297-20

179.   Caprara G, Prosperini E, Piccolo V, Sigismondo G, Melacarne A, Cuomo A, et al. PARP14 Controls the Nuclear Accumulation of a Subset of Type I IFN-Inducible Proteins. J Immunol [Internet]. 2018 Apr 1 [cited 2022 Apr 13];200(7):2439–54. Available from: https://pubmed.ncbi.nlm.nih.gov/29500242/

180.   Wickenhagen A, Sugrue E, Lytras S, Kuchi S, Noerenberg M, Turnbull ML, et al. A prenylated dsRNA sensor protects against severe COVID-19. Science [Internet]. 2021 Oct 29 [cited 2022 Apr 13];374(6567). Available from: https://pubmed.ncbi.nlm.nih.gov/34581622/

181.   Zhu J, Ghosh A, Sarkar SN. OASL – a new player in controlling antiviral innate immunity. Curr Opin Virol [Internet]. 2015 [cited 2022 Apr 13];12:15. Available from: /pmc/articles/PMC4470762/

182. Chattopadhyay K, Ramagopal UA, Mukhopadhaya A, Malashkevich VN, DiLorenzo TP, Brenowitz M, et al. Assembly and structural properties of glucocorticoid-induced TNF receptor ligand: Implications for function. Proc Natl Acad Sci U S A [Internet]. 2007 Dec 4 [cited 2022 Apr 13];104(49):19452–7. Available from: https://pubmed.ncbi.nlm.nih.gov/18040044/

183. Zhou Z, Jia X, Xue Q, Dou Z, Ma Y, Zhao Z, et al. TRIM14 is a mitochondrial adaptor that facilitates retinoic acid-inducible gene-I-like receptor-mediated innate immune response. Proc Natl Acad Sci U S A [Internet]. 2014 [cited 2022 Apr 20];111(2). Available from: https://pubmed.ncbi.nlm.nih.gov/24379373/

184. Veeranki S, Duan X, Panchanathan R, Liu H, Choubey D. IFI16 Protein Mediates the Anti-inflammatory Actions of the Type-I Interferons through Suppression of Activation of Caspase-1 by Inflammasomes. PLoS One [Internet]. 2011 [cited 2022 Apr 21];6(10):e27040. Available from: https://journals.plos.org/plosone/article?id=10.1371/journal.pone.0027040

185. Oshima S, Nakamura T, Namiki S, Okada E, Tsuchiya K, Okamoto R, et al. Interferon regulatory factor 1 (IRF-1) and IRF-2 distinctively up-regulate gene expression and production of interleukin-7 in human intestinal epithelial cells. Mol Cell Biol [Internet]. 2004 Jul 15 [cited 2022 Apr 13];24(14):6298–310. Available from: https://pubmed.ncbi.nlm.nih.gov/15226432/

186. Culley FJ, Pennycook AMJ, Tregoning JS, Dodd JS, Walzl G, Wells TN, et al. Role of CCL5 (RANTES) in viral lung disease. J Virol [Internet]. 2006 Aug 15 [cited 2022 Apr 21];80(16):8151–7. Available from: https://pubmed.ncbi.nlm.nih.gov/16873271/

187. Busse DC, Habgood-Coote D, Clare S, Brandt C, Bassano I, Kaforou M, et al. Interferon-Induced Protein 44 and Interferon-Induced Protein 44-Like Restrict Replication of Respiratory Syncytial Virus. J Virol [Internet]. 2020 Aug 31 [cited 2022 Apr 20];94(18). Available from: https://journals.asm.org/doi/full/10.1128/JVI.00297-20

188. Lai C, Wang K, Zhao Z, Zhang L, Gu H, Yang P, et al. C-C motif chemokine ligand 2 (CCL2) mediates acute lung injury induced by lethal influenza H7N9 virus. Front Microbiol [Internet]. 2017 Apr 4 [cited 2022 Apr 4];8(APR):587. Available from: /pmc/articles/PMC5379033/

189. Pérez-García F, Martin-Vicente M, Rojas-García RL, Castilla-García L, Muñoz-Gomez MJ, Hervás Fernández I, et al. High SARS-CoV-2 Viral Load and Low CCL5 Expression Levels in the Upper Respiratory Tract Are Associated With COVID-19 Severity. J Infect Dis [Internet]. 2022 Mar 15 [cited 2022 Apr 4];225(6):977–82. Available from: https://academic.oup.com/jid/article/225/6/977/6463312

190. Zwarthoff SA, Berends ETM, Mol S, Ruyken M, Aerts PC, Józsi M, et al. Functional characterization of alternative and classical pathway C3/C5 convertase activity and inhibition using purified models. Front Immunol. 2018 Jul 23;9(JUL):1691.

191. Yuan S, Jiang SC, Li ZL. Analysis of Possible Intermediate Hosts of the New Coronavirus SARS-CoV-2. Front Vet Sci [Internet]. 2020 Jun 9 [cited 2022 Apr 18];7:379. Available from: /pmc/articles/PMC7297130/

192. Gupta P, Singh MP, Kapil Goyal •, Tripti P, Mohd •, Ansari I, et al. Bats and viruses: a death-defying friendship. [cited 2022 Jul 20]; Available from: https://doi.org/10.1007/s13337-021-00716-0

193. Bokelmann M, Vogel U, Debeljak F, Düx A, Riesle-sbarbaro S, Lander A, et al. Tolerance and Persistence of Ebola Virus in Primary Cells from Mops condylurus, a Potential Ebola Virus Reservoir. Viruses [Internet]. 2021 Nov 1 [cited 2022 Jul 20];13(11). Available from: https://pubmed.ncbi.nlm.nih.gov/34834992/

194. Ragab D, Salah Eldin H, Taeimah M, Khattab R, Salem R. The COVID-19 Cytokine Storm; What We Know So Far. Front Immunol. 2020 Jun 16;11:1446.

195. Gorbunova V, Seluanov A, Kennedy BK. The World Goes Bats: Living Longer and Tolerating Viruses. [cited 2022 Jul 20]; Available from: https://doi.org/10.1016/j.cmet.2020.06.013

196. Rodrigues TS, de Sá KSG, Ishimoto AY, Becerra A, Oliveira S, Almeida L, et al. Inflammasomes are activated in response to SARS-cov-2 infection and are associated with COVID-19 severity in patients. Journal of Experimental Medicine [Internet]. 2020 Mar 1 [cited 2022 Jul 20];218(3). Available from: https://doi.org/10.1084/jem.20201707

197. Dittmer D, Sheahan T, Mossman K, Banerjee A, Baker ML, Kulcsar K, et al. Novel Insights Into Immune Systems of Bats. Frontiers in Immunology | www.frontiersin.org [Internet]. 2020 [cited 2022 Apr 18];1:26. Available from: www.frontiersin.org

198. Metzemaekers M, Vanheule V, Janssens R, Struyf S, Proost P. Overview of the mechanisms that may contribute to the non-redundant activities of interferon-inducible CXC chemokine receptor 3 ligands. Front Immunol. 2018 Jan 15;8(JAN):1970.

199. Liu M, Guo S, Hibbert JM, Jain V, Singh N, Wilson NO, et al. CXCL10/IP-10 in infectious diseases pathogenesis and potential therapeutic implications. Cytokine Growth Factor Rev [Internet]. 2011 Jun [cited 2022 Apr 18];22(3):121. Available from: /pmc/articles/PMC3203691/

200. Callahan V, Hawks S, Crawford MA, Lehman CW, Morrison HA, Ivester HM, et al. The Pro-Inflammatory Chemokines CXCL9, CXCL10 and CXCL11 Are Upregulated Following SARS-CoV-2 Infection in an AKT-Dependent Manner. Viruses [Internet]. 2021 Jun 1 [cited 2022 Apr 15];13(6). Available from: https://pubmed.ncbi.nlm.nih.gov/34205098/

201. Banerjee A, Baker ML, Kulcsar K, Misra V, Plowright R, Mossman K. Novel Insights Into Immune Systems of Bats. Front Immunol. 2020 Jan 24;11:26.

202. Tyner JW, Uchida O, Kajiwara N, Kim EY, Patel AC, O'sullivan MP, et al. CCL5-CCR5 interaction provides antiapoptotic signals for macrophage survival during viral infection. 2005 [cited 2022 Apr 25]; Available from: http://www.nature.com/naturemedicine

203. Tyner JW, Uchida O, Kajiwara N, Kim EY, O'Sullivan MP, Walter MJ, et al. Chemokine CCL5 signals required for survival during viral infection. Journal of Allergy and Clinical Immunology [Internet]. 2004 Feb 1 [cited 2022 Apr 19];113(2):S49. Available from: http://www.jacionline.org/article/S0091674903029518/fulltext

204. Ichikawa A, Kuba K, Morita M, Chida S, Tezuka H, Hara H, et al. CXCL10-CXCR3 Enhances the Development of Neutrophil-mediated Fulminant Lung Injury of Viral and Nonviral Origin. https://doi.org/101164/rccm201203-0508OC [Internet]. 2013 Mar 5 [cited 2022 Apr 25];187(1):65–77. Available from: www.atsjournals.org

205. Guo J, Huang F, Liu J, Chen Y, Wang W, Cao B, et al. The Serum Profile of Hypercytokinemia Factors Identified in H7N9-Infected Patients can Predict Fatal Outcomes. Scientific Reports

2015 5:1 [Internet]. 2015 Jun 1 [cited 2022 Apr 22];5(1):1–10. Available from: https://www.nature.com/articles/srep10942

206.   Tyner JW, Uchida O, Kajiwara N, Kim EY, Patel AC, O'Sullivan MP, et al. CCL5-CCR5 interaction provides antiapoptotic signals for macrophage survival during viral infection. Nat Med [Internet]. 2005 Nov [cited 2022 Apr 26];11(11):1180. Available from: /pmc/articles/PMC6322907/

207.   Ramadan N, Shaib H. Middle East respiratory syndrome coronavirus (MERS-CoV): A review. Germs [Internet]. 2019 Mar 1 [cited 2022 Apr 28];9(1):35. Available from: /pmc/articles/PMC6446491/

208.   Hemida MG, Chu DKW, Poon LLM, Perera RAPM, Alhammadi MA, Ng HY, et al. MERS Coronavirus in Dromedary Camel Herd, Saudi Arabia. Emerg Infect Dis [Internet]. 2014 [cited 2022 Apr 18];20(7):1231. Available from: /pmc/articles/PMC4073860/

209.   Menachery VD, Mitchell HD, Cockrell AS, Gralinski LE, Yount BL, Graham RL, et al. MERS-CoV accessory orfs play key role for infection and pathogenesis. mBio [Internet]. 2017 Jul 1 [cited 2022 Apr 28];8(4). Available from: https://journals.asm.org/doi/full/10.1128/mBio.00665-17

210.   Siu KL, Yeung ML, Kok KH, Yuen KS, Kew C, Lui PY, et al. Middle East Respiratory Syndrome Coronavirus 4a Protein Is a Double-Stranded RNA-Binding Protein That Suppresses PACT-Induced Activation of RIG-I and MDA5 in the Innate Antiviral Response. J Virol [Internet]. 2014 May [cited 2022 Apr 29];88(9):4866–76. Available from: https://journals.asm.org/doi/full/10.1128/JVI.03649-13

211.   Canton J, Fehr AR, Fernandez-Delgado R, Gutierrez-Alvarez FJ, Sanchez-Aparicio MT, García-Sastre A, et al. MERS-CoV 4b protein interferes with the NF-κB-dependent innate immune response during infection. PLoS Pathog [Internet]. 2018 Jan 1 [cited 2022 Apr 30];14(1). Available from: /pmc/articles/PMC5800688/

212.   Lee T, Pelletier J. The biology of DHX9 and its potential as a therapeutic target. Oncotarget [Internet]. 2016 [cited 2022 May 3];7(27):42716–39. Available from: https://pubmed.ncbi.nlm.nih.gov/27034008/

213.   Ng YC, Chung WC, Kang HR, Cho HJ, Park EB, Kang SJ, et al. A DNA-sensing–independent role of a nuclear RNA helicase, DHX9, in stimulation of NF-κB–mediated innate immunity against DNA virus infection. Nucleic Acids Res [Internet]. 2018 Sep 28 [cited 2022 May 3];46(17):9011. Available from: /pmc/articles/PMC6158622/

214.   Guan D, Altan-Bonnet N, Parrott AM, Arrigo CJ, Li Q, Khaleduzzaman M, et al. Nuclear factor 45 (NF45) is a regulatory subunit of complexes with NF90/110 involved in mitotic control. Mol Cell Biol [Internet]. 2008 Jul 15 [cited 2022 May 3];28(14):4629–41. Available from: https://pubmed.ncbi.nlm.nih.gov/18458058/

215.   Boukakis G, Patrinou-Georgoula M, Lekarakou M, Valavanis C, Guialis A. Deregulated expression of hnRNP A/B proteins in human non-small cell lung cancer: parallel assessment of protein and mRNA levels in paired tumour/non-tumour tissues. 2010 [cited 2022 May 4]; Available from: http://www.biomedcentral.com/1471-2407/10/434

216.   Liu Y, Li H, Liu F, Gao L bin, Han R, Chen C, et al. Heterogeneous nuclear ribonucleoprotein A2/B1 is a negative regulator of human breast cancer metastasis by maintaining the balance of multiple genes and pathways. EBioMedicine [Internet]. 2020 Jan 1 [cited 2022 May

3];51:102583. Available from:
http://www.thelancet.com/article/S2352396419307935/fulltext

217. Wang L, Wen M, Cao X. Nuclear hnRNPA2B1 initiates and amplifies the innate immune response to DNA viruses. Science (1979) [Internet]. 2019 Aug 16 [cited 2022 May 3];365(6454). Available from: https://www.science.org/doi/full/10.1126/science.aav0758

218. Guo W, Huai Q, Zhang G, Guo L, Song P, Xue X, et al. Elevated Heterogeneous Nuclear Ribonucleoprotein C Expression Correlates With Poor Prognosis in Patients With Surgically Resected Lung Adenocarcinoma. Front Oncol. 2021 Jan 25;10:3145.

219. Hu J, Cai D, Zhao Z, Zhong GC, Gong J. Suppression of Heterogeneous Nuclear Ribonucleoprotein C Inhibit Hepatocellular Carcinoma Proliferation, Migration, and Invasion via Ras/MAPK Signaling Pathway. Front Oncol. 2021 Apr 16;11:1301.

220. Ping X, Cheng Y, Bao J, Shi K, Zou J, Shentu X. KPNA4 is involved in cataract formation via the nuclear import of p53. Gene [Internet]. 2021 Jun 20 [cited 2022 May 4];786:145621. Available from: https://doi.org/10.1016/j.gene.2021.145621

221. Xu M, Liang H, Li K, Zhu S, Yao Z, Xu R, et al. Value of KPNA4 as a diagnostic and prognostic biomarker for hepatocellular carcinoma. Aging (Albany NY) [Internet]. 2021 Feb 28 [cited 2022 May 4];13(4):5263. Available from: /pmc/articles/PMC7950262/

222. Bao J, Xu C, Li B, Wu Z, Shen J, Song P, et al. Systematic Characterization of the Clinical Relevance of KPNA4 in Pancreatic Ductal Adenocarcinoma. Front Oncol. 2022 Mar 29;0:1229.

223. Zhang S, Buder K, Burkhardt C, Schlott B, Görlach M, Grosse F. Nuclear DNA Helicase II/RNA Helicase A Binds to Filamentous Actin. Journal of Biological Chemistry. 2002 Jan 4;277(1):843–53.

224. Hale BG, Randall RE, Ortin J, Jackson D. The multifunctional NS1 protein of influenza A viruses. J Gen Virol [Internet]. 2008 [cited 2022 May 9];89(Pt 10):2359–76. Available from: https://pubmed.ncbi.nlm.nih.gov/18796704/

225. Lin L, Li Y, Pyo HM, Lu X, Raman SNT, Liu Q, et al. Identification of RNA Helicase A as a Cellular Factor That Interacts with Influenza A Virus NS1 Protein and Its Role in the Virus Life Cycle. J Virol [Internet]. 2012 Feb 15 [cited 2022 May 9];86(4):1942. Available from: /pmc/articles/PMC3302408/

226. Shi ST, Lai MMC. HCV 5' and 3'UTR: When Translation Meets Replication. Hepatitis C Viruses: Genomes and Molecular Biology [Internet]. 2006 [cited 2022 May 9]; Available from: https://www.ncbi.nlm.nih.gov/books/NBK1624/

227. He QS, Tang H, Zhang J, Truong K, Wong-Staal F, Zhou D. Comparisons of RNAi approaches for validation of human RNA helicase A as an essential factor in hepatitis C virus replication. J Virol Methods. 2008 Dec 1;154(1–2):216–9.

228. Li Y, Masaki T, Shimakami T, Lemon SM. hnRNP L and NF90 Interact with Hepatitis C Virus 5'-Terminal Untranslated RNA and Promote Efficient Replication. J Virol [Internet]. 2014 Jul [cited 2022 May 9];88(13):7199. Available from: /pmc/articles/PMC4054450/

229. Rodenhuis-Zybert IA, Wilschut J, Smit JM. Dengue virus life cycle: viral and host factors modulating infectivity. Cell Mol Life Sci [Internet]. 2010 Aug [cited 2022 May 9];67(16):2773–86. Available from: https://pubmed.ncbi.nlm.nih.gov/20372965/

230. Wang Y, Chen X, Xie J, Zhou S, Huang Y, Li YP, et al. RNA Helicase A Is an Important Host Factor Involved in Dengue Virus Replication. J Virol [Internet]. 2019 Feb 15 [cited 2022 May 9];93(4). Available from: /pmc/articles/PMC6363994/

231. Shi RZ, Pan YQ, Xing L. RNA Helicase A Regulates the Replication of RNA Viruses. Viruses [Internet]. 2021 Mar 1 [cited 2022 May 9];13(3). Available from: /pmc/articles/PMC7996507/

232. Guan D, Altan-Bonnet N, Parrott AM, Arrigo CJ, Li Q, Khaleduzzaman M, et al. Nuclear Factor 45 (NF45) Is a Regulatory Subunit of Complexes with NF90/110 Involved in Mitotic Control. Mol Cell Biol [Internet]. 2008 Jul 15 [cited 2022 May 10];28(14):4629–41. Available from: https://journals.asm.org/doi/full/10.1128/MCB.00120-08

233. Li Y, Belshan M. NF45 and NF90 Bind HIV-1 RNA and Modulate HIV Gene Expression. Viruses [Internet]. 2016 Feb 16 [cited 2022 May 10];8(2). Available from: https://pubmed.ncbi.nlm.nih.gov/26891316/

234. Stricker RLO, Behrens SE, Mundt E. Nuclear factor NF45 interacts with viral proteins of infectious bursal disease virus and inhibits viral replication. J Virol [Internet]. 2010 Oct 15 [cited 2022 Jul 20];84(20):10592–605. Available from: https://pubmed.ncbi.nlm.nih.gov/20702628/

235. Harashima A, Guettouche T, Barber GN. Phosphorylation of the NFAR proteins by the dsRNA-dependent protein kinase PKR constitutes a novel mechanism of translational regulation and cellular defense. Genes Dev [Internet]. 2010 Dec 1 [cited 2022 May 10];24(23):2640–53. Available from: http://genesdev.cshlp.org/content/24/23/2640.full

236. Wang P, Song W, Mok BWY, Zhao P, Qin K, Lai A, et al. Nuclear Factor 90 Negatively Regulates Influenza Virus Replication by Interacting with Viral Nucleoprotein. J Virol [Internet]. 2009 Aug 15 [cited 2022 May 10];83(16):7850–61. Available from: https://journals.asm.org/doi/full/10.1128/JVI.00735-09

237. Shabman RS, Leung DW, Johnson J, Glennon N, Gulcicek EE, Stone KL, et al. DRBP76 Associates With Ebola Virus VP35 and Suppresses Viral Polymerase Function. J Infect Dis [Internet]. 2011 Nov 1 [cited 2022 May 10];204(suppl_3):S911–8. Available from: https://academic.oup.com/jid/article/204/suppl_3/S911/2192823

238. Li T, Li X, Zhu WF, Wang HY, Mei L, Wu SQ, et al. NF90 is a novel influenza A virus NS1-interacting protein that antagonizes the inhibitory role of NS1 on PKR phosphorylation. FEBS Lett [Internet]. 2016 Aug 1 [cited 2022 May 10];590(16):2797–810. Available from: https://onlinelibrary.wiley.com/doi/full/10.1002/1873-3468.12311

239. Castella S, Bernard R, Corno M, Fradin A, Larcher JC. Ilf3 and NF90 functions in RNA biology. Wiley Interdiscip Rev RNA [Internet]. 2015 Mar 1 [cited 2022 May 10];6(2):243–56. Available from: https://onlinelibrary.wiley.com/doi/full/10.1002/wrna.1270

240. Geuens T, Bouhy D, Timmerman V. The hnRNP family: insights into their role in health and disease. Hum Genet [Internet]. 2016 Aug 1 [cited 2022 May 11];135(8):851. Available from: /pmc/articles/PMC4947485/

241. Chaudhury A, Chander P, Howe PH. Heterogeneous nuclear ribonucleoproteins (hnRNPs) in cellular processes: Focus on hnRNP E1's multifunctional regulatory roles. RNA [Internet]. 2010 Aug [cited 2022 May 11];16(8):1449. Available from: /pmc/articles/PMC2905745/

242. Shan J, Moran-Jones K, Munro TP, Kidd GJ, Winzor DJ, Hoek KS, et al. Binding of an RNA Trafficking Response Element to Heterogeneous Nuclear Ribonucleoproteins A1 and A2. Journal of Biological Chemistry. 2000 Dec 8;275(49):38286–95.

243. Vreede FT, Jung TE, Brownlee GG. Model suggesting that replication of influenza virus is regulated by stabilization of replicative intermediates. J Virol [Internet]. 2004 Sep [cited 2022 May 11];78(17):9568–72. Available from: https://pubmed.ncbi.nlm.nih.gov/15308750/

244. Chang CK, Chen CJ, Wu CC, Chen SW, Shih SR, Kuo RL. Cellular hnRNP A2/B1 interacts with the NP of influenza A virus and impacts viral replication. PLoS One [Internet]. 2017 Nov 1 [cited 2022 May 11];12(11). Available from: /pmc/articles/PMC5690641/

245. Japanese encephalitis [Internet]. [cited 2022 May 11]. Available from: https://www.who.int/news-room/fact-sheets/detail/japanese-encephalitis

246. Katoh H, Mori Y, Kambara H, Abe T, Fukuhara T, Morita E, et al. Heterogeneous Nuclear Ribonucleoprotein A2 Participates in the Replication of Japanese Encephalitis Virus through an Interaction with Viral Proteins and RNA. J Virol [Internet]. 2011 Nov [cited 2022 May 11];85(21):10976. Available from: /pmc/articles/PMC3194950/

247. Dechtawewat T, Songprakhon P, Limjindaporn T, Puttikhunt C, Kasinrerk W, Saitornuang S, et al. Role of human heterogeneous nuclear ribonucleoprotein C1/C2 in dengue virus replication. 2011;

248. Tennant BC, Gerin JL. The woodchuck model of hepatitis B virus infection. ILAR J [Internet]. 2001 [cited 2022 May 12];42(2):89–102. Available from: https://pubmed.ncbi.nlm.nih.gov/11406711/

249. Wang F, Kuang Y, Salem N, Anderson PW, Lee Z. Cross-species hybridization of woodchuck hepatitis viral infection-induced woodchuck hepatocellular carcinoma using human, rat and mouse oligonucleotide microarrays. J Gastroenterol Hepatol [Internet]. 2009 Apr 1 [cited 2022 May 12];24(4):605–17. Available from: https://onlinelibrary.wiley.com/doi/full/10.1111/j.1440-1746.2008.05581.x

250. Kelley JB, Talley AM, Spencer A, Gioeli D, Paschal BM. Karyopherin α7 (KPNA7), a divergent member of the importin α family of nuclear import receptors. BMC Cell Biol [Internet]. 2010 Aug 11 [cited 2022 Jul 21];11:63. Available from: /pmc/articles/PMC2929220/

251. DeDiego ML, Nieto-Torres JL, Regla-Nava JA, Jimenez-Guardeño JM, Fernandez-Delgado R, Fett C, et al. Inhibition of NF-κB-Mediated Inflammation in Severe Acute Respiratory Syndrome Coronavirus-Infected Mice Increases Survival. J Virol [Internet]. 2014 Jan 15 [cited 2022 Jul 21];88(2):913. Available from: /pmc/articles/PMC3911641/

252. Canton J, Fehr AR, Fernandez-Delgado R, Gutierrez-Alvarez FJ, Sanchez-Aparicio MT, García-Sastre A, et al. MERS-CoV 4b protein interferes with the NF-κB-dependent innate immune response during infection. PLoS Pathog [Internet]. 2018 Jan 1 [cited 2022 Jul 21];14(1). Available from: /pmc/articles/PMC5800688/

253. Pancer K, Milewska A, Owczarek K, Dabrowska A, Kowalski M, Labaj P, et al. The SARS-CoV-2 ORF10 is not essential in vitro or in vivo in humans. PLoS Pathog [Internet]. 2020 Dec 10 [cited 2022 Jul 13];16(12). Available from: /pmc/articles/PMC7755277/

254. Mena EL, Donahue CJ, Pontano Vaites L, Li J, Rona G, Lignitto L, et al. ORF10-Cullin-2-ZYG11B complex is not required for SARS-CoV-2 infection. [cited 2022 Jul 13]; Available from: https://doi.org/10.1073/pnas.2023157118

255. Stobart CC, Moore ML. RNA Virus Reverse Genetics and Vaccine Design. Viruses [Internet]. 2014 Jun 25 [cited 2022 Jun 9];6(7):2531. Available from: /pmc/articles/PMC4113782/

256. Stobart CC, Moore ML. RNA Virus Reverse Genetics and Vaccine Design. Viruses [Internet]. 2014 Jun 25 [cited 2022 Aug 2];6(7):2531. Available from: /pmc/articles/PMC4113782/

257. Masters PS, Rottier PJM. Coronavirus Reverse Genetics by Targeted RNA Recombination. Coronavirus Replication and Reverse Genetics [Internet]. 2005 [cited 2022 Jun 9];287:133. Available from: /pmc/articles/PMC7122231/

258. Ávila-Pérez G, Nogales A, Martín V, Almazán F, Martínez-Sobrido L. Reverse Genetic Approaches for the Generation of Recombinant Zika Virus. Viruses [Internet]. 2018 Nov 1 [cited 2022 Jun 9];10(11). Available from: /pmc/articles/PMC6266887/

259. Wang W, Peng X, Jin Y, Pan JA, Guo D. Reverse genetics systems for SARS-CoV-2. J Med Virol [Internet]. 2022 Jul 1 [cited 2022 Jun 9];94(7):3017–31. Available from: https://onlinelibrary.wiley.com/doi/full/10.1002/jmv.27738

260. Kouprina N, Larionov V. Transformation-associated recombination (TAR) cloning for genomics studies and synthetic biology. Chromosoma [Internet]. 2016 Sep 1 [cited 2022 Aug 2];125(4):621–32. Available from: https://pubmed.ncbi.nlm.nih.gov/27116033/

261. Xie X, Lokugamage KG, Zhang X, Vu MN, Muruato AE, Menachery VD, et al. Engineering SARS-CoV-2 using a reverse genetic system. Nature Protocols 2021 16:3 [Internet]. 2021 Jan 29 [cited 2022 Aug 2];16(3):1761–84. Available from: https://www.nature.com/articles/s41596-021-00491-8

262. Thi Nhu Thao T, Labroussaa F, Ebert N, V'kovski P, Stalder H, Portmann J, et al. Rapid reconstruction of SARS-CoV-2 using a synthetic genomics platform. Nature 2020 582:7813 [Internet]. 2020 May 4 [cited 2022 Jun 9];582(7813):561–5. Available from: https://www.nature.com/articles/s41586-020-2294-9

263. Thi Nhu Thao T, Labroussaa F, Ebert N, Stalder H, Portmann J, Kelly J, et al. Rapid reconstruction of SARS-CoV-2 using a synthetic genomics platform. Nature | [Internet]. 2020 [cited 2022 Aug 30];582:561. Available from: https://doi.org/10.1038/s41586-020-2294-9

264. Abbas YM, Pichlmair A, Górna MW, Superti-Furga G, Nagar B. Structural basis for viral 5'-PPP-RNA recognition by human IFIT proteins. Nature [Internet]. 2013 Feb 7 [cited 2022 Jun 11];494(7435):60–4. Available from: https://pubmed.ncbi.nlm.nih.gov/23334420/

265. Sarkar SN, Ghosh A, Wang HW, Sung SS, Sen GC. The nature of the catalytic domain of 2'-5'-oligoadenylate synthetases. J Biol Chem [Internet]. 1999 Sep 3 [cited 2022 Jun 11];274(36):25535–42. Available from: https://pubmed.ncbi.nlm.nih.gov/10464285/

266. Kochs G, Janzen C, Hohenberg H, Haller O. Antivirally active MxA protein sequesters La Crosse virus nucleocapsid protein into perinuclear complexes. Proc Natl Acad Sci U S A [Internet]. 2002 Mar 1 [cited 2022 Jun 11];99(5):3153–8. Available from: https://europepmc.org/articles/PMC122488

267. Ramke M, Lee JY, Dyer DW, Seto D, Rajaiya J, Chodosh J. The 5'UTR in human adenoviruses: leader diversity in late gene expression. Scientific Reports 2017 7:1 [Internet]. 2017 Apr 4 [cited 2022 Jun 11];7(1):1–11. Available from: https://www.nature.com/articles/s41598-017-00747-y

268. Liu P, Li L, Millership JJ, Kang H, Leibowitz JL, Giedroc DP. A U-turn motif-containing stem–loop in the coronavirus 5' untranslated region plays a functional role in replication. RNA [Internet]. 2007 May [cited 2022 Jun 11];13(5):763. Available from: /pmc/articles/PMC1852815/

269. Li L, Kang H, Liu P, Makkinje N, Williamson ST, Leibowitz JL, et al. Structural Lability in Stem–Loop 1 Drives a 5' UTR–3' UTR Interaction in Coronavirus Replication. J Mol Biol [Internet]. 2008 Mar 3 [cited 2022 Aug 2];377(3):790. Available from: /pmc/articles/PMC2652258/

270. Vora SM, Fontana P, Mao T, Leger V, Zhang Y, Fu TM, et al. Targeting stem-loop 1 of the SARS-CoV-2 50 UTR to suppress viral translation and Nsp1 evasion. Proc Natl Acad Sci U S A [Internet]. 2022 Mar 1 [cited 2022 Jun 8];119(9). Available from: https://doi.org/10.1073/pnas.2117198119

271. Liu P, Li L, Millership JJ, Kang H, Leibowitz JL, Giedroc DP. A U-turn motif-containing stem–loop in the coronavirus 5' untranslated region plays a functional role in replication. RNA [Internet]. 2007 May [cited 2022 Jun 14];13(5):763. Available from: /pmc/articles/PMC1852815/

272. Miao Z, Tidu A, Eriani G, Martin F. Secondary structure of the SARS-CoV-2 5'-UTR. RNA Biol [Internet]. 2021 [cited 2022 Jun 8];18(4):447. Available from: /pmc/articles/PMC7544965/

273. Sola I, Almazán F, Zúñiga S, Enjuanes L. Continuous and Discontinuous RNA Synthesis in Coronaviruses. Annu Rev Virol [Internet]. 2015 Nov 9 [cited 2022 Aug 2];2(1):265. Available from: /pmc/articles/PMC6025776/

274. Yang D, Leibowitz JL. The structure and functions of coronavirus genomic 3 and 5 ends. Virus Res [Internet]. 2015 [cited 2022 Aug 2];206:120–33. Available from: http://dx.doi.org/10.1016/j.virusres.2015.02.025

275. Escors D, Izeta A, Capiscol C, Enjuanes L. Transmissible Gastroenteritis Coronavirus Packaging Signal Is Located at the 5' End of the Virus Genome. J Virol [Internet]. 2003 Jul 15 [cited 2022 Jun 8];77(14):7890. Available from: /pmc/articles/PMC161917/

276. Paillart JC, Ferhadian D, Soto-Rifo R, Cheng chenganchun A, Liu Y, Zhang Y, et al. Structures and Functions of the 3' Untranslated Regions of Positive-Sense Single-Stranded RNA Viruses Infecting Humans and Animals. Frontiers in Cellular and Infection Microbiology | www.frontiersin.org [Internet]. 2020 [cited 2022 Aug 2];1:453. Available from: www.frontiersin.org

277. Sun L, Li P, Ju X, Rao J, Huang W, Ren L, et al. In vivo structural characterization of the SARS-CoV-2 RNA genome identifies host proteins vulnerable to repurposed drugs. Cell. 2021 Apr 1;184(7):1865-1883.e20.

278. Goebel SJ, Miller TB, Bennett CJ, Bernard KA, Masters PS. A Hypervariable Region within the 3 cis-Acting Element of the Murine Coronavirus Genome Is Nonessential for RNA Synthesis but Affects Pathogenesis. J Virol. 2007;81(3):1274–87.

279. Hegde S, Tang Z, Zhao J, Wang J. Inhibition of SARS-CoV-2 by Targeting Conserved Viral RNA Structures and Sequences. Front Chem. 2021 Dec 23;9:1122.

280. Janowski AB, Jiang H, Fujii C, Owen MC, Bricker TL, Darling TL, et al. Title: The highly conserved stem-loop II motif is important for the lifecycle of astroviruses but dispensable for SARS-CoV-2 Running Title: The s2m is important for astroviruses but dispensable for SARS-CoV-2. [cited 2022 Jun 8]; Available from: https://doi.org/10.1101/2022.04.30.486882

281. Cao C, Cai Z, Xiao X, Rao J, Chen J, Hu N, et al. The architecture of the SARS-CoV-2 RNA genome inside virion. Nature Communications 2021 12:1 [Internet]. 2021 Jun 24 [cited 2022 Jun 8];12(1):1–14. Available from: https://www.nature.com/articles/s41467-021-22785-x

282. Goebel SJ, Hsue B, Dombrowski TF, Masters PS. Characterization of the RNA components of a putative molecular switch in the 3' untranslated region of the murine coronavirus genome. J Virol [Internet]. 2004 Jan 15 [cited 2022 Jun 8];78(2):669–82. Available from: https://pubmed.ncbi.nlm.nih.gov/14694098/

283. Goebel SJ, Taylor J, Masters PS. The 3 cis-Acting Genomic Replication Element of the Severe Acute Respiratory Syndrome Coronavirus Can Function in the Murine Coronavirus Genome. J Virol. 2004;78(14):7846–51.

284. Mian MF, Ahmed AN, Rad M, Babaian A, Bowdish D, Ashkar AA. Length of dsRNA (poly I:C) drives distinct innate immune responses, depending on the cell type. J Leukoc Biol. 2013 Nov;94(5):1025–36.

285. Khalil BA, Elemam NM, Maghazachi AA. Chemokines and chemokine receptors during COVID-19 infection. Comput Struct Biotechnol J. 2021 Jan 1;19:976–88.

286. Gorbunova V, Seluanov A, Kennedy BK. The World Goes Bats: Living Longer and Tolerating Viruses. Cell Metab. 2020 Jul 7;32(1):31–43.

287. Ahn M, Anderson DE, Zhang Q, Tan CW, Lim BL, Luko K, et al. Dampened NLRP3-mediated inflammation in bats and implications for a special viral reservoir host. Nat Microbiol. 2019 May 1;4(5):789–99.

288. Shi RZ, Pan YQ, Xing L. RNA Helicase A Regulates the Replication of RNA Viruses. Viruses [Internet]. 2021 Mar 1 [cited 2022 May 9];13(3). Available from: /pmc/articles/PMC7996507/

289. Zhang X, Chu H, Chik KKH, Wen L, Shuai H, Yang D, et al. hnRNP C modulates MERS-CoV and SARS-CoV-2 replication by governing the expression of a subset of circRNAs and cognitive mRNAs. Emerg Microbes Infect [Internet]. 2022 [cited 2022 Dec 9];11(1):519. Available from: /pmc/articles/PMC8843244/

290. Omrani AS, Al-Tawfiq JA, Memish ZA. Pathogens and Global Health Middle East respiratory syndrome coronavirus (MERS-CoV): animal to human interaction Middle East respiratory syndrome coronavirus (MERS-CoV): animal to human interaction. Global Health [Internet]. 2015 [cited 2022 Feb 8];109(8):354–62. Available from: https://www.tandfonline.com/action/journalInformation?journalCode=ypgh20

291. Zhang N, Tang J, Lu L, Jiang S, Du L. Receptor-binding domain-based subunit vaccines against MERS-CoV. Virus Res [Internet]. 2015 Apr 16 [cited 2022 Feb 7];202:151–9. Available from: https://pubmed.ncbi.nlm.nih.gov/25445336/

292. Hales J, Hales RJ. Investigation and comparison of the human interactions of flaviviral NS5 protein. 1945;

293. Rastogi M, Pandey N, Shukla A, Singh SK. SARS coronavirus 2: from genome to infectome. Respiratory Research 2020 21:1 [Internet]. 2020 Dec 1 [cited 2022 Feb 7];21(1):1–15. Available from: https://respiratory-research.biomedcentral.com/articles/10.1186/s12931-020-01581-z